UNIVERSITÀ DEGLI STUDI DI TRIESTE
XXVIII CICLO DEL DOTTORATO DI RICERCA IN
SCIENZE E TECNOLOGIE CHIMICHE E FARMACEUTICHE

Gold nanoparticles coated by mixtures of ligands: a basic study and their functionalization with gadolinium complexes

Settore scientifico-disciplinare: **CHIM/06**

DOTTORANDA:

MARIA ŞOLOGAN

COORDINATORE:

PROF. MAURO STENER

SUPERVISORE DI TESI:

PROF. LUCIA PASQUATO

ANNO ACCADEMICO 2014 / 2015

Table of contents

2D-	bi-dimensional
3D-	tri-dimensional
A	absorbance
AcCl	acetyl chloride
ACN	acetonitrile
AcOEt	ethyl acetate
AFM	atomic force microscopy
Au	gold
AuNPs	gold nanoparticles
br	broad signal
C12	dodecanethiolate
C16	hexadecanethiolate
C8	octanethiolate
CLSM	confocal laser scanning microscopy
COSY	correlation spectroscopy
CTAB	cetyl trimethylammonium bromide
DCM	dichloromethane
DLS	dynamic light scattering
DMF	dimethylformamide
DMSO	dimethylsulfoxyde
DO3A	1,4,7,10-Tetraazacyclododecane-N,N',N'',N'''-1,4,7-trisacetic acid
DOTA	1,4,7,10-tetraazacyclododecane-1,4,7,10-tetraacetic acid
DPD	Dissipative particle dynamics
EE	ethy ether
ESR	electron spin resonance
EtOH	ethanol
F10	1*H*,1*H*,2*H*,2*H*-perfluorododecanethiolate
F6	1*H*,1*H*,2*H*,2*H*-perfluorooctanethiolate
FITC	fluorescein isothiocyanate
G	gauss
g	grams
Gd	gadolinium
h	hours
HETCOR	heteronuclear correlation spectroscopy
HOESY	Heteronuclear Overhauser Enhacement Spectroscopy

Hz	hertz
i-PrOH	i-propanol
IR	infrared
J	coupling constant
K	Kelvin degree
KF	constant affinity of the radical probe for F-ligand domains
KH	constant affinity of the radical probe for H-ligand domains
KSAc	potassium thioacetate
m	multiplet
M	molar
MD	Molecular dynamics
MeOH	methanol
MeONa	sodium methoxide
mg	milligrams
min	minutes
mL	milliliters
MPA	mercapto proprionic acid
MS	mass spectroscopy
MsCl	methanesulfonyl chloride
MUS	sodim 11-mercapto-1-undecansulfonate
MW	molecular weight
nm	nanometer
NMR	nuclear magnetic resonance
NOESY	Nuclear Overhauser Enhacement Spectroscopy
NPs	nanoparticles
OT	octanethiol
PBS	phosphate buffer solution
PEG	polyethylene glycol
ppm	parts per million
PSD	power spectral density
q	quartet
r.t.	room temperature
rpm	revolutions per minute
s	singlet
SAM	self assembled monolayer
sec	second

SERS	surface enhanced Raman scattering
SPB	surface plasmon band
SPR	surface plasmon resonance
STM	scanning tunnelling microscopy
t	triplet
t-Bu	*tert*-butyl
TEA	triethylamine
TEG	triethylenglycol monomethyl ether
TEM	transmission electron microscopy
TfCl	trifluoromethanesulfonyl chloride
TGA	thermogravimetric analysis
THF	tetrahydrofuran
TOAB	tetraoctylammonium bromide
TsCl	tosylchloride
UV-Vis	ultraviolet-visible
V	volume
W	Watt
XF	molar fraction of the radical probe in *F*-ligand domains
XH	molar fraction of the radical probe in *H*-ligand domains
δ	chemical shift
ε	absorbance coefficient
λ	wavelength
σ	standard deviation

Abstract

In the last twenty years, gold nanoparticles (AuNPs) have received a tremendous attention for applications in the biomedical field for diagnosis, therapy, imaging and drug delivery. Among numerous studies on AuNPs a huge interest was focused on understanding and controlling the properties of these hybrid organic-inorganic nanoparticles. These studies are pushed by the fact that AuNPs can be easily synthesized with a good control over the size, shape, dispersity and composition. Moreover, AuNPs can be protected by different ligands which influence their properties and their interaction with the environment. Indeed, considering that in most cases AuNPs present on the surface mixtures of ligands, it is very important to know not only the relative amount of ligands present into the monolayer, but also how mixtures of ligands can organize on the surface of the gold core.

This thesis is focused on two projects. The first one deals with the study of the morphology of mixed monolayers composed of hydrogenated and fluorinated ligands of different lengths and bulkiness. Previously, our group has demonstrated through ESR experiments that mixtures of immiscible ligands phase segregate forming domains. It was found that the shape of these domains depends on the dimension of the gold core, on relative length and ratio between the ligands and on the ligand composition. The objective of this research project is to study in depth the organization of mixed monolayers protected gold nanoparticles, in particular using blends of hydrogenated and fluorinated thiols. To this aim, we have designed and synthesized AuNPs protected by three classes of binary mixtures of ligands: blend of thiols having different length (NPs-C12/F6 and NPs-C16/F6); ligands having the same length (NPs-C12/F10 and NPs-C8/F6) and nanoparticles protected by ligands of different length and similar bulkiness (NPs-brC12/F6). We have obtained mixed monolayers with different compositions, varying the initial ratio between the two ligands. For all this nanoparticles have recorded different ^{19}F-NMR experiments. The chemical shift variation with the nature of ligands and the monolayer composition reveal to be very diagnostic. The obtained results were supported by *in silico* experiments, in collaboration with the group of dott. P. Posocco, prof. S. Pricl and M. Fermeglia of the University of Trieste, in order to predict the shape of the domains of each type of nanoparticles.

The second project is focused on AuNPs for MRI applications. Nuclear magnetic resonance is a powerful technique for investigating physiopathology *in vitro* and *in vivo*. It

is a non-invasive technique and permits to obtain images using non-radioactive tracers. There are two main classes of materials which have been developed for this technique: compounds to promote the relaxivity of water protons like gadolinium chelates or iron oxide particles (SPIOs) used for ^{1}H-MRI and fluorinated compounds used for ^{19}F-MRI.

Previously, in our group have been reported AuNPs protected by water soluble fluorinated ligands for ^{19}F-MRI applications. These nanoparticles present suitable features for MRI and are also able to bind hydrophobic molecules allowing their applications for imaging and drug delivery. We have decided to improve the characteristics of these nanoparticles in order to have smaller T1 relaxation time and consequently better performances in the magnetic resonance field. In this thesis, we will present in Chapter 4 new preliminary results about three classes of AuNPs for MRI applications: AuNPs protected by fluorinated ligands, AuNPs protected by ligands which complex the Gd (III) and AuNPs protected by fluorinated ligands able to bind Gd(III). Additionally, we have designed and synthesized new thiols used for the synthesis of AuNPs suited for ^{1}H-MRI and ^{19}F-MRI.

Riassunto

Negli ultimi anni, le nanoparticelle di oro (AuNPs) hanno ricevuto un'enorme attenzione per applicazioni nel campo biologico, per la diagnosi, terapia, imaging e veicolazione di farmaci. Tra i vari studi sulle nanoparticelle di oro un'attenzione particolare è stata focalizzata sul controllo e la comprensione delle proprietà di questi materiali ibridi organico-inorganico. Tutti questi studi sono spinti dal fatto che le AuNPs possono essere sintetizzate facilmente con un buon controllo sulla forma, dimensione, dispersità e composizione. In più, le nanoparticelle di oro possono essere funzionalizzate con diversi ligandi che influenzano le loro proprietà e l'interazione con l'ambiente. Infatti, considerando che nella maggiore parte dei casi le nanoparticelle sono protette da miscele di ligandi, è molto importante conoscere non solo la quantità relativa dei ligandi presenti nel monostratto, ma anche sapere come una miscela di tiolati si organizza sulla superficie del nocciolo di oro.

Il lavoro di questa tesi è stato focalizzato su due progetti. Il primo progetto è basato sullo studio della morfologia di miscele di ligandi composti di thioli idrogenati e fluorurati con lunghezze e ingombro sterico diverse. Precedentemente, nel gruppo dove ho lavorato per questa tesi, è stato dimostrato tramite esperimenti ESR, che miscele di ligandi immiscibili danno segregazione di fase e si organizzano a domini. È stato inoltre trovato che la forma di questi domini è influenzata dalla dimensione del nociollo metallico, della lunghezza relativa dei due tiolati e dal rapporto fra essi ma anche dalla composizione del monostratto. Lo scopo di questo progetto di ricerca è stato lo studio più approfondito dell'organizzazzione dei monostratti misti sulla superficie di oro, in particolare usando miscele di tioli idrogenati e fluorurati. Per questo scopo, sono state progettate e sintetizzate nanoparticelle di oro protette da tre tipi di miscele di tioli: ligandi con lunghezze diverse (NPs-C12/F6 e NPs-C16/F6), ligandi avendo la stessa lunghezza (NPs-C12/F10 e NPs-C8/F6) e ligandi con diverse lunghezze e ingombro simile (NPs-brC12/F6). Sono stati ottenuti monostratti misti con diverse composizioni variando il rapporto iniziale fra i due tioli. Per tutte queste nanoparticelle sono stati effettuati esperimenti di ^{19}F NMR ed è stato trovato che la variazione del chemical shift al variare della composizione può dare indicazioni sulla morfologia del monostratto. I risultati ottenuti sono stati sopportati da esperimenti *in silico* realizzati in collaborazione con il gruppo della dott. P. Posocco, prof. S. Pricl e M. Fermeglia dall' University degli Studi di Trieste per predire il tipo di domini che si possono formare per ogni tipo di nanoparticella.

Il secondo progetto è stato concentrato sullo studio di nanoparticelle per l'imaging a

risonanza magnetica (MRI). La risonanza magnetica nucleare e una tecnica molto potente per indagini delle fisiopatologie *in vitro* ed *in vivo*. È una tecnica non-invasiva e permette di ottenere immagini senza usare traccianti irradianti. Sono stati sviluppati due classi di materiali per questa tecnica: composti che sono in grado di diminuire il tempo di rilassamento dei protoni presenti nel acqua come complessi di gadolinio o nanoparticelle di ossido di ferro (SPIO's) usati per ^{1}H MRI e composti fluorurati con applicazioni nel ^{19}F MRI. In precedenza, il nostro gruppo di ricerca ha riportato la sintesi di nanoparticelle di oro solubili in acqua per ^{19}F MRI. Queste nanoparticelle hanno proprietà adatte per MRI e possono essere anche ospiti per molecole idrofobiche permettendo applicazioni per l'imaging e veicolazione di farmaci. Abbiamo deciso di migliorare le proprietà di questi sistemi in modo tale da avere tempi di rilassamento T1 più bassi e di conseguenza prestazioni migliori nel campo di risonanza magnetica. Saranno presentati nel Capitolo 4 dei risultati preliminari di tre classi di nanoparticelle per MRI: AuNPs protette da ligandi fluorurati, AuNPs protette da ligandi che complessano lo ione Gd(III) e nanoparticelle di oro protette da ligandi fluorurati che possono legare lo ione Gd(III). In più, abbiamo progetatto e sintetizzato nuovi tioli per la sintesi di nanoparticelle sia per ^{1}H MRI che per ^{19}F MRI.

1. Introduction

Gold nanoparticles (AuNPs) are among the most extensively investigated nanomaterials and have attracted considerable interest in many fields, from physics, chemistry and biology[1] to material science and medicine.[2,3] Their nanometer-scale dimension bridges bulk materials and molecules, and produce immense changes in the physical and chemical properties with respect to the bulk material.[4] Indeed, gold nanoparticles have unique optical and electronic characteristics which are different from the bulk and are related to their shape and size[5] and arise from quantum confinement of surface electrons. The main property of nanoparticles considered as physical objects is the big surface area to volume ratio determined by the small size resulting in a large number of surface atoms in ratio with the total number of gold atoms.[6] The gold atoms at the surface are coordinately highly unsaturated and can serve as coordination sites for organic ligands such as thiols, phosphines or amines, forming a protecting organic monolayer (Figure 1.1).[7]

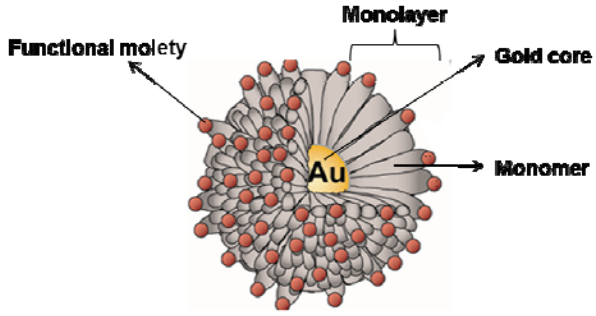

Figure 1.1 Schematic illustration of functionalized AuNPs.

The robustness of gold nanoparticles capped by thiolate ligands deriving from the strong gold−thiolate (Au−S) bond (about 184 kJ/mol)[4,8] and their easy synthetic accessibility made these systems the most studied among the family of gold nanoparticles.

[1] Saha, K.; Agasti, S.; Kim, C.; Li, X.; Rotello, V. *Chem. Rev.* **2012**, 112, 2739 – 2779.
[2] Dykman, L.; Khlebtsov, N. *Chem. Rev.* **2012**, 41, 2256 – 2282.
[3] Salata, O.V. *J. Nanobiotechnology* **2004**, 2, 3 - 8.
[4] Yang, X.; Yang, M.; Pang, B.; Vara, M.; Xia, Y. *Chem. Rev*. **2015**, 115, 10410 – 10488.
[5] The Nguyen, D.; Kim, D. J.; Kim, K. S. *Micron* **2011**, 42, 207 – 227.
[6] Chaudhuri, R. G.; Paria, S. *Chem. Rev.* **2012**, 112, 2373 – 2433.
[7] Daniel, M.C.; Astruc, D. *Chem. Rev.* **2004**, 104, 293 – 346.
[8] Love, J. C.; Estroff, L. A.; Kriebel, J.; Nuzzo, R.; Whitesides, G. *Chem. Rev*. **2005**, 105, 1103 – 1169.

The nature of the monolayer determines the properties of nanoparticles like solubility, reactivity and interaction with other species and the environment. Water-soluble thiolate protected AuNPs can be easily prepared and given the non-toxic nature of gold, these systems are intensively studied for applications in the biomedical field.

In this first chapter, the different methodologies for the synthesis of AuNPs and the main characteristics of the monolayer will be presented. A particular attention is devoted to synthesis and properties of gold nanoparticles protected by fluorinated ligands and in particular by mixtures of hydrogenated and fluorinated thiolates. The main techniques used to study the organization of mixed monolayers will also be presented. In the last section, the state of the art concerning applications of AuNPs protected by fluorinated ligands or by complexes of gadolinium for magnetic resonance imaging (MRI) applications will be briefly reviewed.

1.1. Synthesis of AuNPs protected by organic ligands

1.1.1. Synthesis of homoligand AuNPs

The large number of applications of AuNPs is rooted to the fact that gold nanostructures can be readily prepared with well-controlled sizes, shapes,dispersity and surface properties.

They can be synthesized by both the “top-down” and “bottom up” approaches. In the top-down synthesis, a bulk gold specimen is systematically broken by external forces like those encountered in ion irradiation in air,[9] laser ablation,[10] arc discharge in water,[11] UV irradiation[12] or aerosol technologies.[13] The disadvantage of this pathway is the impossibility to control the size and shape of the particles and the necessity of further stabilization by using surfactants.[5] In the “bottom up“ approach the AuNPs are formed using wet chemistry in solution by chemical or biological reduction of a gold precursor.[14] Typically, chemical reduction involves two steps: a) the production of Au (0) by the reduction of a suitable gold precursor using appropriate reducing agents (borohydrides, aminoboranes, hydrazine, formaldehyde, hydroxylamine, saturated and unsaturated alcohols, citric and oxalic acids, polyols, sugars, hydrogen peroxide, sulfites, carbon monoxide, hydrogen, acetylene); b) the stabilization of the as-obtained AuNPs by suitable capping agents (trisodium citrate, sulfur

[9] Birtcher, R. C.; Donnelly, S. E.; Schlutig, S. *Nucl. Instr. Meth. Phys. Res*. B **2004**, 215, 69 -75.
[10] Tangeysh, B.; Tibbetts, K. M.; Odhner, J.; Wayland, B.; Levis, B. *J. Phys. Chem. C* **2013**, 117, 18719 – 18727.
[11] Lung, J. K.; Huang, J. C.; Tien, D. C.; Liao, C. Y.; Tsieng, K. H.; Tsung, T. T.; Kao, W. S.; Tsai, T. H.; Jwo, C. S.; Lin, H. M.; Stobinski, L. *J. of alloys and Compounds* **2007**, 434 – 435, 655 – 658.
[12] Sakamoto, M.; Fujistuka, M.; Majima, T. *J. Photochem. Photobiol.C: Photochem. Rev.* **2009**, 10, 33 – 56.
[13] Yoo, H. Y.; Bruckenstein, S. *Adv. in Nanopart.* **2013**, 2, 313 – 317.
[14] Parab, H.; Jung, C.; Woo, M.; Park, H. G. *J. Nanopart. Res.* **2011**, 13, 2173 – 2180.

ligands (in particular thiolates), phosphorus ligands, nitrogen-based ligands (including heterocycles), oxygen-based ligands, dendrimers, polymers and surfactant) which prevent aggregation of nanoparticles.[15,16]

In order to obtain monodisperse AuNPs, two approaches can be used: a) an appropriated synthetic method and b) post-synthetic size-selection. The post synthetic size-selection methods are very effective, but are time consuming and in most cases have low yields. Several methods have been reported in order to obtain monodisperse AuNPs like gel electrophoresis,[17] diafiltration,[77] application of magnetic fields,[18] size exclusion chromatography, density gradient centrifugation,[19] selective precipitation,[20] membrane filtration,[21] extraction,[22] or size exclusion separation of alkanethiol-stabilized AuNPs in supercritical ethane.[23]

The most commonly used method to obtain AuNPs is, by far, the aqueous reduction of the gold salt by sodium citrate at reflux, reported by Turkevich *et al* in 1951[24] which gives 20 nm AuNPs. Later, this procedure was improved by Frens in 1973 and Natan in 1995,[25] to obtain colloids between 15 and 150 nm by controlling the initial ratio between trisodium citrate and gold. Recent studies of the mechanism of the reaction suggest that the actual AuNP stabilizer is dicarboxy acetone resulting from the oxidation of citrate, rather than citrate itself.[26] Several other research groups have improved the Turkevich method by controlling the pH and the temperature,[27] the concentration of the reagents, the order of addition of the reactants[28] or the nature of the reducing agents.[29]

Thiolate stabilized gold colloids were first reported by Mulvaney and Giersig in 1993[30] who have shown the possibility to stabilize gold colloids using different alkanethiols. One year

[15] Zhou, J.; Ralston, J.; Sedev, R.; Beattie, D. *J. Colloid Interface Sci.* **2009**, 331, 251 – 262.
[16] Zhao, P.; Li, N.; Astruc, D. *Coord. Chem. Rev.* **2013**, 257, 638 – 665.
[17] Xu, X.; Cawell, C.; Tucker, E.; Kabisatpathy, S.; Brodhacker, L.; Scrivens, W. *J. Chromatogr. A* **2007**, 117, 35 – 41.
[18] Ditsch, A.; Lindenmann, S.; Laibinis, P.; Wang, D.; Hatton,. A. *Int. Eng. Chem. Res.* **2005**, 44, 6824 – 6836.
[19] Chen, G.; Wang, Y.; Tan, L. H.; Yang, M.; Tan, L. S.; Chen, Y.; Chen, H. *J. Am. Chem. Soc*. **2009**, 131, 4218 – 4219.
[20] Zhao, W.Y.; Lin, L., Hsing, I.M. *Langmuir* **2010**, 26, 7405 – 7409.
[21] Akthakul, A.; Hochbaum, A.; Stellacci, F.; Mayes, A.M. *Adv Mater* **2005**, 17, 532 – 535.
[22] Kim, Y.G.; Oh, S. K.; Crooks, R. M. *Chem. Mater.* **2004**,16,167–172.
[23] Williams, D. P.; Satherley, J. *Langmuir* **2009**, 25, 3743–3747.
[24] Turkevich, J.; Stevenson, P. C.; Hillier, *J. Discuss. Faraday. Soc.* **1951**, 11, 55–75
[25] Grabar, K.; Freeman, G.; Hommer, M.; Natan, M. *Anal. Chem.* **1995**, 67, 735 – 743.
[26] a) Wuithschick, M.; Birnbaum, A.; Witte, S.; Sztucki, M.; Vainio, U.; Pinna, N.; Rademann, K.; Emmerling, F.; Kraehnert, R.; Polte, J. *Acs Nano* **2015**, 9 (7), 7052 – 7071; b) Polte, J. *Cryst. Eng. Comm.* **2015**, 17, 6809 – 6830.
[27] Li, C.; Li, D.; Wan, G.; Xu, J.; Hou, W. *Nanoscale Res. Lett.* **2011**, 6, 440 – 449.
[28] Sivaraman, S. K.; Kumar, S.; Santhanam, V. *J. Colloid Interface Sci.* **2011**, 361, 543 – 547.
[29] Hanzic, N.; Jurkin, T.; Maksimovic, A.; Gotic, M. *Radiat. Phys. Chem*. **2015**, 106, 77 – 82.
[30] Giersig, M.; Mulvaney, P. *Langmuir* **1993**, 9, 3408 – 3413.

later, Brust[31] published the first method to prepare AuNPs by reducing tetrachloroauric acid in the presence of thiols using sodium borohydride. This method involves, in the first step, the phase transfer of the gold precursor from an aqueous to an organic phase by using tetraoctylammonium bromide (TOAB). The authors suggested that by the addition of dodecanethiol as capping agent, the Au(III) ions are reduced to Au(I); the further addition of aqueous $NaBH_4$ yield the reduction of Au(I) to Au^0 with nucleation and growth of the nanoparticles imparting a deep brown colored solution.

The high impact of this procedure was due to: (i) the ease of synthesis; (ii) the high thermal and air stability of the AuNPs prepared in this way; (iii) the possibility to repeatedly isolate and re-dissolve the nanoparticles without aggregation or decomposition. The procedure enables control over the size of the nanoparticles by varying the Au-to-thiol ratio, the temperature or the rate at which the reducing agent is added. More specifically, small Au:thiol molar ratios and fast addition of the reducing agent at low temperatures produce smaller and less dispersed particles. The thiolate-protected gold nanoparticles can be easily functionalization and modification by ligand substitution.[16]

The reaction mechanism for the formation of gold nanoparticles proposed by Brust and Schiffrin foresee the formation of polymeric Au(I)-thiolate complexes as a consequence of reduction Au (III) to Au (I) by the added thiol[31] (Scheme 1.1). Later, Shaaf and collaborators[32] have demonstrated that the formation of $[Au(I)SR]_n$ is promoted by the presence of large quantities of water or polar solvents.

[31] Brust, M.; Walker, M.; Bethell, B.; Schiffrin, D.; Whyman, R. *J. Chem. Soc., Chem. Commun.* **1994**, 801 – 802.
[32] Shaaf, T. G.; Knight, G.; Shafigullin, M. N.; Borkman, R. F.; Whetten, R. L. *J. Phys. Chem. B* **1998**, 102, 10643 – 10646.

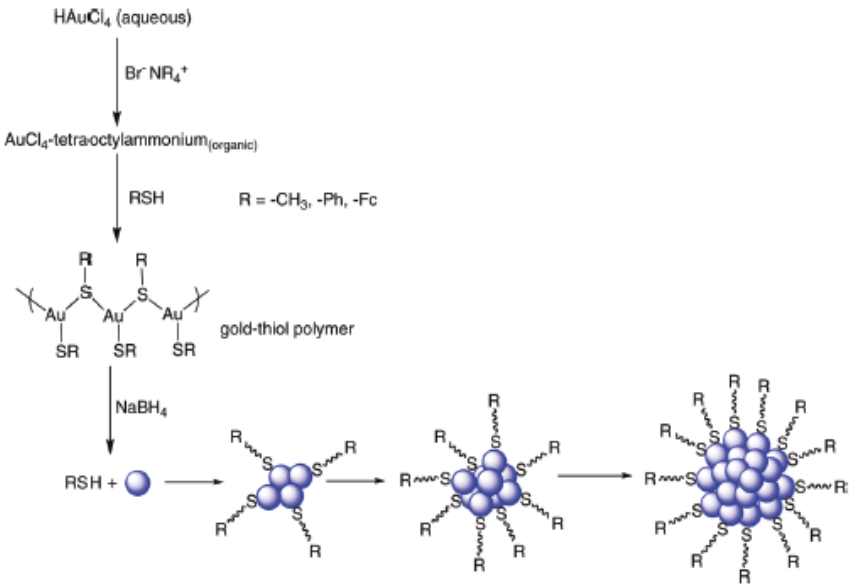

Scheme 1.1 Synthesis of AuNPs using Brust – Schiffrin method.[33]

More recently, Lennox[34] has investigated the nature of the precursors in the Brust-Schiffrin reaction, through NMR experiments. This study displayed that the actual precursors are anionic dihaloaurate(I), or tetrahaloaurate (II) complexes where the tetraoctylmmonium ion serves as counterion. On the other hand, Au(I) thiolates are shown to be precursors of the reaction when the aqueous phase was removed. The same reaction mechanism was found to be operative also in the two phase synthesis of Ag and Cu nanoparticles, and for those reactions in which different phase transfer agents and reducing agents were used. The species present in this reaction have been quantitatively monitored by ^{1}H-NMR spectroscopy. More specifically, the addition of the phase transfer agent to the tetrachloroauric salt determines the formation of anionic Au (III) halide complexes where TOA^{+} acts as the counterion. Upon addition of thiols, Au(III) is reduced to Au(I); the conversion of the reaction depends on the amount of thiol (R-SH) added. When less than 2 equivalents of thiols are used, the reaction mixture contained both $[NR_4][AuX_4]$ and $[NR_4][AuX_2]$ in addition to disulfide (RSSR). When a higher amount of thiol is used, all the $[NR_4][AuX_4]$ is converted in the salt $[NR_4][AuX_2]$ with an excess of free thiol remaining into the solution (Scheme 1.2).

[33] Sardar, R.; Funsston, A. M.; Mulvaney, P.; Murray, R. W. *Langmuir* **2009**, 25, 13840 – 13851.
[34] Goulet, P.; Lennox, B. *J. Am. Chem. Soc. Commun.* **2010**, 132, 9582 – 9584.

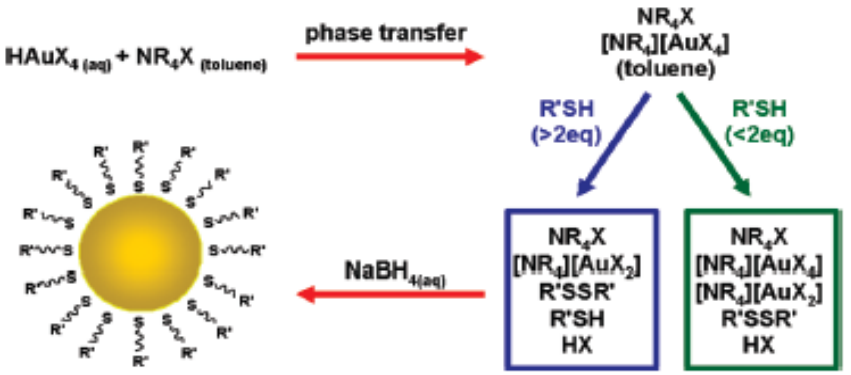

Scheme 1.2 Lennox revised mechanism for Brust AuNPs synthesis.[34]

One year later, on the basis of Raman, NMR, and surface plasmon resonance characterizations, Tong and coworkers have demonstrated[35] no formation of the Au-S bond prior to the addition of the $NaBH_4$, excluding the formation of $[Au(I)SR]_n$ polymers predicted by Brust. According to this study, metal nucleation centers/NPs are first formed inside the inverse micelles of the tetrabutylammonium bromide in the organic solvent (Scheme 1.3), where the metal ions are reduced by $NaBH_4$. Only afterwards, the nanoparticles are passivated by the thiols present in solution.

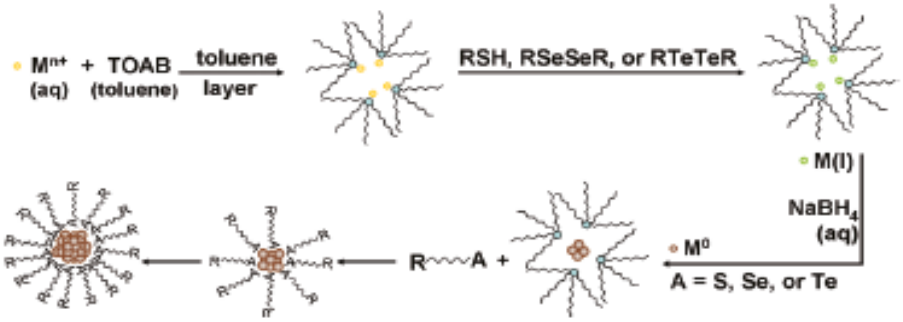

Scheme 1.3 Inverse micelles mechanism proposed by Tong for the two phase Brust Schiffrin synthesis of AuNPs.[35]

Recently, Xue and collaborators[36] observed the formation of Au(I) thiolate complexes in the Brust-Schiffrin synthesis of AuNP using benzylmercaptan as capping agent. The Au (I) thiolate complexes were precipitated by addition of methanol and further characterized by solid state nuclear magnetic resonance (SSNMR), UV-Vis and Raman spectroscopies and

[35] Li, Y.; Zaluzhna, O.; Xu, B.; Gao, Y.; Modest, J.; Tong, Y. *J. Am. Chem. Soc.* **2011**, 133, 2092 – 2095.
[36] Yu, C.; Zhu, L.; Zhang, R.; Wang, X.; Guo, C.; Suo, P.; Xue, G. *J. Phys. Chem. C* **2014**, 118, 10434 – 10440.

TGA. These authors confirm by ^{1}H-NMR and UV-Vis spectroscopy that the first two equivalents of thiol reduce Au(III) to Au(I) completely yielding the corresponding disulfide. The further addition of thiol results in the formation of the $[Au(I)SR]_n$ species.

1.1.2. Biosynthesis of AuNPs

Due to the presence of numerous carboxyl, carbonyl, hydroxyl and phenolic and amines groups, some natural compounds can act as reducing agents for Au (III) and electrostatic stabilizers for AuNPs. The first green synthesis has been reported by Goia[37] who used Arabic gum to obtain 2-14 nm AuNPs. Recently numerous studies have been made in this field[16] and many groups have obtained gold nanoparticles using like reducing agent extract of Lemon grass,[38] Cianmmomum camphora,[39] Castor oil,[40] Tannic acid,[41] Memecylom umbelatum,[42] Allium sativum[43] and many others.[44]

1.1.3. Synthesis of self-assembled mixed monolayers protected gold nanoparticles

There are four main methodologies that can be used in order to obtain mixed monolayers:

1.1.3.1. Direct synthesis

In this procedure, the reduction of Au (III) is made in the presence of a mixture of the thiols to be grafted on the surface of the gold core. This method allows obtaining mixed monolayer AuNPs in short time but the ligands used for the synthesis must be compatible with the reductive conditions, stable during the reaction and available in large amounts.

1.1.3.2. Ligand exchange reaction

With this methodology, the thiolate forming the monolayer is displaced by a new ligand. This method is commonly used when the second ligand it is not compatible with the reducing conditions of the reaction, it is very expensive or it is not commercially available.[45]

---

[37] Goia, D.; Matijevic, E. *Colloids Surf. A* **1999**, 146, 139 – 152.
[38] Shif Shankar, S.; Rai, A.; Ankamwar, B.; Singh, A.; Ahmad, A.; Sastry, M. *Chem. Mater.* **2005**, 17, 566 – 572.
[39] Huang, J.; Li, Q.; Sun, D.; Lu, Y.; Su, Y.; Yang, X.; Wang, H.; Wang, Y.; Shao, W.; He, N.; Hong, J.; Chen, C. *Nanotechnology* **2007**, 18, 105114.
[40] Da Silva, E. C.; da Silva, M. G. A.; Meneghetti, S. M. P.; Machado, G.; Alencar, M. A. R. C.; Hickman, J. M.; Meneghetti, M. R. *J. Nanopart. Res.* **2008**, 10, 201.
[41] Huang, X.; Vu, H.; Liao, X.; Shi, B. *Green. Chem.* **2010**, 12, 395 – 399.
[42] Arunachalam, K.; Anamalai, S. K.; Hari, S. *Int. J. Nanomedicine* **2013**, 8, 1307 – 1315.
[43] Coman, C.; Leopold, L. F.; Rugina, O. D.; Barbu-Tudoran, L.; Leopold, N.; Tofana, M.; Socaciu, C. *J. Nanopart. Res.* **2014**, 16, 2158.
[44] Iravani, S.; *Green Chem*. **2011**, 13, 2638 – 2650.
[45] Hostetler, M.; Wingate, J.; Zhong, C. J.; Harris, J.; Vachet, R.; Clark, M.; Londono, D.; Green, S.; Stokes, J.; Wignall, G.; Glish, G.; Porter, M.; Evans, N.; Murray, R. *Langmuir* **1998**, 14, 17 – 30.

Mechanistic studies of the place exchange reactions have been performed by several groups.[46] The results of these experiments have shown that ligand exchange is an associative process in which the incoming ligand penetrates the monolayer in order to undergo place-exchange and the displaced ligand exits from the monolayer as a thiol. The rate and the equilibrium composition of this reaction depend on: a) the molar ratio of R'SH and RS units, b) the relative steric bulk of the thios and c) the relative length of RSH and R'SH chains.[47] Early investigations by Murray and coworkers[48] have demonstrated that some sites on the surface of the gold core are significantly easy to exchange (like vertex, edge defect sites), while for other sites (like the interior terraces sites) exchange is more difficult because of their different electron densities[49] and steric accessibility.[50] For this reason the rate of exchange on NPs is initially rapid because first thiols on the edges and vertex are exchanged and then the rate of reaction slows down dramatically because thiols on the terraces begin to be exchanged. The rate of this reaction is largely influenced by the chain length of the ligands: the exchange is observed to occur more rapidly onto clusters protected by shorter ligands. It was also demonstrated that disulfides and oxidized sulfur species are not able to undergo place exchange reaction.[39]
Other studies[39] have shown that the rate exchange between the bound and the free thiol depends on the structure of the latter as follow: a) primary thiols are more reactive than the corresponding secondary and tertiary thiols demonstrating that steric hindrance near the thiol group significantly reduces its reactivity in place exchange reactions. b) When the bulky group is far apart from the thiol head group by one carbon the branched (bulkier) thiol exhibited higher reactivity than the linear thiol of the same molecular weight.

1.1.3.3. Preparation of AuNPs capped with citrate, polymers or other weak ligands which are displayed in a second step by blend of thiols. For example, the procedure reported by Peng[51] and modified by Scrimin.[52]

1.1.3.4. Post-synthetic modifications

The chemical reactivities of thiolates are different on nanoparticles with respect to 2D-SAMs because the organization of the ligands on a curved surface is different respect to flat surfaces enabling an easier accessibility to terminal functional groups. This difference makes it possible the use of several classes of reactions which cannot be used on 2D-

[46] Hostetler, M. J.; Templeton, A. C.; Murray, R. W. *Langmuir* **1999**, 15, 3782 -3789.
[47] Donkers, R. L.; Song, Y.; Murray, R. W. *Langmuir* **2004**, 20, 4703 -4707.
[48] Ingram, R. S.; Hostetler, M. J.; Murray, R. W. *J. Am. Chem. Soc.* **1997**, 119, 9175 -9178.
[49] Hakkinen, H.; Barnett, R.N.; Landman, U.; *Phys. Rev. Lett.* **1999**, 82, 3264 -3267.
[50] Luedtke, W. D.; Landman, U. *J. Phys. Chem. B* **1998**, 102, 6566 -6572.
[51] Jana, V.; Peng, X. *J. Am. Chem. Soc*. **2003**, 125, 14280 – 14281.
[52] Manea, F.; Bindoli, C.; Polizzi, S.; Lay, L.; Scrimin, P. *Langmuir* **2008**, 24, 4120 – 4124.

SAMs due to steric effects, such as the S_N2 reactions.[53] Murray and co-workers have studied amide and ester coupling reactions[54] in order to obtain polyfunctionalized gold nanoparticles starting from ω-functionalized materials with carboxylic acid groups or hydroxyl moieties. The click chemistry approach has been recognized as an important tool in gold nanoparticle functionalization since these reactions often give quantitative yields under very mild reaction conditions. In particular copper-catalyzed 1,3-dipolar cycloaddition, between an alkyne and an azide to form a triazole ring,[55] was used by Fleming in 2006[56] for the functionalization of nanoparticles with thiols bearing azide groups. Microwave reactors have been used by Weck[57] to link in a few minutes a library of substituted alkynes onto gold nanoparticles with quantitative conversions. The same methodology was also used to graft alkyne modified DNA duplex on azide functionalized AuNPs obtaining a chain-like assembly of NPs on the DNA template.[58] Finally, another interesting post-synthetic modification is the Michael reaction between maleimide and a nucleophilic gadolinium derivative to obtain gold nanoparticles for MRI applications.[59]

1.1.4. Morphology of self-assembled mixed-monolayers

Control of the topological organization of the ligands in the self-assembled monolayer grafted on solid surfaces is an emerging goal for the nanoscience. AuNPs have shown to be ideal scaffolds for the study of the morphology of self-assembled mixed-monolayers due to their stability and the ease of synthesis and functionalization with different moieties, but spherical nanoparticles remain challenging to modify anisotropically. The properties of gold nanoparticles depend on the features of the monolayer and these also influence the interaction of the nanoparticles with the environment. For example, it has been demonstrated that ripples on the surface of gold nanoparticles, determined by the formation of striated domains, do not allow a net interaction between proteins outer shell and nanoparticles.[60] The explanation for this is that the 5-8 Å small domains on the surface of these particles are more than one order of magnitude smaller than the characteristic size of

[53] Templeton, A. C.; Hostetler, M. J.; Kraft, C. T.; Murray, R. W. J.Am. Chem. Soc. 1998, 120, 1906 – 1911.
[54] Templeton, A. C.; Hostetler, M. J.; Warmoth, E. K.; Chen, S.; Hartshorn, C. M.; Krishnamurthy, M. D. E.; Murray, R. W. *J.Am. Chem. Soc.* **1998**, 120, 4845 – 4849.
[55] a) Demko, Z. P.; Sharpless, K. B. *Angew. Chem. Int. Ed.* **2002**, 41, 2113 -2116. b) Tornøe, C. W.; Christensen, C.; Meldal, M. *J. Org. Chem.* **2002**, 67, 3057 -3064. c) Rostovtsev, V. V.; Green, L. G.; Fokin, V. V. Sharpless, K. B. *Angew. Chem. Int. Ed.* **2002**, 41, 2596 -2599.
[56] Fleming, D. A. Thode, C. J.; Williams, M. E. *Chem. Mater.* **2006**, 18, 2327 -2334.
[57] Sommer, W. J., Weak, M. *Langmuir* **2007**, 23, 11991 -11995.
[58] Fischler, M.; Sologubenko, A.; Mayer, J.; Clever, G.; Burley, G.; Gierlich, J.; Carell, T.; Simon, U. *Chem. Commun.* **2008**, 169 -171.
[59] Milne, M.; Gobbo, P.; McVicar, N.; Bartha, B.; Worketin, M.; Hudson, R. *J. Mater. Chem. B* **2013**, 1, 5628 – 5635.
[60] Jackson, A.; Myerson, J., Stellacci, F. *Nat. Mater.* **2004**, 3, 330 – 336.

a protein globule; independently of the protein conformation, there will always be a series of attractive and repulsive forces between the protein's outer shell and the particle's domains. Recently, the absorption of BSA on the surface of gold nanoparticles (Figure 1.2) with similar composition but different organization of the monolayer was studied[61] by using a combination of DLS, CD spectroscopy, fluorescence quenching, and ITC. Depending on the surface structure of AuNPs, BSA seems to adopt either a "side-on" or an "end-on" conformation on AuNPs. BSA adsorption onto particles with nanoscale stripe-like polar and nonpolar domains behaved differently from AuNPs with randomly distributed polar and non polar groups and AuNPs protected by homoligand with polar end groups. Additionally, the morphology of mixed monolayers influences the toxicity of the NPs.[62]

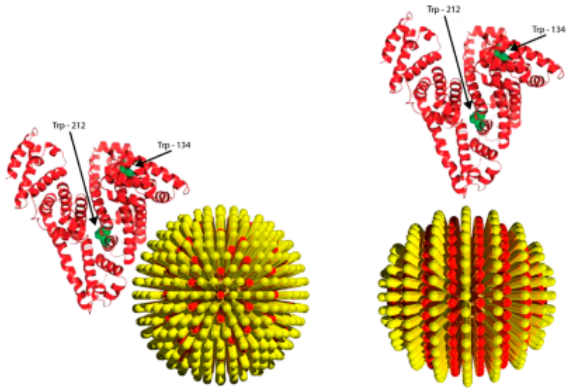

Figure 1.2 Proposed binding geometries for BSA and (left) MUS/brOT or MPA/brOT and (right) MUS/OT or MPA/OT AuNPs based on DLS and fluorescent quenching measurements.[61]

1.1.5. Control of the morphology of self-assembled mixed-monolayers

1.1.5.1. Control of the morphology by using coded ligands

The most easy method to obtain a given organization of the monolayer is to combine ligands coded to self-assemble. The first example of this approach was reported by Stellacci group in 2004.[60] They have shown that mixture of octanethiol (OT) and mercaptopropionic acid (MPA) in a 2:1 molar ratio self organize on the surface of the gold

[61] Huang, R.; Carney, R.; Ikuma, K.; Stellacci, F.; Lau, B. *ACS Nano* **2014**, 8, 5402 – 5412.
[62] Sabella, S.; Carney, R.; Brunetti, V.; Malvindi, M. A.; Al-Juffali, N.; Vecchio, G.; Janes, S.; Bakr, O.; Cingolani, R.; Stellacci, F.; Pompa, P. P. *Nanoscale* **2014**, 6, 7052 – 7061.

core forming stripes with a 5 Å width. The driving force for this organization seems to be the difference in length or the different tail of the two ligands.

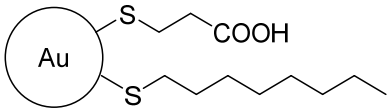

Figure 1.3 AuNPs coated by octanethiol (OT) and mercaptopropionic acid (MPA).

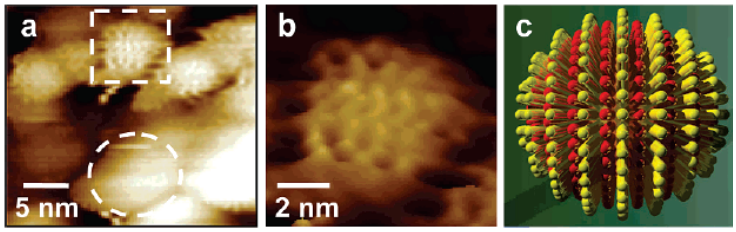

Figure 1.4 a) STM height image of AuNPs, on Au foil, coated with 2:1 molar fraction of octanethiol and mercaptopropionic acid showing ribbon-like stripes, due to the phase separation of the two ligands. b) enlarged image of the NP outlined with the dotted square of figure a and c) schematic drawing to help the reader visualize 3D arrangement (mercaptopropionic acid in red and octanethiol in yellow).[60]

Later, the organization of the thiols was investigated and rationalized by the Glotzer group using atomistic and mesoscale simulations[63] based on particle dissipative dynamics (DPD). These experiments have demonstrated that stripe like patterns formation is entropic in origin. When the two ligands are very short (C3:C3), they are nanophase separating independently by the difference in length, bulkiness or nature of the tail group. For mixtures of thiolates with a sufficiently difference in length (Figure 1.5), the additional conformational entropy gained by creating interfaces at which bulky tail groups are adjacent to less bulky ones, providing the bulky tails with additional free volume, is sufficient to overcome the decrease in enthalpy energy that would be gained from bulk separation and the energetic penalty for creating the extra interfaces. These theoretical studies confirmed also that stripes formation is a function of substrate curvature: stripes are observed only in curved surface with NPs having a core diameter from 2.5 to 8 nm.

[63] a) Singh, C.; Ghorai, P.; Horsch, M.; Jackson, A.; Larson, R.; Stellacci, F.; Glotzer, S. *Phys. Rev. Lett.* **2007**, 99, 226106. b) Singh, C.; Hu, Y.; Khanal, B.; Zubarev, E.; Stellacci, F.; Glotzer, S. *Nanoscale* **2011**, 3, 3244 – 3250. c) Ghorai, P.; Glotzer, S. *J. Phys. Chem. C* **2010**, 114, 19182 – 19186.

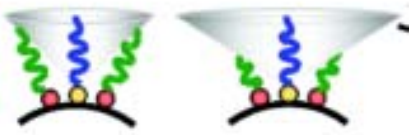

Figure 1.5 Schematic representation of shared free volume of surfactants which are surrounded by thiols having equal or different length.[53]

On the contrary, when the entropic gain is not balancing the enthalpy loss, bulk phase-separated Janus particles are predicted to form (Figure 1.5). Starting from this study, the same group has investigated the design of ternary[64] or quaternary [65] mixture of thiols on the surface of the gold core. Recently, atomistic and mesoscale simulations[66] were used to investigate how the size, bending of thiols and hydration of SAMs are influenced by the organization of a binary mixture of thiols with equal or different length. When they have a random organization, the longer thiolates do not have in the close proximity another long thiolate and hence the probability of bending is larger with respect to other types of organization.

The organization of the monolayer into striped domains leads to different reactivities of the ligands at the pole of the nanoparticles[67] with respect to ligands found in other positions on the gold surface, allowing the introduction of two functionalized thiolates at the poles of the nanoparticles. Thus, chains of nanoparticles have been obtained by exchanging the thiolates at the poles with 11-mercaptoundecanoic acid. Subsequent activation of the acid group with *N*-hydroxysuccinimide and coupling with 1,6-diaminohexane give rise to the formation of a polymeric chain of NPs (Figure 1.6).

[64] Pons-Sieperman, I.; Glotzer, S. *SoftMatter* **2012**, 8, 6226 – 6231.
[65] Pons-Sieperman, I.; Glotzer, S. *ACSNano* **2012**, 6, 3919 – 3924.
[66] Velachi, V.; Bhandary, D.; Singh, J.; Cordeiro, N. *J. Phys. Chem. C* **2015**, 119, 3199 – 3209.
[67] a) DeVries, G. A.; Brunnbauer, M.; Hu, Y.; Jackson, A. M.; Long, B.; Neltner, B. T.; Uzun, O.; Wunsch, B. H.; Stellacci, F. *Science* **2007**, 315, 358 – 361. b) DeVries, G. A.; Talley, F. R.; Carney, R. P.; Stellacci, F. *Adv. Mater.* **2008**, 20, 4243 – 4247.

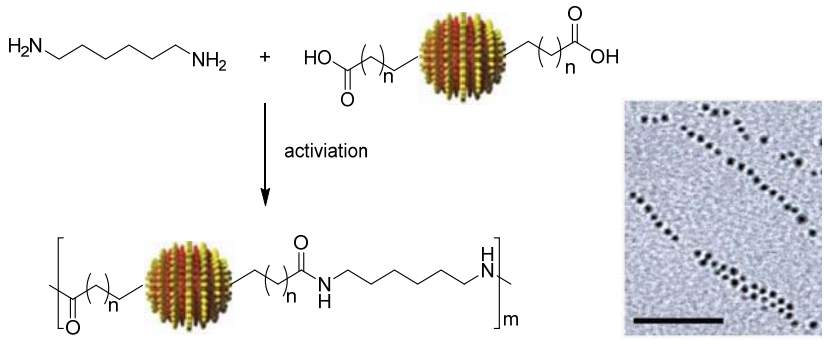

Figure 1.6 Schematic representation of the chain formation reaction (on the left) and TEM image of NPs chains (in the right). Scale bars 200 nm.[67]

1.1.5.2. Chemical assisted organization of mixed-monolayers

Due to their relative strength with respect to van der Waals interactions, hydrogen bonds are very important in nature or in supramolecular chemistry. Moreover, hydrogen bonds are directional and are more dynamic and flexible in geometry than covalent bonding. For example, Binder and collaborators[68] have reported a direct assembly of AuNPs (Figure 1.7) onto 2D gold surfaces via multiple hydrogen bonds.

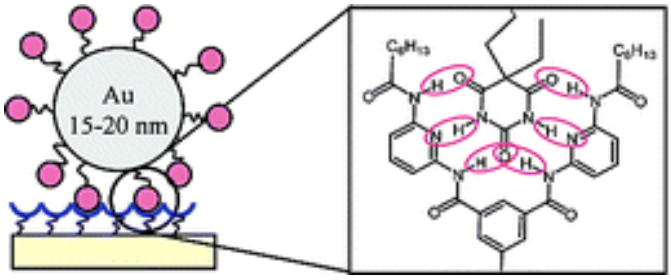

Figure 1.7 Self assembling of AuNPs on surfaces mediated by Hamilton-type receptors.[68]

The same concept was used by P. Rudolf to anchor small gold clusters displaying 1-(8-mercaptooctyl)-thymine (MOT) groups on their surface (Au_{55}-MOT), on a 2D mixed SAM formed by *n*-heptanethiols and DTOT (8-(4,6-diaminol[1,3,5]triazin-2-yl)-octane-1-thiol) molecules. The immobilization of gold nanoparticles on the surface is due to the formation of three hydrogen bonds between MOT and DTOT moieties (Figure 1.8).[69]

[68] Zirbs, R.; Kienberger, F.; Hinterdorfer, P.; ,Binder, W. *Langmuir* **2005**, 21, 8414 – 8421.
[69] van den Brom, C. R.; Arfaoui, I.; Cren, T.; Hessen, B.; Palstra, T.T.M.; de Hosson, J. T. M.; Rudolf, P. *Adv. Funct. Mater.* **2007**, 17, 2045 -2052.

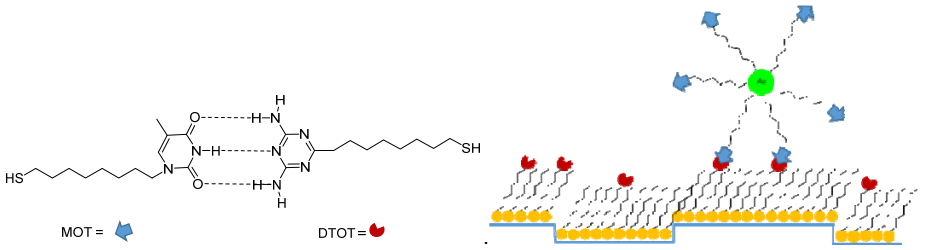

Figure 1.8 Au_{55} clusters functionalized with MOT molecules are immobilized by molecular recognition onto a self-assembled monolayer composed of n-heptanethiol and DTOT molecules.[69]

The segregation of ligands on the surface of nanoparticles can be also directed by an external template. Nanoparticles coated by a mixture of octanethiol, pyrene thiol and 1,6-diamidopyridine thiol has been synthesized by Rotello.[70] The addition of flavin to a solution of such nanoparticles is responsible of NMR chemical shift drift of flavin signals. These shifts are indicative of an enhanced aromatic stacking provided by the complexation of flavin to the 1,6-diaminopyridine and subsequent shift of pyrene thiolate toward this complex. In this case flavin plays as external template that drives a specific organization of the monolayer (Figure 1.9).

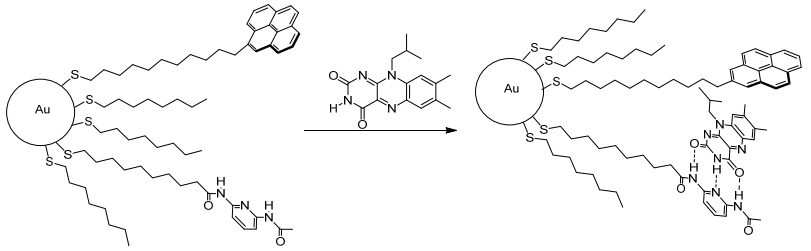

Figure 1.9 Schematic illustration of reorganization of the monolayer upon flavin addition driven by π-stacking.[71]

Another interesting strategy to functionalize NPs on one side only is the one proposed, for example, by Sandar.[72] Colloids are first anchored to a solid functionalized SiO_2 surface and exposed to a solution of 11-mercapto-1-undecanol. In this way colloids are functionalized only on the free, exposed, surface. Nanoparticles are removed from the solid surface by sonication in presence of a solution of 16-mercaptohexadecanoic acid to end up with nanoparticles functionalized on one patchy (Figure 1.10).

[70] Boal, A.K.; Rotello, V. M. *J. Am. Chem. Soc.* **2000**, 122, 734 -735.
[71] Boal, A. K.; Rotello, V. M. *J. Am. Chem. Soc.* **2000**, 122, 734 – 735.
[72] Sandar, R.; Heap, T. B.; Shumaker-Parry, J. S. *J. Am. Chem. Soc.* **2007**, 129, 5356 -5357.

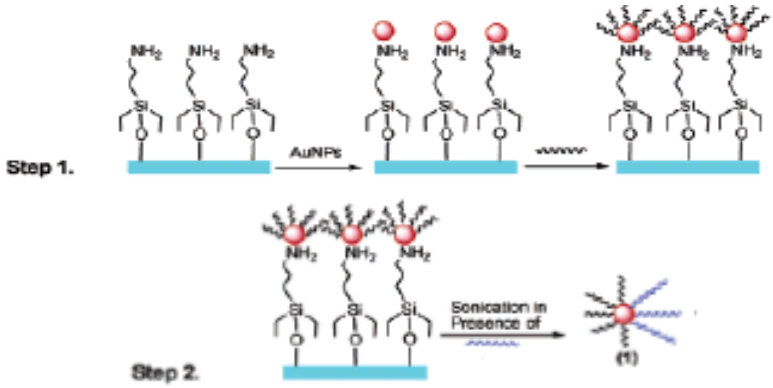

Figure 1.10 Asymmetric functionalization of AuNPs using a solid phase approach.[72]

Recently[73] the partial functionalization of gold nanoparticles using a solid state approach has also been reported. In this approach (Figure 1.11), a glass slide was first activated with a piranha solution which generates silanol groups on its surface. The coverslip was then immersed into a CTAB solution forming self-assembled bilayer. The CTAB modified coverslip was then immersed into the citrate stabilized AuNP solution for 5 min and washed with water. The AuNP-modified glass substrate was then soaked in 2-mercaptoethanol (2-ME) solution and allowed for incubation for 3 h, as a result forming a dense 2-ME monolayer on the NPs surface. Due to the inaccessibility of 2-ME to AuNP surface attached to the substrate, the 2-ME molecules are expected to be asymmetrically bound only to the surface which are exposed to the solution.

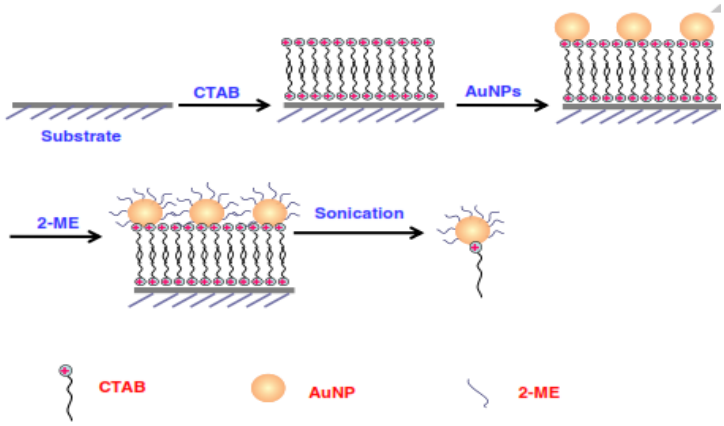

Figure 1.11 CTAB assisted partial functionalization of gold nanoparticles.[73]

[73] Xu, Y.; Guo, L.; Huang, L.; Palanisamy, K.; Kim, D.; Chen, G. *J. Colloid Interface Sci.* **2013**, 409, 32 – 37.

1.2. Purification of AuNPs

It is well known that the purity of nanoparticles can influence their properties. It has been demonstrated[74] that the presence of free ligands determine the rapid decomposition of the nanoparticles as well as the modification of their optical properties.[75] For this reason it is important to find very efficient protocols for their purification. The most common and straightforward procedures are: precipitation, repeated centrifugation or size exclusion chromatography; other more cumbersome, but effective methods like Soxlet extraction[76] or diafiltration[77] have also been used.

1.3. Properties of AuNPs

AuNPs display a variety of shape- and size-dependent properties, with the most known being the characteristic ruby-red color of colloidal gold in contrast to the yellow color of the bulk metal.

The size dependence of the absorption and scattering properties of colloidal gold was first rationalized on the basis of the classical electromagnetism by Mie in 1908.

However, as the size of gold the particle become smaller (< 3 nm) the valence and conduction electron bands become narrower and a gap appear between them causing the disappearance of the metallic character. Under this size regime, discrete transitions are observed with impact on the absorption characteristics, Figure 1.12, and electrochemical properties. [78,79,80]

[74] Woehrle, Warner, M.; Hutchison, J. *Langmuir* **2004**, 20, 5982 – 5988.
[75] Kalyuzhny, G.; Murray, R. W. *J. Phys. Chem B* **2005**, 109, 7012-7021
[76] Waters, C.; Mills, A.; Johnson, K.; Shiffrin, D. *Chem. Commun.* **2003**, 540 – 541.
[77] Sweeney, S.; Whoerle, G.; Hutchison, J. *J. Am. Chem. Soc*. **2006**, 128, 3190 – 3197.
[78] Chen, S.; Ingram, R.; Hostetler, M.; Pietron, J.; Murray, R.; Gregory Shaaff, T.; Khoury, J.; Alvarez, M.; Whetten, R. *Science* **1998**, 280, 2098 – 2101.
[79] Antonello, S.; Holm, A. H.; Instuli, E.; Maran, F. *J. Am. Chem. Soc.* **2007**, 129, 9836
[80] Chirea, M.; Cruz, A.; Pereira, C.; Silva, A. F. *J. Phys. Chem. C* **2009**, 113, 13077 – 13087.

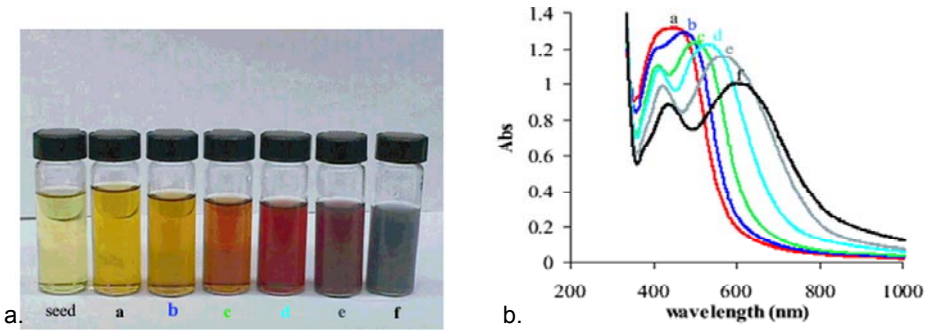

Figure 1.12 a) color variation of gold nanorods with the dimension of the gold core and b) shift of the absorbance band with the dimension of the gold core.[78]

The transition between true molecular species and metal–like nanoparticles occurs when the gold core of the nanoparticles is composed of more than 55 gold atoms. For NPs larger than 3 nm, the free d electrons of the gold can oscillate free through the metal;[81] when irradiated, the free electrons of the AuNPs "sense" the electromagnetic field and begin to oscillate collectively at the same frequency with the incident light. This phenomenon is called Surface Plasmon Resonance (SPR) and is responsible for the ruby-red color of gold colloids.4 The plasmon band arises from the interband transitions between the highly polarizable Au $5d^{10}$ band and the unoccupied states of the conduction band.

The position of the SPR and the ratio between the absorption and scattering intensities is influenced by many parameters,[82] such as the size,[83] shape,[82] structure, morphology and aggregation state.[84] The environment surrounding the nanoparticles surface,[85] the solvent, [86] the nature of the ligands in the monolayer and the temperature[87] also affect the position of the SPR. The SPR of AuNPs shifts slightly when the gold core diameter increases, moving from 520 nm for AuNPs of 3 nm to 550 nm for 100 nm nanoparticles.[88] Gold nanoparticles have an extinction coefficient five orders of magnitude bigger than common dyes and can be computed theoretically as a function of size, shape and composition as reported by El-Sayed.[89] The knowledge of the molar extinction coefficient proved to be sufficient for the simultaneous determination of both nanoparticles size and concentration

[81] Eustis, S.; El-Sayed, M. *Chem. Soc. Rev.* **2006**, 35, 209 – 217.
[82] Carbo-Argibay, E.; Rodrigue-Gonzalez, B. *Isr. J. Chem.* **2015**, 55, 1-14.
[83] Jain, P. K.; Lee, K. S.; El-Sayed, I. H.; El-Sayed, M. A. *J. Phys. Chem. B* **2006**, 110, 7238
[84] Su, K. H.; Wei, Q. H.; Zhang, X.; Mock, J. J.; Smith, D. R.; Schultz, S. *Nano Lett.* **2003**, 3, 1087.
[85] Cobley, C. M.; Chen, J.; Cho, E. C.; Wang, L. V.; Xia, Y. *Chem. Soc. Rev.* **2011**, 40,44-56.
[86] Templeton, A. C.; Pietron, J. J.; Murray, R. W.; Mulvaney, P. *J. Phys. Chem. B* **2000**, 104, 564
[87] Liu, X. O.; Atwater, M.; Wang, J. H.; Huo, Q. *Colloids Surf. B* **2007**, 58, 3.
[88] Xia, Y.; Halas, N. J. *MRS Bull*. **2005**, 30, 338-348
[89] Jain, P. K.; Lee, K. S.; El-Sayed, I. H.; El-Sayed, M. A. *J. Phys. Chem. B* **2006**, 110, 7238.

by simple UV-Vis measurements.[90] The combination of the tunability of the surface plasmon resonance of gold nanoparticles with the inertness of gold makes gold nanostructures well suited for various biomedical applications. [91,92,93]

AuNPs have great ability to quench fluorescence of nearby fluorophores, through fluorescence resonance energy transfer (FRET), the deactivation pathway being based on the overlap between the emission spectrum of excited fluorophores and the surface Plasmon absorbtion band of the AuNPs, which can be useful in sensor fabrication.[94] Despite this property, luminescent AuNPs with sizes ranging from 0.3 to 20 nm can also be synthesized.[94]

AuNPs can also be used as probes for single molecule surface-enhanced Raman scattering (SERS) detection pioneered by Nie[95] and Kneipp[96] who discovered that the large enhancement factors of SERS are on the order of 10^{14}–10^{15}.

Besides the optical properties, other physical characteristics of AuNPs such as density, melting point, mechanical strength and conductivity are different respect to the bulk metal and are sensitive to their size, and shape. Indeed for nanoparticles, the surface area/volume ratio is extremely high and it is inversely proportional to their radius. Smaller is the core size a large percentage of the atoms are on the surface, for example, for 5.0 nm diameter, 25 % of the atoms are on the surface and for NPs of 2.0 nm, 52 % of the atoms are on the last shell. The melting points of the nanomaterials are lower respect to the melting points of bulk metals due to the reduced interaction between the surface and inner atoms, such that the attractive forces of the core are very weak and the surface atoms are able to move at lower temperature. The melting point of the bulk gold is 1337 K and decrease to nearly half when the AuNPs size reaches about 2 nm.[97] The electrical conductivity decreases with the dimension due to the increase of surface scattering.

AuNPs, particularly those below 10 nm size, show efficient catalytic activity even though the bulk metal has been considered to be chemically inert with poor catalytic activity. The catalytic activity is determined by the high fraction of atoms at the surface and the high surface area/volume ratio and the electronic properties of the nanoparticles. AuNPs, which

[90] Haiss, W.; Thanh, N. T. K.; Aveyard, J.; Fernig, D. G. *Anal. Chem.* **2007**, 79, 4215.
[91] Hu, M.; Chen, J.; Li, Z-Y.; Au, L.; Hartland, G. V.; Li, X.; Marquez, M.; Xia, Y. *Chem. Soc. Rev*. **2006**, 35, 1084–1094.
[92] Khlebtsov, N.; Dykman, L. *Chem. Soc. Rev*. **2011**, 40, 1647–1671.
[93] Saha, K.; Agasti, S.; Kim, C.; Li, X.; Rotello, V. *Chem. Rev*. **2012**, 112, 2739 – 2779.
[94] Alex, S.; Tiwari, A. *J. Nanosci. Nanotechnol*. **2015**, 15, 1869 – 1894.
[95] Nie, S.M.; Emery, S. R. *Science* **1997**, 275, 1102–1106.
[96] Kneipp, K.; Wang, Y.; Kneipp, H.; Perelman, L.T.; Itzkan, I.; Dasari, R. *Phys Rev Lett* **1997**, 789, 1667–1670.
[97] Safaei, A. *J. Nanopart. Res.* **2010**, 12, 759 – 779.

are low cost respect to Pt and Pd, can act like very efficient catalyst providing better yield, selectivity[98] and are effective even at lower temperature.[99,100]

1.4. Characterization of AuNPs

1.4.1. Characterization of the gold core

A detailed characterization of the gold core plays and important role not only in optimizing the synthesis pathways, but it is also essential for subsequent applications. Indeed, it was demonstrated that the size[101] and the shape[102] of the nanoparticles are very important for biomedical application because they influence the uptake, biodistribution,[103] and cytotoxicity.[104]

There are some main methods used to characterize the gold core: a) transmission electron microscopy (TEM), scanning electron microscopy (SEM), atomic force microscopy (AFM). Dynamic light scattering (DLS) measures the hydrodynamic diameter of a particles without producing a particle size distribution, but a light-scattering intensity weighted average value. Other techniques such as: centrifugal liquid sedimentation,[105] small angle X-Ray scattering,[106] field flow fractionation[107] (FFF); dark field tracking analysis[108] and X-Ray diffraction (XRD) have been used for the characterization of the gold nanoparticles core.

As was previously mentioned, the dimension of the gold core can be determined from the UV-VIS spectra for AuNPs in the range between 5 nm and 100 nm. These calculations have been performed for perfectly spherical and monodispersed nanoparticles, but the experimental data are always collected over a distribution of particle size and shapes. Moreover, for nanoparticles with a diameter lower than 10 nm, the calculated absorbance curve did not fit the experimental data as well as for bigger nanoparticles and for this reason the results are considered an estimation of the gold core diameter.[109]

---

[98] Huang, J.; Akita, T.; Faye, J.; Fujitani, T.; Takei, T.; Haruta, M. *Angew. Chem. Int. Ed.* **2009**, 48, 7862 – 7866.
[99] Mikami, Y.; Dhakshinamoorthy, A.; Alvaro, M.; Garcia, H. *Catal. Sci. Tecnol*. **2013**, 3, 58 – 69.
[100] Biondi, I.; Laurenczy, G.; Dyson, P. *Inorg. Chem.* **2005**, 50, 8038 - 8045.
[101] Pan, Y.; Neuss, S.; Leifert, A.; Fischler, M.; Wen, F.; Simon, U.; Schmid, G.; Brandau, W.; Jahnen – Dechent, W. *Small* **2007**, 11, 1941 – 1949.
[102] Li, N.; Zhao, P.; Astruc, D. *Angew. Chem. Int. Ed.* **2014**, 53, 1756 – 1789.
[103] Fraga, S.; Brandao, A.; Soares, M. E.; Morais, T.; Duarte, J. A.; Pereira, L.; Soares, L.; Neves, C.; Pereira, E.; de Lourdes Bastos, M.; Carmo, H. *Nanomedicine*, **2014**, 10, 1756 – 1766.
[104] Favi, P. M.; Gao, M.; Sepulveda Arango, L. J.; Ospina, S. P.; Morales, M.; Pavon, J. J.; Webster, T. *J. Biomed. Mater. Res.* **2015**, 103, 3449 – 3462.
[105] Braun, A.; Couteau, O.; Franks, K.; Kenstens, V.; Roebben, G.; Lamberty, A.; Linsinger, T. P. *J. Adv. Powder Technol.* **2011**, 22, 766 – 770.
[106] McKenzie, L.; Habe, P.; Kevan, S.; Hutchison, J. *J. Phys. Chem. C* **2010**, 114, 22055 – 22063.
[107] Gigault, J.; Pettibone, J.; Schmitt, C.; Hackley, V. *Anal. Chim. Acta* **2014**, 809, 9 – 24.
[108] Wagner, T.; Lipinski, L. P.; Wiemann, M. *J. Nanopart. Res.* **2014**, 16, 2419.
[109] Haiss, W.; Thanh, N.; Aveyard, J.; Fernig, D. *Anal. Chem.* **2007**, 79, 4215 – 4221.

Recently, it was reported[110] that inductively coupled plasma mass spectrometry in single particle mode (spICPMS) is a powerful tool to determine the size of the gold core in solution based on the ^{197}Au isotope determination. The main advantage of this technique is the possibility to count a large number of nanoparticles in a very short time (typically in order of 1 000 particles per minute).

1.4.2. Characterization of the monolayer

To better understand the organization of monolayers on curved surfaces, many efforts have been spent to gain more information about 2D-SAMs, a part of this being transferred to nanoparticles.

1.4.2.1. 2D self-assembled monolayers (2D-SAMs)

The molecules or ligands that form SAMs have a head group with a specific affinity for the substrate; the most extensively studied being the thiols for the high stability of the SAMs formed for gold substrates. However, other ligands such as *N*-heterocyclic carbenes (NHCs) have been recently reported to form exceptionally stable SAMs[111] and once bound to gold, NHCs are not displaced even by thiols. In a SAM, the alkane chain attached to the head group represents the spacer, or organic interphase, which acts like a physical barrier between the metal and the surroundings. The terminal group of the ligands forms the organic interface that determines the properties of the SAM (Figure 1.13).

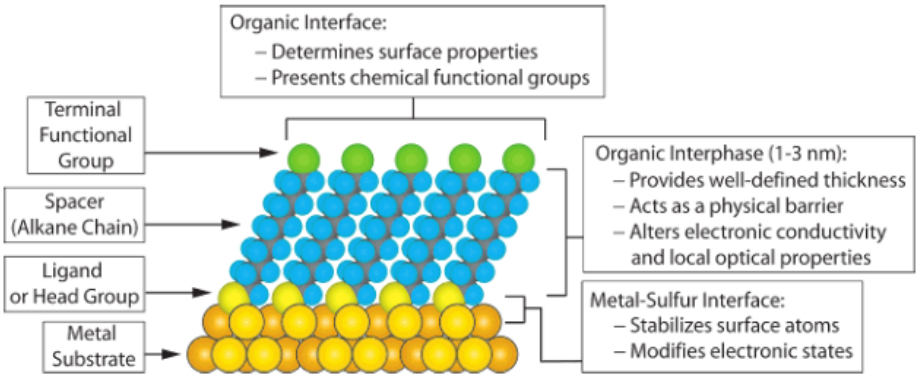

Figure 1.13 Schematic diagram of a SAM on a gold surface.[112]

[110] Loeschner, K.; Jung Braband, M. S.; Sloth, J. Larsen, E. *Anal Bioanal Chem* **2014**, 406, 3845 – 3851.
[111] Crudden, C.; Horton, H.; Ebralidze, I.; Zenkina, O.; McLean, A.; Drevniok, B.; She, Z.; Kraaz, H. B.; Mosey, N.; Seki, T.; Keske, E.; Leake, J.; Rousina-Webb, A.; Wu, G. *Nat. Chem*. **2014**, 6, 409 – 414.

Structure of SAMs: hydrogenated vs. fluorinated alkanethiolates

In analogy to hydrogenated alkane thiolates, also fluorinated alkane thiolates form stable SAMs on the gold surface. AFM measurements indicate that the fluorinated monolayer exists in ordered domains of varied sizes, and the sizes of the domains are similar to those found for the analogous alkanethiolate monolayer.[112] However, several features distinguish the structure of SAMs formed by hydrogenated and fluorinated alkanethiolates. In the SAM, the tilt angle (θ) of the hydrogenated alkyl chain, that is the angle between the ligand axis and the normal to the plane of the substrate, is 30º respects to 16º for the perfluorocarbon chain. In some cases evidence exists that in 2D-SAMs formed by semifluorinated *n*-alkanethiols, the fluorocarbon chains are oriented normal to the surface (Figure 1.14).[113,114]

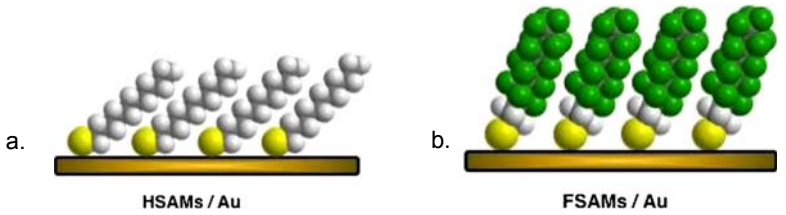

Figure 1.14 Illustration in the differences between the tilt angle of thiolated chains in hydrogenated (H) SAMs compared to fluorinated (F) SAMs.[114]

The perfluorocarbon monolayer presents different packaging respect to the hydrocarbon monolayer due to the van der Waals diameter of 5.6 Å for a perfluoroalkyl chain respect to the 4.2 Å van der Waals diameter for the corresponding alkyl chain.[115] Indeed, the adlayer structure for the alkyl chain is *(43* X *d3)R30° respect to* c(7x7) or p(2x2) for the perfluorinated chains (Figure 1.15).[116] The spacing between the ligands grafted on the gold surface is larger in the case of perfluorinated chains (Figure 1.15).

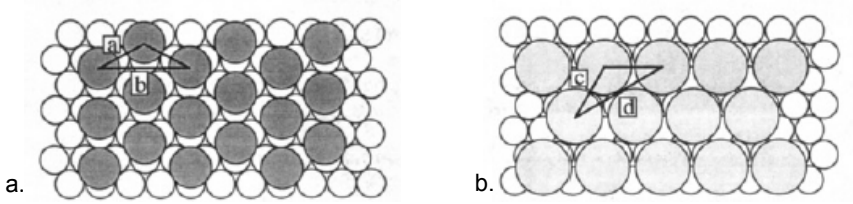

Figure 1.15 Schematic illustration of the adlayer structure for a. HSAMs and b. FSAMs, The spacing between ligands is 0.50 nm (a) and 0.87 nm (b) for the alkyl chain and 0.58 nm (c) and 1.0 nm (d) for the perfluoroalkyl chains.[116]

[112] Alves, C.; Porter, M. *Langmuir* **1993**, 9, 3507 – 3512.
[113] Lenk, T. J.; Hallmark, V. M.; Hoffmann, C. L.; Rabolt, J. F.; Castner, D. G.; Erdelen, C.; Ringsdorf, H. *Langmuir* **1994**, 10, 4610
[114] Tsao, M.-W.; Hoffmann, C. L.; Rabolt, J. F. *Langmuir* **1997**, 13, 4317 – 4332.
[115] Pierre Krafft, M.; Riess, J. *Chemosphere* **2015**, 129, 4 – 19.
[116] Tamada, K. *Langmuir* **2001**, 17, 1913 – 1921.

Hydrogenated alkanethiolate, assembled in the monolayer assume a planar zigzag conformation due to intermolecular stabilization among adjacent chains, while fluorinated alkanethiolate that are already blocked in a helical conformation, maintain this conformation also in the assembled state. The rigidity of the fluorocarbons respect to the alkyl chain was considered to be the main reason for the structural difference of SAMs formed for these two species.[117]

The introduction of a terminal CF_3 group into the aliphatic hydrocarbon was sufficient to generate significant differences in the monolayer properties. For instance, CF_3-terminated alkanethiolated SAM are surprisingly more wettable by polar contacting liquids than analogous hydrocarbon SAMs. The presence of a terminal CF_3 group generates a strong dipole; consequently, a SAM comprising these residues will present an ordered array of oriented dipoles displaying strong interaction with the solvent molecular dipoles increasing the wettability.[118]

In a number of studies, the length of the hydrogenated alkyl chain connecting the sulfur atom to the fluorinated portion of the thiolate was found to have a strong impact on the structure and the properties of the SAMs. Studying by AFM the structure of SAMs derived from a series of semifluorinated alkanethiols of general formula $CF_3(CF_2)_9(CH_2)_nSH$ (F10HnSH, n = 2, 6, 11, 17, 33)[116] it was observed that by increasing the length of the hydrogenated spacer, the fluorocarbon adlayer structure appeared more disordered. This effect was attributed to the tendency of the longer hydrocarbon spacers to pack more tightly than the shorter ones, hindering the packing of the fluorocarbon units. In contrast to the previous data, a recent study comparing the properties of the SAMs obtained from terminally fluorinated alkanethiols bearing ethyl and propyl-hydrocarbon spacers, the latter provided only a slightly improved packing density. Ellipsometric measurements, XPS analysis and contact angle measurements suggest that propyl-spacer FSAMs are consistently 1Å thicker than the ethyl-FSAMs. [119]

The length of the fluorocarbon portion is also important in dictating the structure of the monolayer; decreasing length of the fluorocarbon segment a slight decrease in the packing density was observed and this was accompanied by the increase in the average tilt angle of the fluorinated part.[120] In contrast to the average tilt angles of the fluorocarbon segments (Figure 1.16), the average tilt angles of the hydrocarbon parts are almost the same for all

[117] Alves, C.; Smith, E.; Porter, M. *J. Am. Chem. Soc.* **1992**, 114, 1222 – 1227.
[118] Graupe, M.; Takenaga, M.; Koini, T.; Colorado Jr, R., Randall Lee, T. *J. Am. Chem. Soc*. **1999**, 121, 3222 – 3223.
[119] Zenasni, O.; Jamison, A.; Marquez, M.; Randall Lee, T. *J. Fluorine Chem.* **2014**, 168, 128 – 136.
[120] Lu, H.; Zeysing, D.; Kind, M.; Terfort, A.; Zharnikov, M. *J. Phys. Chem. C* **2013**, 117, 18967 – 18979.

studied semifluorinated monolayers, independent of the length of the fluorocarbon segments.

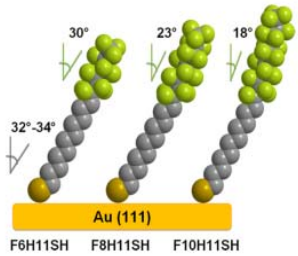

Figure 1.16 The NEXAFS-derived average tilt angles of fluorocarbon and hydrocarbon chains in 2-D SAM are indicated.[120]

The adsorption of a binary mixture of two different semifluorinated thiols of different length was studied in the case of thiols F8H11SH and F8SH observing preferential adsorption of the longer thiol. When a mixture of thiols F8SH and F8H2SH was used, no preferential adsorption of one of the thiols could be observed, consistently with the small difference in length between the thiols.[113]

1.4.2.2. 3D Self assembled monolayer protected gold nanoparticles

Most of the properties of 2D SAMs can be transferred to nanoparticles, but the investigation of the 3D organization of ligands on the surface of the gold core requires more complex techniques. The main difference between 2D and 3D SAM is the curvature of the nanoparticles resulting in a higher flexibility of the terminal portion of the alkane chains. Indeed, measurements of the hydrodynamic radii of monolayer protected gold nanoparticles support the hypothesis that the outer part of the thiol layer is loosely packed.[121] A nanoparticle coated with a well packed SAM (similar to those formed on thin films) is expected to have a hydrodynamic radius equal to the sum of the radius of the gold core and the fully extended alkanethiolate. This is not true because all the hydrodynamic radii measurements of monolayer protected gold nanoparticles are smaller than the prediction, suggesting that the monolayer is not well packed on the outer edge. When the dimension of the gold core is smaller than 5 nm, the 3D monolayers can be characterized using ^{1}H- and ^{13}C NMR. The spectra present broad signals and the broadening is more accentuated when the nuclei are closer to the gold core.

A clear picture about the organization of the self-assembled monolayer on AuNPs has been obtained in 2007[122] when Kornberg and his group have obtained the first X-ray

[121] Wuelfig, P.; Templeton, A.; Hicks, J.; Murray, R. *Anal. Chem.* **1999**, 71, 4069 – 4074.
[122] Jadzinski, P.; Calero, G.; Ackerson, C.; Bushnell, D.; Kornberg, R. *Science* **2007**, 318, 430 – 433.

structure of gold nanoparticles protected by p-mercaptobenzoic acid (p-MBA). These NPs are composed of 102 atoms of gold and are protected by 44 p-MBA molecules and have revealed an unexpected metal core organization and Au-sulfur interaction. The core is composed of 102 gold atoms locked in a Marks decahedron where 13 equatorial atoms impart chirality to the core.[122]

This work revealed the unanticipated existence of RS–Au–SR staple motifs (Figure 1.17), in which gold atoms are sandwiched between two sulfur atoms of the thiolates. The sulfur is in fact bound to three different substituents, two different gold atoms and the organic part R of the thiolate. In principle the organic part R of the thiolate can adopt two positions, the interconversion being possible due to a low energetic barrier between the two.[123]

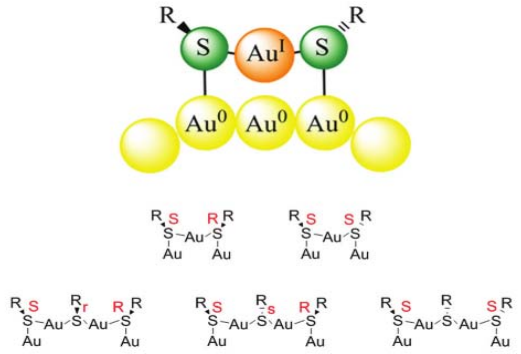

Figure 1.17 Top: schematic drawing of a monomeric Au–SR–Au staple motif (the electron density of the atoms are represented). The organic substituent R of the thiolate can be oriented on the same side with respect to the staple plane (cis) or on opposite sides (trans). Bottom: stereochemistry of monomeric and dimeric staple motifs.[124]

The formation of crystals was possible in this case due to the presence of particles sufficiently uniform in size together with the rigidity given by the presence of the aromatic ligands and by the intermolecular hydrogen bounds between the carboxylate groups present into the monolayer. Three different interactions are present between the ligands that stabilize the monolayer: (1) π-π stacking between two close and parallel phenyl rings with the centers offset by the ring radius, which explain the common finding that distances between neighboring clusters in two dimensional gold particle arrays are less than twice the length of the fully extended thiol[125] (2) H- π phenyl rings interacting at right angles (T-stacking) and (3) a sulfur lone pair – phenyl ring interaction.

Despite the large number of literature reports on the preparation of gold nanoparticles,

[123] Burgi, T. *Nanoscale* **2015**, 7, 15553 – 15567.
[124] Knoppe, S.; Burgi, T. *Acc. Chem. Res.* **2014**, 47, 1318 – 1326.
[125] Wetten, R.; Shafigullin, M.; Khoury, J.; Gregory Shaaf, T.; Vezmar, I.; Alvarez, M.; Wilkinson, A. *Acc. Chem. Res.* ***1999,*** 32, *391 – 406.*

only few studies concerned the preparation of gold nanoparticles protected by fluorinated ligands. The first synthesis of perfluorinated nanoparticles was realized by Korgel group in 2000[126] by using a modified two phase Brust-Schiffrin method and thiol **HS-F6** (Figure 1.18). Later,[127] Yonezawa reported silver and AuNPs synthesis in a single phase solution using thiol **HS-F6** and **HS-F10**. As expected, the gold nanoparticles precipitated from the ethanolic solution due to their poor solubility in common organic solvent. This kind of nanoparticles has good solubility only in fluorinated solvents or supercritical CO_2 and for this reason the applications of these systems are limited. Later, Murray[128] has reported the synthesis of gold nanoparticles protected by **HS-F6** or pentafluorobenzenethiol using a two phase Brust-Schiffrin method: (Figure 1.18).

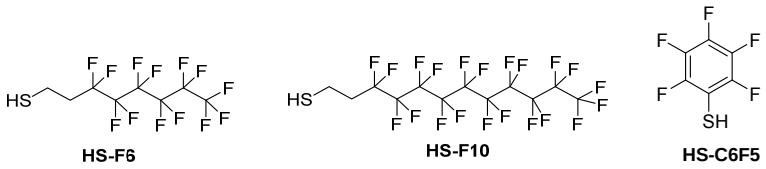

HS-F6 **HS-F10** **HS-C6F5**

Figure 1.18 Fluorinated thiols used for the synthesis of AuNPs.

The solubility limitations and the purification issues due to the presence of the fluorinated ligands have prompted many groups, including ours, to develop alternative strategies to the development of fluorinatd or partially fluorinated nanoparticles. A reliable solution can be the shielding of the fluorinated chain of the ligand from the solvent by using appropriate solubilizing units, especially polyethylene glycol chains.

In 2008 our research group designed and synthesized the first example of gold nanoparticles protected by an amphiphilic thiol (HS-F8PEG),[129] characterized by an external hydrophilic portion formed by a PEG550 and an internal hydrophobic perfluorocarbon moiety. Thanks to the polyethylene glycol chain, the nanoparticles are soluble in many polar organic solvents and, display a remarkable solubility even in water. Moreover, the presence of a highly hydrophobic region hidden by a hydrophilic pegylated shell opens the way to the use of these nanoparticles as vehicles of small hydrophobic molecules through polar environments. The thiol group of this class of ligands suffers of a markedly reduced nucleophilicity (due to the electron withdrawing effect of the fluorinated

[126] Shah, P.; Holmes, J.; Doty, C.; Johnston, K.; Korgel, B. *J. Am. Chem. Soc. Rev*. **2000**, 122, 4245 – 4246.
[127] Yonezawa, T.; Onoue, S.; Kimizuka, K. *Adv. Mater.* **2001**, 13, 140 – 142.
[128] Dass, A.; Guo, R.; Tracy, J.; Balasubramanian, R.; Douglas, A.; Murray, R. *Langmuir* **2008**, 24, 310 – 315.
[129] a) Gentilini, C.; Boccalon, M.; Pasquato, L. *Eur. J. Org. Chem.* **2008**, 3308 - 3313. b) Gentilini, C. Evangelista, F.; Rudolf, P.; Franchi, P.; Lucarini, M.; Pasquato, L. *J. Am. Chem. Soc.* **2008**, 130, 15678 - 15682.

chain in the alpha position respect to the sulfur atom) and for this reason, in the synthesis of AuNPs, the thiolate anion was used instead of the thiol. This effect was never observed with 1*H*,1*H*,2*H*,2*H* perfluoroalkanethiols, indicating that two methylene groups are sufficient to temper the electron withdrawing effect of the *F*-chain.[130]

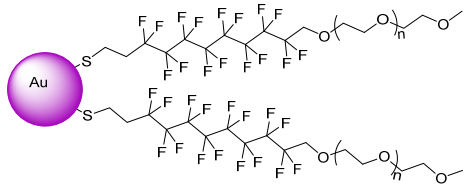

Figure 1.19 Water soluble AuNPs protected by a fluorinated ligand.

In 2012, Niikura used a very similar strategy to develop amphiphilic thiols composed by three parts: an oligo (ethylene glycol) unit; a fluorinated tetraethylene glycol unit and an 11-carbon alkyl chain terminating with a thiol. This species was used for the synthesis of AuNPs of 5, 10 and 20 nm. Interestingly, these nanoparticles produce sub-100 nm NP vesicles in tetrahydrofuran solution without the use of a template.[131] Recently, our group reported the preparation of water soluble gold nanoparticles (Figure 1.20) for ^{19}F MRI applications by using an amphiphilic thiol featuring a fluorinated polyethylene oxide unit.[132]

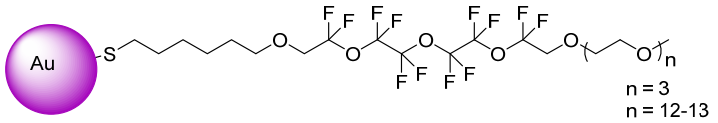

Figure 1.20 Water soluble gold nanoparticles for MRI applications.

1.5. Methodologies to study the morphology of mixed monolayers

The properties of gold nanoparticles depend on type of ligands that form the monolayer but also on the organization that these ligands have on the surface of the gold core. Due to the ease of synthesis, AuNPs have been intensively studied in order to gain information about the morphology of the monolayer. Only few examples have been reported with a direct visualization of the monolayer, but numerous studies of an "indirect" deduction of the organization of a specific mixture of thiols have been reported.

[130] Pengo, P.; Pasquato, L. *J. Fluorine Chem*. **2015**, 177, 2 – 10.
[131] Niikura, K.; Iyo, N.; Higuchi, T.; Nishio, T.; Jinnai, H.; Fujitani, N.; Ijiro, K. *J. Am. Chem. Soc*. **2012**, 134, 7632 -7635.
[132] Boccalon, M.; Franchi, P.; Lucarini, M.; Delgado, J. J.; Sousa, F.; Stellacci, F.; Zucca, I.; Scotti, A.; Spreafico, R.; Pego, P.; Pasquato, L. *Chem. Commun.* **2013**, 49, 8794 – 8796.

1.5.1. Direct methods

Scanning tunneling microscopy (STM) and atomic force microscopy (AFM) are the unique characterization techniques that confer an image about the organization of the monolayer. These are relatively difficult to apply to nanoparticles because have some significant limitations regarding the cleanliness of the sample, the length of the ligands (can be used only for thiols shorter than 12-16 carbons in the alkyl chain). These techniques cannot be applied in the presence of the polyethylene glycol chains and the nanoparticles have to be deposited on a flat surface in order to limit the freedom of the nanoparticles to move over the substrate.[133] STM in air and vacuum was firstly used by Stellacci in 2004[60] to demonstrate the formation of subnanometer ordered domains of mixed monolayers (Figure 1.21).

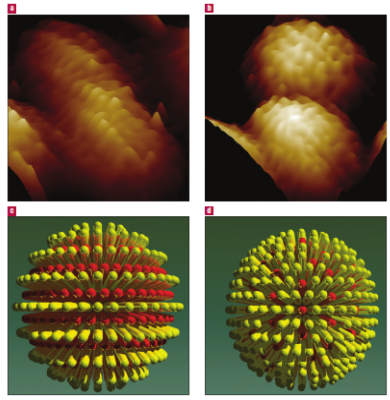

Figure 1.21 STM images of AuNPs.[60]

His group has analyzed a large number of STM images of a variety of nanoparticles protected by different mixtures of ligands. They have studied gold and silver nanoparticles protected by OT and MPA and have found that the organization of the monolayer did not depends on the type of the metal core and its crystallographic structure. The ripple formation was observed for nanoparticles obtained using both methods of synthesis: direct synthesis and place exchange reaction. Moreover, it could be observed that the distance between the ripples can be tuned by varying the dimension of the gold core while keeping the ration MPA/OTconstant (peak-to-peak distance decreases as the nanoparticle diameter increases). Changing the ratio MPA/OT while keeping the core size constant, it was found that the peak-to-peak distance can be changed by quantized increments of 3 Å, going from evenly distributed ripples to unevenly distributed ripples and eventually to the formation of

[133] Kano, S.; Tada, T.; Majima, Y. *Chem. Soc. Rev.* **2015**, 44, 970 – 987.

discrete domains. Octanethiol-coated nanoparticles show an average headgroup spacing of 5.4 Å which, interestingly, seems to increase with nanoparticle diameter. It should be noted that, on flat Au(111), octanethiol monolayers have a constant headgroup spacing of 5.0 Å.[134]

Recently, images in air and liquid (1-phenyloctane) of the sample of nanoparticles protected by nonanethiol and 4-methylbenzenethiol[135,136] in a 1:2 ratio have been obtained (Figure 1.22). The STM images show stripe-like domains with a characteristic spacing of 1 nm that persist over a few images and maintain their direction against scanning angle rotation. The same result was also obtained for nanoparticles protected by a mixture of dodecanethiol and hexanethiol in a 2:1 ratio.

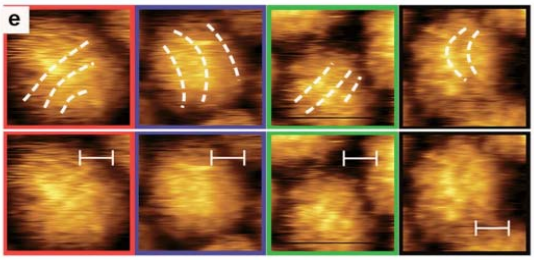

Figure 1.22 STM topography images of the C12:C6 sample. Each particle is shown twice, as indicated by the color Frame. Dashed lines indicate the location and direction of stripe-like domains. Scale bars are 2 nm.[136]

STM data obtained in vacuum and air conditions have been analyzed through power spectral density (PSD) that allows extracting the characteristic spacing of the domains. In Figure 1.23 is presented the typical PSD plot of an STM image. As can be seen from the PSD plots profile, they are practically identical for STM images in air and in phenyloctane suggesting that the stripe like domains persist in both media.

[134] Jackson, A.; Hu, Y.; Silva, P. J.; Stellacci, F. *J. Am. Chem. Soc.* **2006**, 128, 11135 – 11149.
[135] Ong, Q.-K.; Zhao, S.; Reguera, J.; Biscarini, F.; Stellacci, F. *Chem. Commun.* **2014**, 50, 10456 – 10459.
[136] Moglianetti, M.; Ong, K. Q.; Reguera, J.; Harkness, K.; Mameli, M.; Radulescu, A.; Kohlbrecher, J.; Jud, C.; Svergun, D.; Stellacci, F. *Chem. Sci.* **2014**, 5, 1232 – 1240.

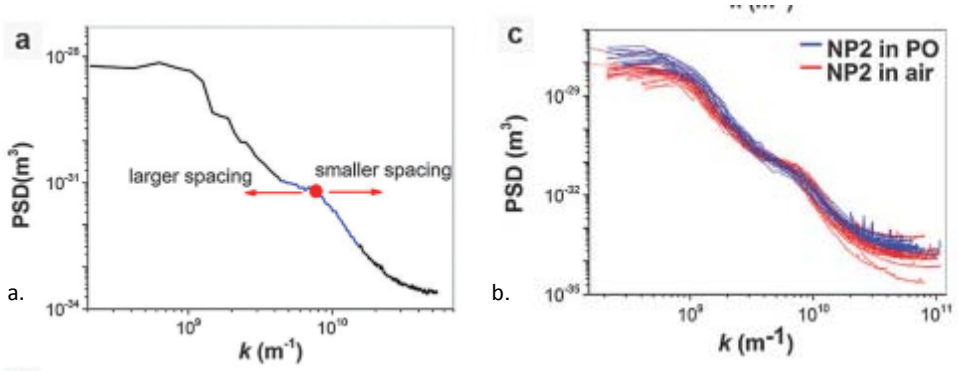

Figure 1.23 a) A typical PSD plot of an STM image; the blue segment is the characteristic ligand spacing. The deflection point marked by the red dot is a good indicator of the characteristic spacing. Its shift to a smaller or a larger value is indicated by the direction of red arrows. b) Comparison for the plots in PO (blue) and air (red).[136]

Small angle neutron scattering (SANS) experiments have been used by von White[137] to characterize homoligand nanoparticles coated by either octadecanethiol (C18) or dodecanethiol (C12), addressing the effect of the solvent on the thickness of the ligand shell. Later[136] with the same technique, the domain formation of a mixture of dodecanethiol and hexanethiol (one of this being deuterated) has been characterized in chloroform.

1.5.2. Indirect methods

There are many techniques which have been proposed to give indirectly informations about the morphology of mixed monolayers protected gold nanoparticles like ESR or NMR or UV-VIS. [138] Other techniques reported to offer information about the organization of the monolayer are MALDI mass spectrometry,[139] fluorescence,[140] infrared spectroscopy,[141] transmission electron microscopy[142] and contact angle measurements[148] or IR.[143]

1.5.2.1. NMR experiments

Nuclear magnetic resonance is a powerful technique for routine characterization of organic compounds and recently has been used to investigate more complex systems like the *in vivo* interaction of proteins with different cellular environments,[144] real time monitoring

[137] Von White, G.; Mohammed, F.; Kitchens, C. *J. Phys. Chem. C* **2011**, 115, 18397 – 18405.
[138] Vilain, C.; Goettmann, F.; Moores, A.; Le Floch, P.; Sanchez, C. *J. Mater. Chem.* **2007**, 17, 3509 – 3517.
[139] Harkness, K.; Balinski, A.; McLean, J.; Cliffel, D. *Angew. Chem. Int. Ed.* **2011**, 4, 10554 – 10559.
[140] Bonomi, R.; Cazzolaro, A.; Prins, L. *Chem. Commun*. **2011**, 47, 445 – 447.
[141] Centrone, A.; Hu, Y.; Jackson, A.; Zerbi, G.; Stellacci, F. *Small* **2007**, 3, 814 – 817.
[142] Wang, Y.; Zeiri, O.; Neyman, A.; Stellacci, F.; Weinstock, I. *ACSNano* **2012**, 6, 629 – 640.
[143] Centrone, A.; Hu, Y.; Jackson, A.; Zerbi, G.; Stellacci, F. *Small* **2007**, 814 – 817.
[144] Barbieri, L.; Luchinat, E.; Banci, L. *Nature* **2015**, 15, 14456.

of metabolic processes[145] or *in vivo* assessment of neurotransmitters and modulators in schizophrenia disease.[146] In the nanoparticles field, NMR techniques have been used for the first time to study Janus nanoparticles protected by hexanethiol and 2-(2-mercaptoethoxy)ethanol by Chen and collaborators[147,148] and later by Stellacci.[149] They have used Nuclear Overhauser Enhacement Spectroscopy (NOESY) experiment to demonstrate the phase separation of the mixture of thiolates on the surface of gold nanoparticles. This is a two-dimensional NMR technique where cross peaks arise from dipole-dipole interactions between nuclear spins in close proximity (typically for distances less than 0.4 nm) and consequently it is useful to determine the nature of the ligands surroundings on the particles surface. The spectrum of ligands randomly distributed on the NP surface shows the presence of two cross peaks between the methyl/methylene protons of the hexanethiolate ligands and the methylene protons of 2-(2-mercaptoethoxy)ethanol ligands whereas these cross peaks were absent in Janus nanoparticles. The absence of these signals in Janus nanoparticles clearly indicates that the hexanethiolate ligands are located far away from 2-(2-mercaptoethoxy)ethanol units because of the segregated arrangement of these two ligands on two different hemispheres of the nanoparticle surface. Ligands at the interface are too few to give rise to a detectable signal. Thus NOESY experiments appear to be useful to obtain information about the spatial organization of ligands on the monolayer.

Recently, a new NMR technique has been developed by Mancin and co-workers based on the paramagnetic relaxation enhancement (PRE) determined by Gd (III) ions[150] or by Yb (III) and Tb (III).[151] These authors studied the organization of mixed monolayers composed of thiols HS-C10 (**1**) and HS-C8TEG (**2**) and HS-C12 (**3**) and **4** depicted in Figure 1.24 by following the broadening or the disappearance of the peaks in the ^{1}H-NMR spectrum upon the addition of Gd^{3+} ions. It was observed that the broadening effect depends on the organization of the mixture of the ligands into the monolayer.

[145] Smith, M.; Marshall, C.; Theillet, F.-X.; Binolfi, A.; Selenko, P.; Ikura, M. *Curr. Opin. Struct. Biol.* **2015**, 32, 39 – 47.
[146] Wijtenburg, A.; Yang, S.; Fischer, B.; Rowland, L. *Neurosci. Biobehav. Rev*. **2015**, 51, 276 – 295.
[147] Pradhan, S.; Brown, L.; Konopelski, J.; Chen, S. *J. Nanopart. Res*. **2009**, 11, 1895 – 1903.
[148] Pradhan, S.; Xu, L. – P.; Chen, S. *Adv. Funct. Mater.* **2007**, 17, 2385 – 2395.
[149] Kim, H.; Carney, R.; Reguera, J.; Ong, Q. K.; Liu, X.; Stellacci, F. *Adv. Mater*. **2012**, 24, 3857 – 3863.
[150] Guarino, G.; Rastrelli, F.; Scrimin, P.; Mancin, F. *J. Am. Chem. Soc.* **2012**, 134, 7200 – 7203.
[151] Guarino, G.; Rastrelli, F.; Mancin, F. *Chem. Commun.* **2012**, 48, 1523 – 1525.

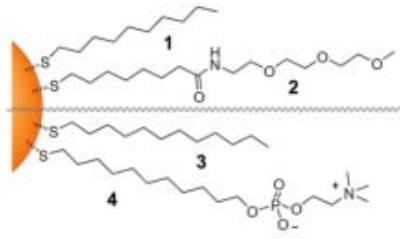

Figure 1.24 AuNPs used for the NMR study.

The data reported suggest that the intramolecular PRE effect driven by the lanthanide is strong enough to cancel not only the signal of the nuclei belonging to the groups bound to the paramagnetic ion, but also the signals of the alkyl chain of the thiolates that are not bound to the ion, but are in close proximity of it. They have recorded NMR spectra of nanoparticles protected by mixtures of **1** and **2** or **3** and **4**, in the presence of increasing amounts of Gd^{3+} (Figure 1.25) and have observed the disappearance of NMR signals of HS-C8TEG **2** and only a lowering of 50 % of the intensity of the signal of decanethiol, suggesting that the latter is only partially affected by the presence of the lanthanide ion. This is in agreement with thiols organized forming large patches or Janus NPs in which the HS-C8TEG units phase segregate and interact with decanethiolates only at the interfaces.

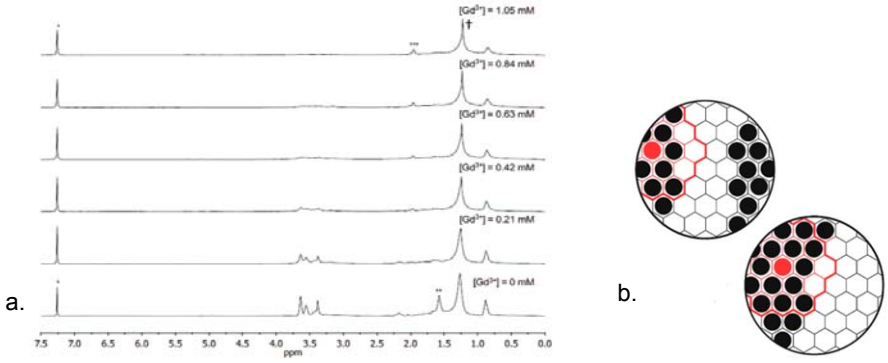

Figure 1.25 a) ^{1}H-NMR spectra of **NP-C10/C8TEG** coated with a mixture of **HS-C8TEG 2** and decanethiol 1 recorded upon addition of increasing amounts of Gd^{3+}; b) schematic representation of Gd^{3+} ion (red) bound to HS-C8TEG. **HS-C8TEG** are grouped in patches and as a consequence only their signals are cancelled while decanthiol is only marginally affected.[150]

On the contrary, NMR spectra of NPs formed by a 1:1 mixture of dodecanethiol and phosphorylcholine thiol have shown the disappearing of the signals pertaining to the two thiols, suggesting that both are in proximity of Gd^{3+} so to be affected by the PRE effect. This result suggests a random organization, formation of stripes or the presence of very small patches.

Recently, Stellacci has reported[152] a study of the morphology of mixed monolayers formed by aliphatic and aromatic ligands (Figure 1.26) using one-dimensional and bidimensional NMR experiments, analyzing the spectral parameters as a function of the ratio between the two ligands. More specifically, they have used mixtures of diphenyl thiol (DPT) and dodecanethiol (DDT) or diphenyl thiol and a branched thiol: 3,7-dimethyloctanethiol (DMOT). The choice of these ligands was made in order to have two well separated peaks in the NMR spectra for each couple.

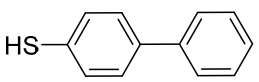

Diphenyl thiol (DPT)

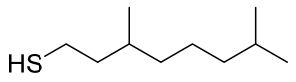

3, 7-Dimethyloctanethiol (DMOT)

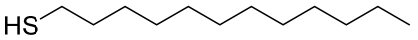

Dodecanethiol (DDT)

Figure 1.26 Schematic representation of thiols used for the study of mixed monolayers gold nanoparticles

Plotting the chemical shift of the aromatic hydrogen peaks against the composition of the monolayer, they have predicted and experimentally demonstrated that are three possible situations (Figure 1.27). For nanoparticles having a random organization a linear trend is obtained because the average composition of the first nearest neighbors shell (FNN) of a thiol coincides with the overall composition of the ligand shell. For Janus nanoparticles only the ligands found at the two component interface have a mixed composition, while for the others the FNN is the same with the homoligand particles. For this reason the coincidence between local and global compositions is removed and a linear dependence becomes a 1/x dependence. For patchy particles, the relationship is more complex (given that the shape of the patches does change with composition) and it leads to a sigmoidal trend whose analytical shape will strictly depend on the shape evolution of the domains.

[152] Liu, X.; Yu, M.; Kim, H.; Mameli, M.; Stellacci, F. *Nat. Commun*. **2012**, 3, 1182.

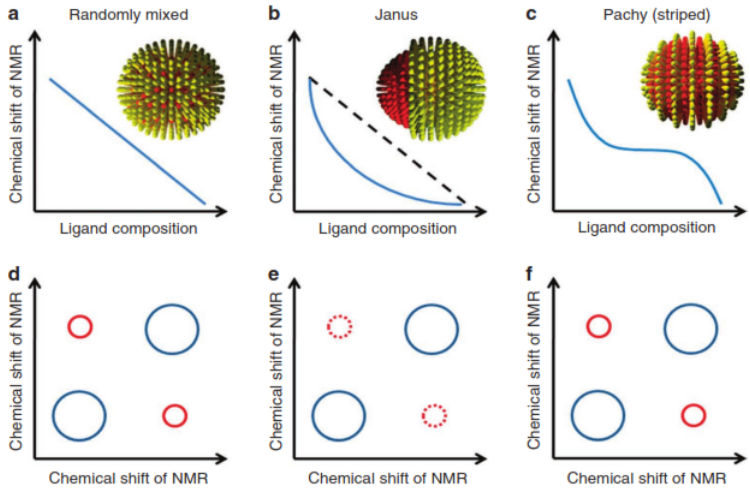

Figure 1.27 Predicted NMR plots for nanoparticles coated with a binary mixture of ligands. a-c Chemical shift of NMR peaks as a function of ligand composition for randomly mixed, Janus and patchy nanoparticles. d-f NOESY of randomly, Janus and patchy nanoparticles, respectively.[152]

Experimentally, they have obtained a linear trend for nanoparticles protected by DMOT and DPT having a random organization, a sigmoidal trend for the ones with a gold core diameter about 4-5 nm protected by DDT and DPT forming patches or stripes and an exponential behaviour when the dimension of the gold core is around 2-3 nm and the two ligands have a Janus organization in the monolayer of the nanoparticles. As shown before, 2D-NMR and in particular NOESY experiments, can be useful to demonstrate that the internuclear distance between two ligands is smaller than 0.4 nm. The NOESY spectra for the systems presented above, present cross peaks between the aromatic thiol peaks and the aliphatic ones for nanoparticles forming stripes or with a random organization. The absence of the cross peaks was instead observed for Janus nanoparticles because in this case the two ligands are interacting only at the interface between the two domains.

1.5.2.2. ESR techniques

Electron Spin Resonance (ESR) has many advantages respect to other indirect methods used to study the morphology of AuNPs monolayer because it is a sensitive technique, it offers the possibility to gain kinetic information in submicrosecond time, it is able to measure the tumbling rates on the nanosecond timescale, it does not require specific functional groups to be present on the ligands and finally it can be applied to both heterogenous and solid samples. In 2002, ESR has been used to investigate the mechanism of place exchange reaction of a stable radical-functionalized disulfide on Au nanoparticles. This study has demonstrated that the two branches of the disulfide molecule

did not adsorb adjacent to each other on the gold surface[153] and that the self-assembly of disulfides on gold proceeds with the breaking of the disulfide bond without the direct adsorption of the disulfide group on the gold surface.[154]

Two years later, in the research group of prof. Pasquato,[155] the ESR has been used to study the exchange of solutes between the ligand shell of protected gold nanoparticles and aqueous solutions. Since gold nanoparticles are ESR silent due to the absence of paramagnetic molecules, in order to get an ESR signal it is necessary to add a paramagnetic material to the sample (spin probe) that has to be a stable radical. The most used classes of spin probes are nitroxide compounds containing a paramagnetic unit N-O.

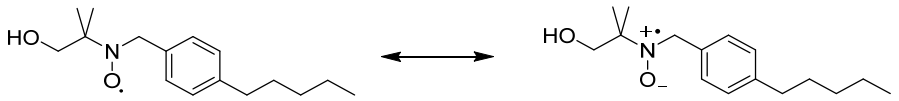

Typical ESR spectra of nitroxide radicals are characterized by the hyperfine interaction between the unpaired electron with the ^{14}N nucleus (I = 1) (α (N) and α ($2H_\beta$) hyperfine constants) and by the *g*-factor shifts due to spin-orbit coupling. Hyperfine splitting constants are known to be very sensitive to the polarity of the environment: grater polarity and/or the hydrogen bonding capability of the medium, the higher are the hyperfine constants because the polar structure is prevalently in these media.[156] When a *p*-substituted benzyl hydroxyalkyl nitroxide radical probe is in the presence of homoligand water soluble nanoparticles protected by the *H*-ligand **HS-C8TEG** (**NP-C8TEG**), the probe is partitioned between the water phase and the monolayer, (Scheme 1.4); this process is an equilibrium reaction characterized by a specific equilibrium constant K_{eq}.

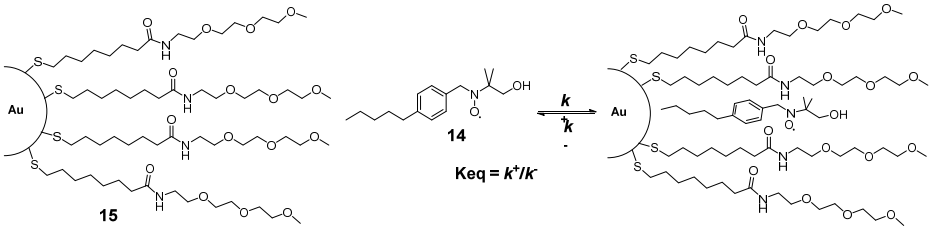

Scheme 1.4 Equilibrium of the nitroxide group between the water phase and the monolayer of AuNPs.

For this reason, the ESR spectrum is characterized by the presence of two set of signals, the hyperfine constants of the signal pertaining to the probe into the monolayer

[153] Ionita, P.; Caragheorgheopol, A. *J. Am. Chem. Soc.* **2002**, 124, 9048 – 9049.
[154] Noh, J.; Hara, M. *Langmuir* **2007**, 16, 2045 – 2048.
[155] Lucarini, M.; Franchi, P.; Pedulli, G. F.; Pengo, P.; Scrimin, P.; Pasquato, L. *J. Am. Chem. Soc.* **2004**, 126, 9326 – 9329.
[156] Lucarini, M.; Pasquato, L. *Nanoscale* **2010**, 2, 668 -676.

having a smaller hyperfine splitting constant from that of signals of the probe in water as can be seen in Figure 1.28.[157]

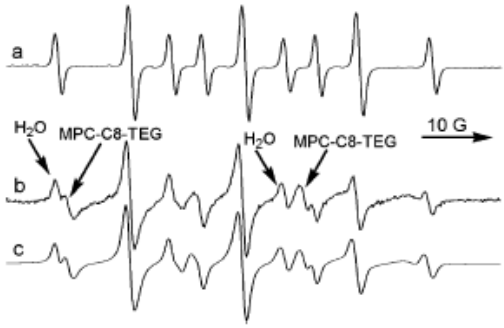

Figure 1.28 ESR spectra of the probe recorded (a) in water and (b) in presence of **NP-C8TEG** 0.3mM and (c) computer simulation of the latter one.[157]

By measuring the concentration ratio between the nitroxide solubilized into the monolayer and the free species by ESR, the affinity constant of the probe for the organic monolayer (K_H) could be calculated . By comparing these constants for nanoparticles having different sizes it was observed that the affinity of the probe for the monolayer increases as the nanoparticle diameter decreases, consistently with the decrease of the packing of the monolayer. Indeed, the hydrophobic probe requires a smaller energetic cost to enter in small NPs monolayers because of the large conformational freedom of the ligands than in bigger nanoparticles.[158]

The same study was performed on nanoparticles protected by fluorinated ligands[159] or by a mixture of hydrogenated and fluorinated ligands.[160]

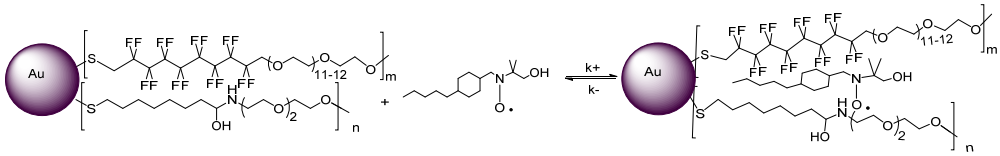

Scheme 1.5 Equilibrium reaction of the nitroxide group between the water phase and the monolayer **NPs-C8TEG/F8PEG**.

[157] Lucarini, M.; Franchi, P.; Pedulli, G. F.; Pengo, P.; Scrimin, P.; Pasquato, L. *J. Am. Chem. Soc.* **2004**, 126 -9326 -9329.
[158] Lucarini, M.; Franchi, P.; Pedulli, G. F.; Gentilini, C.; Polizzi, S.; Pengo, P.; Scrimin, P.; Pasquato, L. *J. Am. Chem. Soc.* **2005**, 127, 16384 -16385.
[159] Lucarini, M.; Pasquato, L. *Nanoscale* **2010**, 2, 668 – 676.
[160] Posocco, P.; Gentilini, C.; Bidoggia, S.; Pace, A.; Franchi, P.; Lucarini, M.; Fermeglia, M.; Pricl, S.; Pasquato, L. *ACSNano* **2012**, 6, 7243 – 7253.

The ESR spectrum of the nitroxide probe located in the monolayer of nanoparticles formed by the *F*-ligands **HS-F8PEG** (**NP-F8PEG**) is characterized by nitrogen and hydrogen splitting constants significantly smaller than those measured for **NP-C8TEG**.[161] This is compatible with the lower polarity of the environment experienced by the probe when dissolved in the **HS-F8PEG** monolayer. Moreover, the affinity constant (K_F) of the probe for fluorinated monolayers is two times higher than that measured for **HS-C8TEG** hydrogenated monolayers.

When the molar fraction of *H*-ligands in the monolayer is lower than 0.71, ESR parameters are independent of the monolayer composition and equivalent to those obtained when using homoligand fluorinated NPs. In presence of a larger amounts of *H*-ligands (molar fractions larger then 0.71), ESR parameters decrease indicating that the probe experiences a monolayer containing also hydrogenated ligands.[162,163]

Combining the results of these studies with an innovative multiscale molecular simulations (Figure 1.29), it could be concluded that: a) the hydrogenated and fluorinated ligands phase segregate forming domains even when about three *F*-chains (4%) are present in the monolayer; the phase segregation is induced by the strong lipophobicity of the *F*-chains. b) The shape of the domains is triggered by the length of the ligands as a consequence of the optimum balance between enthalpic and entropic driving forces. c) The size of the NP core is also a determining factor: below 2 nm Janus domains are formed, whereas stripe-like domains spontaneously form for larger NPs. The shape of the phase segregation domains is also dependent on the composition of the mixed monolayer. When the *H*-chains are present up to a molar fraction of 0.71, a borderline situation is present in which stripe- and patch-like domains coexist. As the molar fraction of the *H*-ligand increases further, the *F*-ligands organize into patches.

[161] Lucarini, M.; Pasquato, L. *Nanoscale* **2010**, 2, 668 – 676.
[162] Gentilini, C.; Franchi, P.; Mileo, E.; Polizzi, S.; Lucarini, M.; Pasquato, L. *Angew. Chem. Int. Ed.* **2009**, 48, 3060 – 3064.
[163] Gentilini, C.; Evangelista, F.; Rudolf, P.; Franchi, P.; Lucarini, M.; Pasquato, L. *J. Am. Chem. Soc*. **2008**, 130, 15678 – 15682.

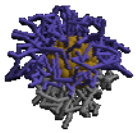

d = 1.6 nm
F-ligands : ***H***-ligands = 1:1
Janus nanoparticle

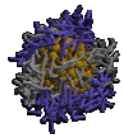

d = 2.2 nm
F-ligands : ***H***-ligands = 1:1
Stripe like pattern

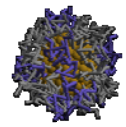

d = 2.5 nm
F-ligands : ***H***-ligands = 0.85:1
Stripe like pattern

Figure 1.29 Multiscale molecular simulations of AuNPs.

1.6. Applications of gold nanoparticles

The optical, electronic, magnetic and mechanical properties of AuNPs make these systems attractive candidates for biomedical applications. Due to the multifunctionality of the nanoparticles, they can be labeled with ligands for different applications as diagnosis, drug delivery, targeting, chemical and biological sensing, magnetic resonance imaging or catalysis.[2]

1.6.1. Drug delivery

Gold nanoparticles (AuNPs) provide good vehicles for delivery of drugs, genetic materials, proteins, and small molecules. The high surface area and tunability of AuNPs provide an excellent platform for attachment of drugs for controlled and sustained release (Figure 1.30). Various covalent and non-covalent strategies have been employed for loading drugs onto AuNPs.[164,165]

[164] Rana, S.; Bajaj, A.; Mout, R.; Rotello, V. *Adv. Drud Deliv. Rev*. **2012**, 64, 200 -216.
[165] Ding, Y.; Jiang, Z.; Saha, K.; Kim, C. S.; Kim, S. T.; Landis, R.; Rotello, V. *Molecular therapy* **2014**, 22, 1075 – 1083.

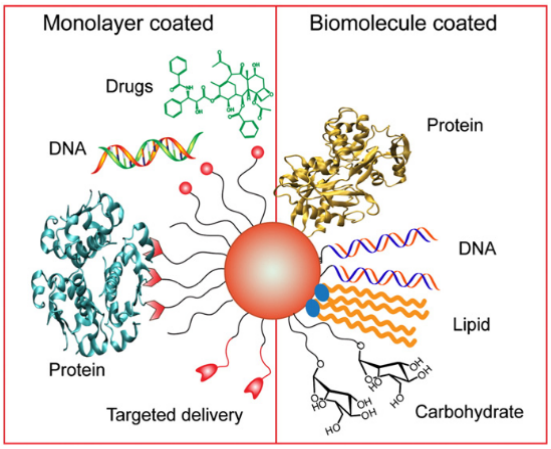

Figure 1.30 Schematic representation of the molecules which can be attached on the surface of the gold core.[164]

Recently, our group reported[166] reported a comparative study of the binding ability of fluorinated and non-fluorinated radical probes for homoligand nanoparticles featuring fluorinated or hydrogenated ligands in their monolayer. The systems analyzed displayed fluorinated moieties with different flexibility located close or distal to the gold core Figure 1.31.

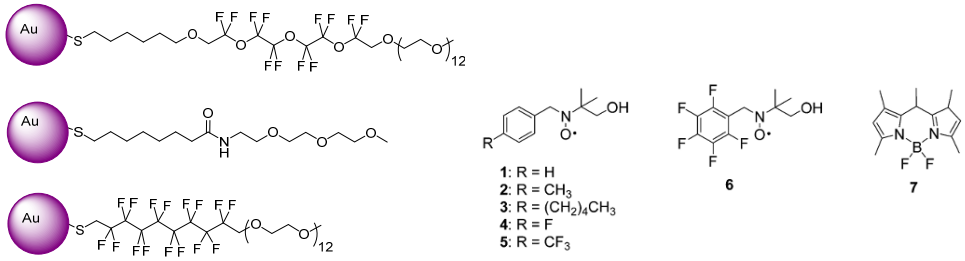

Figure 1.31 Nanoparticles used for the study of host – guest interaction and guests used for the study of the interaction with the nanoparticles.

This study revealed that the binding of both hydrogenated and fluorinated guest are favoured by the presence of the fluorinated monolayers and that a flexible fluorinated monolayer acts as a better hosting system than the more rigid counterpart. Moreover, for nanoparticles protected by ligands with a flexible fluorinated part, increasing the dimension of the gold core, the nanoparticles became better host for the guest even though the inter-ligand distances decrease.

[166] Boccalon, M.; Bidoggia, S.; Romano, F.; Gualandi, L.; Franchi, P.; Lucarini, M.; Pengo, P.; Pasquato, L. *J. Mater. Chem. B* **2015**, 3, 432 – 439.

1.6.2. Diagnosis

The development of methods for early detection of diseases is important in reducing its impact and to improve survival rates. AuNPs have high surface-to-volume ratios and can be functionalized to detect specific targets, offering lower detection limits and higher selectivity than conventional methods.[167] Mirkin has pioneered this field and in a seminal work has used nanoparticles to test the Warfarin metabolism and F5/F2/MTHFR mutations.[168,169] Recently, gold nanoparticles functionalized with antibodies[170] have been reported to improve the diagnosis of prostate cancer.[171]

1.6.3. Magnetic resonance imaging

Magnetic resonance imaging is a powerful non–invasive technique for obtaining 3D maps of living bodies. The advantages offered by MRI are: high spatial (<0.1 mm) and temporal resolution, 3D anatomical images, lack of ionizing radiation, deep tissue penetration, soft tissue contrast, and multiple contrast mechanisms.[172] The conventional MRI techniques exploits the NMR signals arising from the hydrogen nuclei of the water molecules present in the tissue under analysis, however, other heteronuclei such as ^{19}F have been reported to be useful.[173] When water protons are detected, MRI is not a very sensitive technique and for this reason it requires the uses of compounds that are able to change the water protons relaxation times, called MRI contrast agents. The MRI contrast agents can act either on the T1 or T2 relaxation times (SPIO). The former are mainly Gd(III) or Mn(II) complexes while the latter consist of superparamagnetic iron oxide nanoparticles (SPIONs). The presence of these compounds is locally revealed by a lightening (positive contrast, shortening of T1) or darkening (negative contrast, shortening of T2) of the magnetic resonance image.

[167] Mieszawska, A.; Mulder, W.; Fayad, Z.; Cormode, D. *Mol. Pharmaceutics* **2013**, 10, 831 – 847.
[168] Lytton-Jean, A.; Ha, M. S.; Mirkin, C. *Anal. Chem.* **2007**, 79, 6037 – 6041.
[169] Kim, Y. P.; Daniel, W.; Xia, Z.; Xie, H.; Mirkin, C.; Rao, J. *Chem. Commun.* **2010**, 46, 76 – 78.
[170] O'Rourke, D.; Dijohnson, D.; Caiazzo, R.; Nelson, J.; Ure, D.; O'Leary, M.; Richie, J.; Liu, B. *Anal. Chim. Acta* **2012**, 413, 561 – 567.
[171] Kang, B.; Jeun, M.; Jang, G. H.; Song, S. H.; Jeong, I. G.; Kim, C. S.; Searson, P.; Lee, K. H. *Int. J. Nanomed.* **2015**, 10, 6555 – 6569.
[172] Frullano, L.; Caravan, P. *Curr. Org. Synth*. **2011**, 8, 535 – 565.
[173] Kikuchi, K. *Chem. Soc. Rev.* **2010**, 39, 2048 – 2053.

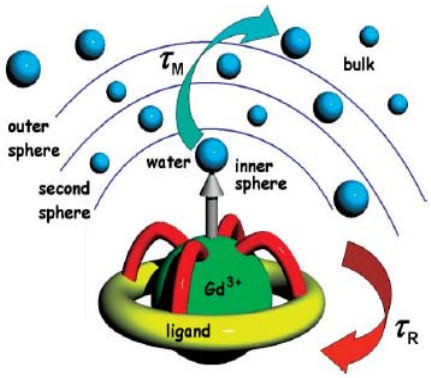

Figure 1.32 Schematic representation of the mechanism of action of a gadolinium contrast agent.

The most common contrast agents for MRI are gadolinium complexes. The increase in the water proton relaxation rate (R1 = 1/T) is linearly proportional to the concentration of Gd(III), with a proportionality constant termed relaxivity, r1. This is given by equation 1 where R_1^0 is the relaxation rate of the solvent in absence of Gd(III). A larger relaxivity indicates a more potent relaxation agent.[172]

$$R_1 = \frac{1}{T_1} = r_1 \cdot [Gd] + R_1^0$$

As far as gadolinium complexes are concerned, the most important parameters that govern the relaxivity are: the hydration number (q), the water exchange rate constant (k), the rotational correlation time (t) and the electron relaxation parameters.[174] However, increasing the parameter q can decrease the stability of the complex determining the displacement of the water molecules with endogenous anions, like carbonate or phosphate.[175] The increase of blood half-life time of contrast agents, which are usually rapidly cleared from the body, can be achieved by decoration with polyethylene oxide.[176] Reduction in the tumbling rate can be achieved by increasing the molecular size of the contrast agent[177] and this can be obtained by conjugating the gadolinium complexes with nanoparticles.

Apart from the reduced tumbling rates, nanoparticle-based contrast agents offer other

[174] Ferreira, M.; Concalvez, J.; Mousavi, B.; Prata, M.; Rodrigues, S.; Calle, D.; Lopez-Larrubia, P.; Cerdan, S.; Rodrigues, T.; Ferreira, P.; Helm, L.; Martins, J.; Geraldez, C. *Dalton. Trans.* **2015**, 44, 4016 – 4031.
[175] Supkowski, R.; Horroks, W. *Inorg. Chem.* 1999, 38, 5616 – 5619.
[176] Ayyagari, A. L.; Zhang, X.; Ghaghada, K. B.; Annapragada, A.; Hu, X.; Bellamkonda, R. V. *Magn. Reson. Med.* **2006**, 55, 1023 - 1029.
[177] Carvan, P. *Chem. Soc. Rev*. **2006**, 35, 512 - 523.

advantages. Arguably the most important feature of these materials is multifunctionality which makes it possible to attach several functional moieties to the same nanostructure enabling multimodal detection or targeted delivery and/or recognition.[178]

Roux pioneered the development of Gd chelate-functionalised AuNPs for MRI and synthesized a multilayered structure containing gadolinium on the surface of Au nanoparticles.[179]

Nonetheless, a 30% increase in the spin–lattice relaxivity per Gd(III) ion (r1) was observed for Gd-functionalized nanoparticles as compared to r1 of a commercially available small molecule analogue, Gd(III) complex with diethylenetriaminepentaacetic acid (Gd–DTPA). Similar results were obtained with Au nanoparticles coated with a DTPA ligand functionalised with two glutathione molecules.

Helm[180] have reported the most impressive relaxivity per Gd(III) chelate unit immobilized on gold nanoparticles: 60 mM^{-1} s^{-1} (30 MHz, 25 °C), using Gd(III) chelates of diethylenetriaminetetraacetic acid (DTTA)-type ligands.

Recently, Milne[181] synthesized water soluble gold nanoparticles decorated with triethylene glycol terminated with maleimide conjugated to over 50 Gd(III) chelators prepared via an interfacial Michael addition in aqueous media. Irure[182] prepared sugar/Gd-coated gold nanoparticles for targeting sugar cell transporters and lectins at the cell surface and demonstrated their efficiency as permeable and highly biocompatible cellular reporter probes for MRI at high magnetic fields. These types of nanoparticles are more stable than those synthesized by Milne[13] due to the presence of a longer alkyl chain in the proximity of gold core.

^{19}F MRI is an emerging diagnostic technique that presents several advantages with respect to proton MRI, ^{19}F is a highly sensitive NMR nuclide, and ^{19}F MRI scarcely shows background signals in animal bodies. However, ^{19}F MRI requires the use of fluorinated contrast agents to provide the MRI signal.

In our group water soluble gold nanoparticles functionalized with a fluorinated polyethylene glycol derivative (Figure 1.33) with features suitable for ^{19}F-MRI were recently reported.[183] These nanoparticles have demonstrated to be compatible with the biological

[178] Warsi, M. F.; Adams, R.; Duckett, S.; Chechik, V., *Chem. Commun.* **2010**, 46, 451 - 453.
[179] Debouttiere, P-J.; Roux, S., Vocanson, F.; Billotey, C.; Beuf, O.; Favre-Réguillon, A.; Lin, Y.; Pellet-Rostaing, S.; Lamartine, R.; Perriat, P.; Tillement, O. *Adv. Funct. Mater.* **2006**, 16, 2330 - 2339.
[180] Moriggi, L.; Cannizzo, C.; Dumas; E.; Mayer, C.; Ulianov, A; Helm, L. *J. Am. Chem. Soc.* **2009**, 131, 10828 – 10829.
[181] Milne, M.; Gobbo, P.; McVicar, N.; Workentin, M.; Hudson, R. *J. Mater. Chem. B* **2013**, 1, 5628 - 5635.
[182] Irure, A.; Marradi, M.; Arnaiz, B.; Genicio, N.; Padro, D.; Penadez, S. *Biomater. Sci*. **2013**, 1, 658 - 668.
[183] Boccalon, M.; Franchi, P.; Lucarini, M.; Delgrado, J. J.; Souza, F.; Stellacci, F., Zucca, I., Scotti, A.; Spreafico, R.; Pengo, P.; Pasquato, L. *Chem. Commun.* **2013**, 49, 8794.

environment because and to be non-cytotoxic towards HeLa cells. The 95% of cells were found to be viable after exposure to nanoparticles concentrations ranging between 0.6 μM and 10 μM. The ^{19}F T1 and T2 relaxation times for this kind of nanoparticles were found to be 588 ms and 67 ms respectively.

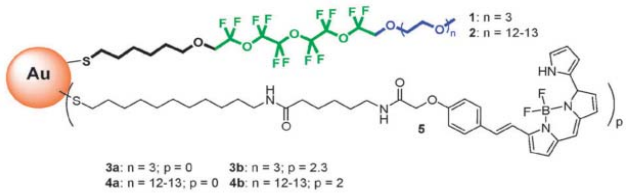

Figure 1.33 Schematic representation of fluorinated AuNPs for MRI applications.[183]

An interesting example of ^{19}F MRI contrast agent was published by Yu and his coworkers consisting of a small, water soluble compound having nine equivalent fluorine atoms which is able to chelate gadolinium ions.[184] Paramagnetic ions were also able to shorten ^{19}F relaxation times of the chelator, improving the signal to noise ratio. In this context, use of more rigid and shorter linkers between the paramagnetic center and the ^{19}F moiety could further improve the relaxation enhancement of ^{19}F by imposing a convenient separation, but the need for long hydrophilic spacers is often related to solubility issues of the fluorinated probe.[185]

Recently, it was demonstrated[186] that the close proximity of a gadolinium center with a fluorinated chain influences the ^{19}F-MRI signal, decreasing the T1.[187,188] In a recent interesting example, gold nanoparticles protected by thiolates carrying Gd(III) complexes and alkanethiolates with phosphonate headgroups, were used as scaffolds for the assembly of a fluorinated guanidinium based amphiphile Figure 1.34. The assembly was triggered by the charge complementarity of the guanidinium and phosphonate moieties and upon complexation, a 27% decrease in ^{19}F T1 of the fluorous shell was observed because of the presence of the gadolinium complexes in the monolayer.[186]

[184] Jiang, Z.-X.; Feng, Y.; Bruce, Y.; Yu, Y. *Chem. Commun.* **2011**, 47, 7233 – 7235.
[185] Tirotta, I.; Dichiarante, V.; Pigliacelli, C.; Cavallo, G.; Terraneo, G.; Baldelli Bombelli, F.; Metrangolo, P.; Resnati, G. *Chem. Rev*. **2015**, 115, 1106 – 1129.
[186] Li, V., Chang, A., William, T. *Tetrahedron* **2013**, 69, 7741 - 7745.
[187] Wu, X.; Dawsey, A.; Siriwardena-Mahanama, B.; Allen, M.; William, T. *J. Fluorine Chem.* **2014**, 168, 177 – 183.
[188] Davies, G. L.; Brown, A.; Blackburn, O.; Tropiano, M.; Faulkner, S.; Beer, P.; Davis, J. *Chem. Commun.* **2015**, 51, 2918 – 2920.

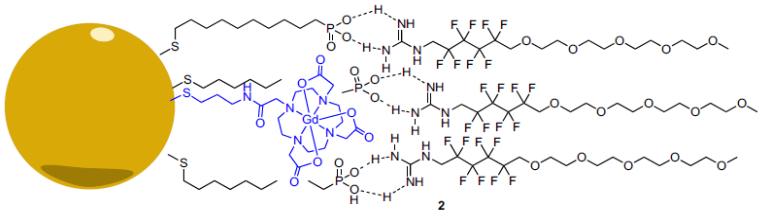

Figure 1.34 AuNPs complexed with gadolinium chelates for MRI.[186]

2. Aim

Gold nanoparticles have found a lot of applications in the biomedical field and part of these applications are based on the surface characteristics of the monolayer protecting the gold core. The importance of understanding and controlling the morphology of mixed monolayers has become a priority for many groups. We focused our attention on the study of the organization on the surface of the gold core of mixed monolayers composed of hydrogenated and fluorinated thiolates and how the structural properties of the ligands may influence the surface characteristics of the nanoparticles.

This PhD thesis has been focused on two projects:

- the synthesis of mixed-monolayers protected gold nanoparticles which coating is composed of hydrogenated and fluorinated ligands and the study of their morphology using NMR techniques and multiscale molecular simulations.
- the design and synthesis of gold nanoparticles protected by hydrogenated and fluorinated gadolinium chelates for MRI applications.

The objective of the first part of this PhD project was to investigate the morphology of mixed monolayers protected gold nanoparticles passivated by blends of dislike thiolates using NMR techniques. To achieve this goal, we designed and synthesized simple systems based on binary blends of hydrogenated and fluorinated ligands having different length mismatch and bulkiness: ligands of different length (NPs-C12/F6 and NPs-C16/F6); ligands having the same length (NPs-C12/F10 and NPs-C8/F6) and nanoparticles protected by ligands of different length and similar bulkiness (NPs-brC12/F6). Samples of nanoparticles have been synthesized presenting different ratios between the two thiolates in the monolayer and it has been investigated how the ^{19}F NMR response depends on the morphology of the monolayer. The obtained results have been supported by multiscale molecular simulations experiments carried out in collaboration with dr. P. Posocco, of the MOSE lab. of the University of Trieste, in order to predict the shape of the domains of each type of nanoparticles.

In the second project, we made a preliminary study of gold nanoparticles for MRI applications. Previously in our group, water soluble gold nanoparticles protected by fluorinated ligands have been found to be promising candidates for ^{19}F MRI applications. Starting from this result, we aim at increasing the MRI performances of these systems by decreasing the longitudinal and transversal relaxation times of selected nuclei, more specifically, of ^{1}H and ^{19}F. In particular, we focused our attention on gold nanoparticles

protected by ligands able to complex the gadolinium ion, commonly used for MRI. For this purpose we designed and synthesized a new ligand for Gd(III) ion which was used to protect the surface of the gold nanoparticles. Apart of this kind of systems we designed another type of nanoparticles, protected by fluorinated ligands able to bind the Gd(III) and we present preliminary results for a potential dual system for both ^{1}H and ^{1}F MRI application.

3. Study of the morphology of mixed - monolayers composed of hydrogenated and fluorinated ligands

As described in the introduction, the features of gold nanoparticles protected by mixed monolayers are determined by the surface characteristic of the nanoparticles. For this reason, it is of paramount importance to understand and to control the morphology. Experimental studies[1] have demonstrated that a binary mixture of dislike thiolates can have three main organizations on the surface of the gold core depending on their structure and on the balance between the entropic gain and enthalpic losses. They can form stripes, when the two ligands have different length; they can separate in two big domains when the two ligands have the same length or they can assume a random organization when one of the two ligands has a branched structure. These results have been rationalized by atomistic and mesoscale simulations.[2]

The study of the morphology of mixed monolayers involving fluorinated compounds is cumbersome because of the large number of limitations like their low solubility in common solvents and purifications problems. In principle, the use of binary blends of hydrogenated and fluorinated thiolates may permit to obtain anisotropic mixed monolayers since these ligands are expected to self-sort on the surface of the gold core because of their reciprocal phobicity. Previously, our group has demonstrated by ESR experiments[3] that mixtures of hydrogenated and fluorinated ligands on the surface of AuNPs phase segregate forming domains even at lower percentages of the fluorinated ligand into the monolayer (lower than 4%). This conclusion was supported by *in silico* simulations realized on water soluble

[1] a) Jackson, A. M.; Myerson, J. W.; Stellacci, F. *Nat. Mat*. **2004**, 3, 330–336; b) Jackson, A. M.; Hu, Y.; Silva P. J.; Stellacci, F. *J. Am. Chem. Soc*. **2006**, 128, 11135–11149; c) Centrone, A.; Hu, Y.; Jackson, A. M.; Zerbi, G.; Stellacci, F. *Small* **2007**, 3, 814–817; d) Ong, Q. K.; Reguera, J.; Silva, P. J.; Moglianetti, M.; Harkness, K.; Longobardi, Mali, K.S.; Renner, C.; De Feyter, S.; Stellacci, F. *ACS Nano* **2013**, 7, 8529–8539; e) DeVries, G. A.; Brunnbauer, M.; Hu, Y.;. Jackson, A. M; Long, B.; Neltner, B. T.; Uzun, O.; Wunsch B. H.; Stellacci, F. *Science* **2007**, 315, 358–361; f) Kim, H.; Carney, R. P.; Reguera, J.; Ong, Q. K.; Liu, X.; Stellacci, F. *Adv. Mater*. **2012**, 24, 3857–3863; g) Hu Y.; Uzun, O.; Dubois, C.; Stellacci, F. *J. Phys. Chem. C*, **2008**, 112, 6279–6284;

[2] a) Singh, C.; Ghorai, P. K.; Horsch, M. A.; Jackson, A. M.; Larson, R. G.; Stellacci, F.; Glotzer, S. C. *Phys. Rev. Lett.* **2007**, 99, 226106-1−226106-4; b) Pons-Siepermann, I. C.; Glotzer, S. C. *ACS Nano* **2012**, 6, 3919-3924; c) Singh, C.; Jackson, A. M.; Stellacci, F.; Glotzer, S. C. *J. Am. Chem. Soc.* **2009**, 131, 16377–16379; d) Santos, A.; Singh, C.; Glotzer, S. C. *Phys. Rev. E*, **2010**, 81, 011113; e) Carney, R. P.; DeVries, G. A.; Dubois, C.; Kim, H.; Kim, J. Y.; Singh, C. P.; Ghorai, K.; Tracy, J. B.; Stiles, R. L.; Murray, R. W.; Glotzer, S. C.; Stellacci, F. *J. Am. Chem. Soc*. **2008**, 130, 798−799.

[3] Gentilini, C.; Evangelista, F.; Rudolf, P.; Franchi, P.; Lucarini, M.; Pasquato, L. *J. Am. Chem. Soc.* **2008**, 130, 15678−15682; Gentilini, C.; Franchi, P.; Mileo, E.; Polizzi, S.; Lucarini, M; Pasquato, L. *Angew. Chem. Int. Ed.* **2009**, 48, 3060–3064; c) Posocco, P.; Gentilini, C.; Bidoggia, S.; Pace, A.; Franchi, P.; Lucarini, M.; Fermeglia, M.; Pricl, S.; Pasquato, L. *ACS Nano* **2012**, 6, 7243−7253

AuNPs protected by mixtures or hydrogenated and fluorinated ligands in collaboration with the group of dr. Paola Posocco, prof. Maurizio Fermeglia and prof. Sabrina Pricl of the MOSE lab. of from the University of Trieste. In particular, specific ratios of amphiphilic fluorinated and hydrogenated thiolates were found to give rise to domains like stripes or patches. To this aim we decide to investigate 3D mixed monolayers composed of simple blend of fluorinated and hydrogenated ligands in order to understand how dissimilarities between the ligands and their geometrical mismatches arising from differences in length and steric bulk influence the formation of domains and eventually their size and shape.

Synthesis of AuNPs protected by mixed - monolayers

In this work we aim to investigate the morphology of mixed monolayers, grafted on the surface of the gold NPs, composed of hydrogenated and fluorinated ligands of different length and steric bulk using NMR techniques. The obtained results are supported by multiscale molecular simulations realized at MOSE, which predict the organization of mixed monolayers on the surface of the gold core.

Aiming at exploring a broad range of nanoparticles compositions and mixtures of dislike ligands, we have used four types of hydrogenated thiols (octanethiol, **HS-C8**; dodecanethiol, **HS-C12**; hexadecanethiol, **HS-C16**; 3-methyl-dodecanethiol, **HS-brC12**) and two fluorinated ones (1*H*,1*H*,2*H*,2*H*-perfluorodecanethiol, **HS-F6** and 1*H*,1*H*,2*H*,2*H*-perfluorododecanethiol, **HS-F10**), displayed in Figure 3.1.

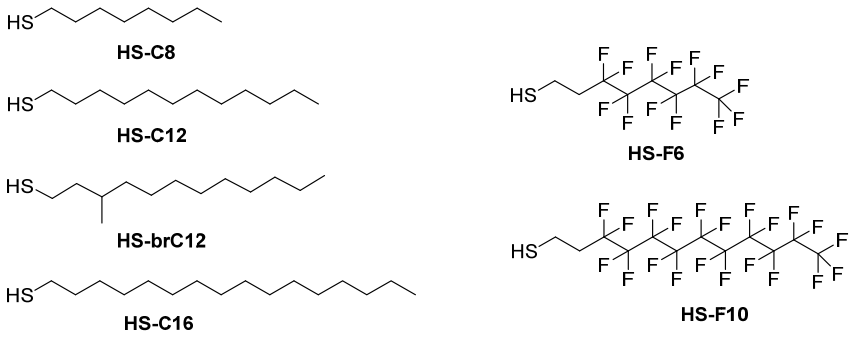

Figure 3.1 Library of hydrogenated and fluorinated ligands used for this study.

The thiols **HS-C8**, **HS-C12**, **HS-C16** and **HS-F6** are commercially available, **HS-brC12** was synthesized as described in Section 3.7 and **HS-F10** was prepared according to literature procedures.[4]

[4]Tokuyasu, T. *J. Org. Chem.* **2005**, 70, 251−260.

The structural diversity of these thiols was chosen in order to investigate how the strong immiscibility between fluorinated and hydrogenated alkyl chains and the structural parameters such as thiols length, steric bulk and length mismatch influence the synthetic process, the solubility properties and the organization of the monolayer. AuNPs protected by mixtures of hydrogenated and the fluorinated ligands with different molar fractions were synthesized varying the initial ratio between the two thiols. All these nanoparticles were characterized using UV-VIS, TEM, TGA and NMR experiments. We have investigated how the type of thiols used for the synthesis influence the organization of the monolayer and we have realized a basic study of the morphology of these nanoparticles using NMR techniques. Moreover, for these nanoparticles multiscale molecular simulations were performed in collaboration with the group of Dr. P. Posocco of the University of Trieste.

Using binary mixtures of ligands presented in Figure 3.1, we have synthesized three classes of nanoparticles.

1. AuNPs protected by ligands of different length

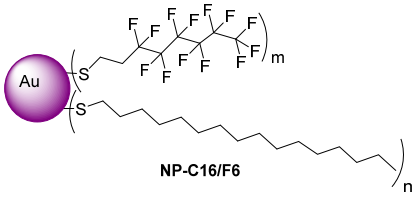

NP-C16/F6

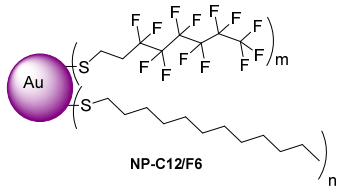

NP-C12/F6

2. AuNPs protected by ligands having the same length

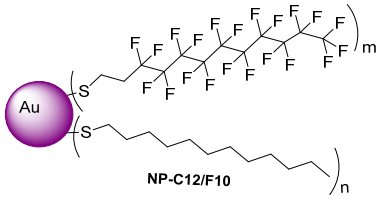

NP-C12/F10

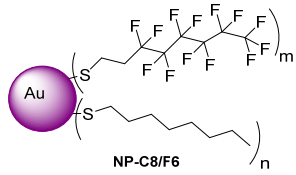

NP-C8/F6

3. AuNPs protected by ligands of similar bulkiness and different length

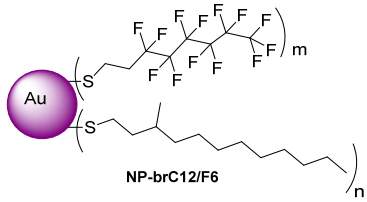

NP-brC12/F6

The combination of thiols **HS-C12** and **HS-F10** in nanoparticles **NP-C12/F10** or thiols **HS-C8** and **HS-F6** in nanoparticles **NP-C8/F6** will allow an analysis of the conditions

required for the preparation of NPs displaying *H*- and *F*-ligands of the same length. The combination of thiols **HS-C12** and **HS-F6** in nanoparticles **NP-C12/F6** or thiols **HS-C16** and **HS-F6** in nanoparticles **NP-C16/F6**, allows instead an analysis of the role played by the length mismatch (4 atoms and 8 atoms respectively) in the outcome of the syntheses and in the morphology of the monolayer. By combining thiols **HS-brC12** and **HS-F6** in nanoparticles **NP-brC12/F6** we will explore the effect of using a branched thiol preventing the formation of domains stabilised by van der Waals interactions,[5] in association with a four atom shorter fluorinated thiol.

The synthesis of these AuNPs was achieved by exploiting two procedures: a direct synthesis following a modified Brust-Schiffrin method for the preparation of the **NP-C16/F6**, **NP-C8/F6**, and **NP-brC12/F6** (Scheme 3.1) or a place exchange reaction (Scheme 3.2) between narrowly dispersed **NP-C12**, prepared following the method of Miyake,[6] and the fluorinated ligand for the synthesis of **NP-C12/F6** and **NP-C12/F10**. The choice for one of the two methods was rationalized considering the ease of synthesis, the availability of the ligands and the costs involved for the synthesis.

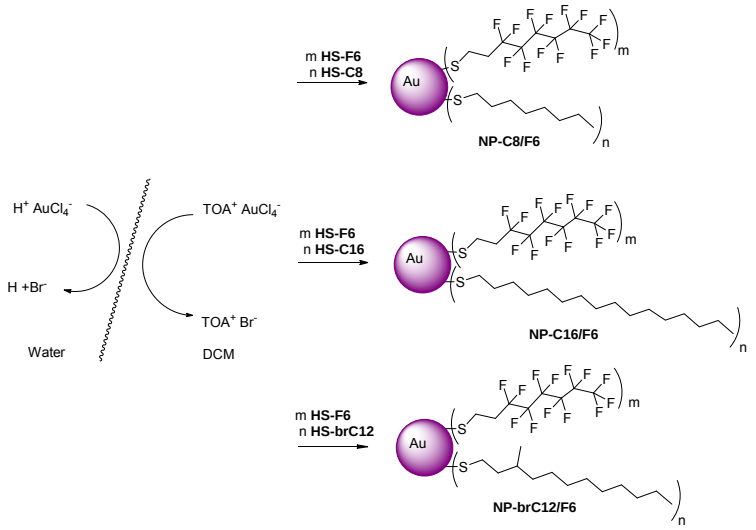

Scheme 3.1 Direct synthesis of AuNPs.

[5] X. Liu, M. Yu, H. Kim, M. Mameli and F. Stellacci, *Nat. Commun*. **2012**, 3,1182.
[6] T. Shimizu, T. Teranishi, S. Hasegawa and M. Miyake, *J. Phys. Chem B*. **2003**, 107, 2719−2724

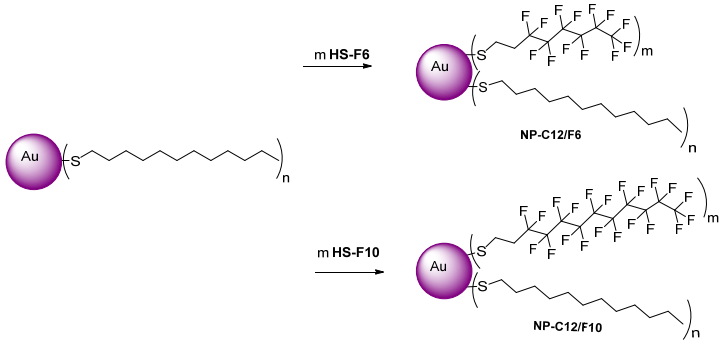

Scheme 3.2 Place exchange reaction method for the synthesis of AuNPs.

3.1. Synthesis of AuNPs protected by ligands having different length

3.1.1. Synthesis of NP-C16/F6

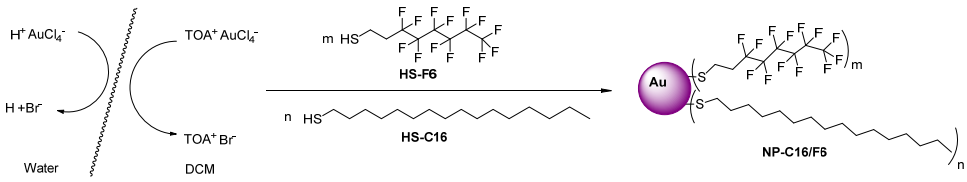

Scheme 3.3 Direct synthesis of **NP-C16/F6**.

As previously mentioned, the **NP-C16/F6** have been obtained using a direct synthesis in which the tetrachloroauric acid was reduced with $NaBH_4$ in the presence of a mixture of hexadecanethiol (**HS-C16**) and 3,3,4,4,5,5,6,6,7,7,8,8,8-tridecafluorooctane-1-thiol (**HS-F6**), both commercially available. Briefly, an aqueous solution of tetrachloroaurate salt (1 Equiv.) was transferred to the organic phase using 2.5 Equiv. of tetraoctylammonium bromide (TOAB) in dichloromethane. The mixture was vigorously stirred observing the fading of the aqueous phase while the organic phase turned orange. To this solution, a freshly prepared mixture of the two ligands in dichloromethane (DCM) was added in a 3:1 Au:thiol ratio (see Table 3.8). The total amount of thiols and the **HS-C12**/**HS-F6** used ratios vary (Table 3.8), depending on the desired final loading of the fluorinated ligand and on the dimension of the gold core. Subsequent addition of an aqueous solution of $NaBH_4$ in water produced the reduction of gold salt to Au (0) and the mixture turned brown or violet depending on the diameter of the nanoparticles core; the time required for adding the $NaBH_4$ solution varied from 5s to 35 minutes, as reported in Table 3.8, in order to obtain gold nanoparticles with a gold core diameter around 3 nm. The reaction mixture was let to stir overnight then the two layers were separated and the organic phase was washed with brine (1 x 20 mL). The

nanoparticles were purified by precipitations and repeated washings with methanol (see section 3.7, Experimental part). The pure nanoparticles were subjected to selective extractions with $CHCl_3$ and afterwards with hexane. The insoluble material eventually present was tested for solubility in hexafluorobenzene.

^{1}H NMR characterization of these nanoparticles (Figure 3.2) confirmed the absence of free thiols or disulfides, indicating that the purification protocol was successful.

At least 1 mg of nanoparticles was decomposed by treatment with 3 mL of iodine (2 mg/mL) in chloroform overnight. The iodine and solvent excess was let to evaporate under a fume cupboard. The disulfides were dried under vacuum and the ratio between the two ligands was determined from the ^{1}H NMR spectrum by integration of the methylene groups in the alpha position with respect to the sulfur atom (Figure 3.2). As can be seen in Table 3.1, we have obtained mixed monolayers nanoparticles comprising from the 2.6% to the 80.4% of the fluorinated ligand, thus covering the entire span of compositions (Table 3.1). The characteristics and the average composition of these nanoparticles are presented in Table 3.1.

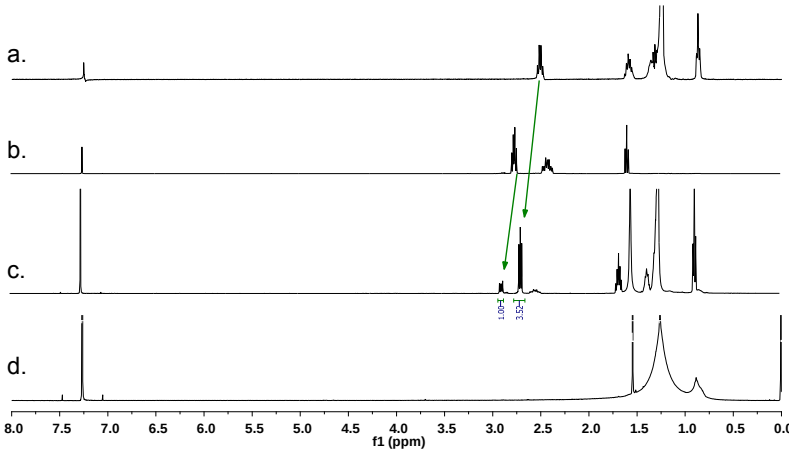

Figure 3.2 a) ^{1}H-NMR (400 MHz, $CDCl_3$) spectrum of **HS-C16**; b) ^{1}H-NMR (500 MHz, $CDCl_3$) spectrum of **HS-F6**; c) ^{1}H-NMR (500 MHz, $CDCl_3$) spectrum of decomposed **NP-C16/F6-e** d) ^{1}H-NMR (500 MHz, $CDCl_3$) spectrum of **NP-C16/F6-e**.

Table 3.1 Characterization data for nanoparticles **NP-C16/F6**.

Nanoparticles	Diameter (nm)[a]	Composition[b]	X_{F6}[c]	Solubility Score[d]	% C_6F_6 added[e]
NP-C16/F6-a	2.9 ± 0.5	$Au_{976}(C16)_{177}(F6)_6$	0.026	1	0
NP-C16/F6-b	3.2 ± 0.6	$Au_{1289}(C16)_{213}(F6)_8$	0.036	1	0
NP-C16/F6-c	2.6 ± 0.5	$Au_{475}(C16)_{114}(F6)_5$	0.042	1	0
NP-C16/F6-d	3.0 ± 0.5	$Au_{976}(C16)_{178}(F6)_{11}$	0.055	1	0
NP-C16/F6-e	3.2 ± 0.6	$Au_{976}(C16)_{147}(F6)_{42}$	0.217	1	0
NP-C16/F6-f	2.9 ± 0.5	$Au_{800}(C16)_{142}(F6)_{79}$	0.357	1	0
NP-C16/F6-g(C)	2.1 ± 0.4	$Au_{309}(C16)_{42}(F6)_{35}$	0.455	1	0
NP-C16/F6-g(F)	2.1 ± 0.5	$Au_{309}(C16)_{26}(F6)_{52}$	0.666	0	37.5
NP-C16/F6-h(C)	2.1 ± 0.4	$Au_{309}(C16)_{40}(F6)_{44}$	0.524	1	0
NP-C16/F6-i(C)	2.6 ± 0.4	$Au_{475}(C16)_{70}(F6)_{80}$	0.533	1	0
NP-C16/F6-i(H)	2.7 ± 0.6	$Au_{527}(C16)_{55}(F6)_{74}$	0.574	0.5	12.5
NP-C16/F6-j(C)	2.5 ± 0.3	$Au_{475}(C16)_{71}(F6)_{96}$	0.573	1	0
NP-C16/F6-j(H)	2.0 ± 0.4	$Au_{309}(C16)_{31}(F6)_{44}$	0.586	0.5	12.5
NP-C16/F6-k(C)	2.3 ± 0.4	$Au_{314}(C16)_{23}(F6)_{63}$	0.730	1	0
NP-C16/F6-k(F)	2.2 ± 0.5	$Au_{314}(C16)_{18}(F6)_{72}$	0.804	0	37.5
NP-C16/F6-h(H)	2.2 ± 0.4	$Au_{314}(C16)_{19}(F6)_{61}$	0.762	0.5	37.5
NP-C16/F6-h(F)	2.1 ± 0.3	$Au_{309}(C16)_{19}(F6)_{62}$	0.764	0	25

[a] Average diameters and standard deviation of a population of at least 300 particles.[b] Calculated on the basis of the TGA and TEM and ^{1}H NMR analyses of decomposed nanoparticles. [c] Molar fraction of the fluorinated ligand in the monolayer of nanoparticles **NP-C16/F6** determined by ^{1}H NMR analysis of decomposed nanoparticles. [d] The solubility scores are defined arbitrarily as follows: score 1 is assigned to nanoparticles fully soluble in chloroform; score 0.5 is assigned to nanoparticles fully soluble in hexane; score 0 is assigned to nanoparticles fully soluble in hexafluorobenzene; [e]percentage of C_6F_6 in the mixture $CDCl_3/C_6F_6$ added to solubilise the nanoparticles for NMR experiments.

The size of the gold core has been determined using transmission electron microscopy, by depositing a dilute (0.1 mg/mL) solution of nanoparticles onto a carbon coated copper or nickel grid and left the solvent to gently evaporate at air. The TEM images were analyzed manually, measuring the sizes of at least 300 nanoparticles for each sample. A combination of the information obtained from NMR, TEM and TGA allowed us to determine the average composition of each nanoparticle, as reported in Table 3.1.

The syntheses of **NP-C16/F6** give rise to samples of nanoparticles displaying different solubility properties: soluble in chloroform only, in hexane or in mixtures of chloroform and hexafluorobenzene (C_6F_6). More specifically, at percentages of **F6** into the monolayer smaller than 60 %, the nanoparticles are very soluble in chloroform, at percentages of **HS-F6** bigger than 60% three types of nanoparticles are obtained: soluble in chloroform, samples soluble in hexane or in mixtures chloroform/hexafluorobenzene. The solubility properties and the dimension of the gold core are better described in Chapter 3.4.3.

For all the samples of nanoparticles reported in Table 3.1, we have recorded ^{19}F-NMR spectra (Figure 3.3) by dissolving 4-5 mg of nanoparticles in an appropriate solvent. More specifically, the nanoparticles soluble only in $CHCl_3$ have been dissolved in $CDCl_3$ and the other samples were solubilized in different mixtures $CDCl_3/C_6F_6$, as reported in Table 3.1.

All the ^{19}F NMR spectra have been recorded using $CFCl_3$ as external reference. As expected, the signals of the nanoparticles are broadened respect to the signals of the free thiols, as it was also observed in the ^{1}H-NMR spectra. Even though in the ^{1}H NMR spectra reported in Figure 3.2, no free thiols were identified, in the ^{19}F NMR spectra, very small sharp peaks are seen suggesting that traces of free thiol are present. An explanation for this discordance could be the sensibility of the technique and small quantity of free fluorinated thiols do not display any signal in the ^{1}H NMR spectra but only in the more sensitive ^{19}F NMR.

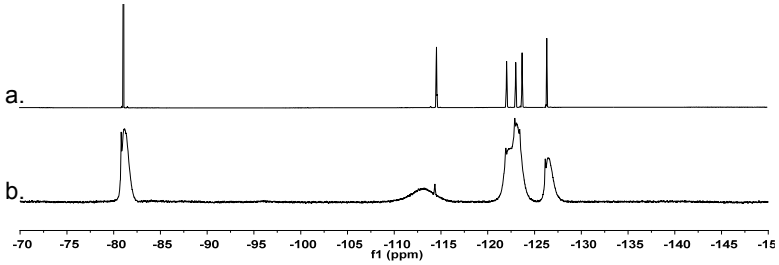

Figure 3.3 ^{19}F-NMR (470 MHz, $CDCl_3$) spectrum of a) **HS-F6** and b) **NP-C16/F6-e**.

3.1.1.1. Assignment of the peaks

The correct interpretation of the NMR spectra is essential for our study. It is very important to identify the chemical shift of the signals of each thiol used for the synthesis of the nanoparticles. The hydrogenated ligands are well known and completely characterized; instead, the assignment of the ^{19}F-NMR resonances of the fluorinated ligands required a more detailed study. The ^{19}F NMR spectrum with assignment of the resonances for thiol **HS-F6** is reported in Figure 3.4.

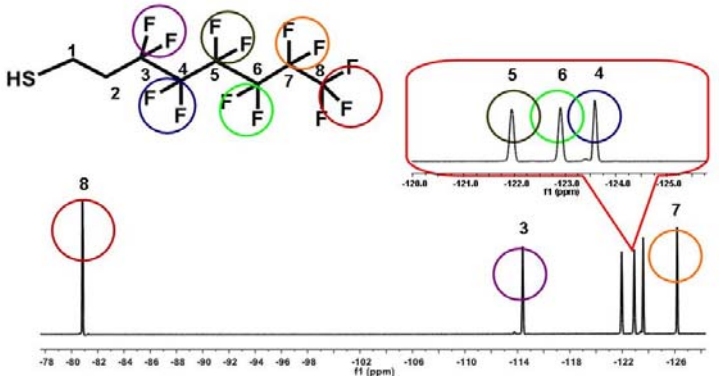

Figure 3.4: ^{19}F NMR (470 MHz, $CDCl_3$) spectrum of **HS-F6** and the assignment of the peaks.

In order to assign the peaks corresponding to each CF_2 group, we have first recorded a series of mono- and bi-dimensional NMR experiments (^1H, ^{19}F, ^1H-^1H COSY, ^{19}F-^{19}F COSY ^1H-^{19}F HETCOR) on free **HS-F6.** The obtained results then can be translated to the peaks signals present on the nanoparticles spectra. A first information arises from ^1H-^{19}F HETCOR bidimensional experiment (Figure 3.5) realized on **HS-F6**, in which a correlation between the CH_2 peak at 2.4 ppm corresponding to the methylene group in alpha position respect to the thiol moiety (Figure 3.4) and the CF_2 peak at -114.6 ppm can be observed. The presence of this cross peak suggests that these two groups are directly linked.

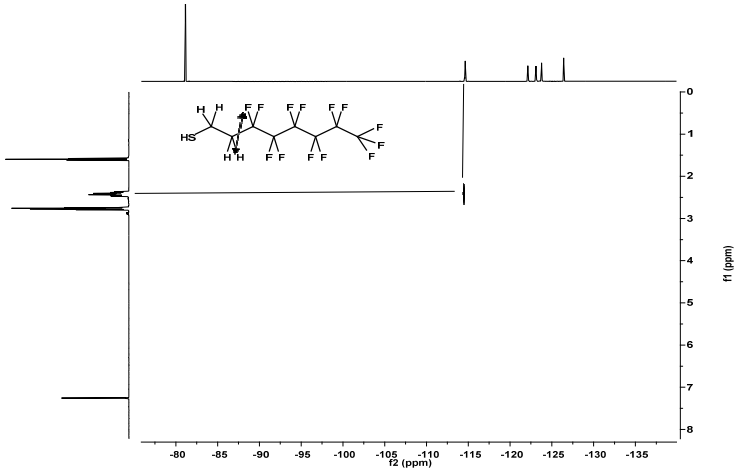

Figure 3.5 ^1H-^{19}F HETCOR (500 MHz, $CDCl_3$) experiment on **HS-F6**.

This assignment is consistent with the observation that, in the spectrum of **NP-C16/F6-e**, the signal at -114 ppm (Figure 3.3) is more broad than the other signals because more close to the gold atoms than the others CF_2. From a qualitative evaluation of the integration of the signals in the ^{19}F-NMR spectrum of **HS-F6** arises other information: the peak at -81 ppm integrate 1.5 with respect to the other peaks present in the spectrum, suggesting that this signal pertain to the CF_3-. In perfluorinated compounds, the four bond coupling constant (^4J) is usually larger than the vicinal coupling constant (^3J).[7] As a consequence weak or no cross peaks can be seen between adjacent CF_2 groups in bidimensional ^{19}F-^{19}F COSY experiments (Figure 3.6). For **HS-F6** no correlations were observed between the peak at -81 ppm and -114.6 with the peak at -126.6 ppm (blue circles in Figure 3.6). There are two possibilities which determine this absence: the groups are too distant to give a signal or are neighbors in the molecule.

[7] Battiste, J.; Jing, N.; Newmark, R. *J. Fluorine Chem.* **2004**, 125, 1331 – 1337.

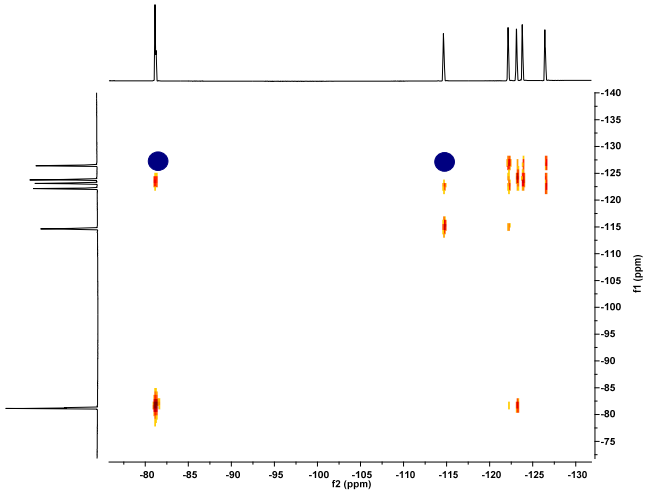

Figure 3.6 ^{19}F-^{19}F COSY (500 MHz, $CDCl_3$) experiment on **HS-F6**.

From this data we can conclude that the peak at -126 ppm perteins to the CF_2 group in position 7 and the remaining peaks at -125 ppm represent the CF_2 central groups. The same assignment of chemical shifts can be transferred to the spectrum of the nanoparticles.

3.1.1.2. Influence of solvent composition on the chemical shift of the NP-C16/F6

As it can be seen in Table 3.1, some of the nanoparticles needed the addition of hexafluorobenzene, in order to dissolve completely, especially when the percentage of **F6** into the monolayer is very high. Considering that the NMR response can be influenced by the solvent, we decided to investigate the influence of the solvent composition used to dissolve each sample on the chemical shift of the nanoparticles signals. To this aim we dissolved about 5 mg of nanoparticles **NP-C16/F6-e** in $CDCl_3$ and added increasing amounts of C_6F_6. After each step, we performed ^{19}F NMR experiments determining the chemical shifts of the peaks using $CFCl_3$ as external standard. The ^{19}F-NMR spectra obtained is presented in Figure 3.7.

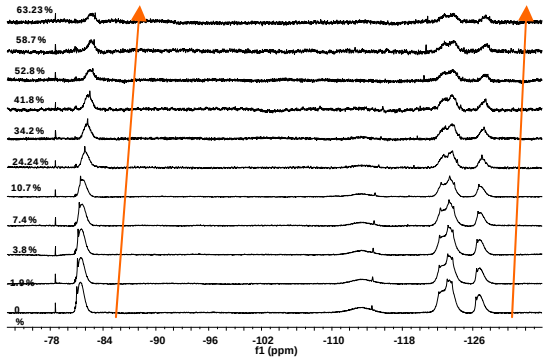

Figure 3.7 Chemical shift of **NP-C16/F6-e** function of the solvent composition.

The ^{19}F-NMR spectra displays that the peaks of nanoparticles shift by changing the composition of the solvent. In the case of nanoparticles only two peaks are well separated enabling an accurate measure of the chemical shift at the maximum: the peak at around -81 ppm representing the CF_3 end group and the peak at -126.5 ppm that is assigned at the CF_2 group in position 7 (Figure 3.4). By plotting the observed chemical shift as a function of the percentage of C_6F_6 into the solvent mixture, the linear correlations displayed in Figure 3.8 were obtained. Regarding the peak of nanoparticles, we represented the difference between the chemical shift of the CF_3 or CF_2 groups at a certain percentage of C_6F_6 into the solvent mixture and the chemical shift of the corresponding group when no C_6F_6 was added, indicated as delta chemical shift (Δδ) (Figure 3.8).

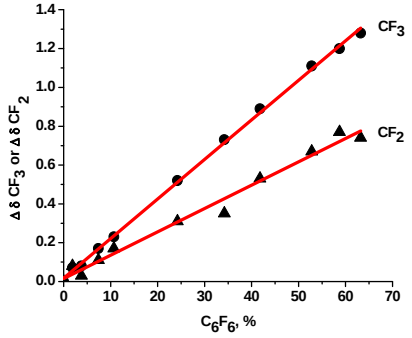

Figure 3.8 Delta chemical shift* of CF_3 (circles) and CF_2 (triangles) groups of nanoparticles as a function of the percentage of C_6F_6 into the mixture of solvents used to dissolve the nanoparticles. * delta chemical shift = chemical shift of the nanoparticle at a certain percentage of C_6F_6 in the solvent mixture - chemical shift of nanoparticles in the absence of C_6F_6.

A linear trend was observed for the nanoparticles signals *vs*. the increase amount of C_6F_6. Comparing the influence of the solvent composition on the chemical shift of the CF_3 and CF_2 groups we obtained two linear trends (Figure 3.8) the slope of the straight line

pertaining to the CF_2 in the position 7 is smaller than the slope of the straight line corresponding to the CF_3 chemical shift. This was an expected behavior considering that the CF_2 group is less exposed to the solvent respect to the CF_3 group. These data suggested the necessity of further NMR studies to better understand how the nanoparticles interact with the solvent and how these interactions influence the NMR response of different samples of nanoparticles. Starting from the consideration that by varying the composition of the monolayer different arrangement of the two ligands could be obtained possibly producing a different response to the solvent, we decided to investigate other two samples of nanoparticles (Figure 3.9) having higher percentage of the fluorinated thiol into the monolayer: 35.7% for **NP-C16/F6-f** and 57.26% for **NP-C16/F6-j(C)**. For this study we have followed the same procedure used for **NP-C16/F6-e**. More specifically, we dissolved the nanoparticles in chloroform and we have added different amounts of C_6F_6, measuring after each step the chemical shift of the CF_3 and CF_2 of the nanoparticles. By plotting delta chemical shift of CF_3 or CF_2 group we obtained an identical behavior with **NP-C16/F6-e**, namely the influence of the solvent composition on the chemical shift of the CF_2 group is less pronounced with respect to the influence on the CF_3 chemical shift for all three samples of nanoparticles analyzed (Figure 3.9).

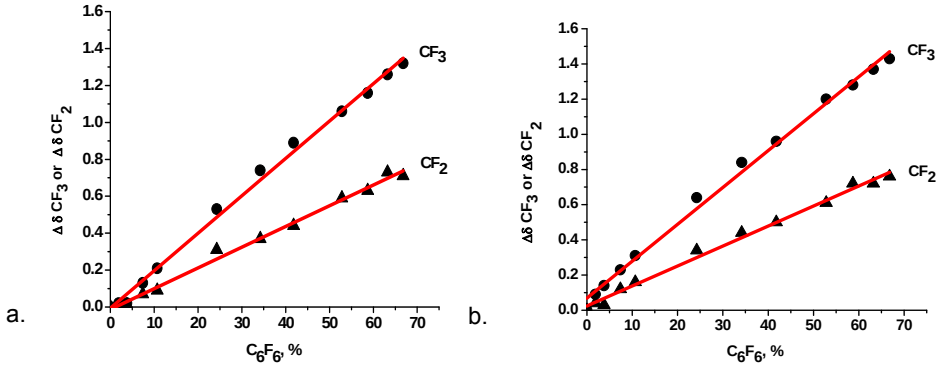

Figure 3.9 Chemical shift of CF_3 (circles) and CF_2 (triangles) groups for **NP-C16/F6-f** and **NP-C16/F6-j(C)**.

In order to observe better the differences between these three samples of nanoparticles, we plotted the delta chemical shift of CF_3 and CF_2 peaks for all three samples, as a function of the percentage of the fluorinated ligand into the monolayer, as can be seen in Figure 3.10.

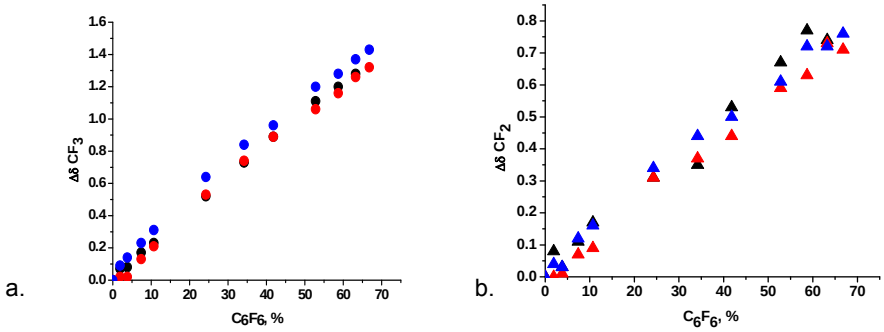

Figure 3.10 Representation of a) delta chemical shift of CF_3 and b) delta chemical shift of CF_2 as a function of % of C_6F_6 for three samples of **NP-C16/F6** in black: **NP-C16/F6-e**; in red **NP-C16/F6-f** and in blue **NP-C16/F6-j(C)**.

This study has revealed that the influence of the solvent mixture on the chemical shift of nanoparticles is the same for the three samples. This means that the composition of the monolayer and eventually different organization of the blend of these two ligands are not decisive factors for the chemical shift of the nanoparticles signals. This behavior has to be taken into account when analyzing the NMR spectra of various nanoparticles and the chemical shift of the nanoparticles signals must be accurately measured and corrected in order to obtain the real chemical shift of the signals eliminating the influence of the solvent. With all this in mind, we have realized ^{19}F-NMR experiments of the nanoparticles presented in Table 3.1. For the samples soluble in only chloroform, the crude data were not modified and the chemical shift presented is the chemical shift as measured from the spectra. For nanoparticles which need addition of fluorinated solvent to be completely solubilized, we revised the crude chemical shift data obtained from the ^{19}F-NMR modified by the influence of the solvent composition to the chemical shift of the signals of nanoparticles.

3.1.1.3. Synthesis of perfluorinated NP-F6

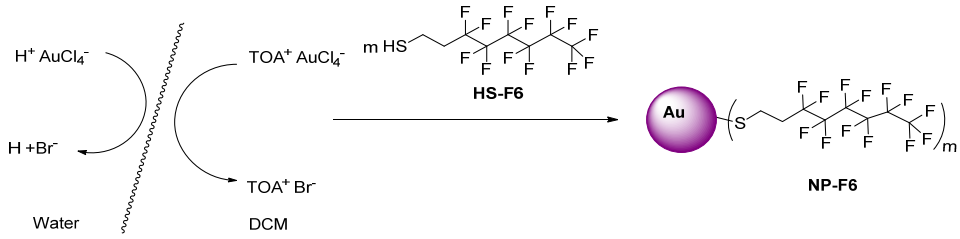

Scheme 3.4 Synthesis of **NP-F6**.

As presented in Table 3.1, we have synthesized **NPs-C16/F6** with loadings of the fluorinated thiol into the monolayer varying from 2.6% to 80.4%. In order to complete this

study, we aim at determining the chemical shift of the peaks of the nanoparticles at 100% of the fluorinated ligand into the monolayer. For this purpose, we synthesized **NP-F6** (Scheme 3.4) which are nanoparticles protected only by **HS-F6**. *A priori* we have indentified two main problems which can appear during the synthetic process. The first one is the low solubility of these nanoparticles in common organic solvents, as already reported in literature.[8] Due to this behavior, **NP-F6** synthesized in solvents like toluene, chloroform or dichloromethane are expected to precipitate. The precipitation of the nanoparticles during the growth of the gold core produces polydisperse samples. A theoretical solution to this problem could be the use of fluorinated solvents for the synthesis, avoiding in this way the precipitation, but introducing together with this a lot of impurities present into fluorinated solvents. The second problem which derives from the first one could be the difficulty to purify these nanoparticles due to the intercalation between the chains of the monolayer of other small species present into the reaction mixture (Figure 3.11) which remain entrapped.

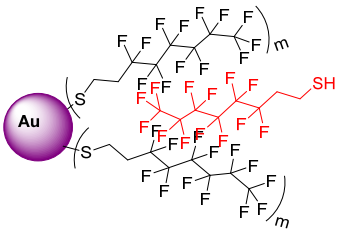

Figure 3.11 Intercalation of free **HS-F6** into the monolayer of **NP-F6**.

Following the Brust-Schiffrin method for the preparation of the NPs there are two species which can give this kind of problems: the tetraoctylammonium bromide and the free fluorinated ligands. Since the TOAB can be removed by repeated precipitations of the nanoparticles with a polar solvent, the presence of free thiol into the monolayer is more difficult to remove. The presence of free thiol or small organic compounds can be identified from the ^{1}H NMR experiments. When small molecules are in the presence of nanoparticles, the ^{1}H NMR spectra show broadened peaks for the nanoparticles and sharp peaks for the impurities.

For the synthesis of these nanoparticles, a solution of 2.5 Equiv. of TOAB in DCM was added to an aqueous solution of tetrachloroauric acid (2.5 Equiv.) and the mixture was let to stir for 15 minutes while was seen the shading of the aqueous phase and the coloration of the organic one. At this point the solution of thiol or thiolate (previously prepared by adding NaOMe to the **HS-F6** and let to stir for 1h) (See Table 3.2) was added and the color turned

[8] Dass, A.; Guo, R.; Tracy, J.; Balasubramanian, R.; Douglas, A.; Murray, R. *Langmuir* **2008**, 24, 310 – 315.

from deep to pale orange. At the mixture a freshly prepared solution of $NaBH_4$ was added at 0 ºC or room temperature using different addition times as reported in Table 3.3. The mixture was let to stir overnight. Samples **NP-F6-a** and **NP-F6-b** were not precipitated, but in the other cases a black precipitate was formed.

The nanoparticles which were not precipitated during the synthesis, were washed with brine and methanol was added in order to precipitate them. At this point we have taken off the supernatant and the precipitate was soluble in dichloromethane, chloroform and toluene and less soluble in acetone and methanol. These solubility properties suggest that our assumptions were correct and there is an intercalation process which makes difficult the purification process.

Table 3.2 Synthetic details for the synthesis of **NP-F6**.

Sample	Ratio Au/thiol	Time of addition $NaBH_4$	Temperature of addition (ºC)	Solvent	Activation of thiol
NP-F6-a	3/1	3'40''	0	Dry deoxygenated toluene	yes
NP-F6-b	3/1	3'40''	0	toluene	no
NP-F6-c	4/1	5''	r.t.	DCM	no
NP-F6-d	6/1	5''	r.t.	DCM	no
NP-F6-e	3/1	35'	r.t.	DCM	no

At this point, all samples of nanoparticles were washed six times with acetone, then ten times with DCM, but a part of the material was lost because was soluble in the solvent. After the purification process, differences in the solid color were observed: **NP-F6-b** and **NP-F6-d** appear as a yellow solid but for the other two samples the precipitate was black. In order to achieve NMR spectra, we tried to dissolve the samples in mixture of C_6F_6 and $CDCl_3$, but only **NP-F6-a**, **NP-F6-c** and **NP-F6-e** were soluble, suggesting that the yellow color obtained for the other two samples was an indication of the failure of the synthesis.

From TEM images of **NP-F6-a** (Figure 3.12) we could observed that the dimension of the gold core is smaller respect to what was expected and this can be due to the bulkiness of the fluorinated thiol respect to hydrogenated one because bulky thiols tend to favor the formation of smaller nanoparticles.[9]

[9] R. S. Ingram, M. J. Hostetler and R. W. Murray, *J. Am. Chem. Soc*. **1997**, 119, 9175−9178

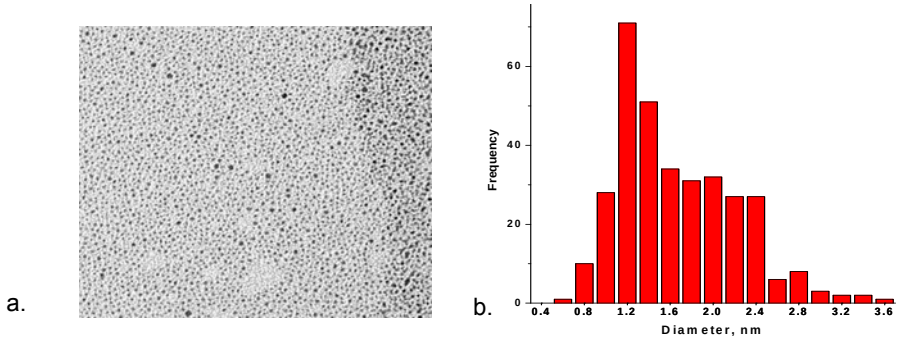

Figure 3.12 a) TEM image and b) size histogram of **NP-F6-a**.

For this reason we increased the ratio between gold and thiol to 4/1 and 6/1 but we didn't obtain bigger nanoparticles. Additionally, was observed that using a Au/thiol ratio of 6/1, **NP-F6-d** have formed aggregates.

At this point we tried to obtain bigger nanoparticles by increasing the addition time of $NaBH_4$ from 5 seconds to 35 minutes in order to allow to the nanoparticles to growth. A small difference between the gold core of **NP-F6-a** and **NP-F6-e** was observed.

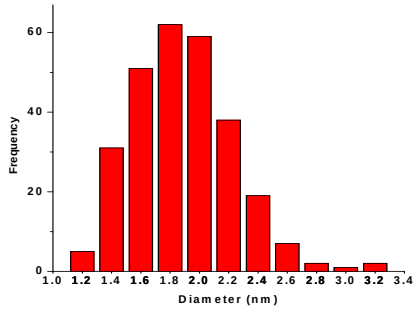

Figure 3.13 Size histogram of **NP-F6-c**.

With reference to a previously reported procedure[6,11] in which AuNPs protected by **HS-C12** with a gold core diameter around 3 nm were obtained by heat treatment of small nanoparticles, we tried to use the same procedure for perfluorinated NPs in order to increase the gold core diameter of **NP-F6-e** using heat ripening. For this purpose, three procedures were experimented: a) a sample of crude **NP-F6-e** (without washes) was dried and heated at 150 ºC for 30 minutes with a heating rate of 2 ºC/minute. At this point, the solid was dissolved in trifluorotoluene obtaining a brown solution, with no visual evidences of the core size increase and we let the sample to stir after addition of a small amount of **HS-F6**. The explanation for this result could be the absence of TOAB which acts like a solvent in the ripening process. Trying to overcome this problem, two additional procedures

were tried. First, a small quantity of TOAB was added to the previously obtained solution and the solvent was evaporated to dryness. Then the sample of nanoparticles was heated using the same conditions reported before. In the second approach, the TOAB was added to the solid state nanoparticles **NP-F6-e** before the heat treatment. After the ripening process, both solids were dissolved in trifluorotoluene and let under stirring for one night.

Then both samples resulted from the ripening trials were washed with brine and ten times with methanol. After the purification process, only the first sample of nanoparticles was soluble in C_6F_6, the other one is not soluble in any solvent. From TEM images of the first sample can be seen that only a slight increase of the dimension of the gold core (Figure 3.14) was observed suggesting that in this case the ripening process was not successful. We suppose that this problem is due to the fact that these nanoparticles are not soluble in melt TOAB during the ripening process and for this reason they are not able to grow.

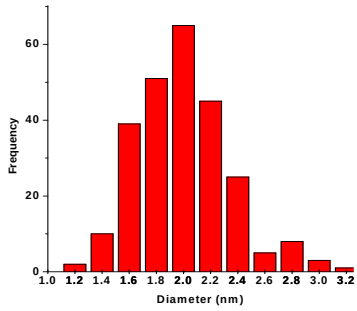

Figure 3.14 Size histogram of **NP-F6-a** after the heat treatment.

We rationalized that a possible solution to this problem could be the use of fluorinated phase transfer agents with a melting point which allow the increasing of the nanoparticles size and also the use of fluorinated solvents for the synthesis to not allow the precipitations of the **NP-F6**, but we realized that this approach will have produced very impure nanoparticles.

In fact, analysing the ^{1}H-NMR and ^{19}F-NMR spectra (Figure 3.15) of these samples the signal of several impurities can be seen concluding that they are not very clean, but it should be considered that part of the impurities are due to the fluorinated solvents used to dissolve the samples.

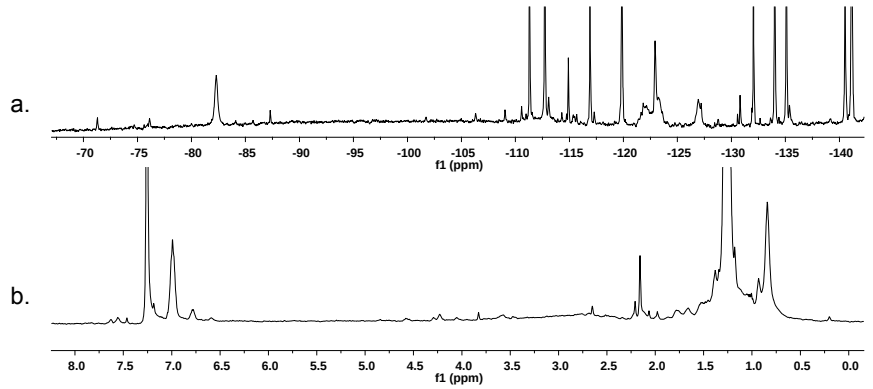

Figure 3.15 a) ^{19}F-NMR (470 MHz, $CDCl_3/C_6F_6$) and b) ^{1}H-NMR (500 MHz, $CDCl_3/C_6F_6$) of **NP-F6-a**.

From these experiments we can conclude that it is difficult to obtain nanoparticles **NP-F6** bigger than 2 nm using a two phase Brust-Schiffrin method. This is probably due to the fact that the dimension of the gold core depends on the ratio between Au/thiol and **HS-F6** is more bulkier respect to the hydrogenated alkanethiolates and, therefore, a smaller number of thiols is sufficient to protect the surface of the gold core. In conclusion, the CF_3 and CF_2 chemical shifts in the ^{19}F NMR reported in the next section have been measured on **NP-F6-c** with a core diameter of 1.6 nm.

3.1.1.4. Study of the chemical shift of NPs-C16/F6 as a function of the monolayer composition

We analysed the ^{19}F NMR spectra obtained for all samples of nanoparticles reported in Table 3.1 and we plotted the chemical shift of the CF_3 and CF_2 groups as a function of the percentage of the fluorinated ligand into the monolayer. As previously discussed, the chemical shift of the nanoparticles which are soluble in mixtures of $CDCl_3$ and C_6F_6 was corrected by the contribution of the solvent. The results obtained are presented in Figure 3.16.

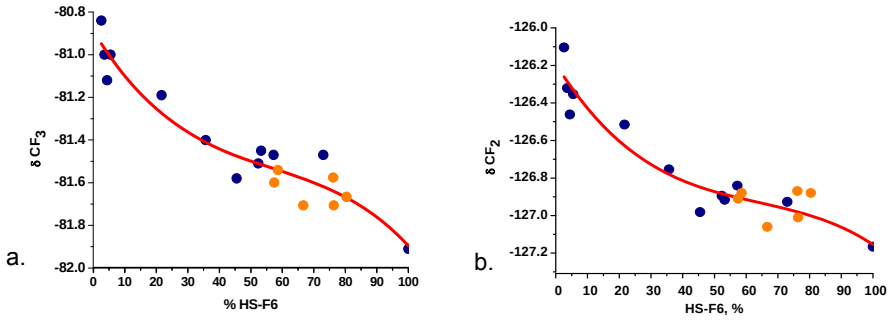

Figure 3.16 Representation of the ^{19}F chemical shift of the a) CF_3 and b) CF_2 groups as a function of the ligand composition of **NP-C16/F6**.

As it was observed in previous experiments (Figure 3.10), the solvent composition has a smaller influence on the chemical shift of the peak corresponding to CF_2 groups respect to that of the CF_3 groups. For this reason, our initial suppositions were that the variation of the chemical shift of CF_3 and CF_2 groups as a function of the loading of the fluorinated thiol into the monolayer will be different. At the contrary, even though the CF_3 group is more exposed to the solvent respect to the CF_2 group, the variation of the chemical shift of these groups as a function of the monolayer composition is similar (Figure 3.16). These results further support that the chemical shift variations reported here are not a consequence of the variation of the solvent composition but, instead, result of a different organization of the monolayer. As can be seen in the graphs of Figure 3.16, at percentages of the fluorinated ligand lower than 40% a linear decay was obtained, suggesting that increasing the amount of fluorinated ligand into the monolayer these species experiences very different chemical surroundings. In the region between 40% and 80% the chemical shift of the CF_3 group is less sensitive to the composition of the monolayer, indicating that the thiolate **F6** experiences very similar surroundings even though the percentage of the fluorinated ligand into the monolayer increases. When more than 80% of the **F6** thiolate is introduced in the monolayer, the chemical shift of the terminal CF_3 group becomes again sensitive to the influence of the neighboring thiols.

An interesting solubility behavior was observed at higher percentages of the fluorinated ligand into the monolayer, where two set of signals can be individualized. The orange points represent samples that are soluble only in mixtures of $C_6F_6/CDCl_3$ and the blue points are nanoparticles soluble in only chloroform. It can be observed that the orange points have a blu ‘‘twin’’ point in terms of the percentage of the fluorinated ligand into the monolayer, these points belong to nanoparticles having the same composition of the monolayer but displaying different solubility properties. These solubility characteristics can be due to a diverse organization of the monolayer or, more likely, by different arrangement of the thiols

on the surface of the metal core, maintaining the same morphology. To analyze these different possibilities, the samples were subjected to thermal treatment. If the organization of the monolayer was not at equilibrium, we reason that the heat treatment could help in reaching the final stable organization. At the contrary, if the morphology attained represents a thermodynamic equilibrium state, the heating process will not induce reorganization.

We have used for this investigation two samples of nanoparticles having the same composition of the monolayer but different solubility properties: one soluble only in $CHCl_3$, **NP-C16F6-j(C)** and another one soluble in hexane, **NP-C16F6-j(H)**. The nanoparticles were dissolved in $CHCl_3$ and hexane respectively and kept at 60 ºC for 4 hours. After this time, the solvent was removed, then the nanoparticles were redissolved in chloroform (**NP-C16F6-j(C)**) or in a mixture 1.25/1 of $CDCl_3/C_6F_6$ (identical with the solvent composition used to dissolve the nanoparticles before the heat treatment for **NP-C16F6-j(H)**). The ^{1}H- and ^{19}F-NMR spectra of the samples before and after thermal treatment were identical (Figure 3.17).

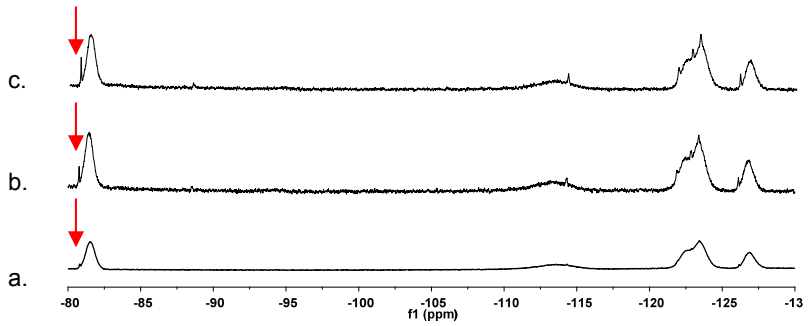

Figure 3.17 ^{19}F NMR (470 MHz, $CDCl_3$) of **NP-C16F6-j(C)** a) before heat treatment; b) after 2 h, 60 °C; c) after 4 h, 60 °C. Red arrows indicate the appearance of a sharp peak in the spectrum of nanoparticles.

Two main conclusions can be drawn from this analysis: firstly, we can conclude that after the heat treatment using the procedure reported above, the nanoparticles didn't change their NMR response and since the chemical shifts of nanoparticles depend on the organization of the monolayer, it can be concluded that the monolayers didn't changed their morphology. This means that the organization of the monolayer is sufficiently stable and small variations of the experimental conditions or storage method have no influence on the morphology of the monolayer. From this preliminary data results that no modifications happen during the NMR experiments considering that they are realized at 25 ºC and the samples stored at 4 ºC. Secondly, in the NMR spectra the appearance of sharp peaks corresponding to the free unbound species could be observed, suggesting that during the heat treatment the thiolates detach from the surface of the gold core and free ligands

remain after the heating.

In order to confirm that the corrections regarding the influence of the solvent on the chemical shift of the nanoparticles are correct, we made another study: we added C_6F_6 to a sample of nanoparticles soluble in $CHCl_3$ only (the percentage of added C_6F_6 was the same used for **NP-C16/F6** which have the same composition, but are not soluble in $CHCl_3$), we measured the chemical shift of the peaks of the nanoparticles and we corrected the crude chemical shift considering the influence of the solvent mixture. If our considerations were correct then the chemical shift of the nanoparticles dissolved only in $CHCl_3$ or in the mixture $C_6F_6/CDCl_3$ should be the same. For this purpose, we have chosen two samples of nanoparticles soluble in $CHCl_3$: **NP-C16F6-j(C)** and **NP-C16F6-h(C)** having 52.38% and 57.26% of fluorinated ligand into the monolayer respectively. We dissolved these samples in $CDCl_3$ only and in a solvent mixture containing 12.5 % and 37.5 % respectively of C_6F_6. We have performed ^{19}F NMR experiments and we have measured the chemical shift of the CF_3 group. By comparing the chemical shift of the CF_3 group obtained for **NP-C16F6-j(C)** and **NP-C16F6-h(C)** in $CDCl_3$ and the chemical shift of these samples when we have added C_6F_6 (calculated considering the influence of the solvent composition) we have obtained the same value. These results clearly show that our considerations for the corrections of the influence of the solvent composition on the chemical shift of the peak of the nanoparticles are consistent with the real situation.

3.1.1.5. Multiscale molecular simulations

Multiscale molecular simulations have been carried out in collaboration with dott. P. Posocco of the Molecular Simulation Engeneering Laboratories (MOSE) of the University of Trieste, in order to predict the mixed – monolayer organization of protected gold nanoparticles. Briefly, an *ad hoc* multiscale molecular modeling was developed which consist in using the informations obtained at lower level simulations (atomistic molecular dynamic (MD) simulations) to parameterize mesoscale dissipative particle dynamic (DPT) that incorporate the essential physics/phenomena observed at the finer level. Accordingly, the lattice of Au model is faced centered cubic (fcc), but also eicosahedral. Practically, the technique consist in simulating the interface between the gold surface, the ligands and the solvent by building a cell which is ‘’streched’’ along the c-direction. For our studies, considering that some nanoparticles are soluble in $CHCl_3$ and others only in presence of C_6F_6, multiscale molecular simulations have been realized choosing as solvent both $CHCl_3$ and C_6F_6.

This method has been validated by applying it *in toto* to a well known system consisting in AuNPs protected by a mixture of mercaptoundecanesulfonate (MUS) and octanethiol (OT) in a 2:1 ratio.

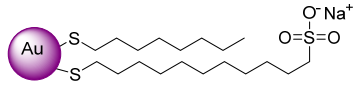

Figure 3.18 NP-OT/MUS.

This type of mixed monolayers has been intensively studied and STM data of these nanoparticles suggest a stripe organization of the two ligands on the surface of the gold core as shown by Stellacci.[10] Moreover, the reliability of this approach was also demonstrated by the fact that the average height found for the ripple domains (0.8 - 0.9 nm) was also comparable with the experimentally estimation (1 ± 0.2 nm).

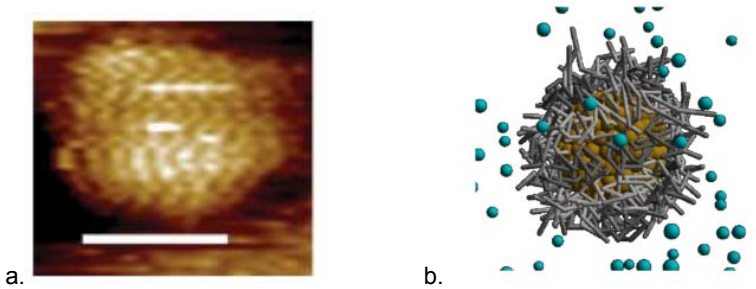

Figure 3.19 a) Experimentally obtained STM images for AuNPs-MUS/OT 2:1 and b) Rippled morphology predicted using multiscale molecular simulation approach in the presence of water like solvent. Legend of the colors: brown, gold core; light grey, OT; dark grey, MUS; turquoise, water molecules.[10]

Considering the innovation of this new molecular simulation protocol this was applied on **NPs-C16/F6** to gain more information about the organization of the monolayer involving hydrogenated and fluorinated ligands. The results are presented for two examples of nanoparticles in Figure 3.20.

NP-C16/F6-e
$Au_{976}HT_{147}F_{42}$
21.7% **F6**

NP-C16/F6-j(C)
$Au_{475}HT_{71}F_{96}$
57.26% **F6**

Figure 3.20 Multiscale molecular simulations of **NP-C16/F6** (dark blu-C16; turquoise-F6).

[10] Uzun, O.; Hu, Y.; Verma, A.; Chen, S.; Centrone, A.; Stellacci, F. *Chem. Commun*. **2008**, 196-198.

As it can be seen, the simulations have revealed that the two ligands organize in stripes on the surface of the gold core, even when 20 % of the **F6** thiolate is present in the monolayer. In this case, the gain in entropy due to the difference in length and the immiscibility of hydrogenated and fluorinated ligands are sufficient to overcome the loss of van der Waals interactions between the hydrogenated alkyl chains. These results are in perfect agreement with the previously reported data about the organization of the mixed monolayer composed of a mixture of hydrogenated and fluorinated thiols having different length.[3]

The striped organization explains why some samples of **NP-C16/F6** are soluble in chloroform even at higher percentages of the fluorinated ligands into the monolayer (around 80%). The fluorinated ligands are masked by the longer hydrogenated ones and in this way the solvent does not interact with the fluorinated domains. The results revealed by multiscale modeling are consistent also the behavior of the curve representing the chemical shift of the peaks of the fluorinated thiolates as a function of the monolayer composition. At percentages of the **F6** lower than 50 %, a linear decay of the chemical shift was observed, suggesting that the local composition of the environment surrounding the fluorinated thiols changes even when small variations in the monolayer composition occur. This is explained by the fact that increasing the number of fluorinated ligands into the monolayer, stripes with different sizes are formed and for this reason the interface surface area change rapidly. Once the stripes are formed, the subsequent addition of more fluorinated ligands did not influence the number of thiolates at the interface. The incoming thiols enter inside a previously formed fluorinated stripe. At percentages of the fluorinated thiolate higher than 80% another decrease of the chemical shift of the CF_3 group was observed because at this level, the hydrogenated thiolates are in minority.

These interesting results have encouraged us to continue the study of this class of nanoparticles, protected by ligands with different length. A useful point could be to find the minimum length mismatch between the two ligands necessary to obtain striped organization on the surface of the gold core. For this purpose, we maintained the same fluorinated ligand (**HS-F6**) used for the synthesis of previous nanoparticles, but the hydrogenated thiol was shorter (**HS-C12** *vs.* **HS-C16**), with a length mismatch between the two ligands of only four carbon atoms instead of eight.

3.1.2. Synthesis of NP-C12/F6

For the synthesis of this type of nanoparticles we have chosen a place exchange reaction method. Briefly, small **NP-C12** were obtained using a two phase Brust-Schiffrin method, heat treated in order to increase the dimension of the gold core and used in the place exchange reaction with fluorinated thiols (Scheme 3.5)

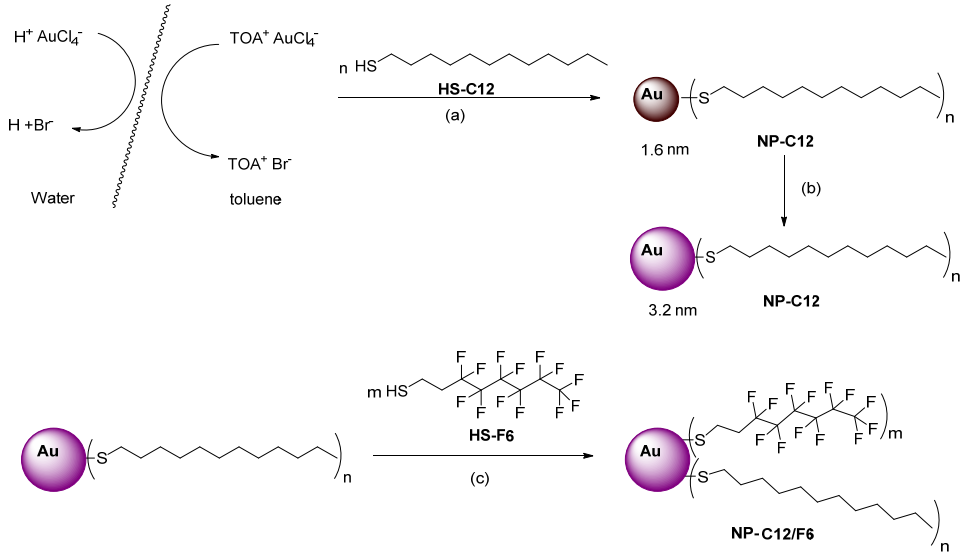

Scheme 3.5 Synthesis of **NP-C12/F6** by place exchange reaction: a) Synthesis of **NP-C12**; b) heat treatment of **NP-C12** and c) Place exchange reaction of **NP-C12** with **HS-F6**.

3.1.2.1. Synthesis of monodisperse NP-C12

Dodecanthiol-protected gold nanoparticles (**NP-C12**) were synthesized in a two phase reaction (toluene/water). The $AuCl_4^-$ ions (1 Equiv.) were transferred to the organic phase using 2.5 Equiv. of a surfactant (TOAB). At this point the yellow aqueous phase became colorless and the colorless organic phase turned orange. Then, 3 Equiv. of **HS-C12** were added and the solution fades. After the addition of a freshly prepared $NaBH_4$ aqueous solution (11.4 Equiv.), the organic phase turned dark brown due to the reduction of gold species to Au (0). After 18 h, in the UV-VIS spectrum of the brown solution can be observed a weak surface plasmon absorbtion at around 520 nm, suggesting the formation of quite small nanoparticles (Figure 3.21). To evolve the size of the **NP-C12**, the crude solid prepared,[11] by evaporating toluene, is then heated at 150 ^oC at a heating rate of 2 ^oC/min and held for 30 minutes at the maximum temperature. After this process a change in color from brown to violet can be observed (Figure 3.21).

[11] Shimizu, T.; Teranishui, T.; Hasegawa, S.; Miyake, M. *J. Phys. Chem. B* **2003**, 107, 2719 – 2724.

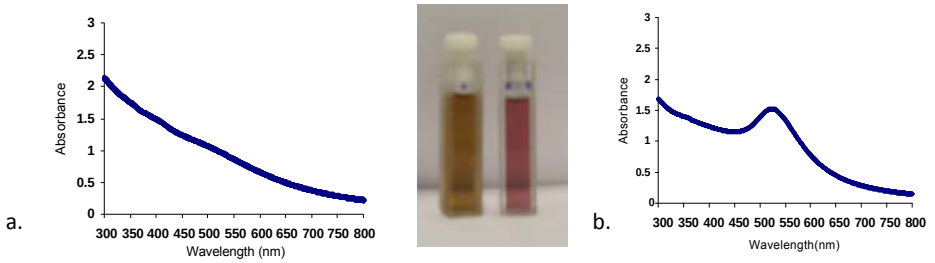

Figure 3.21 UV-VIS spectra of **NP-C12** a) before and b) after heat treatment.

The UV-VIS spectra shown the appearance of a surface plasmon band at around 520 nm after the heat treatment. This is an indication of the fact that the gold core diameter is bigger than 3 nm, in fact this was demonstrated by TEM images (Figure 3.22). The main diameter was found to be 3.2 nm with a standard deviation of 0.4 nm.

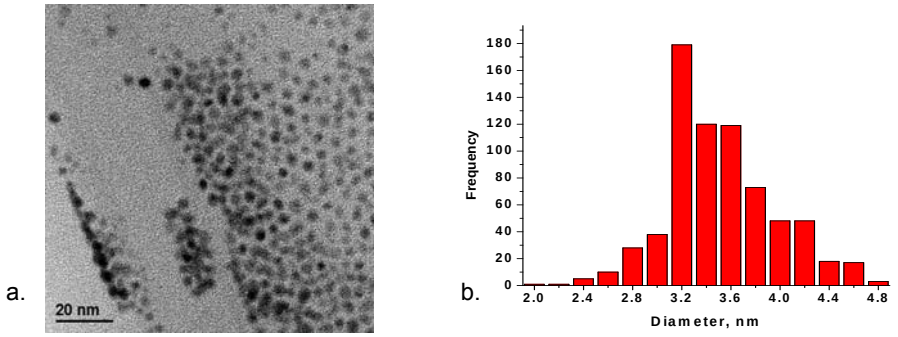

Figure 3.22 a) TEM images and b) size histogram of **NP-C12**, precursor of **NP-C12/F6**.

Previous data suggest that the heat treated nanoparticles form aggregates after few days which can be explained by the fact that during the heat treatment some of the thiols come off the gold core and a part of the core surface remain unprotected. For this reason, these nanoparticles were put in the presence of another one equivalent of **HS-C12** and let to stir in toluene for 18 h. Then the solvent was removed under reduced pressure, the nanoparticles were dissolved in chloroform and transferred in two centrifuge tubes. They were washed with methanol (7 x 20 mL, 10 minutes, 4000 rpm, 20 °C) and acetone (7 x 20 mL) followed by decanting of the supernatant solution. The solvent was removed under argon and ^{1}H-NMR spectra prove the absence of –S-S- bounds and clean nanoparticles were obtained. Using this method, monodisperse AuNPs are obtained with a gold core diameter of 3.2 nm and a standard deviation of 0.4 nm, as can be seen in Figure 3.22 which presents the TEM histogram of one sample of **NP-C12**.

3.1.2.2. Synthesis of NP-C12/F6

The previously obtained **NP-C12** have been dissolved in deoxygenated DCM and then different quantities of **HS-F6** were added in order to obtain mixed monolayers nanoparticles with various final ratios **C12/F6** (see Experimental part, Table 3.9). The reaction was let to stir for three days at 40 ºC. Then the nanoparticles were purified by precipitations and washes with MeOH. The dimension of the gold core, the final composition of the monolayer and the solubility properties are reported in Table 3.3.

Table 3.3 Characterization data of nanoparticles **NP-C12/F6**, obtained by place exchange from **NP-C12**.

Nanoparticles	Diameter[a] (nm)	Composition[b]	X_{F6}[c]	Solubility Score[d]	% C_6F_6 added[e]
NP-C12/F6-a	3.4 ± 0.4	$Au_{1340}(C12)_{213}(F6)_{26}$	0.106	1	0
NP-C12/F6-b	3.3 ± 0.3	$Au_{1310}(C12)_{210}(F6)_{30}$	0.125	1	0
NP-C12/F6-c	3.4 ± 0.6	$Au_{1340}(C12)_{208}(F6)_{30}$	0.126	1	0
NP-C12/F6-d	3.2 ±0.4	$Au_{1289}(C12)_{194}(F6)_{35}$	0.154	1	0
NP-C12/F6-e	3.2 ±0.3	$Au_{1289}(C12)_{190}(F6)_{35}$	0.156	1	0
NP-C12/F6-f	3.3 ±0.6	$Au_{1340}(C12)_{174}(F6)_{40}$	0.188	1	0
NP-C12/F6-g	3.2 ± 0.4	$Au_{1289}(C12)_{185}(F6)_{46}$	0.200	1	0
NP-C12/F6-h	3.8 ±0.3	$Au_{2267}(C12)_{232}(F6)_{68}$	0.227	1	0
NP-C12/F6-i(C)	3.6 ±0.6	$Au_{1830}(C12)_{197}(F6)_{73}$	0.270	1	0
NP-C12/F6-i(H)	3.6 ±0.6	$Au_{1830}(C12)_{180}(F6)_{100}$	0.357	0.5	26.6
NP-C12/F6-j	3.6 ±0.6	$Au_{1830}(C12)_{209}(F6)_{85}$	0.286	1	0
NP-C12/F6-k(C)	3.6 ±0.6	$Au_{1830}(C12)_{206}(F6)_{86}$	0.294	1	0
NP-C12/F6-k(H)	3.6 ±0.6	$Au_{1830}(C12)_{184}(F6)_{123}$	0.400	0.5	26.6
NP-C12/F6-l	2.5 ±0.7	$Au_{488}(C12)_{81}(F6)_{48}$	0.370	1	0
NP-C12/F6-m	3.2 ±0.8	$Au_{1289}(C12)_{123}(F6)_{112}$	0.478	0	26.6
NP-C12/F6-n	3.0 ±0.8	$Au_{976}(C12)_{74}(F6)_{108}$	0.600	0	60
NP-C12/F6-o	3.1 ±0.4	$Au_{1200}(C12)_{73}(F6)_{160}$	0.720	0	62.5

[a] Average diameters and standard deviation obtained by analysis of a population of at least 300 particles. [b] Calculated on the basis of the TGA and TEM and ^{1}H NMR analyses of decomposed nanoparticles. [c] Molar fraction of the fluorinated ligand in the monolayer of nanoparticles **NP-C12/F6** determined by ^{1}H NMR analysis of decomposed nanoparticles. [d] The solubility scores are defined arbitrarily as follows: score 1 is assigned to nanoparticles fully soluble in chloroform; score 0.5 is assigned to nanoparticles fully soluble in hexane; score 0 is assigned to nanoparticles fully soluble in hexafluorobenzene. [e]Percentage of C_6F_6 in the mixture $CDCl_3/C_6F_6$ used to solubilize the nanoparticles for NMR experiments.

The ^{1}H-NMR analysis supports (Figure 3.23) the efficacy of the purification process, because the nanoparticles are very clean and no sharp peaks corresponding to free thiols were observed.

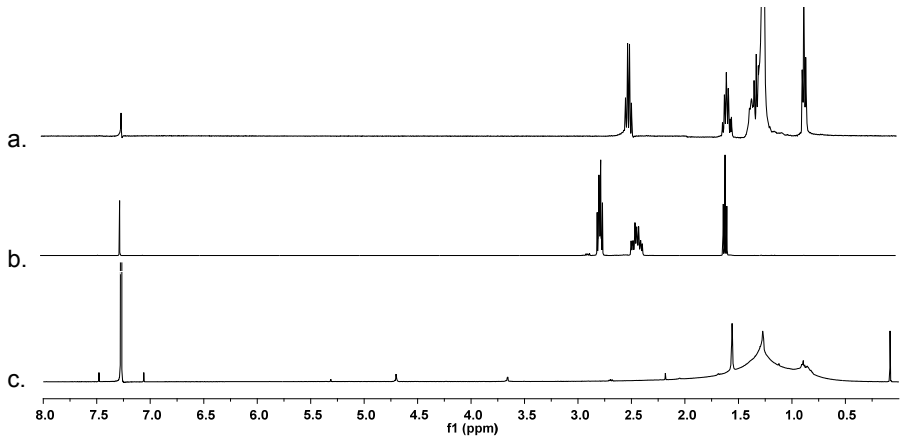

Figure 3.23 ^{1}H NMR (500 MHz, $CDCl_3$) of a) **HS-C12**; b) **HS-F6**; c) **NP-C12/F6-d**.

The final ratio between the two ligands has been obtained by decomposition of at least 1 mg **NP-C12/F6** in the presence of an excess of iodine. Then the solvent and iodine were evaporated at room temperature and the ratio between the thiolates determined from the integration of the signals pertaining to the methylene groups in the alpha position to the sulphur atom. The relationship between the initial ratio between the two ligands and the final ratio obtained after the decomposition of the monolayer will be further discussed in Chapter 3.4. For the dimension of the gold core we have realized TEM analysis of the precursor **NP-C12** because it was verified that the dimension of the gold core did not change during the place exchange reaction and consequently, the diameter of **NP-C12/F6** is identical with the dimension of the nanoparticles used as precursor.

As can be seen in Table 3.3, at higher loadings of the fluorinated ligand into the monolayer, the nanoparticles are no longer soluble in $CHCl_3$ and for this reason we have used mixture of hydrogenated and fluorinated solvents ($CDCl_3/C_6F_6$) to dissolve them. Precedent experiments on **NP-C16/F6** suggest that the peaks of nanoparticles shift as a function of the solvent composition and for this reason some corrections of the crude NMR response are needed in order to obtain the real chemical shift. This is the reason why we have investigated how the peak of the nanoparticles depends on the solvent composition (Figure 3.24). For this study, we dissolved **NP-C12F6-f** in $CHCl_3$ and we have added increasing amounts of C_6F_6 into the solvent mixture. We have measured the position of the maxima of the peaks corresponding to the CF_3 and CF_2 groups. Plotting the chemical shift of the delta chemical shift (defined as difference between the chemical shift of nanoparticles at a certain percentage of C_6F_6 into the solvent mixture and the chemical shift of nanoparticles when no C_6F_6 was added) of CF_3 and CF_2 groups of the nanoparticles, we

have obtained the graph reported in Figure 3.24.

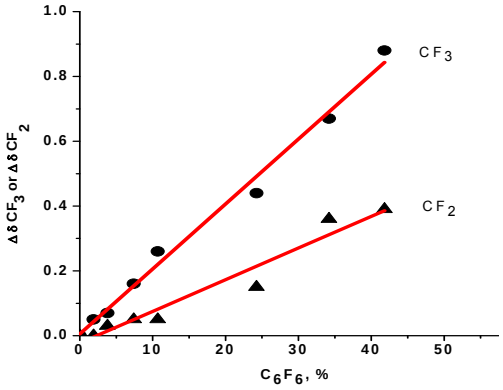

Figure 3.24 Influence of the solvent composition on the chemical shift of CF_3 (circles) and CF_2 (triangles) groups of the nanoparticles.

This graph demonstrates that the shift of the CF_3 and CF_2 bands of the nanoparticles change linearly with the addition of C_6F_6. The influence of the solvent composition on the chemical shift of the CF_2 group is less pronounced with respect to that of the CF_3 group. This is reasonable because the CF_3 group is more exposed to the solvent respect to CF_2. Taking into account these contributions of the solvent mixture, we have further corrected all the chemical shifts of the nanoparticles soluble in mixtures of hydrogenated and fluorinated solvents, the other ones being reported as obtained from the NMR spectra.

For all the nanoparticles reported in Table 3.3 ^{1}H- and ^{19}F-NMR experiments were performed and the chemical shifts of the CF_3 and CF_2 groups were plotted as a function of the ligand composition. It has to be mentioned that the peak at 100% loading of the fluorinated thiolates was obtained by measuring the chemical shift of CF_3 and CF_2 groups of **NP-F6-a** (Figure 3.15). The obtained results are presented in Figure 3.25.

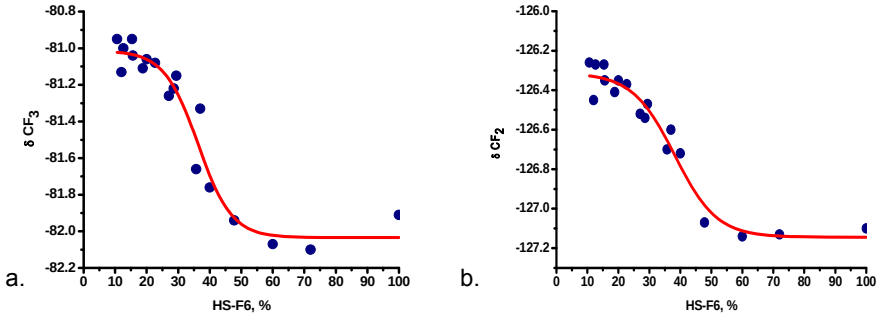

Figure 3.25 Chemical shift of a) CF_3 and b) CF_2 groups as a function of the percentage of the fluorinated ligand into the monolayer of **NP-C12/F6**.

As it can be seen, for **NP-C12/F6** a sigmoidal behavior was obtained which is very different with respect to that obtained for **NP-C16/F6** even though both types of nanoparticles are protected by ligands having different length. In this case plateau region was found until the 25% of fluorinated thiolate was introduced in the monolayer; this trend is followed by a sudden decrease of the chemical shift with a small increase of **F6** introduced into the monolayer. At higher percentages, a plateau region is observed up to the 100% **F6**. This can be an indication of the fact that at lower and higher loadings of **F6** there is no marked difference in the surroundings of the fluorinated thiol at the interface and a similar NMR response is obtained. This can be true only if in this interval of composition identical regions are gradually formed and this does not influence the overall ratio between thiols at the interface and thiols inside these regions. When the loading of the fluorinated thiols arrive to 50%, there is a steep decrease of the chemical shift suggesting that the thiols experiments very different surroundings with a small variation of the composition.

In order to gain more informations about the morphology of this second type of mixture of ligands multiscale molecular simulations were realized using the same approach presented above. The images obtained for some selected samples are presented in Figure 3.26.

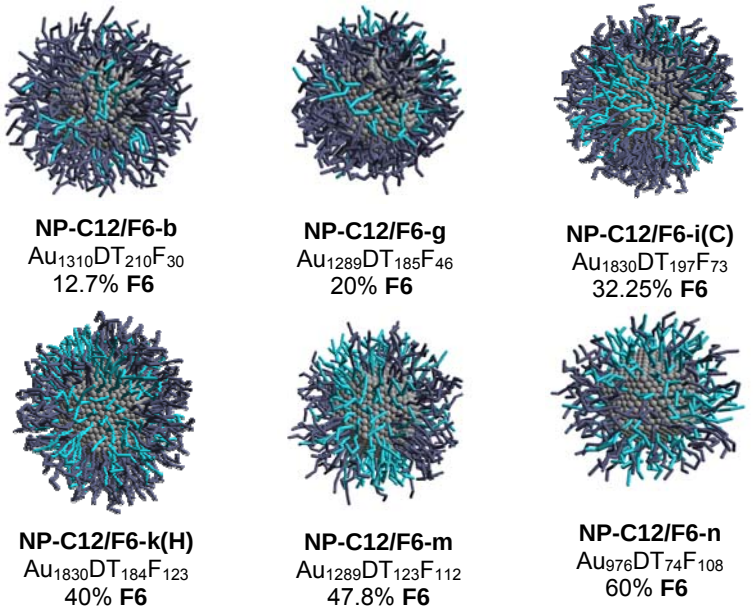

Figure 3.26 Multiscale molecular simulations of some selected **NP-C12/F6** (dark blu-C12; turquoise-F6).

As can be seen from these images, the nanoparticles do not present an ordered organization of the monolayer, in some case are formed stripes, but in the most cases irregular patches are observed. Initially, at 10-15 % of the fluorinated ligands into the monolayer, they are forming very small patches formed by 5-6 fluorinated chains or isolated thiolates are present. When the loading of **F6** increase to 30%, elongated patches or even stripes are observed. This is also the composition where the decrease of the chemical shift for the CF_3 and CF_2 groups of **F6** starts, indicating the generation of different environments around the fluorinated ligands. At percentages higher than 40% of the fluorinated ligand, the shape of the domains became irregular, with a transition between stripes and defined domains. After 60% of the fluorinated thiol, the chemical shift of the CF_3 group becomes insensitive to any further variation of composition, suggesting no important changes in the neighboring environment.

From these experiments we can conclude that the length mismatch of four carbon atoms is not sufficient to create a highly ordered system, but it can be surely stated that the obtained organization is not random. This means that the ligands are able to phase segregate forming domains, but the smaller difference in length is not sufficient to gain the entropy necessary to organize in stripes or regular patches.

From the NMR and simulations experiments realized on nanoparticles protected by ligands having different length, it can be concluded that the difference in length is important

in order to obtain phase segregation of the two ligands on the surface of the gold core. When the mismatch between the two ligands is only four carbon atoms, the gain in entropy at the interfaces is not sufficient to determine an ordered organization of the monolayer and for this reason both irregular patches or stripes are observed in the molecular simulation.

3.2. Synthesis of AuNPs protected by ligands having the same length

The theoretical investigations by S. Glotzer and experimental data reported in literature suggest that mixtures of ligands having the same length form Janus nanoparticles, with the thiolates separated in two big domains on the surface of the gold core. In order to study this kind of systems, AuNPs protected by mixtures of dodecanethiol (**HS-C12**) and 1*H*,1*H*,2*H*,2*H*-perfluordodecanethiol (**HS-F10**), **NP-C12/F10** nanoparticles protected by mixtures of octanethiol (HS-C8) and 1*H*,1*H*,2*H*,2*H*-perfluorooctanethiol (**HS-F6**), **NP-C8/F6** have been synthesized. The nanoparticles **NP-C12/F10** have been synthesized using the place exchange reaction method, while the direct synthesis was used for **NP-C8/F6**.

3.2.1. Synthesis of NP-C12/F10

3.2.1.1. Synthesis of thiol HS-F10

A first attempt for the synthesis of **HS-F10** occurs (Scheme 3.6) via nucleophilic substitution of TrtSH with iodide **A** in the presence of potassium carbonate. The reaction was performed in a mixture of H_2O/EtOH 10:1 and refluxed for 18 h. Then the product was purified using silica gel chromatography, but the trityl derivate was obtained in 47% yield only.

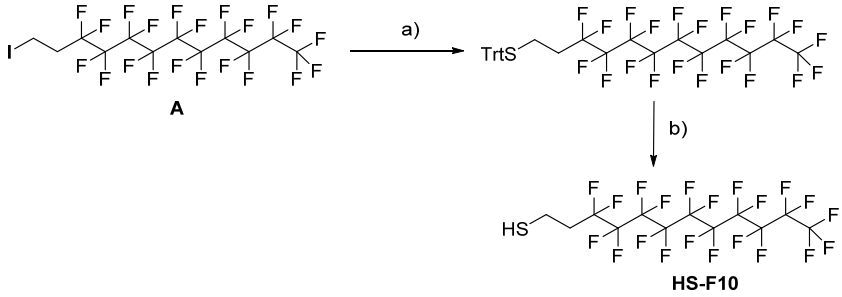

Scheme 3.6 First strategy for the synthesis of **HS-F10**: a) TrtSH, K_2CO_3, EtOH/H_2O, reflux, overnight; b) TFA, TIPS, 2 h.

The low yield pushed us to use a more straightforward procedure, presented in Scheme 3.7, previously reported in literature.[12] Briefly, the iodo-perfluoroalkane derivative **A** was reacted with thiourea in ethanol at reflux overnight forming an *S*-alkyl thiouronium intermediate insoluble in the reaction mixture. The thiol **HS-F10** was obtained as a white solid with a 78% yield.

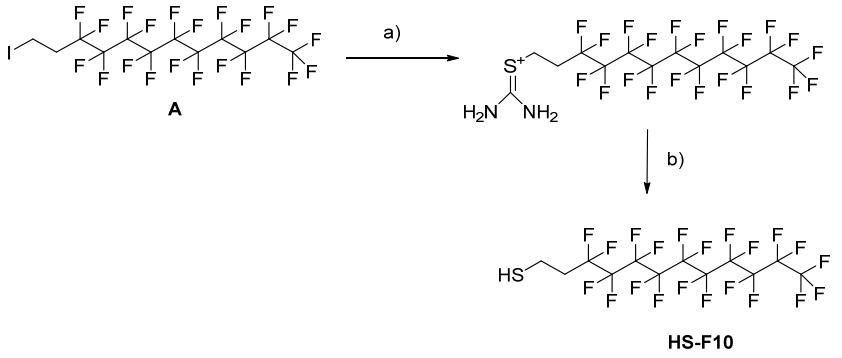

Scheme 3.7 Second strategy for the synthesis of **HS-F10**: a) thiourea, EtOH, 78 ºC; b) KOH, 2 h, HCl.

The thiol **HS-F10** has been characterized by ^{1}H-NMR and ^{19}F-NMR spectra presented in Figure 3.27.

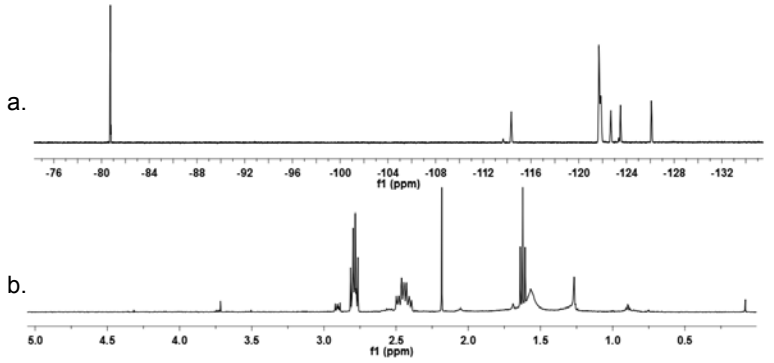

Figure 3.27 a) ^{19}F NMR (470 MHz, $CDCl_3$) and b) ^{1}H NMR (500 MHz, $CDCl_3$) of **HS-F10**.

As expected, the ^{1}H-NMR and ^{19}F-NMR of **HS-F10** are very similar to that of the shorter thiol, **HS-F6** and consequently the assignment of the peaks is very similar to those presented before. Therefore, in the ^{19}F-NMR spectrum, the isolated peak at about -81 ppm corresponds to the terminal CF_3 group (the integration of the peaks in the ^{19}F NMR spectrum shown a ratio 3:2 between this peak and the other ones). From bidimensional

[12] Da Costa, R. C.; Jurisch, M.; Gladysz, *J. Inorg. Chim. Acta* **2008**, 361, 3205 – 3214.

heteronuclear ^{1}H-^{19}F HETCOR experiments it was found that the peak at -114.5 ppm pertains to the CF_2 in position 3. The rightmost peak corresponds to the absorbtion of the CF_2 group in position 7 and other peaks are due to the absorbance of central CF_2 groups.

3.2.1.2. Synthesis of NP-C12/F10

For the synthesis of **NP-C12/F10** we have used the same approach as for **NP-C12/F6**.

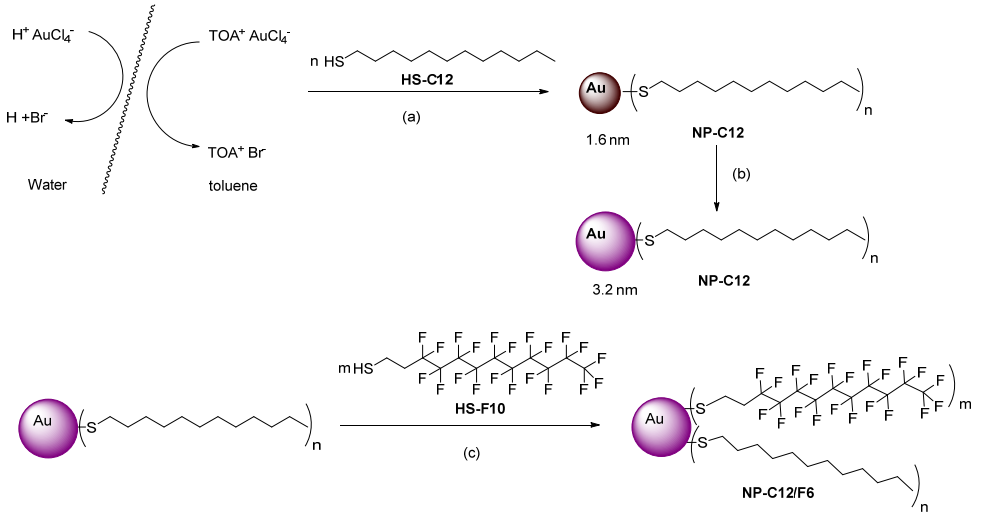

Scheme 3.8 Synthesis of **NP-C12/F10**: a) synthesis of **NP-C12**; b) heat treatment of **NP-C12** and c) place exchange reaction of **NP-C12** with **HS-F10**.

First, we have synthesized small dodecanethiol protected gold nanoparticles using the two phase Brust-Schiffrin method. Then the gold core diameter has been increased by heat treatment, procedure reported by Miyake.[11] At this point, the purified **NP-C12** were dissolved in methylene chloride and different quantities of **HS-F10** (see Experimental part, Table 3.10) were added in various ratios with respect to the **C12** thiolate present into the monolayer in order to obtain **NP-C12/F10** with increasing molar fraction of the fluorinated thiol. The reaction mixture was let to stir for three days at 40 °C. Then the nanoparticles were precipitated with MeOH, centrifuged and purified by repeated washing cycles with methanol. Nanoparticles **NP-C12/F10** with loading of the fluorinated ligand into the monolayer varying from 13.9% to 87.3% have been obtained (Table 3.4).

Table 3.4 Characterization data for **NP-C12/F10**.

Nanoparticles	Diameter[f] (nm)[a]	Composition[b]	X_{F10}[c]	Solubility Score[d]	% C_6F_6 added[e]
NP-C12/F10-a(C)	3.2 ± 0.3	$Au_{1289}(C12)_{194}(F10)_{31}$	0.139	1	0
NP-C12/F10-a(H)	3.2 ± 0.3	$Au_{1289}(C12)_{161}(F10)_{60}$	0.272	0.5	20
NP-C12/F10-b(C)	3.2 ± 0.3	$Au_{1089}(C12)_{187}(F10)_{35}$	0.157	1	0
NP-C12/F10-b(H)	3.2 ± 0.3	$Au_{1289}(C12)_{136}(F10)_{78}$	0.366	0.5	20
NP-C12/F10-c	3.6 ± 0.6	$Au_{1830}(C12)_{176}(F10)_{43}$	0.200	1	0
NP-C12/F10-d(C)	3.6 ± 0.6	$Au_{1830}(C12)_{211}(F10)_{73}$	0.258	1	0
NP-C12/F10-d(H)	3.6 ± 0.6	$Au_{1830}(C12)_{170}(F10)_{112}$	0.400	0.5	33
NP-C12/F10-e	4.0 ± 0.6	$Au_{2406}(C12)_{126}(F10)_{200}$	0.615	0	71
NP-C12/F10-f	3.2 ± 0.5	$Au_{1289}(C12)_{27}(F10)_{186}$	0.873	0	82.8

[a] Average diameters and standard deviation obtained by analysis of a population of at least 300 particles. [b] Calculated on the basis of the TGA and TEM and ^{1}H NMR analyses of decomposed nanoparticles. [c] Molar fraction of the fluorinated ligand in the monolayer of nanoparticles **NP-C12/F6** determined by ^{1}H NMR analysis of decomposed nanoparticles. [d]The solubility scores are defined arbitrarily as follows: score 1 is assigned to nanoparticles fully soluble in chloroform; score 0.5 is assigned to nanoparticles fully soluble in hexane; score 0 is assigned to nanoparticles fully soluble in hexafluorobenzene. [e]percentage of C_6F_6 in the mixture $CDCl_3/C_6F_6$ added to solubilise the nanoparticles for NMR experiments.

The final ratio between the two ligands in the monolayer has been determined after the decomposition of at least 1 mg of nanoparticles with a solution of 4 mg/mL of I_2 for one day. Then the solvent was removed and the ratio **C12**/**F10** ratio was determined by integrating the signals of the methylene protons in the alpha position to the sulphur pertaining to the two disulfides. The dimension of the gold core was obtained from TEM images analysis counting at least 300 nanoparticles. For all these nanoparticles the ^{19}F chemical shifts of the terminal CF_3 and CF_2 groups were measured; before plotting the chemical shift of the CF_3 and CF_2 group as a function of the monolayer composition we have investigated the contribution of the solvent composition to the chemical shift.

For this study we dissolved a sample of **NP-C12/F10-b(C)** with a 5.4/1 ratio between the two ligands and we added to the solvent mixture increasing amounts of C_6F_6. We have measured the maximum of the broad peak corresponding to the nanoparticles signals (Figure 3.28). Both peaks shifted downfield increasing the percentage of C_6F_6 into the solvent mixture as can be seen in the graphs below.

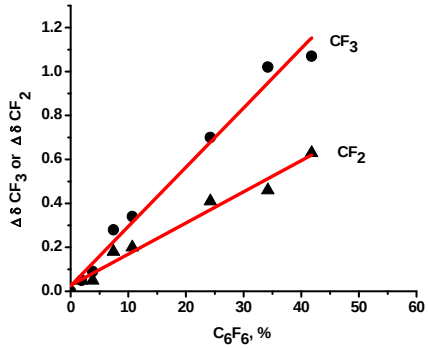

Figure 3.28 The influence of the solvent composition on the chemical shift of CF_3 (circles) and CF_2 (triagles) groups of the nanoparticles.

3.2.1.3. Study of the chemical shift of NP-C12/F10 as a function of the monolayer composition

At this point, we have measured for each sample presented in Table 3.4, the chemical shift of the peaks of the fluorinated ligand present in the monolayer protecting nanoparticles. For the calculation of the real chemical shift, we have considered the contribution of the solvent composition to the shift of the nanoparticles peaks. In Figure 3.29 we have represented the chemical shift of the CF_3 and CF_2 groups of each monolayer composition of **NP-C12/F6** *versus* the percentage of the fluorinated ligand into the monolayer.

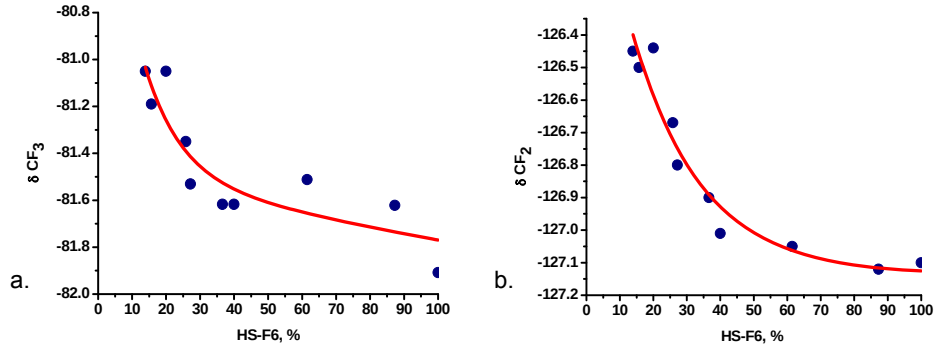

Figure 3.29 Chemical shift of a) CF_3 and b) CF_2 groups as a function of the percentage of the fluorinated ligand into the monolayer.

The behavior curves obtained for **NP-C12/F10** are different from those pertaining to **NP-C12/F6** and **NP-C16/F6**. In this case the interpolation of the points gave an exponential decay of the chemical shift of the CF_3 and CF_2 peak as a function of the percentage of the fluorinated ligand into the monolayer. A steep decay was observed when the loading of the fluorinated ligand was less than 40%, followed by a smooth decrease of the chemical shift

up to the 100% of **F6**. This indicates a strong evolution of the surface area at the interface in the first region of the curve which determines a significant downfield shift of the signals of the fluorinated ligands. When the loading increases over 60%, no significant changes at the interface are observed and the chemical shift remains nearly constant.

For selected samples of these nanoparticles, multiscale molecular simulations were performed; the images of the equilibrium morphologies are presented in Figure 3.30.

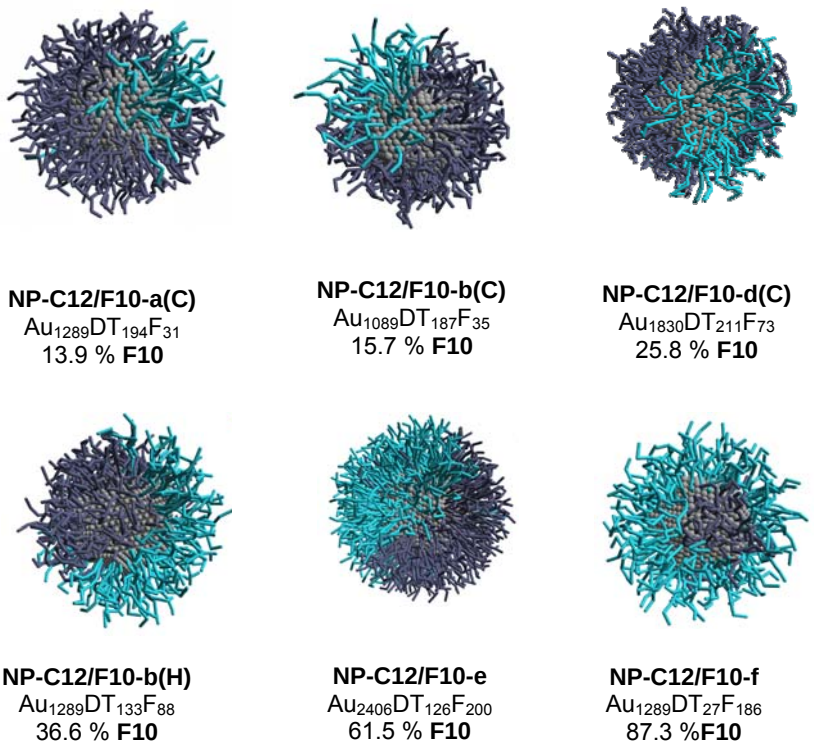

Figure 3.30 Multiscale molecular simulations of **NP-C12/F10** (dark blu-C12, turquoise-F6).

Multiscale molecular simulations reveal that for **NP-C12/F6** the two ligands are separated in two big domains, indicating the formation of Janus nanoparticles. These data are in good agreement with previously reported studies on nanoparticles protected by ligands having equal length. This organization of the monolayer well explains the behavior of the chemical shift of the CF_3 and CF_2 groups when increasing the percentage of the fluorinated ligand into the monolayer: increasing the loading of **F10** bigger domains are formed and probably the ratio between the number of thiolates at the interface and that of the thiolates found inside the domains rises exponentially. The analysis of the TEM images of these nanoparticles obtained by deposition of a very diluted chloroform solution onto the TEM support (10^{-6} mg/mL) disclosed an interesting behavior: upon drying, the nanoparticles

displayed a marked tendency to form dimers and trimmers accounting for the 50 % of the nanoparticles population, as can be seen in Figure 3.31.

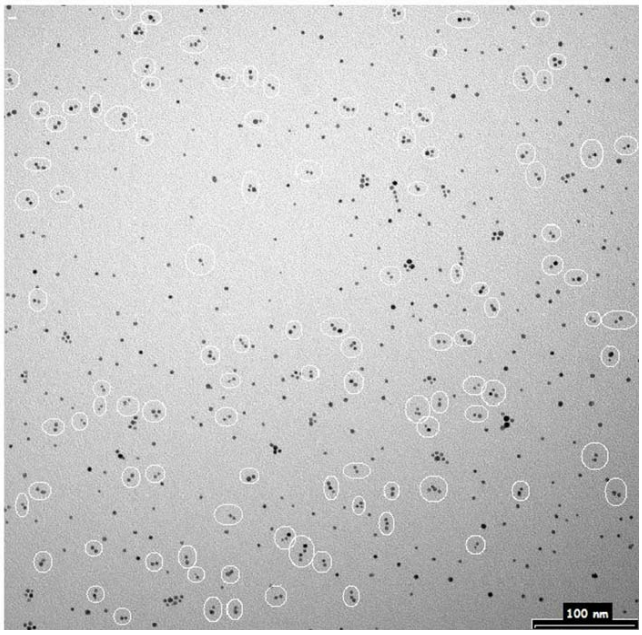

Figure 3.31 TEM image of **NP-C12/F10**, ratio 1.5:1, c = 10 ng/mL.

This result is in agreement with the information gained from multiscale molecular simulations, since the separation in two big domains of the two ligands allows the interaction of the fluorinated part of one nanoparticle with the fluorinated part of another nanoparticle through fluorophilic interactions favoured by the interdigitation of the monolayers (Figure 3.32).

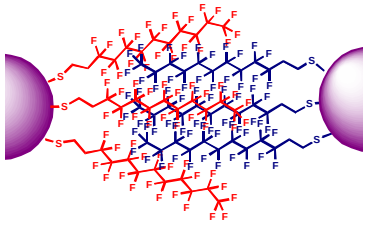

Figure 3.32 Illustrative representation of the interactions between Janus nanoparticles.

The same TEM experiment has performed using **NP-C12/F6** and **NP-C12**. Nanoparticles **NP-C12/F6** with a loading of the fluorinated ligand around 50% present only 15 % dimers and this is probably determined by the fact that, as shown before, they form elongated patches that are to slim to interact intramolecularly. Instead, for **NP-C12** we could

not observe the formation of dimers suggesting that the interaction between nanoparticles are favored only if are present fluorinated thiolates. This can be explained by the fact that the driving forces for dimerization of two particles are the formation of fluorophilic interactions between fluorinated ligands due to the interdigitation of the monolayers.

3.2.2. Synthesis of NP-C8/F6

In order to gain more information about the morphology of the monolayer of gold nanoparticles protected by ligands having the same length, we have decided to synthesize AuNPs protected by octanethiolate, **C8** and fluorinated alkanethiolate, **F6**. The aim of this study was to investigate wheater the length of the fluorinated thiolate can influence the morphology in comparison to **NP-C12/F10** presenting longer ligands.

These nanoparticles have been synthesized using a modified Brust-Schiffrin method following the same procedure reported for **NP-C16/F6**. Briefly, to 3 Equiv. of tetrachloroauric acid were added 3.6 Equiv. of TOAB and the reaction mixture was let to stir for 15 minutes. One equivalent of the mixture of thiols **HS-C8**/**HS-F6** was then added to the solution; the mixtures of thiols contain different **HS-C8**/**HS-F6** ratios in order to obtain mixed monolayers with various compositions (see Experimental part, Table 3.11). After addition of thiols, the solution gradually faded. After the addition of 11.4 Equiv. of $NaBH_4$ in different periods of time, the solution became brown or violet, depending on the dimension of the gold core. Other synthetic details are presented in Table 3.11.

At least 1 mg of nanoparticles was decomposed using an excess of iodine solution for one night in order to determine the final ratio between the ligands. After removal of the solvent the ratio between the two ligands present into the monolayer was determined from the integration of the signals belonging to methylene groups in the alpha position respect to the sulfur atom of the two different disulfides. The ratio between the hydrogenated and fluorinated ligands, associated with the results of the TEM and TGA analyses allowed us to establish the composition of the different nanoparticles samples, in Table 3.5. The nanoparticles **NP-C8/F6** were obtained with a percentage of **F6** in the range 4.5% to 83 %, see Table 3.5.

Table 3.5 Characterization data for nanoparticles **NP-C8/F6**.

Nanoparticles	Diameter (nm)[a]	Composition[b]	X_{F6}[c]	Solubility Score[d]	% C_6F_6 added[e]
NP-C8/F6-a	3.0 ± 0.6	$Au_{976}(C8)_{229}(F6)_{11}$	0.045	1	0
NP-C8/F6-b	3.3 ± 0.8	$Au_{1340}(C8)_{246}(F6)_{18}$	0.068	1	0
NP-C8/F6-c	3.8 ± 0.7	$Au_{1634}(C8)_{283}(F6)_{29}$	0.093	1	0
NP-C8/F6-d	2.7 ± 0.5	$Au_{527}(C8)_{139}(F6)_{38}$	0.213	1	0
NP-C8/F6-e	3.0 ± 0.6	$Au_{976}(C8)_{166}(F6)_{46}$	0.217	1	0
NP-C8/F6-f(C)	2.8 ± 0.6	$Au_{780}(C8)_{114}(F6)_{67}$	0.370	1	0
NP-C8/F6-g(C)	2.6 ± 0.5	$Au_{475}(C8)_{75}(F6)_{53}$	0.417	1	0
NP-C8/F6-h	3.1 ± 0.6	$Au_{976}(C8)_{126}(F6)_{90}$	0.417	1	0
NP-C8/F6-g(H)	2.4 ± 0.5	$Au_{465}(C8)_{57}(F6)_{57}$	0.500	0.5	40
NP-C8/F6-i(C)	2.3 ± 0.5	$Au_{459}(C8)_{57}(F6)_{57}$	0.500	1	0
NP-C8/F6-f(F)	2.4 ± 0.5	$Au_{459}(C8)_{53}(F6)_{59}$	0.522	0	40
NP-C8/F6-f(H)	2.9 ± 0.5	$Au_{807}(C8)_{86}(F6)_{98}$	0.533	0.5	40
NP-C8/F6-i(F)	2.4 ± 0.4	$Au_{459}(C8)_{32}(F6)_{80}$	0.717	0	40
NP-C8/F6-j	2.5 ± 0.4	$Au_{460}(C8)_{16}(F6)_{78}$	0.830	0	40
NP-C8/F6-k (H)*	1.9 ± 0.4	$Au_{225}(C8)_{42}(F6)_{38}$	0.475	0.5	20
NP-C8/F6-k (F)*	2.2 ± 0.6	$Au_{309}(C8)_{25}(F6)_{70}$	0.736		60

[a] Average diameters and standard deviation of a population of at least 300 particles. [b] Calculated on the basis of the TGA and TEM and ^{1}H NMR analyses of decomposed nanoparticles. [c] Molar fraction of the fluorinated ligand in the monolayer of nanoparticles **NP-C8/F6** determined by ^{1}H NMR analysis of decomposed nanoparticles. [d] The solubility scores are defined arbitrarily as follows: score 1 is assigned to nanoparticles fully soluble in chloroform; score 0.5 is assigned to nanoparticles fully soluble in hexane; score 0 is assigned to nanoparticles fully soluble in hexafluorobenzene; [e]percentage of C_6F_6 in the mixture $CDCl_3/C_6F_6$ added to solubilise the nanoparticles for NMR experiments. * obtained by place exchange reaction between **NP-C8** and **HS-F6**.

For these nanoparticles, at percentages of the fluorinated thiol into the monolayer higher than 50%, the nanoparticles are no longer soluble in $CHCl_3$ and C_6F_6 was added in order to obtain homogeneous solutions. In order to analyze the influence of the solvent on the chemical shift of the CF_3 and CF_2 groups we have used the same protocol discussed for the previous types of nanoparticles. The trend we obtained for the **NP-C8/F6** is very similar to that found before for the other types of mixed monolayers, more specifically, increasing amounts of C_6F_6 in the solvent mixture determine a downfield shift of the C_6F_6 and nanoparticles peaks (Figure 3.34).

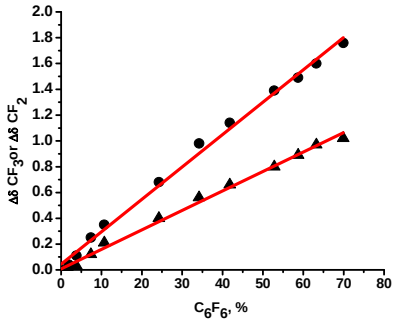

Figure 3.33 The influence of the solvent composition on the chemical shift of CF_3 (circles) and CF_2 (triangles) groups of the nanoparticles.

The influence of the solvent composition on the chemical shift of the signals pertaining to the CF_2 groups is less pronounced with respect to the influence on the CF_3 chemical shift and this is an expected behavior considering that the CF_3 group is more exposed to the solvent respect to the CF_2 group. By correcting the influence of the solvent composition on the chemical shift, we have obtained the real chemical shift of the CF_3 and CF_2 groups as a function of the ligand composition, as can be seen in the graphs of Figure 3.34.

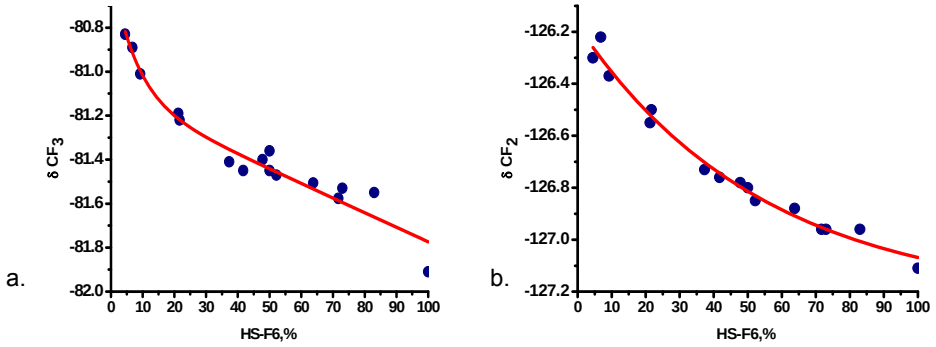

Figure 3.34 Chemical shift of a) CF_3 and b) CF_2 groups as a function of the percentage of the fluorinated ligand into the monolayer.

The behavior of the chemical shift *vs*. the percentage of **F6** in the monolayer obtained for **NP-C8/F6** is different with respect to the previous types of nanoparticles and seems to be an intermediate situation between an exponential and a linear decay. This trend is somewhat unexpected since we thought that **NP-C8/F6** and the previously discussed **NP-C12/F10** should have had a very similar Janus organization of the monolayer. To further investigate the structure of monolayer organization, some the nanoparticles presented in Table 3.5 analyzed by multiscale molecular simulations and the results obtained are

presented in Figure 3.35.

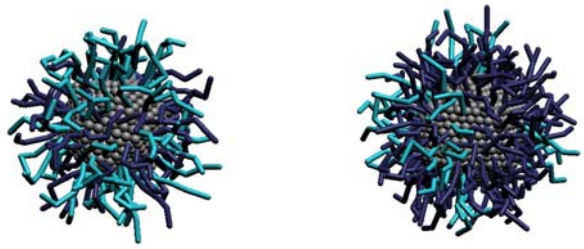

NP-C8/F6-g(C)
$Au_{475}OT_{75}F_{53}$
41.6% **F6**

NP-C8/F6-d(C)
$Au_{527}OT_{139}F_{38}$
21.3% **F6**

Figure 3.35 Multiscale molecular simulations of **NP-C8/F6** (dark blu-C8; turquoise-F6).

As it can be seen, the **C8** and **F6**, even though similar in length, are not separated in two big domains on the surface of the gold core. On the contrary, at smaller percentages of the fluorinated ligand into the monolayer, the fluorinated thiolates prefer to remain isolated and an essentially random organization is observed. By increasing the loading, the fluorinated ligand do not form extended domains but rather, they tend to remain confined in small patches. Overall, the morphology of nanoparticles **NP-C8/F6** remains ill-defined since no clear evidence for a preferred organization exists. This system has to be more deeply investigated in order to understand why, despite matching in length between the two thiolates, **NP-C8/F6** behave differently with respect to **NP-C12/F6**. A working hypothesis could be that the shorter length of **F6** respect to the **F10** used for **NP-C12/F6** reduces the overall strength of the fluorophilic interactions, making the formation of fluorinated domains less favorable. In addition, the difference in steric bulk between hydrogenated and fluorinated thiolates may represent a bias for the organization of the thiolates when this geometrical mismatch is not counterbalanced by the occurrence of strong fluorophilic interactions.

3.3. Synthesis of AuNPs protected by ligands having different length and similar bulkiness

The presence on the surface of gold nanoparticles of branched thiols disrupts the tightly packing of the ligands in the monolayer and consequently a disordered morphology is expected. Trying to investigate if similar results are obtained when mixtures of hydrogenated and fluorinated ligands are composing the mixed – monolayer protected AuNPs, we have designed and synthesized a new branched hydrogenated thiol, 3-methyl-dodecanethiol, Figure 3.36.

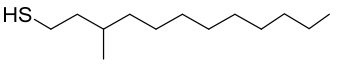

Figure 3.36 Structure of 3-methyl-dodecanethiol (**HS-brC12**).

This thiol will be used together with the fluorinated ligand, **HS-F6** to synthesize **NP-brC12/F6**. The structure of **HS-brC12** presents a methyl group at the gamma position respect to the sulfur atom; the position of the methyl group with respect to the thiol moiety has been chosen in order to be distant enough from the gold core to give stable nanoparticles while being sufficiently inside the monolayer to avoid Van der Waals interactions.

3.3.1. Synthesis of the branched thiol HS-brC12

The strategy developed for the synthesis of thiol **HS-brC12**, Scheme 3.11, involves, as a key step the cross - metathesis reaction allowing to increase the length of the alkyl chain and to introduce the methyl group in the desired position.

In a first attempt for the synthesis of **HS-brC12** we performed the cross metathesis reaction between the commercially available alcohol 3-methyl-3-buten-1-ol and 1-decene, in the presence of the Hoveyda-Grubbs catalyst: dichloro[1,3-bis(2,6-isopropylphenyl)-2-imidazolidinylidene](2-isopropoxyphenylmethylene)ruthenium(II) **Cat 1** (Figure 3.37) following the procedure reported by Grubbs.[13]

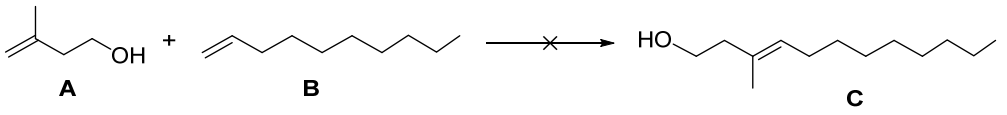

Scheme 3.8 First strategy for the cross metathesis reaction.

[13] Stewart, I.; Douglas, C.; Grubbs, R. *Org. Lett.* **2008**, 10, 441 – 444.

The choice of this ruthenium catalyst was based on literature data suggesting that it is very effective for the cross metathesis reactions involving sterically demanding olefins.[14] Briefly, a mixture of the two alkenes **A** and **B** (in a 1:3 or 3:1 ratio **A**:**B**) was added to a solution of catalyst **Cat 1** in dry deoxygenated dichloromethane. After 2 h the reaction was stopped by adding ethyl vinyl ether that deactivates the catalyst.[15]

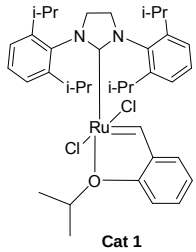

Cat 1

Figure 3.37 Structure of ruthenium catalyst used for the cross metathesis reaction.

From the reaction mixture two main fractions could be separated: a catalyst derivative (probably a complex with ethyl vinyl ether) and an alkene. This main product was analysed using mono- and bi-dimensional NMR experiments and was identified as the cross-metathesis product of 1-decene **D** (Figure 3.38) without formation of the desired heterodimer.

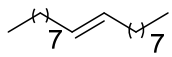

D

Figure 3.38 Homodimer of 1-decene.

To circumvent the problem of the formation of **D**, we modified the synthetic procedure by using a large excess of alcohol **A**, and working in the conditions reported by Wang,[14] Scheme 3.10.

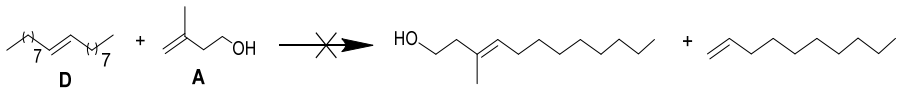

D **A**

Scheme 3.9 Second strategy for the cross metathesis reaction.

Briefly, a solution of homodimer **D** and alcohol **A** in dry deoxygenated toluene were added under argon atmosphere at a solution of **Cat 1** in toluene. The mixture was let to stir at reflux overnight, the reaction was stopped by filtering the crude mixture on a short column of silica gel in order to remove the catalyst. Unfortunately, from this reaction only

[14] Wang, Z.; Jackson, R.; Robinson, A. *Org. Lett.* **2013**, 15, 3006 – 3009.
[15] Minenkov, Y.; Occhipinti, G.; Jensen, V. *Organometallics* **2013**, 32, 2099 – 2111.

the starting reagents and derivatives of **Cat 1** were obtained. These unfavorable results can be the consequence of the interactions between the hydroxyl group of **A** and the catalyst **Cat 1**, thus blocking the heterodimerization reaction.

In order to avoid this possible source of interference, the alcohol **A** was converted to the corresponding bromide **E** following the procedure reported by Leach.[16] This reaction was performed in two steps: the activation of the alcohol group using mesityl chloride (MsCl) and the reaction of this with lithium bromide (LiBr) in anhydrous THF obtaining light sensitive oil

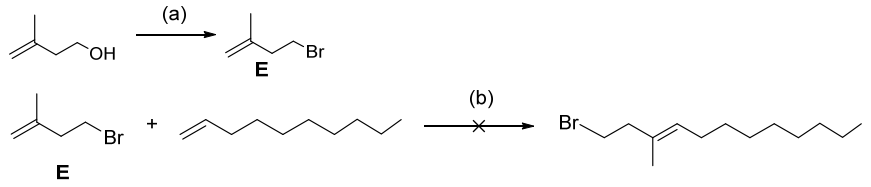

Scheme 3.10 Third strategy for the cross metathesis reaction (a) 1. MsCl, DCM, quantitative; 2. LiBr, THF, 30 %; (b) Cat 1, DCM.

The bromo-alkene **E** was used as the substrate for the metathesis reaction using catalyst **Cat 1** and the same conditions reported for the second strategy (Scheme 3.11), but after one day no traces of the desired product could be observed, the only product being detected was the homodimerization compound **D** (Figure 3.38).

At this point we decided to mask the alcohol function with a suitable protecting group. We explored the protection of the hydroxyl group of alcohol **A** by conversion to the corresponding acetyl[17] or benzyl ester. The preparation of the acetate ester was hindered by its low boiling point, resulting in low isolated yield. The benzoate ester, instead, could be isolated in good yield and purity.

The preparation of the benzyl ester was achieved by adding benzoyl chloride to a solution of **A** in anhydrous DCM at 0 °C. After addition of Et_3N and 4 h under argon atmosphere, the reaction mixture was washed with 10% HCl, saturated $NaHCO_3$ and brine. After the purification by flash chromatography (hexane/diethyl ether = 98/2) the pure compound **F** was obtained with a 78% yield.

[16] Leach, A.; Wang, R.; Wohlhieter, E.; Khan, S.; Jung, M.; Houk, K. N. *J. Am. Chem. Soc.* **2003**, 125, 4271 – 4278.
[17] Breton, G. W. *J. Org. Chem*. **1997**, 62, 8952 – 8954.

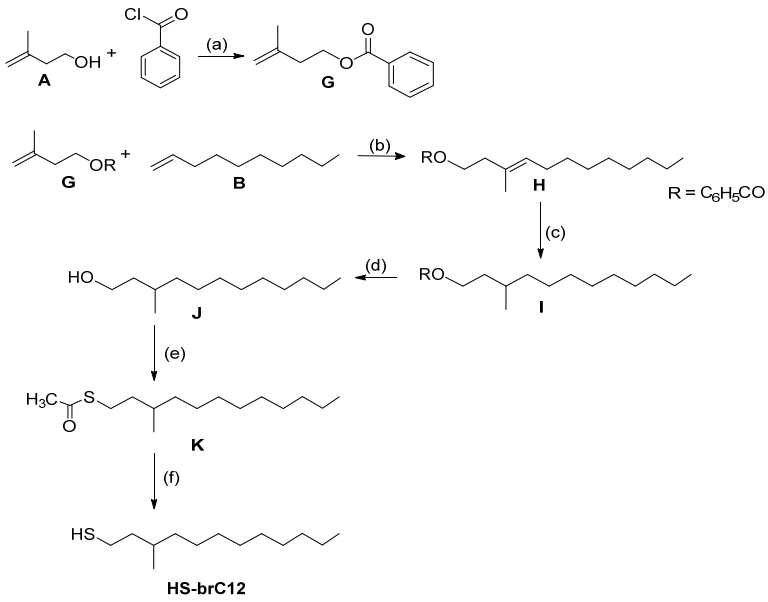

Scheme 3.11 Synthesis of branched thiol **HS-brC12**: (a) C_6H_5COCl, Et_3N, DCM, RT, 3.5 h, 90% (b) Ru Catalyst, DCM, 40 °C, overnight, 88% (c) H_2, Pd/C, RT, overnight, 90% (d) KOH 10% in MeOH, RT, overnight, 55% (e) 1. MsCl, Et_3N, RT, 4 h 2. K^+SAc, EtOH, reflux, 4 h, 65% (f) $NaBH_4$, degassed EtOH, RT, 4h, 75%.

The compound **G** was used for the cross metathesis reactions screening two types of Ru catalyst: the catalyst **Cat 1** and the second generation Grubbs catalyst **Cat 2,** Figure 3.37. The use of catalyst **Cat1** was found to be more convenient, even if less reactive than **Cat 2** because it allows an easier purification of the product. The mixture of the two alkenes **A** and **B** was added to the solution of the catalyst under argon atmosphere. The reaction was left at room temperature for 1 day; the mixture was concentrated and passed through a short silica gel column using hexane as eluent. After the purification by flash chromatography, the pure compound **H** was obtained in 57% yield.

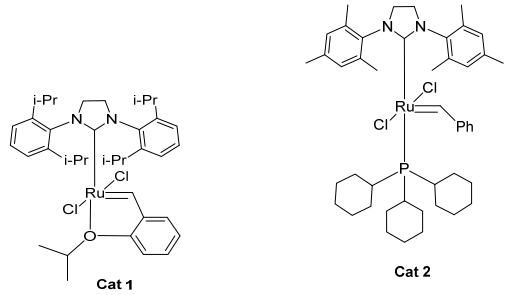

Figure 3.39 Ruthenium based catayst used for the cross metathesis reaction.

The pure cross coupling product **H** was used for the successive hydrogenation step with H_2 and Pd/C catalyst which gives the pure compound **I** in quantitative yield. The hydroxyl group was deprotected by using a NaOH/MeOH solution and the desired product **J** was obtained as colorless oil in 50% yield. In order to introduce the thiol group, necessary for grafting the ligand to the nanoparticle surface, the hydroxyl group was activated with mesyl chloride in the presence of triethylamine. After removal of the volatile species, the crude product was treated with potassium thioacetate in refluxing ethanol for 4 h affording compound **G** in 65% yield. The deprotection of the thiol group was achieved by trans-esterification using sodium borohydride in ethanol; the desired thiol **HS-brC12** was obtained with an overall yield of 25 %. In order to increase the yield of the last reactions: the introduction of the protected thiol and the subsequent deprotection, we have decided to choose another route for these steps,[18] presented in Scheme 3.12.

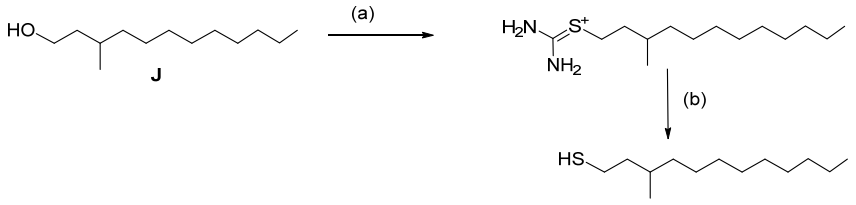

Scheme 3.12 Second attempt for the synthesis of thiol 1: (a) thiourea, HBr; (b) NaOH, HCl, 40%.

Briefly, a mixture of alcohol, thiourea and HBr 48% was refluxed for 9 h under stirring. Then a solution of NaOH was added and the reaction was refluxed for another 2 h, keeping a stream of argon over the surface of the liquid without stirring. The two layers were separated and after extraction of the acidified aqueous layer, the product **HS-brC12** was obtained with a 40% yield. Considering that the overall yield of this strategy was not improved and due to the toxicity of using HBr, we have decided to use the first procedure reported in Scheme 3.11 to synthesize the branched thiol **HS-brC12**.

The as-obtained thiol was used as such for the synthesis of **NP-brC12/F6**.

[18] Franck, R.; Smith, P. *J. Am. Chem. Soc*. **1946**, 68, 2103 – 2104.

3.3.2. Synthesis of NP-brC12/F6

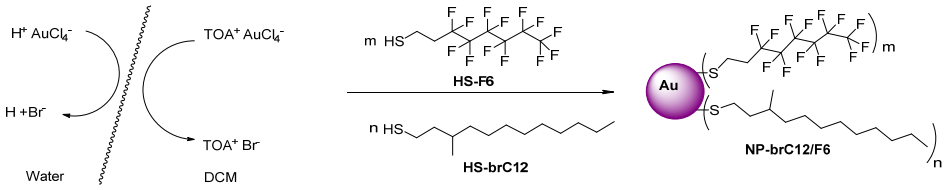

Scheme 3.13 Direct synthesis of NP-brC12/F6.

Briefly, a solution of $HAuCl_4$ (1 Equiv) in milliQ water was added at a solution of TOAB (2.5 Equiv) in DCM. The reaction was left to stir for 15 minutes and subsequently, a mixture of **HS-brC12** and **HS-F6** in different initial ratios (see Experimental part, Table 3.12) was added at the solution. After another 15 minutes, the solution faded becoming light yellow. After the addition of an aqueous solution of $NaBH_4$, the solution turned to dark brown or violet, depending on the dimension of the gold core. The two layers were separated and the organic layer was washed with brine (1 x 20 mL). The nanoparticles were precipitated by addition of methanol. The turbid suspension was centrifuged and the residue was purified by repeated washing cycles with methanol. The purified nanoparticles were subjected to selective extractions with chloroform and afterwards with hexane. The insoluble material eventually present was tested for solubility in hexafluorobenzene.

All samples were characterised by ^{1}H NMR, UV-VIS, TGA, TEM. The ^{1}H NMR spectra (Figure 3.40) suggest that the purification process was successful and the nanoparticles are very clean, without traces of free thiols.

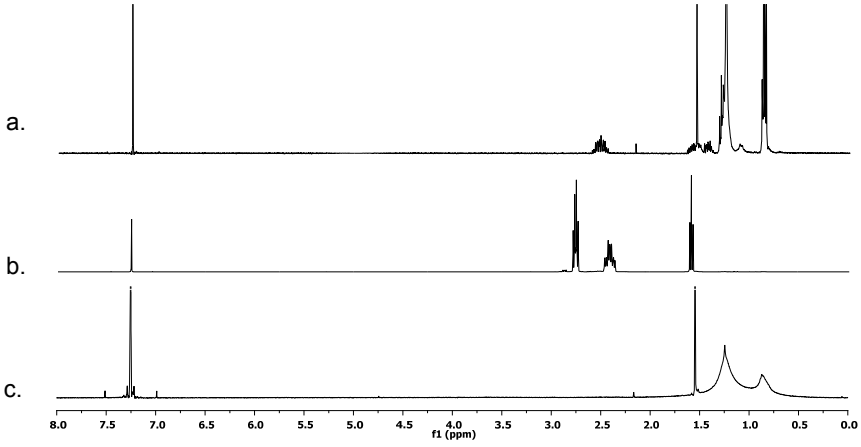

Figure 3.40 ^{1}H NMR (500 MHz, $CDCl_3$) of a) **HS-brC12**; b) **HS-F6**; c) **NP-brC12/F6-f**.

The ratio between *H*- and *F*-thiolates in the monolayer was assessed by decomposing a small amount of nanoparticles in the presence of excess iodine. The mixture of disulfides thus obtained was analysed by ^{1}H NMR and the ratio between the two thiolates present in the monolayer was determined by integration of the signals pertaining to the methylene groups in the alpha position to the sulfur atom. The diameters of the nanoparticles core were determined by TEM and the amount of organic material was assessed by thermogravimetric analyses. Characterization data are reported in Table 3.6.

Table 3.6 Characterization data for nanoparticles **NP-brC12/F6**.

Nanoparticles	Diameter (nm)[a]	Composition[b]	X_{F6}[c]	Solubility score[d]	% C_6F_6 used[e]
NP-brC12/F6-a	3.7 ± 0.6	$Au_{2230}(brC12)_{305}(F6)_{22}$	0.068	1	0
NP-brC12/F6-b	3.6 ± 0.7	$Au_{1830}(brC12)_{250}(F6)_{43}$	0.147	1	0
NP-brC12/F6-c	3.4 ± 0.8	$Au_{1340}(brC12)_{202}(F6)_{47}$	0.192	1	0
NP-brC12/F6-d	2.1 ± 0.6	$Au_{270}(brC12)_{68}(F6)_{17}$	0.198	1	0
NP-brC12/F6-e	3.1 ± 0.9	$Au_{976}(brC12)_{148}(F6)_{62}$	0.294	1	0
NP-brC12/F6-f	1.6 ± 0.5	$Au_{208}(brC12)_{30}(F6)_{24}$	0.446	1	0
NP-brC12/F6-g	2.8 ± 0.6	$Au_{807}(brC12)_{76}(F6)_{92}$	0.545	0	40
NP-brC12/F6-h	2.7 ± 0.9	$Au_{500}(brC12)_{28}(F6)_{139}$	0.833	0	60
NP-brC12/F6-i	1.9 ± 0.9	$Au_{201}(brC12)_{11}(F6)_{63}$	0.851	0	46.7

[a] Average diameters and standard deviation of a population of at least 300 particles. [b] Calculated on the basis of the TGA and TEM and ^{1}H NMR analyses of decomposed nanoparticles. [c]Molar fraction of the fluorinated ligand in the monolayer of nanoparticles **NP-brC12/F6** determined by ^{1}H NMR analysis of decomposed nanoparticles. [d] The solubility scores are defined arbitrarily as follows: score 1 is assigned to nanoparticles fully soluble in chloroform; score 0.5 is assigned to nanoparticles fully soluble in hexane; score 0 is assigned to nanoparticles fully soluble in hexafluorobenzene. [e]percentage of C_6F_6 in the mixture $CDCl_3/C_6F_6$ added to dissolve the nanoparticles.

There are some interesting aspects in the synthesis of this type of AuNPs. As can be seen in Table 3.12 (Experimental section. Part 1), the samples **NP-brC12F6-c, NP-brC12F6-e** and **NP-brC12/F6-f** are synthesized applying the same procedure, using the same ratio between the two thiols and adding the $NaBH_4$ at the same rate. The only difference between these three syntheses is the ratio between the amount of gold salt and the overall amount of thiols. More specifically, when we used a ratio Au/thiols = 3/1, a small gold core diameter of 1.6 nm was obtained while core diameters of 3.1 and 3.0 nm were obtained when 4/1 and 5/1 ratios were used. Moreover, **NP-brC12/F6-f**, *i.e.* the smallest one, turned out to be the sample with the higher loading of the fluorinated thiol into the monolayer, around 45.5%. This can be rationalized considering that for smaller gold core diameter, the curvature radius of the nanoparticles is higher and for this reason the bulky thiols can easily be accommodated. On the contrary, increasing the gold core diameter, the ligands are tightly packed preventing the bulky thiols to enter in high percentage. From

these experiments it can be deduced that when the monolayer is well packed, the bulky hydrogenated thiols enter with more facility respect the fluorinated ones, even though the bulkiness is similar. This can be rationalized considering that van der Waals interactions established between the alkyl chains are stronger respect to the fluorophilic ones between the fluorinated thiolates.

Another interesting information can be deduced from the synthesis of the sample **NP-brC12/F6-d**. For this sample we have used the same Au/thiol ratio and the same composition of the mixture of thiols used for **NP-brC12/F6-c**, the only difference was in the order of addition of $NaBH_4$. For **NP-brC12/F6-d** the solution of $HAuCl_4$, TOAB and thiols was added to the solution of $NaBH_4$ because literature data previously reported[19] suggest that the inverse order of addition can improve the monodispersity of the gold core. We observed that by changing the order of addition, the dimension of the gold core decreases significantly from 3.4 nm to 2.1 nm. This reversal of the addition did not change the loading of the fluorinated ligand into the monolayer which remains almost the same compared to the previous case in which the decreasing of the gold core diameter determines a bigger loading of the fluorinated ligand. The obtaining of smaller nanoparticles can be explained by the fact that in this case, the gold salt is added gradually to a concentrated solution of $NaBH_4$, meaning that a small quantity of gold is in the presence of a large amount of reducing agent. In these conditions, the growth of the core of the nanoparticles is not allowed. Regarding the standard deviation of the gold core diameter, we could not observe a significant improvement of the dispersity, which decreases from 0.8 nm observed for **NP-brC12/F6-c** to 0.6 nm for **NP-brC12/F6-d**. Analyzing the histograms of the two samples (Figure 3.41) it can be seen that **NP-brC12/F6-c** contains two populations of nanoparticles, one with a core diameter of 2.4 nm and another with a gold core diameter of 4 nm.

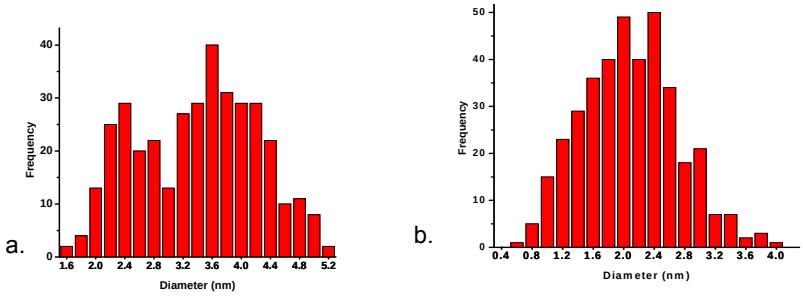

Figure 3.41 Size histograms of a) **NP-brC12/F6-c** and b) **NP-brC12/F6-d**.

The large dispersity of **NP-brC12/F6-c** and the presence of two populations of nanoparticles prompted us to try isolating the two fractions observed in the TEM images. A

[19] Sivaraman, S. K.; Kumar, S.; Santhanam, V. *J. Colloids Interface*, **2011**, 361, 543 – 547.

first attempt was to separate them by size exclusion chromatography using SEPHADEX LH-20 and eluting with $CHCl_3$. Using this procedure we have been obtained four fractions. TEM images of the first and fourth fractions are presented in Figure 3.42.

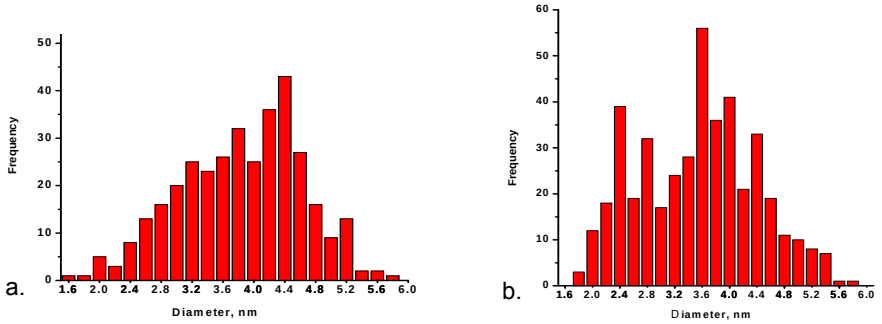

Figure 3.42 Size histograms of **NP-brC12/F6-c**, F1 X_m = 3.8 ± 0.8; F4 X_m = 3.5 ± 0.9.

As can be seen in these two histograms, we didn't obtain monodisperse nanoparticles. In the first fraction are present big nanoparticles, with a gold core diameter of 3.8 nm, but the histogram of the fourth fraction have the same profile with the one of the **NP-brC12/F6-c**. Both fractions have the standard deviation similar to the one of the initial sample, around 0.8 nm. It might be that using a very long column with a high ratio between the stationary phase and the sample, monodispersed fractions could be obtained, but we did not try.

A second attempt that we made in order to decrease the dispersion of the gold core diameter consisted in the heat treatment of the sample **NP-brC12/F6-c** in refluxing toluene for one hour. TEM analysis of this sample, Figure 3.43, displays an increase of the gold core diameter, but the standard deviation obtained from the histogram of was 0.95 nm.

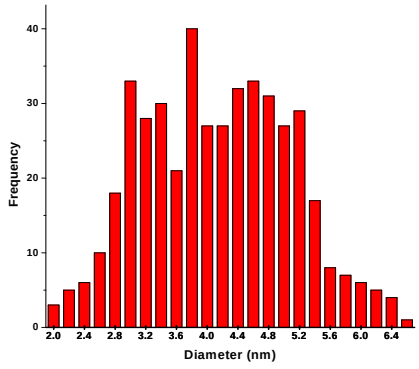

Figure 3.43 Size histogram of **NP-brC12/F6-c** after the heat treatment, X_m = 4.1 nm ± 0.95.

Other synthetic details and the relation between the initial ratio between the two ligands and the final ratio found into the monolayer after the decomposition of the nanoparticles, but

also the influence of the initial quantity of fluorinated ligand and the dimension of the gold core will be further discussed in Chapter 3.4. All these samples were analyzed by ^{19}F NMR in order to determine the chemical shift of the CF_3 and CF_2 absorbtion peaks. The real chemical shift of the CF_3 and CF_2 signals as a function of the monolayer composition, was determined by applying the correction scheme outlined in the preceding cases. We have first studied the influence of the solvent composition on the chemical shift of the selected samples of nanoparticles. For this purpose, we have dissolved 4-5 mg of **NP-brC12/F6-b** in $CDCl_3$ and we added increasing amounts of C_6F_6. After each addition we have recorded ^{19}F NMR spectra measuring the chemical shift of signals pertaining to the CF_3 and CF_2 signals. By plotting the chemical shift as a function of the percentage of C_6F_6 into the solvent mixture, we have obtained the graphs reported below in Figure 3.44.

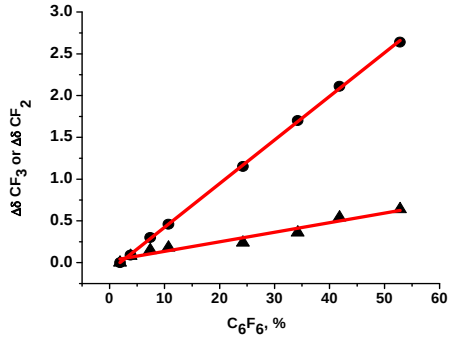

Figure 3.44 The influence of the solvent composition on the chemical shift of CF_3 (circles) and of CF_2 (triangles) groups of the nanoparticles.

For this kind of nanoparticles, the delta chemical shift of the peaks of the nanoparticles show linear dependence with the percentage of the fluorinated solvent in the mixture. As observed for the other types of nanoparticles, the influence of the solvent on the chemical shift of the CF_2 group is smaller with respect to the influence on the CF_3 group.

For the nanoparticles **NP-brC12/F6** we recorded ^{1}H and ^{19}F NMR spectra to determine the chemical shift of the CF_3 and of the CF_2 groups. The chemical shift data were corrected by considering the role of the solvent; the corrected chemical shifts plotted against the monolayer composition are presented in Figure 3.45.

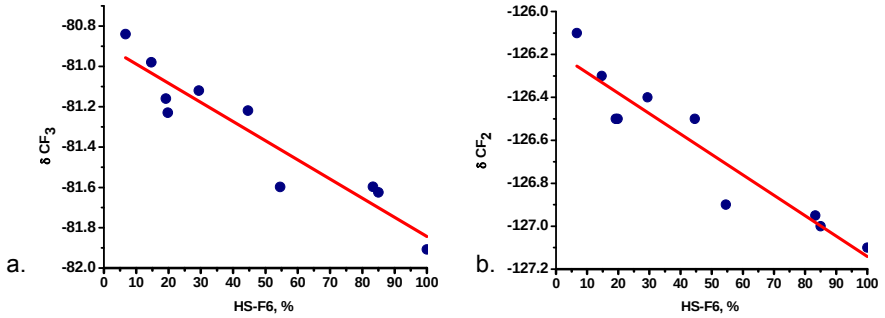

Figure 3.45 Chemical shift of a) CF_3 and b) CF_2 groups as a function of the percentage of the fluorinated ligand into the monolayer.

As it can be observed in these graphs, the broad peak of the nanoparticles shifts gradually downfield when the composition of the **F6** into the monolayer increases from 6% to 100%. In the case of these nanoparticles, the linear decay suggests that the average composition of the first nearest neighbor shell for one ligand coincides with the overall composition of the monolayer. This is in agreement with the initial hypothesis that the branched structure of the hydrogenated ligand, not allowing an ordered crystalline arrangement on the surface of the gold core, reduced the formation of phase-segregated domains. To get more informations about the organization of the monolayer, all these nanoparticles have been analyzed in the molecular simulation experiments. The morphologies resulting from the multiscale simulations are presented in Figure 3.46.

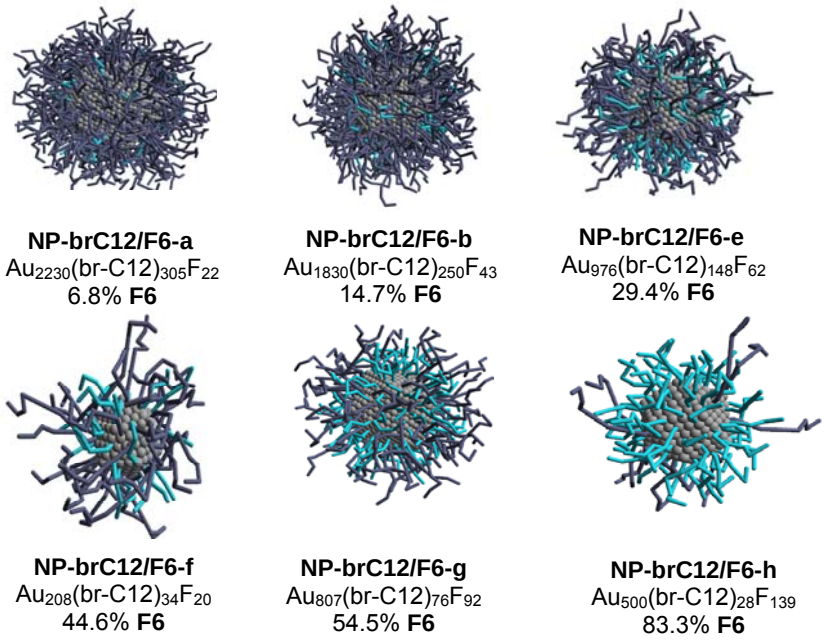

Figure 3.46 Multiscale molecular modeling of **NP-brC12/F6** (dark blu-brC12; turquoise-F6).

As it can be seen in these images, the two ligands have no tendency to form compact domains and they prefer to stay isolated resulting in a random organization of the monolayer independently of the ligand composition and of the dimension of the gold core. These data are in keeping with previous literature data on the organization of monolayers comprising branched thiolates.[26]

3.4. Analysis of the monolayer composition and composition-related properties

Understanding how the final monolayer composition depends on the initial composition of the reaction mixture in either the direct synthesis or in the place exchange reaction is thus instrumental to any approaches based on the use of *F*- and *H*-thiols for the preparation of NPs. Based on the experimental data previously reported, we discuss the correlation between the initial ratio of the thiols and the final composition of the monolayer in relation to the structure of the ligands. We also correlate the core size of the NPs to the nature of the thiols. Finally, we analyse the effect of the monolayer composition on the solubility properties of NPs.[20]

[20] Şologan, M.; Cantarutti, C.; Bidoggia, S.; Polizzi, P.; Pengo, P.; Pasquato, L. *Faraday Discussions* **2016**, Accepted manuscript, DOI: 10.1039/C6FD00016A.

Prior to presenting our analysis of the composition of mixed monolayers as a function of the relative amount of thiols in the initial reaction mixture, we find it useful defining the limiting behaviours expected under place exchange conditions or in the direct synthesis. We considered the following cases: (i) the preparation of NPs by place exchange of thiol **B** from homoligand nanoparticles comprising thiolates **A** only. (ii) The preparation of NPs obtained by direct synthesis using a blend of thiols **A** and **B**. For the sake of simplicity, we shall consider the formation of a single population of nanoparticles.

Mixed monolayer obtained by place exchange. The relationship between the molar fraction of ligand **B** in the monolayer and its initial molar fraction in the reaction mixture can conveniently be represented in the plot of Figure 3.47. In this plot, the x-axis represents the initial molar fraction of thiol **B** in the reaction mixture, while the y-axis represents the final composition of the monolayer expressed as molar fraction of the thiolate **B**.

Three different limiting cases are theoretically possible depending on the relative affinity of thiols **A** and **B** and the thermodynamics of the monolayer formation. If we assume that the ligands **B** have a very high tendency to assemble in the monolayer and that this is much higher than that of thiols **A**, in the place exchange reaction ligands **B** will displace the ligands **A** completely. The amount of ligand **B** introduced in the monolayer is only limited by its initial molar fraction. This process will lead, eventually, to the complete conversion of the homoligand **A**-monolayer into homoligand **B**-monolayer when the initial molar fraction of **B** is just 0.5, red curve in Figure 3.48; any further increase of initial molar fraction of thiol **B** cannot produce further changes. A second limiting behaviour is obtained when no preference between ligand **A** and ligand **B** in forming the monolayer exists. The final compositions of the monolayers as a function of the initial compositions will thus cluster along the diagonal of the plot, blue line in Figure 3.48. A third limiting case is the one pertaining to a situation in which the grafting of ligand **B** is strongly disfavoured, green line in Figure 3.47. In this case, no **B** ligands will be found in the monolayer at any initial molar fraction.

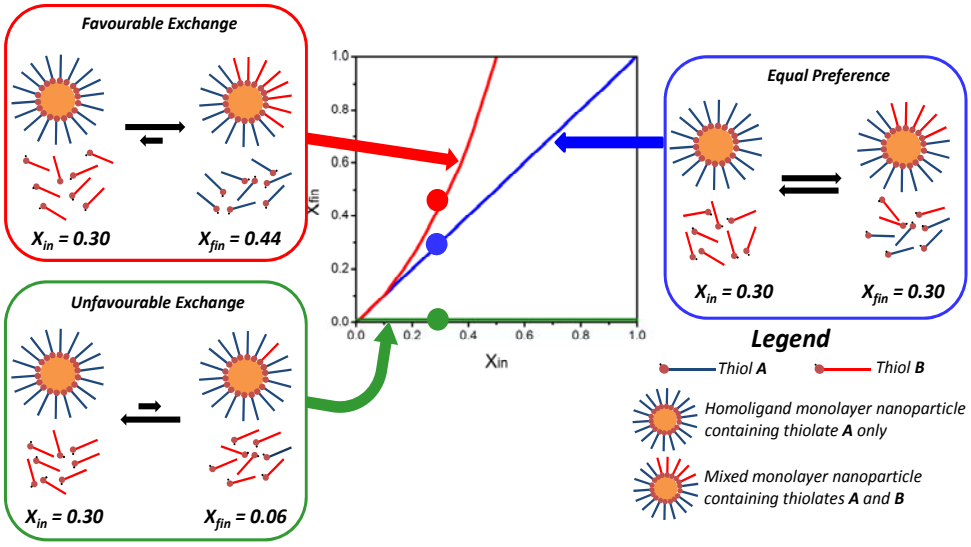

Figure 3.47 Limiting cases theoretically possible in the place exchange between thiols B and homoligand nanoparticles featuring the thiolate A only. If the grafting of thiols B is favoured, top left of the figure; complete consumption of thiols B can take place with displacement of an equal amount of thiolate A. In this case, the experimental data points will cluster along the red curve. If the grafting of thiol B is disfavoured, bottom left of the figure, only little exchange will be observed and the experimental data will be found close to the green line of the plot. If there is equal preference for the grafting of ligands A or B, right hand side of the figure, the composition of the mixed monolayer will reflect the initial composition of the reaction mixture and the experimental data points will cluster along the diagonal of the plot.

Mixed monolayer obtained by direct synthesis. In the direct synthesis of NPs, the thiols are in excess with respect to the available grafting sites on the nanoparticle surface. This is a remarkable difference with respect to place exchange. If ligands **B** have a very high affinity for the monolayer and this is much higher than the affinity of the thiols **A**, it is theoretically even possible to end-up with homoligand **B**-monolayers even if the initial molar fraction of thiol **B** is relatively small. In this case the experimental data point could be found either above the red line of Figure 3.48 or close to it. On the other hand, if there is no preference for the grafting of the **A** or **B** thiolates, the experimental data point will cluster along the diagonal of the plot. If the grafting of thiols **B** is disfavoured the experimental points will be found beneath the diagonal or approaching the green line of the plot of Figure 3.47.

3.4.1. Analysis of the experimental data for the synthesis of the mixed monolayer nanoparticles[20]

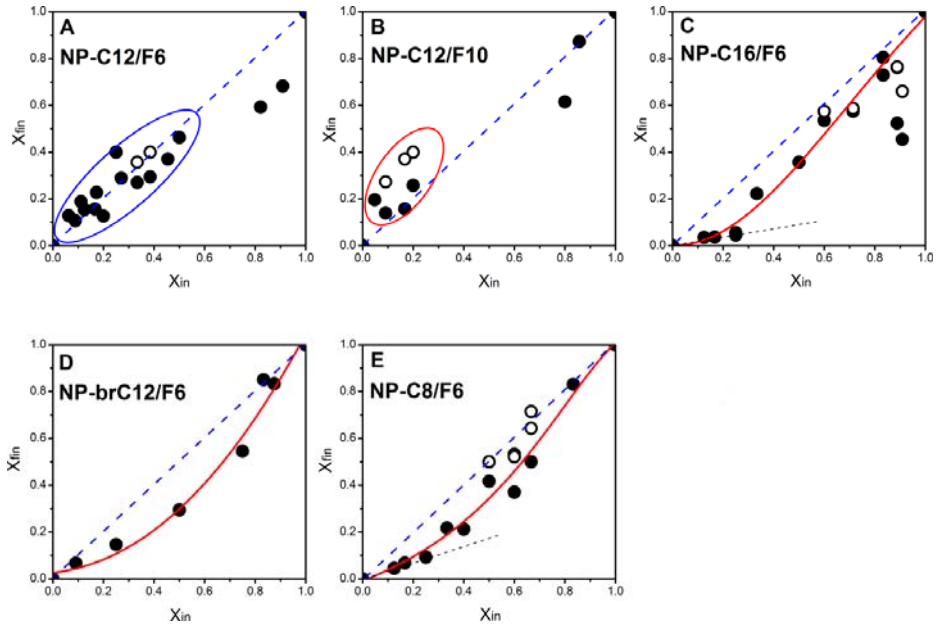

Figure 3.48 Panel **A** and **B**: experimental data of the monolayer compositions for nanoparticles **NP-C12/F6** and **NP-C12/F10**, respectively, as a function of the composition of the initial reaction mixture. Panel C, **D**, and **E**: experimental data of the monolayer compositions for nanoparticles **NP-C16/F6**, **NP-brC12/F6**, and **NP-C8/F6**, respectively, as a function of the composition of the initial reaction mixture.

For nanoparticles **NP-C12/F6**, Figure 3.48 A, the experimental data cluster along the diagonal of the plot, with some deviations only at very high initial loading of the fluorinated component. Hence, from a synthetic point of view, the preparation of nanoparticles **NP-C12/F6** containing up to 50% of the fluorinated ligand is straightforward, since the initial molar fraction of the reaction mixture is maintained in the final product. This indicates that there is essentially no energetic penalty or gain in introducing thiol **HS-F6** in the monolayer of preformed **NP-C12**. Instead, some energetic penalty, resulting in a less facile introduction of the *F*-ligand in the monolayer, occurs only when the initial molar fraction is very high. In some cases, the synthesis of nanoparticles **NP-C12/F6** gives rise to a sub-population of nanoparticles with different solubility properties and richer in the fluorinated component that could be isolated, nanoparticles **NP-C12/F6-i(H)** and **NP-C12/F6-k(H)**, Table 3.5. The compositions of these systems are reported as open symbols in the plot of Figure 3.48 A.

Similarly, for nanoparticles **NP-C12/F10**, Figure 3.48 B, the experimental data points tend to cluster slightly above the diagonal; as in the previous case, in the preparation of

nanoparticles **NP-C12/F10**, a small fraction of nanoparticles with monolayer very rich in the fluorinated component could be isolated, nanoparticles **NP-C12/F10-a(H)**, **NP-C12/F10-b(H)** and **NP-C12/F10-d(H)**, Table 3.4. The monolayer composition of these nanoparticles is reported with open symbols in the plot of Figure 3.48 B. These data indicate a facile introduction of the fluorinated ligands in the monolayer of the nanoparticles even at low molar fraction of the fluorinated component in the reaction mixture. This behaviour is suggestive of a slightly favourable introduction of thiol **HS-F10** in the monolayer of pre-formed **NP-C12**.

Increasing the length difference between the ligands, as in nanoparticles **NP-C16/F6,** a completely different behaviour was observed, Figure 3.48 C. In facts, the introduction of few *F*-ligands in the monolayer of these nanoparticles proved to be extremely unfavourable with a strong negative deviation from the diagonal of the plot in the region of small initial fraction of the *F*-component. In these syntheses more than 20% of fluorinated ligand in the reaction mixture was necessary to achieve a mixed monolayer containing a mere 5% of fluorinated thiolates. After this threshold, however, the introduction of fluorinated ligands becomes more facile, with the experimental data points approaching the diagonal of the plot. Also in this case we observed the formation of sub-population of nanoparticles richer in the fluorinated component; but at variance with **NP-C12/F6** and **NP-C12/F10**, this was observed only at initial molar fractions of the *F*-component higher than 60%; the compositions of these systems are reported with open symbols in the plot of Figure 3.48 C.

For nanoparticles **NP-brC12/F6**, Figure 3.48 D, yet a different behaviour appears. In this case the introduction of *F*-ligands remains unfavourable in all of the conditions explored. This is not unexpected because, by design and in analogy with literature evidences, these nanoparticles are believed to display a poorly organised monolayer and as suggested by ^{19}F NMR data and molecular simulations. Notably for nanoparticles **NP-brC12/F6**, we could not identify sub-populations of nanoparticles with different contents of the fluorinated ligands obtained in the same synthesis.

A somewhat intermediate behaviour was observed for nanoparticles **NP-C8/F6**, Figure 3.48 E, for which more than 20% of *F*-ligand in the reaction mixture was needed to achieve a 10% of the *F*-thiolate in the final monolayer composition. After this threshold the introduction of *F*-ligands becomes more favourable, with the experimental data points slowly approaching the diagonal of the plot at higher molar fraction of the fluorinated component. In some cases, the preparation of nanoparticles **NP-C8/F6** yielded a small fraction richer in the fluorinated component when the initial composition of the reaction mixture contained more than 50% of the *F*-ligand. The compositions of these systems are reported with open symbols in the plot of Figure 3.48 E.

From these data it is clear that the formation of mixed monolayers comprising fluorinated thiolates may be favoured or disfavoured depending on the structure of the ligands and the degree of substitution that is achieved; relatively subtle structural changes impact considerably on the outcome of the syntheses. Most importantly, these data display that the final composition of the NPs cannot be *a priori* predicted on the basis of the composition of the reaction mixture, neither in the direct synthesis, nor in the place exchange reaction.

3.4.2. Effect of the fluorinated ligand loading on the nanoparticles size

It is well established by a large number of experimental evidences that in the Brust-Schiffrin synthesis, the size of gold nanoparticles can be tuned by varying the initial gold/thiol ratio, the larger the ratio, the larger the resulting nanoparticles.[21] There are also evidences that bulky thiols tend to favour the formation of smaller gold nanoparticles.[22] Fluorocarbons have a cross-sectional area of 28.3 $Å^2$ while for hydrocarbons the molecular cross section is 18.9 $Å^2$ only.[23] The fluorinated thiols used in this study are therefore much bulkier (1.5 times higher cross-sectional area) than the hydrogenated ligands, with the possible exception of the branched **HS-brC12**. It is expected that the introduction of *F*-ligands in the monolayer of gold nanoparticles may result in systems of smaller size. In the Brust-Schiffrin synthesis of NPs we indeed observed a monotonous decrease of the nanoparticles size increasing the molar fraction of the *F*-component in the initial reaction mixture while maintaining constant the total gold/thiols ratio. The experimental data for the nanoparticles **NP-C8/F6**, **NP-C16/F6** and **NP-brC12/F6** are reported in Figure 3.49 A, Figure 3.49 B, and Figure 3.49 C respectively. This behaviour was found to be general; regardless the difference in length between the *F*- and *H*-ligands and the steric bulk of the hydrogenated thiols and has clearly a significant impact in the choice of the reaction conditions. In addition, it is also likely to have an impact on the organization of the ligands in the monolayer since the morphology of mixed monolayers depends also on the nanoparticle curvature radius and in turn on the free volume available per chain.

[21] Brust, M.; Walker, M.; Bethell, D.; Schiffrin D. J.; Whyman, R. *J. Chem. Soc., Chem. Commun.* **1994**, 801−802.
[22] Da Costa, R.; Jurisch, M.; Gladysz, J. *Inorg. Chim. Acta.* **2008**, 361, 3205−3214.
[23] Harkness, K. M.; Balinski, A.;. McLean, J. A; Cliffel, D. E. *Angew. Chem. Int. Ed.* **2011**, 50, 10554 – 10559.

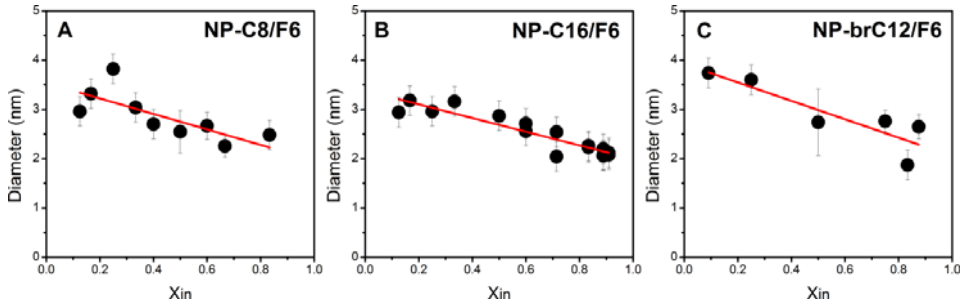

Figure 3.49 Dependence of the nanoparticles core diameter on the initial molar fraction of the fluorinated ligand. Error bars represent the standard deviation of the average diameter measured from TEM analyses. In the case of multiple preparations with the same initial loading of the fluorinated component, the experimental points represent the average of the diameters and error bars represent their standard deviation.

3.4.3. Solubility behaviour of NP

The solubility properties of these nanoparticles systems are very informative and were found to vary according to the amount of fluorinated ligand in the monolayer and the structure of the fluorinated and hydrogenated thiolates. At low molar fraction of the fluorinated component, the nanoparticles were freely soluble in chloroform and methylene chloride. At intermediate content of the fluorinated component, the nanoparticles were soluble in hexane, while at the higher molar fractions, they were soluble in fluorinated solvents only. In all of the cases, the solubility limit in the different solvents was higher than about 10 mg/mL. To qualitatively analyse the solubility behaviour in relation to the monolayer composition, we found it useful to use the solubility in the different solvent as a categorical variable and to plot this variable against the monolayer composition expressed as molar fraction of the *F*-ligand, Figure 3.50.

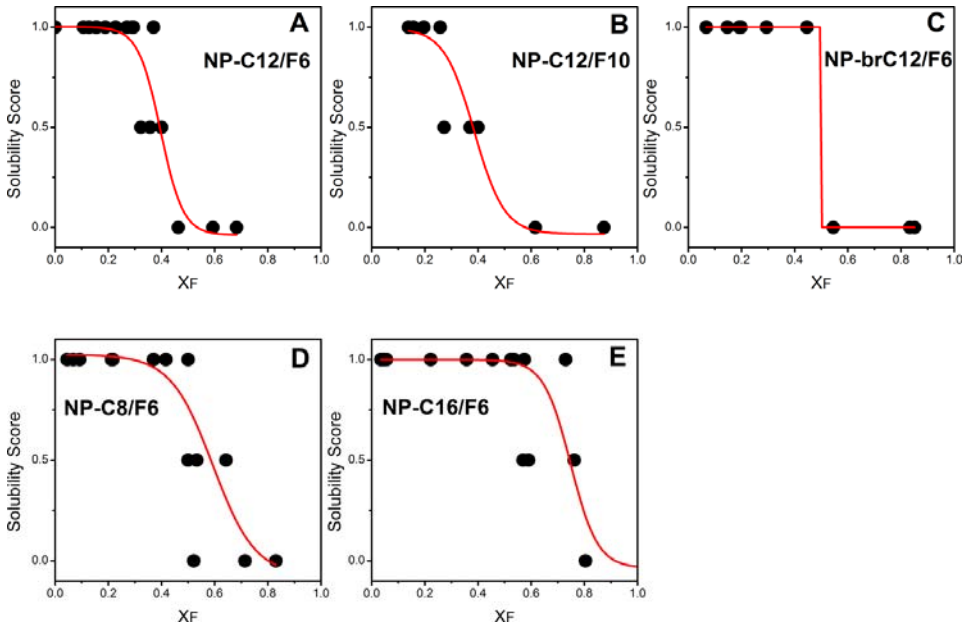

Figure 3.50 Comparison of the solubility transitions for the NPs as a function of the molar fraction of fluorinated component in the monolayer. The solubility is expressed according to the following score: score = 1 is assigned to the nanoparticles soluble in chloroform. Score = 0.5 is assigned to the nanoparticles soluble in hexane, score = 0 is assigned to the nanoparticles soluble in hexafluorobenzene.

As previously mentioned, to the systems fully soluble in chloroform we arbitrarily assigned a score of 1, the nanoparticles systems soluble in hexane were ranked with a score of 0.5 and those soluble in fluorinated solvents only (C_6F_6) were ranked with a score of zero. This approach allows to simply comparing the solubility properties of different set of nanoparticles. Nanoparticles **NP-C12/F6** display a solubility transition, corresponding to the onset of solubility in hexane, when about 40% of the fluorinated thiolate is present in the monolayer; the same percentage was found for nanoparticles **NP-C12/F10**. A significant difference was instead observed for nanoparticles **NP-C16/F6** that remained fully soluble up to a molar fraction of fluorinated ligand of 0.8. For nanoparticles **NP-brC12/F6**, the transition occurred when the molar fraction of the *F*- ligand was 0.5, the same behaviour was found for nanoparticles **NP-C8/F6**.

A rationalization of the experimental evidences presented above can be put forth by considering that the immiscibility of *H*- and *F*-ligands may lead to self-sorting of the two species and that their difference in length may substantially contribute to the driving force for the self-sorting process.

From a general point of view, if short fluorinated thiols tend to cluster in a monolayer of longer hydrogenated ligands, the introduction of a very small number of *F*-ligands in the

monolayer will be unfavourable, because it will decrease the number of van der Waals contacts between hydrogenated ligands without offering a significant enthalpic gain deriving from the establishment of fluorophilic interactions and forming an unfavourable H/F interface. At this stage the entropic gain due to the increased conformational mobility of the hydrogenated thiolates will also be minimal. Only when the amount of the *F*-ligands exceeds a certain threshold, the introduction of more fluorinated ligands should become favourable because of the increased number of fluorophilic interactions and the increased entropic gain due to the conformational mobility of the longer hydrogenated thiolates. This is reminiscent of a cooperative process, where the (unfavourable) introduction of the first few fluorinated ligands generates the conditions for a more favourable assembling. We can clearly trace this phenomenon to the synthetic conditions explored for the preparation of nanoparticles **NP-C16/F6**, Figure 3.48 C. In this case the introduction of up to 5% of fluorinated ligands is strongly disfavoured, while after this threshold the introduction of the fluorinated ligands becomes more favourable. The change in slope in the plot of Figure 3.48 C is consistent with the cooperative mechanism outlined above; in the first phase a few nucleation centres are formed that eventually evolve towards the growth of fluorinated domains. Nucleation and growth of alkanethiolate monolayers by displacement of weakly bound ligands on the surface of gold nanoparticles have indeed ben reported.[24] Our data may be taken as an indication that in the case of nanoparticles **NP-C16/F6**, 10 % of the *F*-ligand is sufficient to trigger the formation of fluorinated domains. This percentage is very close to the results of our previous studies displaying that already at the 5% loading, domains are formed in mixed monolayers comprising amphiphilic *H*- and *F*- ligands.[25] Another remarkable property of **NP-C16/F6** is that up to 80% of the fluorinated ligand can be introduced without significantly affecting the solubility of the system. This implies that the *F*-ligands cannot form large domains that would trigger particles aggregation. On the other hand, the synthetic conditions do suggest that domains indeed exist implying that these should be relatively small and/or shielded from the solvent and from the fluorinated domains of other nanoparticles by the longer *H*-ligands.

For nanoparticles **NP-C12/F10**, the experimental data cluster slightly above the diagonal of the plot of Figure 3.48 B indicating that the introduction of the *F*-ligands in the monolayer it is not unfavourable even at low loading of the fluorinated component. When, as in this case, there is no length mismatch between the thiolates, the enthalpic balance due to the loss of interactions between hydrogenated ligands and the establishment of

[24] Hostetler, M. J.; Wingate, J. E.; Zhong, C.-J.;. Harris, J. E.; Vachet, R. W.; Clark, M. R.; Londono, J. D.; Green, S. J.; Stokes, J. J.; Wignall, G. D.; Glish, G. L.; Porter, M. D.; Evans N. D.; Murray, R. W. *Langmuir* **1998**, 14, 17−30.
[25] Posocco, P.; Gentilini, C.; Bidoggia, S.; Pace, A.; Franchi, P.; Lucarini, M.; Fermeglia, M.; Pricl, S.; Pasquato, L. *ACS Nano* **2012**, 6, 7243−7253.

interactions between fluorinated chains will be a significant contribution to the overall ΔG of reaction. It should be noted that for nanoparticles **NP-C12/F10** in some cases we observed the formation of a second population of nanoparticles with high content of the fluorinated even when a very low initial loading of the thiol **HS-F10** was used. In this case it is reasonable to think that clustering of ligands is likely to occur initially with the formation of small patches, eventually evolving towards larger compact domains. Given the absence of length mismatch between the two ligands **HS-C12** and **HS-F10**, the observed behaviour is consistent with Glotzer theoretical prediction of Janus nanoparticles.

As in the preceding case, the experimental data for nanoparticles **NP-C12/F6**, Figure 3.48 A indicate that there is essentially no energetic penalty or gain in introducing thiol **HS-F6** in the monolayer of preformed **NP-C12** up to a final composition of 50%. In nanoparticles **NP-C12/F6** a docecanethiolate unit is replaced by the four atom shorter **F6** thiolate. If clustering of the fluorinated ligands takes place, this geometrical mismatch should produce an increased conformational freedom for the hydrogenated ligands at the boundaries of the *F*- ligands clusters. Since the introduction of the fluorinated ligand is easy even at very low loading, we expect the formation of small domains with a large interfacial area to surface ratio.

The solubility properties of both nanoparticles **NP-C12/F6** and **NP-C12/F10**, are in line with the formation of clusters of ligands, leading to the onset of low solubility already when about only 40% of the *F*- ligands are introduced in the monolayer, Figure 3.50 A and Figure 3.50 B ,respectively.

For nanoparticles **NP-brC12/F6**, the experimental data points cluster beneath the diagonal of the plot of Figure 3.49 D, suggesting an unfavourable incorporation in the nanoparticles monolayer. Since in this case the branched nature of the **HS-brC12** thiolate hinders the formation of a compact monolayer, the formation of domains will be unlikely and a random distribution of the thiolates on the monolayer will results, in analogy to the observation of Stellacci and co-workers[26] for branched hydrogenated alkyl thiolates. The absence of fluorinated domains is consistent with the solubility properties of these systems that remain soluble in chloroform up to the introduction of 50% of the fluorinated component. Experimental evidence that is consistent with a random distribution of the thiolates is also the absence of sub-populations of nanoparticles, obtained in the same synthesis and displaying different average content of *F*-ligands. Indeed these sub-populations are likely to be formed only if the introduction of *F*-ligands is favoured as the result of some ligands clustering in the monolayer. A somewhat intermediate behaviour is displayed by nanoparticles **NP-C8/F6**, the graph of Figure 3.48 E share some features with

[26] Liu, X.; Yu, M.; Kim, H.; Mameli M.; Stellacci, F. *Nat. Commun.* **2012**, 3,1182.

that obtained for nanoparticles **NP-brC12/F6** and nanoparticles **NP-C16/F6**. This is peculiar since given the absence of length mismatch between the two thiols, the formation of Janus particles should be expected and the synthetic data should be close to those obtained for nanoparticles **NP-C12/F10**.

3.5. Study of mixed monolayer AuNPs using bidimensional NMR experiments

Previous studies[26,27] on mixed - monolayer nanoparticles have demonstrated that bidimensional NMR experiments can be useful to gain information about ligands which are closer than 0.4 nm into the monolayer. This kind of experiments is based on Nuclear Overhauser Effect which is the transfer of nuclear spin polarization from one spin to another spin via cross-relaxation. This experiment allows obtaining information about spin systems not directly bound but close in space. Considering that the nanoparticles previously presented display mixtures of hydrogenated and fluorinated ligands in their monolayer, an interesting bidimensional experiment which could give some information about ligands organization which are in close proximity are the ^{1}H-^{19}F HOESY. These experiments permit to see cross peaks between signals of fluorinated ligands which are neighboring to hydrogenated ones. In the case of mixed - monolayer gold nanoparticles, with defined domains, the fluorinated ligands can be in close proximity to the hydrogenated ones only at the interface between the two regions. Otherwise, when the two ligands are not close enough, no cross peak should be seen. Assuming that mixed monolayers may have different organizations on the surface of the gold core, the number of ligands at the interface will be different for each type organization. Starting from these indications, for nanoparticles with monolayers displaying a random organization or organized in stripe-like domains a large number of ligands are expected at the interface between hydrogenated and fluorinated regions. This is the reason why we expect for this types of nanoparticles to observe a cross peak in the HOESY spectra between the CF_2 central groups of the fluorinated ligand and the methylene groups of the hydrogenated ones (Figure 3.51). More specifically, we expect to observe cross peaks for nanoparticles **NP-brC12/F6**, **NP-C16/F6**, **NP-C12/F6** and **NP-C8/F6**, not for **NP-C12/F10**.

[27] Kim, H.; Carney, R.; Reguera, J.; Ong, Q.; Liu, X.; Stellacci, F. *Adv. Mater*. **2012**, 24, 3856 – 3863.

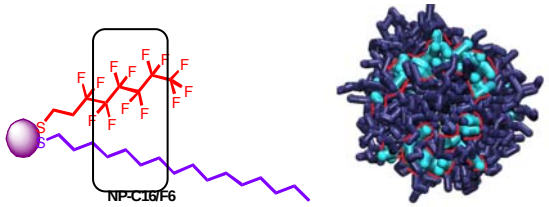

Figure 3.51 NP-C16/F6 and illustrative representation of the interface (red dashed line) between the hydrogenated and the fluorinated regions (dark blu-C16; turquoise-F6).

On the contrary, in the case of nanoparticles having a Janus organization, the two ligands are closer to each other only at the interface between the two big regions (Figure 3.52) and for this reason the number of fluorinated ligands interacting with the hydrogenated ones is smaller with respect to the other types of morphologies and in the ^{1}H-^{19}F HOESY spectra no cross peaks are expected.

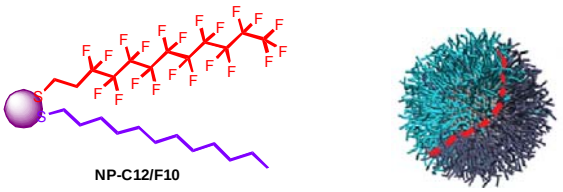

Figure 3.52 NP-C12/F10 and illustrative representation of the interface (red dashed line) between the hydrogenated and the fluorinated regions (dark blu-C12; turquoise-F10).

The ^{1}H-^{19}F HOESY experiment has been realized by dissolving one sample of each type of AuNPs in deoxygenated solvent at a concentration of 10 mg/mL. The solvent must be very well deoxygenated because it is well known that oxygen has a high solubility in fluorinated solvents/compounds and the presence of this species can prevent the transmission of spin relaxation from one molecule to another determining a false negative result. The samples we have chosen to realize these experiments were AuNPs with a ratio hydrogenated/fluorinated around 1/1. The first results obtained for **NP-C16/F6**, **NP-C12/F6** and **NP-brC12/F6** and **NP-C8/F6** and are presented in Figure 3.53.

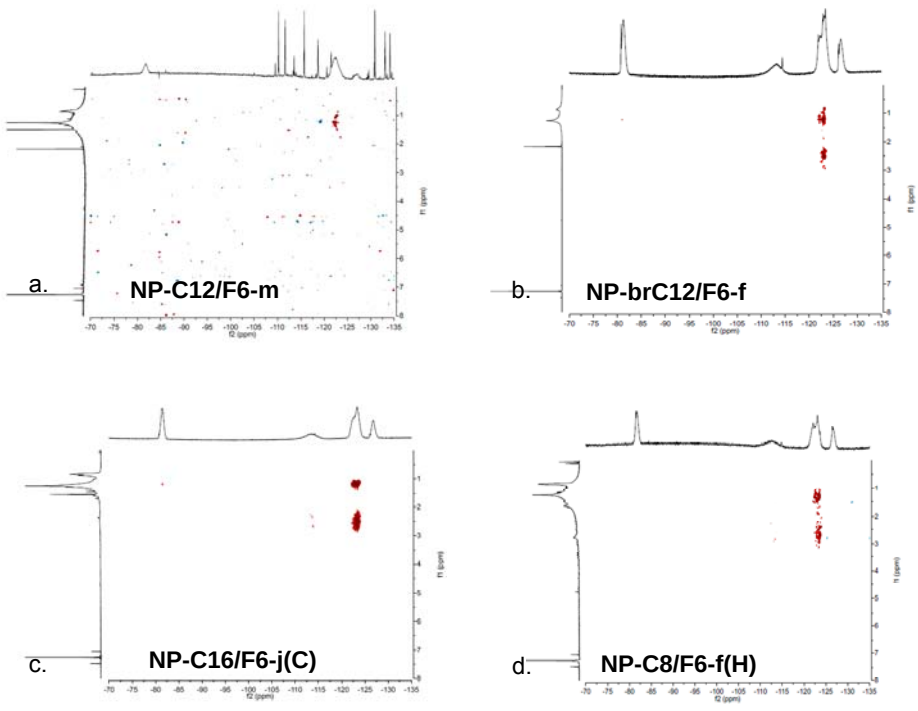

Figure 3.53 ^{1}H-^{19}F HOESY experiments on nanoparticles a) (500 MHz, $CDCl_3/C_6F_6$) **NP-C12/F6-m**; b) (500 MHz, $CDCl_3$) **NP-brC12/F6-f**; c) (500 MHz, $CDCl_3$) **NP-C16/F6-j(C)**; d) (500 MHz, $CDCl_3/C_6F_6$) **NP-C8/F6-f(H)**.

As it can be seen in these HOESY spectra, in all of the four cases cross peaks are present between the peak at around -123 ppm corresponding to the 4- and 5-CF_2 central groups of the fluorinated ligands and the methylene groups of the hydrogenated ones represented by the peak at 1.2 ppm in the f1 axis. This result suggests that the two thiolates are in close proximity into the monolayer consistent with multiscale molecular simulations. In the HOESY spectra of nanoparticles **NP-brC12/F6** and **NP-C16/F6** a second cross peak between the same CF_2 central groups and a signal at around 2.5 ppm in the ^{1}H-NMR could be observed. This cross peak can be due to either an intra- or intermolecular interaction. In order to clarify this point, we performed HOESY experiment on homoligand nanoparticles, **NP-F6** (Figure 3.55) and on the free **HS-F6** (Figure 3.54).

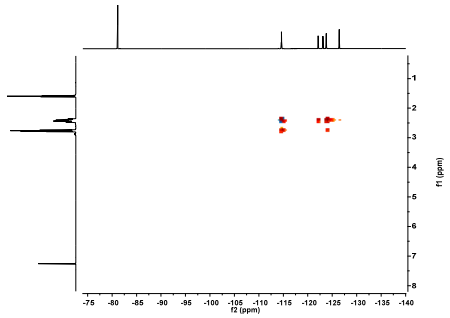

Figure 3.54 ^{1}H-^{19}F HOESY (500 MHz, $CDCl_3$) experiments of **HS-F6**.

The HOESY spectrum of **HS-F6** (Figure 3.54) shows cross peaks between the two methylene groups of the **HS-F6** and the 3-CF_2 groups in the third position could be observed; cross peaks were also present between the 4- and 5- CF_2 central groups and the methylene group in the beta position with respect to the sulfur atom. This experiment demonstrates that the second cross peak present in the HOESY spectrum of the nanoparticles is due to the intramolecular interaction between the hydrogenate methylene group and CF_2 groups of the same molecule of thiolate **F6**.

The HOESY spectrum of **NP-F6-c** (Figure 3.55) shows a cross peak between the methylene group in alpha position to sulfur of the fluorinated thiol and the CF_2 central groups.

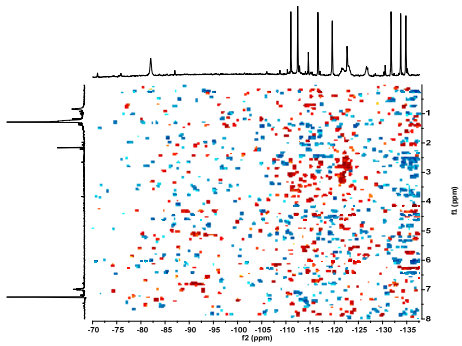

Figure 3.55 ^{1}H-^{19}F HOESY (500 MHz, $CDCl_3$) experiments of **NP-F6-c**.

Our investigation regarding the use of bidimensional HOESY experiment for the study of mixed monolayers was extended to the study of **NP-C12/F10-b(H)** which have a Janus organization of the monolayer. The spectrum obtained, Figure 3.56 presented an unexpected cross peak, between the signal of the central CF_2 groups of the fluorinated ligand and the methylene groups of the hydrogenated one.

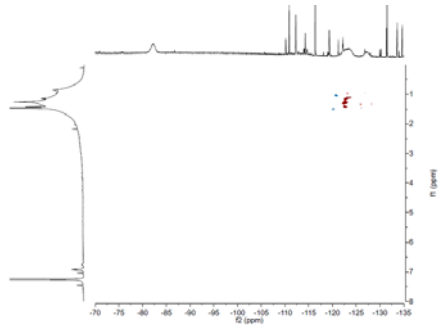

Figure 3.56 ^{1}H-^{19}F HOESY (500 MHz, $CDCl_3/C_6F_6$) experiments on nanoparticles **NP-C12/F10-b(H**).

Since for Janus nanoparticles the fluorinated and hydrogenated thiolates are interacting solely at the interface between two domains, the intensity of this cross peak should be vanishingly small. An explanation for the observation of this cross peak can be the length and consequently the number of fluorine nuclei of the fluorinated ligand; thiolate F10 has seven CF_2 groups capable of determining a high number of interactions able to produce an NMR signal. For this reason, even though the two ligands are interacting only at the interface between the two regions, the higher number of CF_2 groups may be sufficient to determine the appearance of the cross peak. This can be an indication of the fact that the ^{1}H-^{19}F HOESY is a very sensitive experiment which allows to monitor a low number of contacts between hydrogenated and fluorinated ligands.

In order to demonstrate this sensitivity of the ^{1}H-^{19}F HOESY experiment, we performed another HOESY analysis on a sample of the same class of nanoparticles, **NP-C12/F10-a(C)**, presenting a small percentage of the fluorinated thiolate into the monolayer, only 13% of **F10**. In this case, as can be seen in the image obtained from multiscale molecular simulations (Figure 3.57 a), the fluorinated ligands form a small patch and the number of fluorinated ligands that are close to the hydrogenated ones is lower respect to the previously used sample of nanoparticles. However, even in this case, the HOESY spectrum has shown (Figure 3.57 b) an intense cross peak between the methylene groups of **C12** and the central CF_2 groups of **F10**.

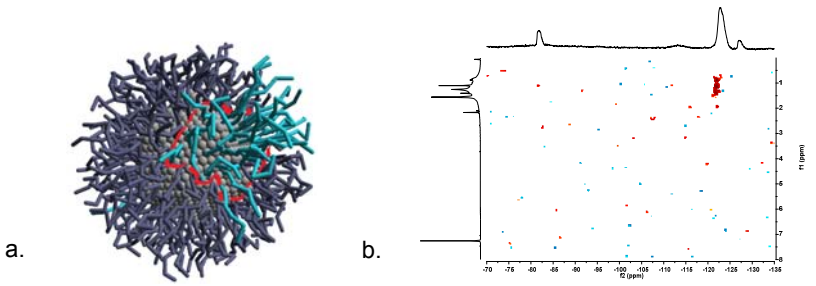

Figure 3.57 a) Interaction at the interface (red dashed line) between the hydrogenated (dark blu) and the fluorinated (turquoise) regions b) ^{1}H – ^{19}F HOESY experiment (500 MHz, $CDCl_3$) on **NP-C12/F10**.

From these experiments it can be concluded that the ^{1}H-^{19}F HOESY is a very sensitive technique and cross peaks can be observed even though in the monolayer only a small number of interactions between the hydrogenated and fluorinated thiolates is present.

In conclusion, it was demonstrated that mixtures of hydrogenated and fluorinated ligands phase segregated forming domains, the self sorting depending on the structure of the two thiols and the geometrical mismatch between them. NMR techniques can give important informations about the organization of the monolayer. A linear decay of the chemical shift for nanoparticles protected by ligands having similar bulkiness and different length (**NP-brC12/F6**) and the multiscale molecular simulations have demonstrated that this kind of nanoparticles have a random morphology. Phase segregation in two main patches has been found when **HS-C12** and **HS-F10** have been used to synthesized the AuNPs. By plotting the chemical shift of the CF_3 and CF_2 groups of the fluorinated ligand an exponential decay was found which is in agreement with previous studies on Janus nanoparticles. If the mixture of ligands is made by thiols with a difference in length of eight carbon atoms, the ligands phase segregate in the monolayer forming stripes. This is because the length mismatch between the two ligands allows a gain in entropy only if this morphology is attained. In other cases, the ligands are forming irregular patches or a non-defined organization. It has been demonstrated that bidimensional heteronuclear experiments and in particular, ^{1}H-^{19}F HOESY, are very sensitive but are not suited to distinguish between different organization of the monolayer because cross peaks between the CF_2 central groups of the fluorinated ligand and the methylene groups of the either hydrogenated or fluorinated thiolates can be observed even when a small number of interactions are present.

3.6. Design and synthesis of fluorinated ligands for AuNPs soluble in polar solvents

3.6.1. Synthesis of fluorinated ligand, HS-F6-OH

HOESY bidimensional NMR techniques give unexpected results even though previously NOESY data have been reported to be successful in studying the morphology of mixed monolayer nanoparticles. The usefulness of the HOESY experiments prompted us to design and synthesized a new fluorinated thiol (**HS-F6-OH**, Figure 3.58) which present two very well separated peaks in the ^{1}H NMR spectrum. The nanoparticles obtained by using this thiol can be investigated with both ^{1}H-^{19}F HOESY, and NOESY experiments.

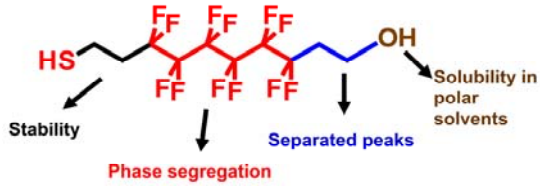

Figure 3.58 New fluorinated thiol, **HS-F6-OH**, for the synthesis of AuNPs.

In the structure of **HS-F6-OH** four moieties can be identified: two methylene groups close to the thiol group in order to give stability to the monolayer; a fluorinated part formed by six CF_2 groups able to induce phase segregation, two methylene groups close to the OH group which give a well separated signal in the ^{1}H NMR spectra and, finally, an hydroxyl group that determines solubility in polar solvents. Additionally, the presence of a hydroxyl function that can be further modified with different moieties enables a variety of applications.

The structure of this thiol was conceived to overcome two main problems encountered when we have used the fluorinated ligands, **HS-F6** and **HS-F10**. In first place, it allows having two set of well separated signals in the ^{1}H NMR spectra, enabling the use of both NOESY and HOESY experiments to study the morphology of the monolayer. Secondly, the hydroxyl group allows the preparation of nanoparticles soluble in polar solvents. This is possible because, once assembled in the monolayer of the nanoparticles, the fluorinated units of thiolates **F6OH** are masked from the solvent. Hence an increase in the percentage of the fluorinate ligand into the monolayer will not influence the solubility too much, in this way the use of fluorinated solvents could be avoided. The aim of this study was to investigate if bidimensional experiments such as HOESY and NOESY give indications about the morphology of the monolayer when **HS-F6OH** was used.

Using this thiol we have synthesized two types of nanoparticles. For the first class of nanoparticles we have used thiols having a small difference in length between the ligands, **HS-C12** and **HS-F6-OH**; for the second one, we used a mixture of ligands with a larger length mismatch: **HS-C16** and **HS-F6-OH**.

For the synthesis of the new fluorinated thiol **HS-F6-OH** (Scheme 3.14) we started from the commercially available diiodoperfluorohexane which reacts with vinyl acetate in the presence of a radical initiator, AIBN. After one day, $LiAlH_4$ in THF was added to the crude product and the reaction was left to stir overnight. The symmetrical diol **B** was obtained with an overall yield of 25% and further used for the reaction with TsCl following a procedure reported by Bouzide[28] The reaction was performed in THF, in the presence of Ag_2O and KI. The product was reacted with TrtSH in the presence of K_2CO_3 to give compound **D**. The thiol **HS-F6-OH** was obtained by deprotection of the trityl derivative using TFA and TIPS in 30% overall yield.

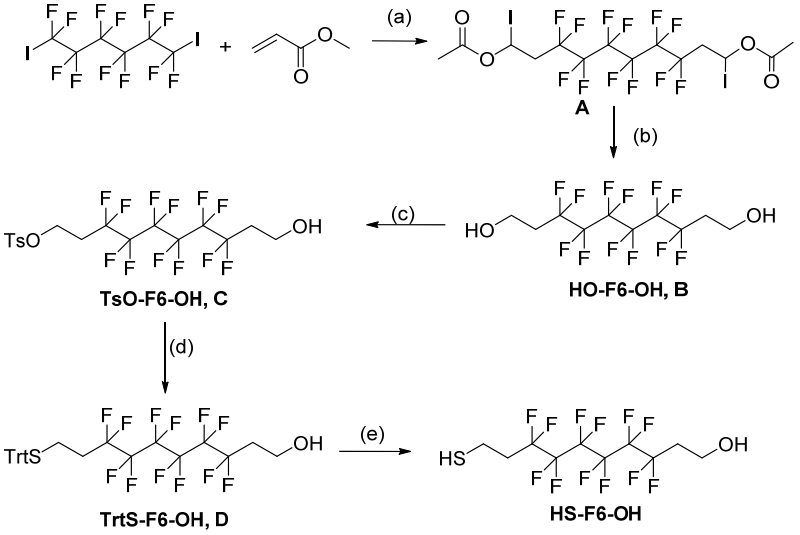

Scheme 3.14 Synthesis of **HS-F6-OH**: (a) AIBN, vinyl acetate, overnight; (b) $LiAlH_4$, THF, overnight; (c) TsCl, Ag_2O, Ki, THF, overnight; (d) TrtSH; K_2CO_3, overnight; (e) TFA, TIPS, DCM.

3.6.2. Synthesis of NP-C12 and NP-C16

The mixed monolayer nanoparticles were synthesized by place exchange reaction using the narrowly dispersed **NP-C12** and **NP-C16** and **HS-F6-OH**. For the synthesis of monodisperse **NP-C12** and **NP-C16** we have modified the procedure reported by Miyake (Scheme 3.5).[11]

[28] Bouzide, A., LeBerre, N., Sauve, G. *Tetrahedron Lett*. **2001**, 42, 8781.

In the thermal treatment the small **NP-C12** and **NP-C16** were heated up to 154 ºC with a rate of temperature rise of 2 ºC/min and let at 154 ºC for 30 minutes. Then, the nanoparticles were dissolved in toluene and left to stir overnight with a small amount of the corresponding thiol, **HS-C12** or **HS-C16** respectively. The purification process of **NP-C16** needed some optimization to ensure the obtainment of samples free of residual TOAB. The optimized protocol requires three precipitations with methanol before the concentration of the solution and afterwards six washings with methanol. The ^{1}H NMR spectra of these samples of nanoparticles (Figure 3.59) suggest that they are clean without traces of free thiols, but very small quantities of disulfides can be noticed.

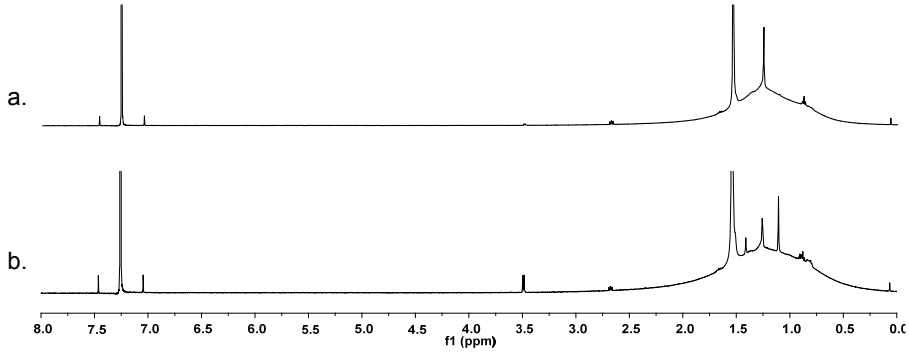

Figure 3.59 ^{1}H NMR (500 MHz, $CDCl_3$) spectra of a) **NP-C16** and b) **NP-C12**.

The histograms of the size distribution obtained by analysis of the TEM images of both samples of nanoparticles are reported in Figure 3.60. The size histograms suggest that the decreasing of the maximum heating temperature determined a decrease of the gold core diameter. In this case NPs with gold core diameters of 4.4 nm ± 0.96 (**NP-C12**) and 4.1 nm ± 0.6 (**NP-C16**) have been obtained.

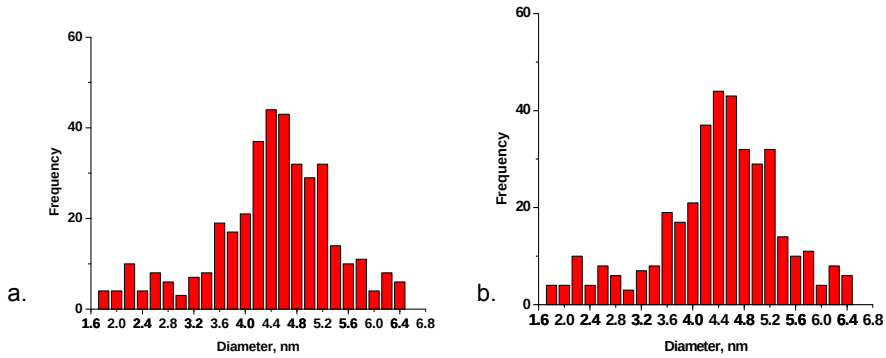

Figure 3.60 Size histograms of a) **NP-C12** and b) **NP-C16**.

These samples of nanoparticles have been used for the place exchange reactions with **HS-F6-OH**, described in the next section.

3.6.3. Synthesis of NP-C12/F6-OH

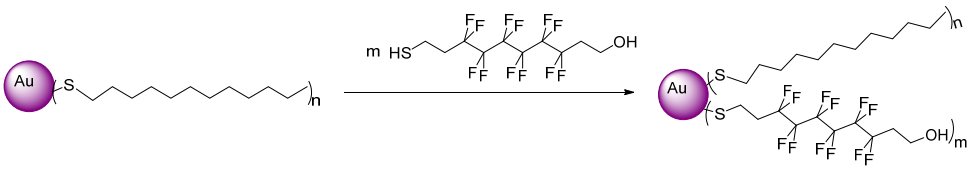

13-15 mg of **NP-C12** were dissolved in deoxygenated methylene chloride and **HS-F6-OH** was added in various ratios respect to the **C12** thiolate present in the monolayer. The 3/1, 1/1.5, 1/3 and 1/8 **HS-C12**/**HS-F6-OH** ratios were used: (Table 3.7). The reaction mixture was left stirring for three days at 40 ºC. After this period of time, all nanoparticles were found precipitated. They were transferred in centrifuge tubes and washed nine times with dichloromethane and chloroform. The ^{1}H NMR spectra shown that the samples were very clean.

The ratio between the two ligands in the monolayer has been determined after the decomposition of 1-2 mg of each sample of nanoparticles with a solution of I_2 in MeOH overnight. After the removal of the solvent, the final ratio between the two ligands was determined from the integration of the ^{1}H NMR signals corresponding to the methylene groups of the disulfides obtained, the data of the final composition of the monolayer are presented in Table 3.7.

Table 3.7 Synthetic details for the synthesis of **NP-C12/F6**.

Sample	**Initial ratio C12/F6-OH**	**Final ratio C12/F6-OH**
NP-C12/F6-OH-a	3/1	1.2/1
NP-C12/F6-OH-b	1/1.5	1.2/1
NP-C12/F6-OH-c	1/3	1.2/1
NP-C12/F6-OH-d	1/8	1/3.1

From these four syntheses it seems that there is a preference for the 1/1 final ratio between the two ligands because varying the initial ratio **HS-C12**/**HS-F6-OH** from 3/1 to 1/3, the final percentage of the fluorinated ligand into the monolayer is the same: 1.2/1. By further increasing the initial amount of the fluorinated ligand with respect to **C12**, a final ratio **C12**/**F6-OH** of 1/3.1 could be obtained.

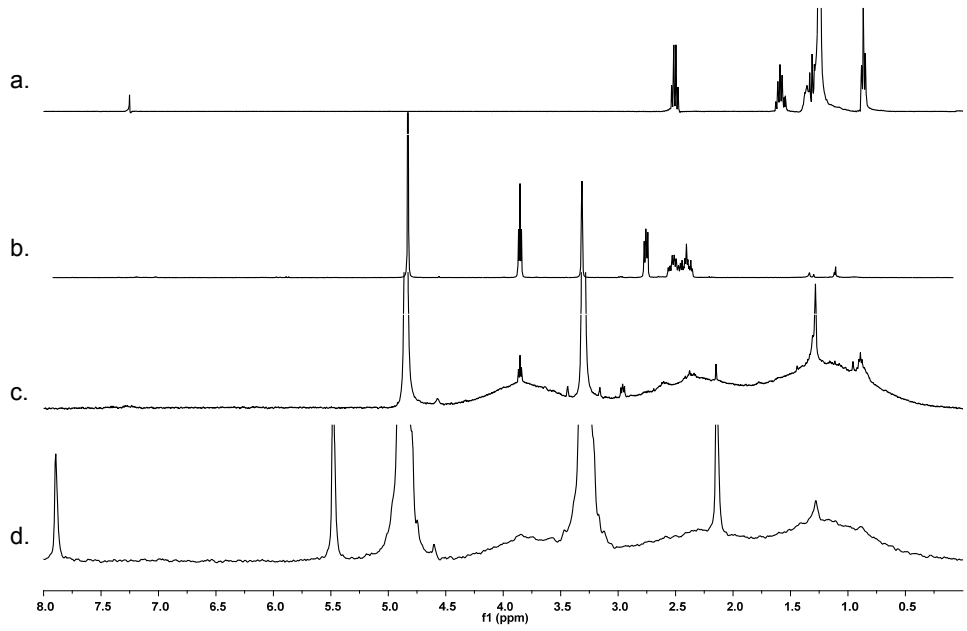

Figure 3.61 a) ^{1}H NMR (400, $CDCl_3$) of **HS-C12**; b) ^{1}H NMR (500, CD_3OD) of **HS-F6-OH**; c) ^{1}H NMR (500, CD_3OD) of **NP-C12/F6-OH-b** after one week; ^{1}H NMR (500, CD_3OD) of **NP-C12/F6-OH-b**.

In Figure 3.61 the ^{1}H NMR of the thiols used for the synthesis of these nanoparticles (Figure 3.61 a) and b)) and the ^{1}H NMR spectrum of nanoparticles are presented (Figure 3.61 d). As it can be seen, the peaks of the nanoparticles are broadened respect to the peaks of the free thiols. When the NMR spectra were recorded immediately after the synthesis, no free thiols have been observed. On the contrary, after one week sharp peaks corresponding to the free thiol appeared in the NMR spectra. This suggests that the nanoparticles are not very stable and the thiols detach from the surface of the metal core. This will be further investigated in order to find an explanation to this behavior.

Sharp peaks were present also in the ^{19}F NMR spectra (Figure 3.62) of **NP-C12/F6-OH-b**.

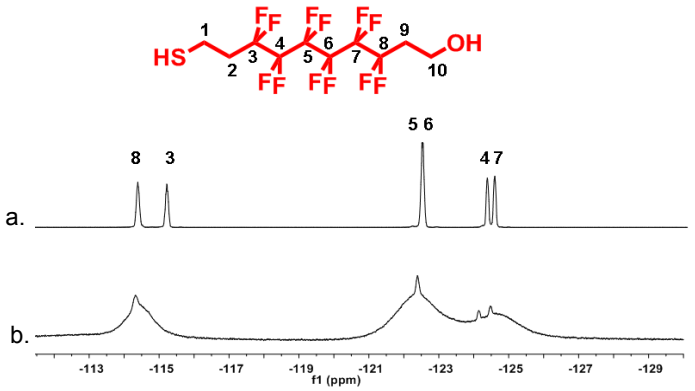

Figure 3.62 a) Assignment of the peaks of thiol **HS-F6-OH** and b)^{19}F NMR (470 MHz, CD_3OD) of **NP-C12/F6-OH-b**.

The resonances were assigned by analysis of the ^{19}F NMR and the bidimensional HETCOR experiments. The ^{1}H–^{19}F HETCOR experiments present a cross peak between the peaks at -114 - 115 ppm and the peaks at 2.3 ppm corresponding to the methylene groups in position 2 and 9. This suggests that the two peaks at -114 ppm and -115 ppm in the ^{19}F NMR spectra are due to the 3- and 8- CF_2 groups. From the integration of the signals we could conclude that the peak at -122 ppm represent the two central CF_2 groups, the other two peaks at around -125 ppm are the CF_2 groups in position 4 and 7.

^{19}F NMR spectra also revealed the presence of some small sharp peaks that can be due to presence of traces of free unbond thiol. In the ^{19}F NMR spectra of the nanoparticles only four sharp peaks are observed and not five like in the free thiol spectrum. The absent signal is that corresponding to the 3- CF_2, i.e. the CF_2 nearest to the gold core.

We have performed bidimensional ^{1}H-^{19}F HOESY and NOESY experiments on **NP-C12/F6-OH-b** by dissolving 10 mg of nanoparticles in deoxygenated methanol. The spectra are reported in Figure 3.63.

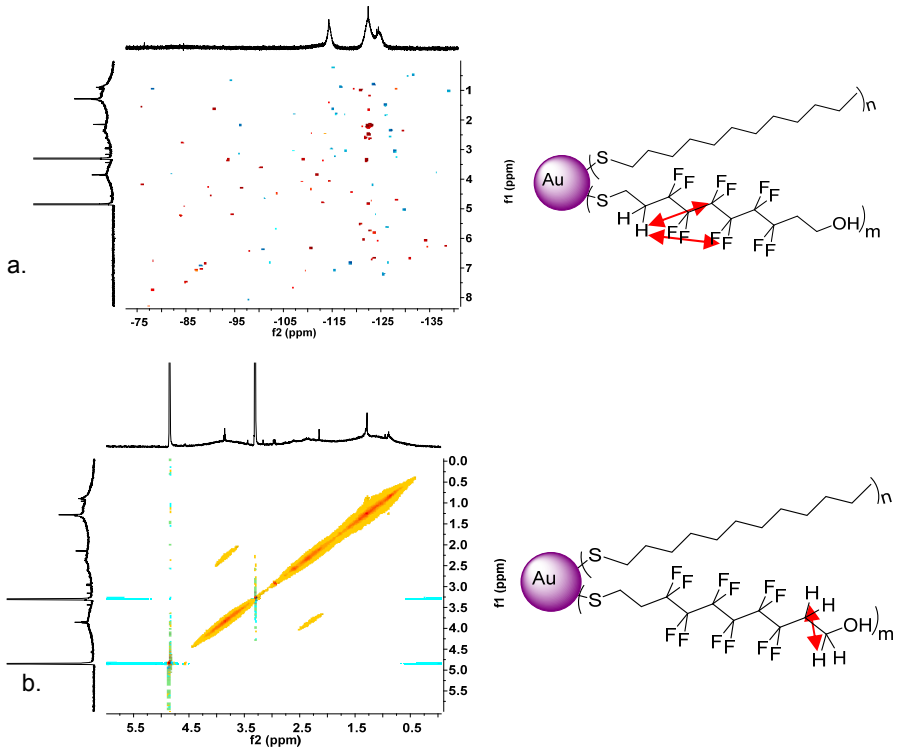

Figure 3.63 a) ^{1}H-^{19}F HOESY and b) NOESY (500 MHz, CD_3OD) spectra of **NP-C12/F6-OH**.

In the HOESY spectrum a weak cross peak between the 5- and 6- CF_2 of the fluorinated thiol and the methylene groups at 2.2 – 2.5 ppm was observed. This resonance is assigned to the CH_2 groups in position 2 and 9. In the NOESY spectrum an intramolecular cross peak between the CH_2 group in 1 and 2 and CH_2 group in 9 and 10 was observed. In addition to these intramolecular interactions, no intermolecular cross peaks between the two ligands were detected. These NMR data suggest a phase segregation of the ligands forming Janus nanoparticles. In order to analyze if AuNPs protected by ligands of different length have a different behavior, we have synthesized **NP-C16/F6-OH**.

3.6.4. Synthesis of NP-C16/F6-OH

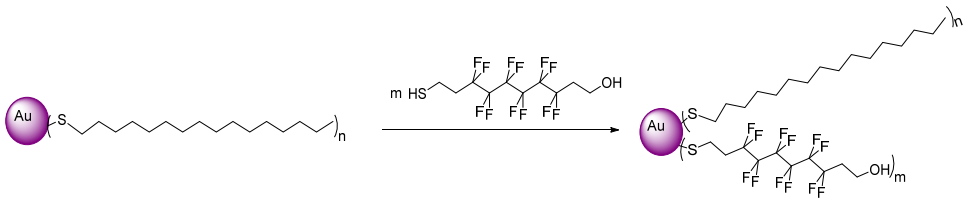

For the preparation of these nanoparticles we have used **NP-C16** previously synthesized with a gold core diameter of 4.1 nm. Briefly, 12.7 mg of **NP-C16** were dissolved in deoxygenated dichloromethane. At this solution **HS-F6-OH** in a 1/2 ratio with respect to the **C16** thiolate present into the monolayer was added. The reaction was left stirring for three days observing the formation of a black precipitate. The supernatant was taken off and the solid was found to be very soluble in MeOH. After that the nanoparticles were precipitated twice with dichloromethane and washed several times with dichloromethane and chloroform. Even for these nanoparticles we have carried out ^{1}H-^{19}F HOESY and NOESY experiments (Figure 3.64) after dissolving the nanoparticles in deoxygenated methanol.

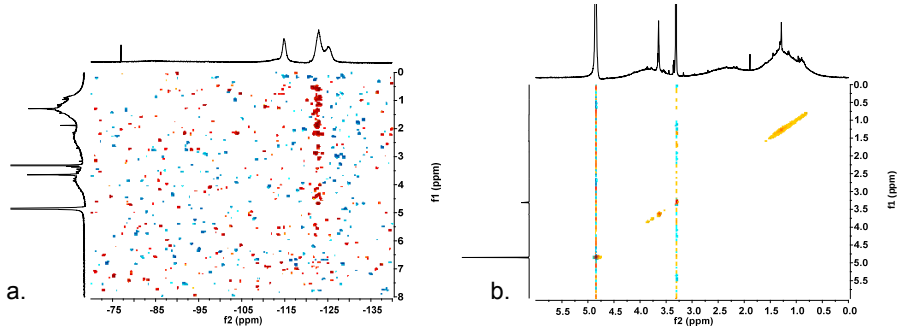

Figure 3.64 ^{1}H - ^{19}F HOESY and NOESY experiments (500 MHz, CD_3OD) of **NP-C16/F6-OH**.

The bidimensional experiments of these nanoparticles give different signals respect to those observed for **NP-C12/F6-OH**. In this case, one extended cross peak appears in the HOESY spectra between the signals found from 0.8 to 3 ppm in the ^{1}H NMR spectrum and the 5- and 6- CF_2 of the fluorinated ligand. This can be an indication that this peak is originated by an intermolecular interaction between the alkyl chain of **C16** and the fluorinated chain of **F6-OH**. Moreover, analyzing NOESY experiment no correlation peak could be observed between the signal of the fluorinated and hydrogenated ligands even though our previous studies suggest that for this length mismatch between the two ligands the nanoparticles monolayer should organize in

stripes.

These preliminary results on nanoparticles protected by mixtures of hydrogenated ligands and the thiolate **F6-OH** suggest that this species can be very useful in order to understand better the contribution of specific groups to the organization of mixed monolayer nanoparticles. Further investigations are needed in order to understand the applicability and scope of bidimensional NMR experiments on mixed monolayer gold nanoparticles protected by hydrogenated and fluorinated ligands.

3.7. Experimental part

3.7.1. General information

All commercially available reagents were from Aldrich and Alfa Aesar, and used without purification unless otherwise mentioned. Solvents were purchased from Aldrich and VWR, deuterated solvents from Cambridge Isotope Laboratories and Aldrich. Dry solvents were obtained from Aldrich and Alfa Aesar. Chlorinated solvents were kept over K_2CO_3 with occasional shaking for at least 24 h prior to use. All other solvents were reagent grade and used as received. Reactions were monitored by TLC on Merck silica gel plates (0.25 mm) and visualized by UV light, I_2, or by $KMnO_4$–H_2SO_4. Chromatography was performed on Merck silica gel 60F-254 (230–400 mesh).

Nuclear Magnetic Resonance spectra were recorded on a Varian 500 spectrometer (operating at 500 MHz for proton, at 125 MHz for carbon), or on a Jeol GX-400 MHz (operating at 400 for proton). ^{1}H NMR spectra were referenced to the residual protons in the deuterated solvent. ^{13}C NMR spectra were referenced to the solvent chemical shift. Chemical shifts (δ) are quoted in ppm and the multiplicity of each signal is designated by the conventional abbreviations: s, singlet; d, doublet; t, triplet; q, quartet; m, multiplet; br, broad; dd, doublet of doublets. Coupling constants (*J*) are quoted in Hz.

Mass spectroscopy measurements were obtained by electrospray ionization (ESI) with a Perkin Elmer APII at 5600 eV and recorded by Dr Fabio Hollan, Department of Chemical and Pharmaceutical Sciences, University of Trieste, Italy.

UV-Visible spectroscopy measurements were recorded on a Shimadzu UV-1800 spectrophotometer.

Thermogravimetric analysis (TGA) were performed on TGA Q-500 V6.3 Build 189 using platinum pans and a heating rate of 10 °C/min up to 1000 °C or on a Netzsch STA 409 using alumina crucibles and a heating rate of 10 °C/min up to 650 °C.

Transmission electron microscopy (TEM) images were obtained with either a Philips EM 208 operating at 100 kV or with a Joel 3010 high resolution electron microscope (1.7 nm point-to-point) operating at 300 keV using a *Gatan* slow-scan CCD camera (mod. 794).

3.7.2. Synthesis of 3,3,4,4,5,5,6,6,7,7,8,8,9,9,10,10,10-heptadecafluoro-1-decanethiol (HS-F10)

A mini-reactor flask was charged with 3,3,4,4,5,5,6,6,7,7,8,8,9,9,10,10,10-heptadecafluoro-1-iodine (0.052 g, 0.077 mmol), thiourea (0.0062 g, 0.0814 mmol) and ethanol (0.314 mL). The mixture was refluxed for 24 h. An aqueous KOH (0.320 mL, 0.1 M) was added. After 2 h, the mixture was allowed to cool at room temperature and

concentrated HCl was added until the sample was acidic. The mixture was extracted with hexane (2x10 mL). The organic phase was dried and the solvent was removed by rotary evaporation to give a white solid. Yield 34%.

The ^{1}H-NMR, ^{13}C-NMR, SM are in accordance with those reported in literature[29].

3.7.3. Synthesis of 3-methyldodecane-1-thiol (HS-brC12)

3-methylbut-3-enylbenzoate

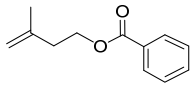

Benzoyl chloride (700 µL, 6 mmol) was added to a solution of 3-methyl-3-buthen-1-ol (608 µL, 6 mmol) in dry DCM (8 mL) at 0-5 °C under argon. Et_3N (1.69 mL, 12 mmol) was added in 15 minutes and the reaction mixture was stirred 15 minutes. DCM (2 mL) was added and the reaction mixture was stirred at room temperature for 3.5 h. 10 mL of DCM was added and the organic layer was washed with 10% HCl (2x15 mL) then saturated $NaHCO_3$ (15 mL) and brine (15 mL). The solvents were removed under reduced pressure and the crude product was purified by flash chromatography using hexane to hexane/ diethyl ether 96/4. Yield 78%.

The ^{1}H-NMR, ^{13}C NMR and Mass-spectra are in agreement with the literature.[30]

(3*E*)-3-methyldodec-3-en-1-yl benzoate

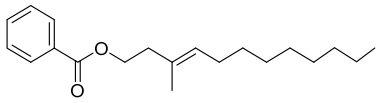

1-decene and **3-methylbut-3-enylbenzoate** were simultaneously added *via* a syringe to a stirring solution of catalyst **Cat 1** (Figure 3.37) in dry deoxygenated DCM. The reaction was refluxed under argon atmosphere for 24 h. The reaction mixture was then reduced in volume to 0.5 mL and purified directly on silica gel column, eluting with hexane.[7]

^{1}H-NMR (500 MHz, $CDCl_3$): δ = 8.05 (d, 2H, Bz), 7.43-7.55 (m, 3H, Bz), 5.26- 5.35 (m, 1H, CH_2-~~CH~~=), 4.36 (t, 2H, ~~CH_2~~O), 2.46 (m, 2H, ~~CH_2~~-CH_2-O), 2.00 (m, 2H, ~~CH_2~~-CH_2=CH), 0.87-1.78 (m, 20H, ~~CH_2~~). **^{13}C-NMR** (500 MHz, $CDCl_3$): δ = 166 (C=O), 128.2-132.7 (Bz), 121.25 (CH_2-~~CH~~=), 63.6 (~~CH_2~~O), 38.7 (~~CH_2~~-CH_2-O), 13.8-30 (~~CH_2~~).

[29] Da Costa, R., Jurisch, M., Gladysz, J., *Inorg. Chim. Acta.*, **2008**, *361*, 3205.
[30] Tokuyasu, T., *J. Org. Chem.*, **2005**, *70*(1), 251;

3-methyl-1-dodecan-benzoate

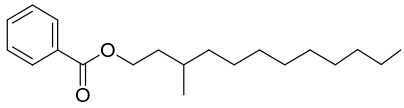

Pd/C (0.018 g) was added to 0.045 g (0.1488 mmol) of compound **2** dissolved in 2 mL of MeOH. The reaction was left under hydrogen atmosphere for 1 day. Then the reaction was stopped and the mixture was centrifuged. The supernatant was separated and the solvent was evaporated under reduced pressure obtaining a pale yellow oil.

^{1}H-NMR (500 MHz, $CDCl_3$): δ = 8.05 (d, 2H, Bz), 7.43-7.55 (m, 3H, Bz), 4.36 (t, 2H, $\underline{CH_2}O$), 2.46 (m, 2H, $\underline{CH_2}$-CH_2-O), 0.87-1.78 (m, 20H, $\underline{CH_2}$). **^{13}C-NMR** (500 MHz, $CDCl_3$): δ = 166 (C=O), 128.2-132.7 (Bz), 63.6 ($\underline{CH_2}O$), 38.7 ($\underline{CH_2}$-CH_2-O), 13.8-30 ($\underline{CH_2}$).

3-methyldodecan-1-ol

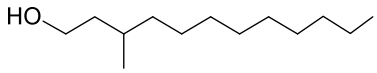

A 1% solution of KOH in methanol (1 mL) was added to 0.037 g (0.115 mmol) of 3-methyl-1-dodecan-benzoate, the reaction mixture was stirred at room temperature for 1 day. The solvent was removed under reduce pressure and the residue was dissolved first in 30 mL water and then 30 mL of hexane were added. The aqueous layer was extracted with hexane (4 x 30 mL) and ethyl acetate (4 x 30 mL). The pure product was obtained in a 56% yield.

^{1}H-NMR (500 MHz, $CDCl_3$): δ = 3.6 (m, 2H, $\underline{CH_2}$-OH), 0.87-1.78 (m, 25H, $\underline{CH_2}$).

***S*-(3-methyldodecyl) ethanethioate**

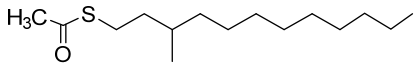

a. Triethylamine (0.125 mL, 1.24 mmol) was slowly added to an aliquot of alcohol **3-methyldodecan-1-ol** (0.050 g, 0.249 mmol) diluted in 7 mL of hexane. The reaction mixture was left stirring at room temperature for 30 minutes. The solution was cooled in an ice bath and MsCl (0.085 mL, 0.747 mmol) was added dropwise. The reaction mixture was stirred for 4 hours at room temperature and afterwards, excess MsCl was destroyed by adding 20 mL of water. The organic layer was separated and the aqueous layer was extracted with diethyl ether (8 x 30 mL). The combined organic layers were washed with 0.1 M HCl (3 x 30 mL), saturated aqueous $NaHCO_3$ (3 x 30 mL) and brine (3 x 30 mL). The organic solution was dried, filtered and brought to dryness to give 80 mg of crude product which was used in the next step without further purification. **^{1}H-NMR** (270 MHz, $CDCl_3$): δ = 4.28 (m, 2H, $\underline{CH_2}$-OMs), 3.00 (s, CH_3-O), 0.87-1.78 (m, 25H, $\underline{CH_2}$).

b. Under argon atmosphere, potassium thioacetate (65 mg, 0.498 mmol) was dissolved in 20 mL of degassed absolute ethanol. The crude mesylate, obtained in the preceding step (80 mg, 0.249 mmol) diluted with degassed ethanol (1 mL) was added over 5 minutes to the stirring solution of potassium thioacetate. The mixture was brought to reflux and kept at this temperature for 4 hours. After cooling, the precipitate was filtered off and rinsed with ethanol. The solvent was removed and the residue was taken up with a mixture of hexane (50 mL) and water (50 mL). The aqueous layer was extracted with hexane (3 x 30 mL) and the combined organic layers were washed with brine (4 x 30 mL), dried over anhydrous Na_2SO_4, and brought to dryness. The crude product was purified by column chromatography on silica gel using hexane as eluent.

^{1}H-NMR (500 MHz, $CDCl_3$): δ = 2.84-2.92 (m, 2H, $\underline{CH_2}$-SAc), 2.32 (s, 3H, CH_3-CO), 1.56, 1.4 (m, $\underline{CH_2}$- CH_2-S), 1.48 (m, 1H, CH), 1.1-1.35 (m, 14 H, CH_2), 0.89 (6H, CH_3). **^{13}C-NMR** (500 MHz, $CDCl_3$): δ = 196.09 (CO), 36.47 ($\underline{CH_2}$- CH_2-S), 32.26 (CH), 30.56 (CH_3-CO), 29.04-29.8 (CH_2), 27.04 ($\underline{CH_2}$-SAc), 22.59 (CH_2-CH_3), 19.16 (CH_3), 14.02 (CH_3-CH_2).

3-methyldodecane-1-thiol, HS-brC12

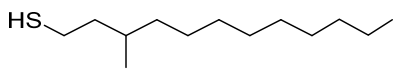

$NaBH_4$ (6.74 mmol) was added to a solution containing 0.087 g (0.337 mmol) of ***S*-(3-methyldodecyl) ethanethioate** in 5 mL of deoxygenated ethanol. The reaction mixture was stirred at room temperature for 4 hours and afterwards, the reaction mixture was treated with 20 mL of water and 20 mL of AcOEt. The phases were separated and the organic layer was extracted with water (1 x 30 mL) and dried over Na_2SO_4. The solvent was removed *in vacuo* to give 0.054 mg of colorless oil.

^{1}H-NMR (500 MHz, $CDCl_3$): δ = 2.50 (m, 2H, $\underline{CH_2}$-SH), 2.69 (m, 3H, $\underline{CH_2}$-S-S), 1.1-1.65 (m, 14 H, CH_2), 0.89 (6H, CH_3). **^{13}C-NMR** (500 MHz, $CDCl_3$): δ = 41.56 ($\underline{CH_2}$- CH_2-S), 31.947 (CH), 30.56 (CH_3-CO), 29.34-29.91 (CH_2), 22.79 ($\underline{CH_2}$-SH), 22.77 (CH_2-CH_3), 19.22 (CH_3), 14.10 (CH_3-CH_2).

3.7.4. Synthesis of the fluorinated thiol HS-F6-OH

3,3,4,4,5,5,6,6,7,7,8,8,-dodecafluorodecane-1,10,diol, HO-F6-OH

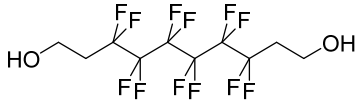

a. Vinyl acetate (0.2 mL) was added under argon atmosphere to 0.5 g (0.902mmol) of 1,6-diiodoperfluorohexane AIBN (0.020 g). The mixture was let to stir for 18 hours. The reaction was stopped and the product was purified by flash chromatography on silica gel

(eluent hexane) obtaining an air sensitive white solid. (Yield: 24%)

^{1}H-NMR (500 MHz, $CDCl_3$): δ = 7.07 (ddt, 2H, CH-SAc), 3.02, 3.29 (m, 2H, CH_2-CF_2), 2.08 (CH_3-CO). **^{19}F-NMR** (500 MHz, $CDCl_3$): δ = -112.11 to -114.61 (CF_2-CH_2); -121.69, -123.54 (-CF_2-).

b. To a solution of the pure compound obtained at point a) (140 mg, 0.192 mmol) in 7 mL dry THF, $LiAlH_4$ (1.4 mL) was added under argon atmosphere. The reaction was let to stir for 18 hours and afterwards the mixture was taken up with ethyl acetate (4 mL) and water (10 mL). The aqueous phase was extracted with diethyl ether (5x 30 mL). the combined organic layers were washed with $KHSO_4$ (2x30 mL), water (2x30 mL), dried over anhydrous Na_2SO_4, filtered and evaporated to dryness. Were obtained 85 mg of **HO-F6-OH** (Yield: 94%)

^{1}H-NMR (500 MHz, $CDCl_3$): δ = 4.00 (t, 4H, CH_2-OH), 2.4 (m, 4H, CH_2-CF_2). **^{13}C-NMR** (500 MHz, $CDCl_3$): δ = 55.3 (CH_2- OH), 33.9 (CH_2-CF_2). **^{19}F-NMR** (500 MHz, $CDCl_3$): δ = -121.84, -123.54 (CF_2), -113.45 (-CF_2-CH_2).

3,3,4,4,5,5,6,6,7,7,8,8,-dodecafluoro-10-hydroxydecyl-4-methylbenzenesulfonate, TsO-F6-OH

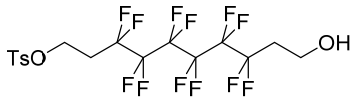

To a stirred solution of **HO-F6-OH** (0.04 g, 0.103 mmol) in THF (1 mL) were added Ag_2O (0.036 g, 0.205 mmol), TsCl (0.021 g, 0.113 mmol), KI (0.003 g, 0.02 mmol). The reaction was let to stir at room temperature for one night. The product was purified by flash chromatography on silica gel (EP/AcOEt = 95/5). Yield 60 %.

^{1}H-NMR (500 MHz, $CDCl_3$): δ = 7.8 (d, 2H, Ts), 7.35(d, 2H, Ts), 4.28 (t, 2H, CH_2-Ts), 4 (t, 2H, CH_2-OH), 2.45 (s, 3H), 2.5 (tt, 2H, CH_2-CH_2-OTs), 2.37 (tt, 2H, CH_2-CH_2-OH). **^{13}C-NMR** (500 MHz, $CDCl_3$): δ = 130.00 (Ts), 127.4 (Ts), 61.6 (CH_2-OTs), 55.28(CH_2-OH), 33.94 (CH_2-CH_2-OH), 31.08 (CH_2-CH_2-OTs), 21.64 (CH_3). **^{19}F-NMR** (500 MHz, $CDCl_3$): δ = -126.98, -126.88 (CF_2-CF_2–CH_2), -116.65 (-CF_2-CH_2–CH_2), -125.00 (CF_2).

3,3,4,4,5,5,6,6,7,7,8,8,-dodecafluoro-10-hydroxydecyl ethanethioate, AcS- F6-OH

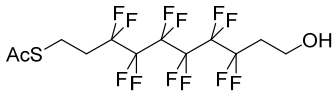

A solution of **TsO-F6-OH** (0.02 g, 0.036 mmoli) in 1 mL deoxygenated THF was added to a solution of KSAc (0.008 g, 0.072 mmoli) in 2 mL deoxygenated THF. The solution was let to stir at reflux for 3 h and after that the organic phase was washed with water (1 x 5 mL), dried and the solvent was evaporated under reduced pressure.

^{1}H-NMR (500 MHz, $CDCl_3$): δ = 4 (dd, 2H, $\underline{CH_2}$-OH), 3.1 (t, 2H, $\underline{CH_2}$ – SAc), 2.4 (tt, 2H, $\underline{CH_2}$-CH_2-OH), 2.36 (s, 3H, CH_3).). **^{13}C-NMR** (500 MHz, $CDCl_3$): δ = 194.75 (CO), 55.5 ($\underline{CH_2}$-OH), 33.90, 31.67 ($\underline{CH_2}$-CF_2), 30.5 (CH_3–CO), 19.8 (CH_2-SAc). **^{19}F-NMR** (500 MHz, $CDCl_3$): δ = -123.56, -123.86 ($\underline{CF_2}$-CF_2–CH_2), -114.6 (-$\underline{CF_2}$-CH_2–CH_2-OH), -113.43 ($\underline{CF_2}$-CH_2–CH_2-OTs), -121.83 (CF_2).

3,3,4,4,5,5,6,6,7,7,8,8,-dodecafluoro-10-mercaptodecane-1-ol, TrtS-F6-OH

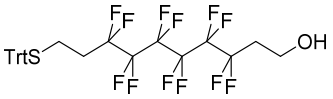

K_2CO_3 (0.020 g, 0.146 mmol) was added to a solution of TrtSH (0.020 g, 0.073 mmol) in 0.06 mL anhydrous DMF at 0 °C and let to stir for 30 min. Afterwards a solution of **TsO-F6-OH** (0.04 g, 0.073 mmol) in 0.07 mL anhydrous DMF was added dropwise. The reaction was let to stir overnight when the mixture was acidified with HCl 10% at pH = 6. The aqueous layer was washed with DCM (2 x 10 mL). The organic phase was washed with water (1 x 10 mL), brine (1 x 10 mL) dried over Na_2SO_4 and the solvent was evaporated. The mixture was purified by column chromatography on silica gel (eluent EP/AcOEt = 90/10) obtaining the pure product **TrtS-F6-OH** with in 91% yield.

^{1}H-NMR (500 MHz, $CDCl_3$): δ = 7.28 (d, 2H, Trt), 7.43 (d, 2H, Trt), 3.98 (dd, 2H, $\underline{CH_2}$-OH), 2.45 (t, 2H, $\underline{CH_2}$-STrt), 2.4 (tt, 2H, $\underline{CH_2}$-CH_2-OH), 1.8 (2H, $\underline{CH_2}$-CH_2-STrt). **^{13}C-NMR** (500 MHz, $CDCl_3$): δ = 146.66 (Trt), 129.37 (Trt), 127.97, 126.85 (Trt), 55.35 ($\underline{CH_2}$-OH), 34.02 ($\underline{CH_2}$-CH_2-OH), 31.15 ($\underline{CH_2}$-STrt), 22.56 ($\underline{CH_2}$-CH_2-STrt). **^{19}F-NMR** (500 MHz, $CDCl_3$): δ = -123.84 (CF_2), -121.87 (-$\underline{CF_2}$-CF_2-), -114.68 (TrtS–CH_2–CH_2–$\underline{CF_2}$), -113.48 (-$\underline{CF_2}$-CH_2–CH_2-OH).

3,3,4,4,5,5,6,6,7,7,8,8,-dodecafluoro-10-(trithylthio)decan-1-ol, HS-F6-OH

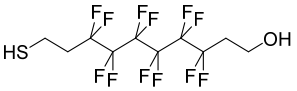

To the compound **TrtS-F6-OH** (0.13 g, 0.2 mmol), TFA (0.295 mL, 0.4 mmol) was added and the solution became intense yellow. After the addition of $^{i}Pr_3Si$ (0.1 mL, 2.2 mmol) the reaction was let to stir for 1.5 h. The product was purified by flash chromatography on silica gel (eluent EP).

^{1}H-NMR (500 MHz, $CDCl_3$): 3.85 (dd, 2H, $\underline{CH_2}$-OH), 2.79 – 2.68 (m, $\underline{CH_2}$-SH), 2.58 – 2.3 (tt, 2H, CF_2-$\underline{CH_2}$-CH_2-OH), 1.8 (2H, $\underline{CH_2}$-CH_2-SH). **^{19}F-NMR** (500 MHz, $CDCl_3$): δ = -114.2 (-$\underline{CF_2}$-CH_2 – CH_2 - OH), -115.23 ($\underline{CF_2}$–CH_2–CH_2-SH), -122.24 $(CF_2)_2$,-124.28 ppm,-124.49 (-$\underline{CF_2}$-CF_2-CH_2).

3,3,4,4,5,5,6,6,7,7,8,8,-dodecafluoro-10-(trithylthio)decane-1-methanesulfonate, TrtS-F6-OMs

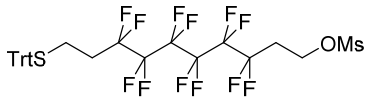

To a solution of **TrtS-F6-OH** (0.3 g, 0.462 mmol) in 1.2 mL DCM, Et_3N and MsCl were added at 0 ºC under argon atmosphere. The reaction was let to stir for 2h at room temperature. After this time, 3 mL of DCM were added and the organic phase was washed twice with saturated NH_4Cl. The organic phase was dried on anhydrous Na_2SO_4 and the solvent was removed under argon. The compound **TrtS-F6-OMs** was used for the next reaction without further purifications.

3,3,4,4,5,5,6,6,7,7,8,8,-dodecafluoro-10-bromo-1-ol, TrtS-F6-Br

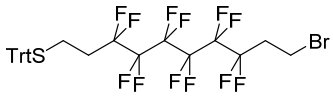

The compound **TrtS-F6-OMs** was dissolved in 1 mL anhydrous THF and at this solution LiBr (0.080 g, 0.924 Equiv.) was added under argon atmosphere. The reaction was let to stir overnight. The solvent was evaporated and the product was purified by flash chromatography (eluent EP) obtaining an yellow oil (135 mg, Yield 41%).

^{1}H-NMR (500 MHz, $CDCl_3$): δ = 7.47 (d, J=7.4 Hz, 6H, Trt), 7.43 (t, J=7.6 Hz, 6H, Trt), 7.26 (t, J=6.8 Hz, 6H), 3.55-3.48 (m, 2H, $\underline{CH_2}$-Br), 2.70 (ddd, 2H, J= 25.6, 17.3, 8 Hz, $\underline{CH_2}$-CH_2-Br), 2.50 (dd, J = 16.1, 7.4 Hz, 2H, $\underline{CH_2}$ -STrt), 1.86 (ddd, J = 26.9, 18.0, 8.7 Hz, 2H, $\underline{CH_2}$-CH_2-STrt). **^{13}C-NMR** (500 MHz, $CDCl_3$): δ = 144.28 (Trt), 129.50 (Trt), 128.06, 126.88 (Trt), 67.30 ($\underline{C}Ph_3$), 34.94 (t, $\underline{CH_2}$-CH_2-Br), 31.07 (t, $\underline{CH_2}$-CH_2-STrt), 22.69 ($\underline{CH_2}$-STrt), 20.16 ($\underline{CH_2}$-Br).

3.7.5. Synthesis of nanoparticles

The preparation of the gold nanoparticles **NP-F6**, **NP-C16/F6**, **NP-C8/F6**, and **NP-brC12/F6** was achieved by exploiting the direct synthesis following the Brust-Schiffrin procedure employing a blend of the *H*- and *F*-thiols. Otherwise, **NP-C12/F6**, **NP-C12/F10, NP-C12/F6-OH** and **NP-C16/F6-OH** were prepared by place exchange on nanoparticles bearing monolayers comprising hydrogenated thiolates only. For the preparation of the NPs by place exchange, narrowly dispersed **NP-C12** were prepared by the method of Miyake.[53]

The final ratio between the ligands has been determined from NMR spectra of the decomposed nanoparticles. At least 1 mg of nanoparticles was decomposed after the treatment with 3 mL of iodine (2 mg/mL) in chloroform overnight. The iodine and solvent excess was let to evaporate under a fume cupboard. The disulfides were dried under

vacuum and the ratio between the two ligands was determined by integration of the methylene groups in the alpha position with respect to the sulphur atom.

The diameters of the nanoparticles core were determined by TEM and the amount of organic material was assessed by thermogravimetric analyses. In some cases in both the direct synthesis and the place exchange reactions, two or three minor fractions of nanoparticles (all fractions from the same synthesis are indicated in the tables with the same lowercase letter) could be separated by exploiting their different solubility in chloroform, hexane and/or hexafluorobenzene. All of these fractions have been completely characterised. The solubility properties of these nanoparticles are indicated by adding (C); (H) or (F) to their designation, to indicate solubility in chloroform, hexane or hexafluorobenzene respectively.

3.7.5.1. Synthesis of NP-F6

Thiol **HS-F6** (0.030 mL, 0.073 mmol) was dissolved under stirring in 7 mL deoxygenated toluene. To this solution was added 0.440 mL (0.219 mmol) of a solution 0.5M sodium methoxide in methanol. The solution was stirred for an hour before use for the synthesis of the nanoparticles.

A $HAuCl_4 \cdot 3H_2O$ (0.086 g, 0.218 mmoli) aqueous solution (22.5 mL) was added to tetraoctylammonium bromide (TOAB, 0.238 g, 0.436 mmol) in toluene (60 mL) and the mixture was vigorously stirred. The yellow aqueous solution became colorless, and the toluene phase turned orange. After stirring the solution mixed with 3,3,4,4,5,5,6,6,7,7,8,8,8-tridecafluoro-octane-1-thiolate (F6-S^-Na^+, 0.07 mmol) in toluene (7 mL) for 20 minutes at room temperature and a freshly prepared aqueous solution (22.5 mL) of $NaBH_4$ (0.083, 2.19 mmol) was added to the vigorously stirred solution and the resulting solution is stirred for more than 18 h. After the separation of the two layers, the organic phase is concentrated ad reduced pressure. After the solvent removal, the solid was washed with MeOH (8x15 mL), DCM/K_2CO_3 (5x15 mL) and toluene (8x15 mL) when the ^{1}H-NMR spectra of the surnatant solution show no traces of the free thiols.

Solubility properties: soluble in chloroform/hexafluorobenzene, insoluble in dichloromethane and toluene. UV-VIS: weak surface plasmon band at around 520 nm. ^{1}H-NMR (500 MHz, $CDCl_3/C_6F_6$): δ = 0.90 (br, CH_3), 1.27 (br, $(CH_2)_9$). ^{19}F-NMR (470 MHz, $CDCl_3/C_6F_6$): δ = -82.02 (br, CF_3), -120.30 – (-122.70) $(CF_2)_3$, -125.60 (br, $\underline{CF_2}$-CF_3). TEM: 1.66 nm; σ = 0.55; n = 334. TG Analysis: 63.71%.

3.7.5.2. Synthesis of NP-F10

To an aqueous solution of $HAuCl_4$ was added a solution of TOAB in deoxygenated toluene and the mixture was let to stir for 15 minutes. Then Na^+-S-F10 (in a 3/1 Au/thiol

ratio) prepared by adding a solution of NaOMe to **HS-F10** in dry deoxygenated MeOH and let to stir for 30 minutes. A freshly prepared solution of $NaBH_4$ in deoxygenated water was added in 3'40'' and the color changed from colorless to violet. The reaction mixture was let to stir overnight when a black precipitate was observed. After repeated washes with MeOH, the nanoparticles were not soluble in any solvent, including the fluorinated ones, suggesting the formation of aggregates.

3.7.6. General procedure for the direct synthesis of nanoparticles NP-C16/F6, NP-C8/F6 and NP-brC12/F6

A solution of tetraoctylammonium bromide, 2.5 Equiv., in DCM was added to an aqueous solution of $HAuCl_4 \cdot 3H_2O$ (1 Equiv.), see Table 3.8 for **NP-C16/F6,** Table 3.11 for **NP-C8/F6** and Table 3.12 for **NP-brC12/F6**. The mixture was vigorously stirred observing fading of the aqueous phase while the organic phase turned orange. After the phase transfer was completed, a freshly prepared solution of the hydrogenated and fluorinated thiols in DCM was added to the reaction mixture. The concentration of the thiols solution, the volume used vary in the different syntheses, the total amount of thiols and their molar ratio are reported in Table 3.8 for **NP-C16/F6**, Table 3.11 for **NP-C8/F6** and Table 3.12 for **NP-brC12/F6**. The reaction mixture was left stirring at room temperature for 10 minutes and afterwards, a freshly prepared aqueous solution of $NaBH_4$ was added under vigorous stirring; the time required for adding the $NaBH_4$ solution is reported in Table 3.8 for **NP-C16/F6**, Table 3.11 for **NP-C8/F6 and** Table 3.12 for **NP-brC12/F6**. The reaction mixture was left stirring for 18 hours at room temperature.

General procedures for work-up

Nanoparticles ***NP-C16/F6.*** The organic and the aqueous layers were separated and the organic layer was washed with brine (1 x 20 mL). The nanoparticles were precipitated by addition of methanol. The turbid suspension was transferred into two centrifuge tubes and centrifuged for 3 minutes at 4500 rpm at 15 °C. The supernatant was discarded and the precipitate was washed with methanol. The crude nanoparticles preparation was recovered by centrifugation. The nanoparticles were dissolved with 1.0 mL of $CHCl_3$, the solvent was removed in an argon stream and the residue was washed with methanol (7 x 15 mL). The purified nanoparticles were subjected to selective extractions with $CHCl_3$ and afterwards with hexane. The insoluble material eventually present was tested for solubility in hexafluorobenzene. All of the fractions were characterised by ^1H NMR, UV-VIS, TGA, TEM. Synthetic details are reported in Table 3.8.

Nanoparticles ***NP-brC12/F6*** *and* ***NP-C8/F6****.* The organic and the aqueous layers were separated and the organic layer was washed with brine (1 x 20 mL) and the nanoparticles

were precipitated by addition of methanol to the organic phase. The turbid suspension was transferred into two centrifuge tubes and centrifuged for 30 minutes at 4500 rpm at 15 °C. The supernatant was discarded and the solid residue was dissolved in 1 mL of $CHCl_3$; the nanoparticles were precipitated a second time by addition of methanol and recovered by centrifugation. After removal of the supernatant, the solid was washed with MeOH (3 x 15 mL) and acetone (3 x 15 mL). The purified nanoparticles were subjected to selective extractions with $CHCl_3$ and afterwards with hexane. The insoluble material eventually present was tested for solubility in hexafluorobenzene. All of the fractions were characterized by ^{1}H NMR, UV-VIS, TGA, TEM (see Results and discussions Table 3.1 for **NP-C16/F6**, Table 3.5 for **NP-C8/F6** and Table 3.6 for **NP-brC12/F6**). Synthetic details are reported in Table 3.11 for **NP-C8/F6** and Table 3.12 for **NP-brC12/F6**.

3.7.7. General procedure for the synthesis of NP-C12/F6 and NP-C12/F10 by place exchange reaction

Synthesis of NP-C12 of 3.2 nm

A $HAuCl_4 \cdot 3H_2O$ (0.6 mmoli) aqueous solution (60 mL) was added to tetraoctylammonium bromide (TOAB, 1.2 mmol) in toluene (160 mL) and the mixture was vigorously stirred. The yellow aqueous solution became colorless, and the toluene phase turned orange. After stirring the solution mixed with dodecanthiol (DT, 1.2 mmol) in toluene (20 mL) for 10 minutes at room temperature and a freshly prepared aqueous solution (60 mL) of $NaBH_4$ (6 mmol) was added to the vigorously stirred solution and the resulting solution is stirred for more than 18 h. After the separation of the two layers, the organic phase is evaporated at reduced pressure.

^{1}H-NMR (500 MHz, $CDCl_3$): δ = 0.90 (br, CH_3), 1.27 (br, $(CH_2)_9$). UV-VIS ($CHCl_3$, c=0,1 mg/mL) λ_{max} (nm): monotonic decay from 200 nm. TEM: X_m = 1.6 nm;

The crude solid obtained was heat-treated at 150 ^{o}C at the heating rate of 2 ^{o}C/min and held for 30 minutes at this temperature. The heat-treated product was dissolved in 30 mL toluene, mixed with 1.2 mmol DT and put to react overnight. After the solvent removal, the solid was washed with MeOH (12x15 mL) and acetone (12x15 mL). ^{1}H-NMR (500 MHz, $CDCl_3$): δ = 0.90 (br, CH_3), 1.27 (br, $(CH_2)_9$). UV-VIS ($CHCl_3$, c=0,1 mg/mL) λ_{max} (nm): surface plasmon band at 520 nm. TEM: X_m = 3.2 nm; σ = 0.4 nm; n = 725. TG Analysis: 14.3%. Average composition: $Au_{1289}(C12)_{221}$.

Synthesis of nanoparticles NP-C12/F6 and NP-C12/F10.

A solution of **NP-C12** dissolved in DCM at a concentration of 2 mg/ml was deoxygenated and used for the synthesis. To the nanoparticles, was added a solution of fluorinated thiols in deoxygenated DCM (the proper amount is reported in Table 3.9 for **NP-C12/F6** and Table 3.10 for **NP-C12/F10**). The reaction mixture was kept stirring at 40 °C in a pressure-tight screw-capped reaction vessel for three days. After this time the solution was concentrated to a small volume (about 5 mL) and the nanoparticles were precipitated by addition of methanol. The supernatant was discarded and the precipitated nanoparticles were taken-up in 1 mL of $CHCl_3$ and precipitated a second time by addition of methanol. The supernatant was discarded and the solid residue was dissolved in a small amount of $CHCl_3$ and transferred in a centrifuge tube. The solvent was removed by aid of a gentle argon stream and then the residue was washed with methanol (4 x 20 mL) and acetone (4 x 20 mL). To improve the purification process, the nanoparticles were dissolved in $CHCl_3$, the solvent was removed under an argon flux, and residue washed with methanol (4 x 20 mL) and acetone (4 x 20 mL). The purified nanoparticles were subjected to selective extractions first with $CHCl_3$ and afterwards with hexane. The insoluble material eventually present was tested for solubility in hexafluorobenzene. All of the fractions were characterised by ^1H NMR, UV-VIS, TGA, TEM.

3.7.8. Synthetic details for the synthesis of mixed-monolayer protected gold nanoparticles and NMR characterization data

3.7.8.1. Synthetic details and NMR characterization data for NP-C16/F6

Table 3.8 Synthetic details for nanoparticles **NP-C16/F6**, obtained by direct synthesis.

Nanoparticles	$HAuCl_4$ (mmol)[a]	TOAB (mmol)[b]	Au/(total thiols)[c]	HS-C16/HS-F6[c] Initial ratio	$NaBH_4$ (mmol)[d]	Addition time
NP-C16/F6-a	0.129	0.322	3.0/1.0	7.0/1.0	1.29	all at once
NP-C16/F6-b	0.129	0.322	3.0/1.0	5.0/1.0	1.29	all at once
NP-C16/F6-c	0.152	0.375	3.0/1.0	3.0/1.0	1.52	3'50''
NP-C16/F6-d	0.167	0.418	3.0/1.0	3.0/1.0	1.68	3'30''
NP-C16/F6-e	0.190	0.472	3.0/1.0	2.0/1.0	1.90	3'40''
NP-C16/F6-f	0.248	0.615	3.0/1.0	1.0/1.0	2.48	4'30''
NP-C16/F6-g(C) **NP-C16/F6-g(F)**	0.152	0.375	3.0/1.0	1.0/10.0	1.52	30'
NP-C16/F6-h(C) **NP-C16/F6-h(H)** **NP-C16/F6-h(F)**	0.165	0.412	3.0/1.0	1.0/8.0	1.65	30'
NP-C16/F6-i(C) **NP-C16/F6-i(H)**	0.123	0.307	3.0/1.0	1.0/1.5	1.23	35'
NP-C16/F6-j(C) **NP-C16/F6-j(H)**	0.138	0.345	3.0/1.0	1.0/2.5	1.38	31'
NP-C16/F6-k(C) **NP-C16/F6-k(F)**	0.098	0.240	3.0/1.0	1.0/5.0	0.99	35'

[a] Used as a 34 mM solution in deoxygenated milliQ water. [b] Added as a 35 mM solution in deoxygenated DCM. [c] The thiols were added as a solution in deoxygenated DCM, the solution was prepared with the specified **HS-C16**/**HS-F6** ratio. The total concentration of the thiols (**HS-C16+HS-F6**) was adjusted in order to add exactly 1.0 ml of the solution to the mixture containing $HAuCl_4$·and TOAB. [d] Added as a 0.44 M solution.

- **NP-C16/F6-a**

^{1}H-NMR (500 MHz, $CDCl_3$): δ = 0.90 (br, CH_3), 1.27 (br, (CH_2)); **^{19}F-NMR** (470 MHz, $CDCl_3$): δ = -80.84 (br, CF_3), -120.3 to -124.1 $(CF_2)_3$, -126.10 (br, $\underline{CF_2}$-CF_3).

- **NP-C16/F6-b**

^{1}H-NMR (500 MHz, $CDCl_3$): δ = 0.90 (br, CH_3), 1.27 (br, (CH_2)); **^{19}F-NMR** (470 MHz, $CDCl_3$): δ = -81.00 (br, CF_3), -121.0 to -124.1 $(CF_2)_3$, -126.30 (br, $\underline{CF_2}$-CF_3).

- **NP-C16/F6-c**

^{1}H-NMR (500 MHz, $CDCl_3$): δ = 0.90 (br, CH_3), 1.27 (br, (CH_2)); **^{19}F-NMR** (470 MHz, $CDCl_3$): δ = -81.12 (br, CF_3), -120.8 to -124.2 $(CF_2)_3$, -126.43 (br, $\underline{CF_2}$-CF_3).

- **NP-C16/F6-d**

^{1}H-NMR (500 MHz, $CDCl_3$): δ = 0.90 (br, CH_3), 1.27 (br, (CH_2)); **^{19}F-NMR** (470 MHz, $CDCl_3$): δ = -81.00 (br, CF_3), -120.8 to -124.0 $(CF_2)_3$, -126.33 (br, $\underline{CF_2}$-CF_3).

- **NP-C16/F6-e**

^{1}H-NMR (500 MHz, $CDCl_3$): δ = 0.90 (br, CH_3), 1.27 (br, (CH_2)); **^{19}F-NMR** (470 MHz, $CDCl_3$): δ = -81.19 (br, CF_3), -120.9 to -124.7 $(CF_2)_3$, -126.43 (br, $\underline{CF_2}$-CF_3).

- **NP-C16/F6-f**

^{1}H-NMR (500 MHz, $CDCl_3$): δ = 0.90 (br, CH_3), 1.27 (br, (CH_2)); **^{19}F-NMR** (470 MHz, $CDCl_3$): δ = -81.40 (br, CF_3), -120.8 to -125.2 $(CF_2)_3$, -126.70 (br, $\underline{CF_2}$-CF_3).

- **NP-C16/F6-g(C)**

^{1}H-NMR (500 MHz, $CDCl_3$): δ = 0.90 (br, CH_3), 1.27 (br, (CH_2)); **^{19}F-NMR** (470 MHz, $CDCl_3$): δ = -81.58 (br, CF_3), -121.2 to -124.6 $(CF_2)_3$, -126.91 (br, $\underline{CF_2}$-CF_3).

- **NP-C16/F6-g(F)**

^{1}H-NMR (500 MHz, $CDCl_3/C_6F_6$): δ = 0.90 (br, CH_3), 1.27 (br, (CH_2)); **^{19}F-NMR** (470 MHz, $CDCl_3/C_6F_6$): δ = -82.11 (br, CF_3), -121.4 to -124.4 $(CF_2)_3$, -127.06 (br, $\underline{CF_2}$-CF_3).

- **NP-C16/F6-h(C)**

^{1}H-NMR (500 MHz, $CDCl_3$): δ = 0.90 (br, CH_3), 1.27 (br, (CH_2)); **^{19}F-NMR** (470 MHz, $CDCl_3$): δ = -82.51 (br, CF_3), -121.9 to -124.6 $(CF_2)_3$, -126.83 (br, $\underline{CF_2}$-CF_3).

- **NP-C16/F6-h(H)**

^{1}H-NMR (500 MHz, $CDCl_3/C_6F_6$): δ = 0.90 (br, CH_3), 1.27 (br, (CH_2)); **^{19}F-NMR** (470 MHz, $CDCl_3/C_6F_6$): δ = -81.98 (br, CF_3), -122.2 to -124.4 $(CF_2)_3$, -126.87 (br, $\underline{CF_2}$-CF_3).

- **NP-C16/F6-h(F)**

^{1}H-NMR (500 MHz, $CDCl_3/C_6F_6$): δ = 0.90 (br, CH_3), 1.27 (br, (CH_2)); **^{19}F-NMR** (470 MHz, $CDCl_3/C_6F_6$): δ = -82.11 (br, CF_3), -122.3 to -124.4 $(CF_2)_3$, -127.01 (br, $\underline{CF_2}$-CF_3).

- **NP-C16/F6-i(C)**

^{1}H-NMR (500 MHz, $CDCl_3$): δ = 0.90 (br, CH_3), 1.27 (br, (CH_2)); **^{19}F-NMR** (470 MHz, $CDCl_3$): δ = -81.51 (br, CF_3), -121.2 to -124.6 $(CF_2)_3$, -126.85 (br, $\underline{CF_2}$-CF_3).

- **NP-C16/F6-i(H)**

^{1}H-NMR (500 MHz, $CDCl_3/C_6F_6$): δ = 0.90 (br, CH_3), 1.27 (br, (CH_2)); **^{19}F-NMR** (470 MHz, $CDCl_3/C_6F_6$): δ = -82.00 (br, CF_3), -121.6 to -124.7 $(CF_2)_3$, -126.91 (br, $\underline{CF_2}$-CF_3).

- **NP-C16/F6-j(C)**

^{1}H-NMR (500 MHz, $CDCl_3$): δ = 0.90 (br, CH_3), 1.27 (br, (CH_2)); **^{19}F-NMR** (470 MHz, $CDCl_3$): δ = -81.45 (br, CF_3), -121.2 to -124.4 $(CF_2)_3$, -126.78 (br, $\underline{CF_2}$-CF_3).

- **NP-C16/F6-j(H)**

^{1}H-NMR (500 MHz, $CDCl_3/C_6F_6$): δ = 0.90 (br, CH_3), 1.27 (br, (CH_2)); **^{19}F-NMR** (470 MHz, $CDCl_3/C_6F_6$): δ = -81.95 (br, CF_3), -121.5 to -124.7 $(CF_2)_3$, -126.88 (br, $\underline{CF_2}$-CF_3).

- **NP-C16/F6-k(C)**

^{1}H-NMR (500 MHz, $CDCl_3$): δ = 0.90 (br, CH_3), 1.27 (br, (CH_2)); **^{19}F-NMR** (470 MHz, $CDCl_3$): δ = -81.47 (br, CF_3), -121.5 to -124.5 $(CF_2)_3$, -126.86 (br, $\underline{CF_2}$-CF_3).

- **NP-C16/F6-k(F)**

^{1}H-NMR (500 MHz, $CDCl_3/C_6F_6$): δ = 0.90 (br, CH_3), 1.27 (br, (CH_2)); **^{19}F-NMR** (470 MHz, $CDCl_3/C_6F_6$): δ = -82.07 (br, CF_3), -121.5 to -124.4 $(CF_2)_3$, -126.88 (br, $\underline{CF_2}$-CF_3).

3.7.8.2. Synthetic details and NMR characterization data of NP-C12/F6

Table 3.9 Synthetic details for the preparation of nanoparticles **NP-C12/F6**, obtained by place exchange reaction from **NP-C12**.

Nanoparticles	Mass NP-C12 (mg)[a]	HS-F6 (mmol)	HS-C12/HS-F6 initia ratio
NP-C12/F6-a	30.6	0.0023[b]	10.3/1.0
NP-C12/F6-b	36.5	0.0018[c]	15.0/1.0
NP-C12/F6-c	31.9	0.0059[d]	4.0/1.0
NP-C12/F6-d	30.0	0.0032[b]	7.0/1.0
NP-C12/F6-e	30.5	0.0045[d]	5.0/1.0
NP-C12/F6-f	31.9	0.0029[d]	8.0/1.0
NP-C12/F6-g	15.0	0.0054[d]	3.0/1.0
NP-C12/F6-h	31.3	0.0038[d]	4.8/1.0
NP-C12/F6-i(C) **NP-C12/F6-i(H)**	23.9	0.0079[d]	2.0/1.0
NP-C12/F6-j	23.2	0.0060[d]	2.7/1.0
NP-C12/F6-k(C) **NP-C12/F6-k(H)**	24.1	0.0105[d]	1.6/1.0
NP-C12/F6-l	26.0	0.0213[b]	1.2/1.0
NP-C12/F6-m	44.7	0.0345	1.0/1.0
NP-C12/F6-n	33.3	0.1231[c]	1.0/4.6
NP-C12/F6-o	37.0	0.0274[d]	1.0/10.0

[a] Dissolved in deoxygenated DCM to a concentration of 2.0 mg/ml. [b] Added as a 26.3 mM solution in deoxygenated DCM. [c] Added as a 131.5 mM solution in deoxygenated DCM. [d] Added as a 13.15 mM solution in deoxygenated DCM.

- **NP-C12/F6-a**

^{1}H-NMR (500 MHz, $CDCl_3$): δ = 0.90 (br, CH_3), 1.27 (br, (CH_2)); **^{19}F-NMR** (470 MHz, $CDCl_3$): δ = -80.95 (br, CF_3), -120.5 to -123.5 $(CF_2)_3$, -126.60 (br, $\underline{CF_2}$-CF_3).

- **NP-C12/F6-b**

^{1}H-NMR (500 MHz, $CDCl_3$): δ = 0.90 (br, CH_3), 1.27 (br, (CH_2)); **^{19}F-NMR** (470 MHz, $CDCl_3$): δ = -81.13 (br, CF_3), -120.4 to -124.4 $(CF_2)_3$, -126.45 (br, $\underline{CF_2}$-CF_3).

- **NP-C12/F6-c**

^{1}H-NMR (500 MHz, $CDCl_3$): δ = 0.90 (br, CH_3), 1.27 (br, (CH_2)); **^{19}F-NMR** (470 MHz, $CDCl_3$): δ = -81.00 (br, CF_3), -120.2 to -124.6 $(CF_2)_3$, -126.45 (br, $\underline{CF_2}$-CF_3).

- **NP-C12/F6-d**

^{1}H-NMR (500 MHz, $CDCl_3$): δ = 0.90 (br, CH_3), 1.27 (br, (CH_2)); **^{19}F-NMR** (470 MHz, $CDCl_3$): δ = -80.95 (br, CF_3), -120.8 to -124.2 $(CF_2)_3$, -126.27 (br, $\underline{CF_2}$-CF_3).

- **NP-C12/F6-e**

^{1}H-NMR (500 MHz, $CDCl_3$): δ = 0.90 (br, CH_3), 1.27 (br, (CH_2)); **^{19}F-NMR** (470 MHz, $CDCl_3$): δ = -81.04 (br, CF_3), -120.4 to -124.4 $(CF_2)_3$, -126.35 (br, $\underline{CF_2}$-CF_3).

- **NP-C12/F6-f**

^{1}H-NMR (500 MHz, $CDCl_3$): δ = 0.90 (br, CH_3), 1.27 (br, (CH_2)); **^{19}F-NMR** (470 MHz, $CDCl_3$): δ = -81.11 (br, CF_3), -120.6 to -124.3 $(CF_2)_3$, -126.41 (br, $\underline{CF_2}$-CF_3).

- **NP-C12/F6-g**

^{1}H-NMR (500 MHz, $CDCl_3$): δ = 0.90 (br, CH_3), 1.27 (br, (CH_2)); **^{19}F-NMR** (470 MHz, $CDCl_3$): δ = -81.06 (br, CF_3), -120.6 to -124.3 $(CF_2)_3$, -126.45 (br, $\underline{CF_2}$-CF_3).

- **NP-C12/F6-h**

^{1}H-NMR (500 MHz, $CDCl_3$): δ = 0.90 (br, CH_3), 1.27 (br, (CH_2)); **^{19}F-NMR** (470 MHz, $CDCl_3$): δ = -81.08 (br, CF_3), -120.2 to -124.3 $(CF_2)_3$, -126.37 (br, $\underline{CF_2}$-CF_3).

- **NP-C12/F6-i(C)**

^{1}H-NMR (500 MHz, $CDCl_3$): δ = 0.90 (br, CH_3), 1.27 (br, (CH_2)); **^{19}F-NMR** (470 MHz, $CDCl_3$): δ = -81.26 (br, CF_3), -120.5 to -124.5 $(CF_2)_3$, -126.52 (br, $\underline{CF_2}$-CF_3).

- **NP-C12/F6-i(H)**

^{1}H-NMR (500 MHz, $CDCl_3/C_6F_6$): δ = 0.90 (br, CH_3), 1.27 (br, (CH_2)); **^{19}F-NMR** (470 MHz, $CDCl_3/C_6F_6$): δ = -81.66 (br, CF_3), -120.8 to -124.8 $(CF_2)_3$, -126.7 (br, $\underline{CF_2}$-CF_3).

- **NP-C12/F6-j**

^{1}H-NMR (500 MHz, $CDCl_3$): δ = 0.90 (br, CH_3), 1.27 (br, (CH_2)); **^{19}F-NMR** (470 MHz, $CDCl_3$): δ = -81.22 (br, CF_3), -120.8 to -124.5 $(CF_2)_3$, -126.54 (br, $\underline{CF_2}$-CF_3).

- **NP-C12/F6-k(C)**

^{1}H-NMR (500 MHz, $CDCl_3$): δ = 0.90 (br, CH_3), 1.27 (br, (CH_2)); **^{19}F-NMR** (470 MHz, $CDCl_3$): δ = -81.15 (br, CF_3), -120.8 to -124.2 $(CF_2)_3$, -126.47 (br, $\underline{CF_2}$-CF_3).

- **NP-C12/F6-k(H)**

^{1}H-NMR (500 MHz, $CDCl_3/C_6F_6$): δ = 0.90 (br, CH_3), 1.27 (br, (CH_2)); **^{19}F-NMR** (470 MHz, $CDCl_3/C_6F_6$): δ = -81.76 (br, CF_3), -120.6 to -124.3 $(CF_2)_3$, -126.72 (br, $\underline{CF_2}$-CF_3).

- **NP-C12/F6-l**

^{1}H-NMR (500 MHz, $CDCl_3$): δ = 0.90 (br, CH_3), 1.27 (br, (CH_2)); **^{19}F-NMR** (470 MHz, $CDCl_3$): δ = -81.33 (br, CF_3), -120.2 to -124.6 $(CF_2)_3$, -126.6 (br, $\underline{CF_2}$-CF_3).

- **NP-C12/F6-m**

^{1}H-NMR (500 MHz, $CDCl_3$): δ = 0.90 (br, CH_3), 1.27 (br, (CH_2)); **^{19}F-NMR** (470 MHz, $CDCl_3$): δ = -81.94 (br, CF_3), -121.4 to -124.5 $(CF_2)_3$, -127.07 (br, $\underline{CF_2}$-CF_3).

- **NP-C12/F6-n**

^{1}H-NMR (500 MHz, $CDCl_3$): δ = 0.90 (br, CH_3), 1.27 (br, (CH_2)); **^{19}F-NMR** (470 MHz, $CDCl_3$): δ = -82.07 (br, CF_3), -120.8 to -123.9 $(CF_2)_3$, -127.14 (br, $\underline{CF_2}$-CF_3).

- **NP-C12/F6-o**

^{1}H-NMR (500 MHz, $CDCl_3$): δ = 0.90 (br, CH_3), 1.27 (br, (CH_2)); **^{19}F-NMR** (470 MHz, $CDCl_3$): δ = -82.1 (br, CF_3), -120.8 to -123.8 $(CF_2)_3$, -127.13 (br, $\underline{CF_2}$-CF_3).

3.7.8.3. Synthetic details and NMR characterization of NP-C12/F10

Table 3.10 Synthetic details for the preparation of **NP-C12/F10**, obtained by place exchange reaction

Nanoparticles	Mass NP-C12 (mg)[a]	HS-F10 (mmol)	HS-C12/ HS-F10 initial ratio
NP-C12/F10-a(C) **NP-C12/F10-a(H)**	43.0	0.0032 [b]	10.0/1.0
NP-C12/F10-b(C) **NP-C12/F10-b(H)**	47.0	0.0069[b]	5.0/1.0
NP-C12/F10-c	28.1	0.0009 [c]	21.0/1.0
NP-C12/F10-d(C) **NP-C12/F10-d(H)**	27.4	0.0045 [d]	4.2/1.0
NP-C12/F10-e	30.0	0.0517 [e]	1.0/4.0
NP-C12/F10-f	23.4	0.1053 [d]	1.0/6.0

[a] Dissolved in deoxygenated DCM to a concentration of 2.0 mg/ml. [b] Added as a 15.8 mM solution in deoxygenated DCM. [c] Added as a 22.8 mM solution in deoxygenated DCM. [d] Added as a 22.4 mM solution in deoxygenated DCM. [e] Added as a 100 mM solution in deoxygenated DCM.

- **NP-C12/F10-a(C)**

^{1}H-NMR (500 MHz, $CDCl_3$): δ = 0.90 (br, CH_3), 1.27 (br, (CH_2)); **^{19}F-NMR** (470 MHz, $CDCl_3$): δ = -81.05 (br, CF_3), -120.4 to -124.0 $(CF_2)_3$, -126.45 (br, $\underline{CF_2}$-CF_3).

- **NP-C12/F10-a(H)**

^{1}H-NMR (500 MHz, $CDCl_3/C_6F_6$): δ = 0.90 (br, CH_3), 1.27 (br, (CH_2)); **^{19}F-NMR** (470 MHz, $CDCl_3/C_6F_6$): δ = -81.53 (br, CF_3), -120.4 to -124.5 $(CF_2)_3$, -126.80 (br, $\underline{CF_2}$-CF_3).

- **NP-C12/F10-b(C)**

^{1}H-NMR (500 MHz, $CDCl_3$): δ = 0.90 (br, CH_3), 1.27 (br, (CH_2)); **^{19}F-NMR** (470 MHz, $CDCl_3$): δ = -81.19 (br, CF_3), -120.6 to -124.2 $(CF_2)_3$, -126.50 (br, $\underline{CF_2}$-CF_3).

- **NP-C12/F10-b(H)**

^{1}H-NMR (500 MHz, $CDCl_3/C_6F_6$): δ = 0.90 (br, CH_3), 1.27 (br, (CH_2)); **^{19}F-NMR** (470 MHz, $CDCl_3/C_6F_6$): δ = -81.62 (br, CF_3), -120.9 to -124.1 $(CF_2)_3$, -126.90 (br, $\underline{CF_2}$-CF_3).

- **NP-C12/F10-c**

^{1}H-NMR (500 MHz, $CDCl_3$): δ = 0.90 (br, CH_3), 1.27 (br, (CH_2)); **^{19}F-NMR** (470 MHz, $CDCl_3$): δ = -81.25 (br, CF_3), -120.4 to -124.1 $(CF_2)_3$, -126.44 (br, $\underline{CF_2}$-CF_3).

- **NP-C12/F10-d(C)**

^{1}H-NMR (500 MHz, $CDCl_3$): δ = 0.90 (br, CH_3), 1.27 (br, (CH_2)); **^{19}F-NMR** (470 MHz, $CDCl_3$): δ = -81.35 (br, CF_3), -120.2 to -124.2 $(CF_2)_3$, -126.67 (br, $\underline{CF_2}$-CF_3).

- **NP-C12/F10-d(H)**

^{1}H-NMR (500 MHz, $CDCl_3/C_6F_6$): δ = 0.90 (br, CH_3), 1.27 (br, (CH_2)); **^{19}F-NMR** (470 MHz, $CDCl_3/C_6F_6$): δ = -81.62 (br, CF_3), -120.1 to -123.7 $(CF_2)_3$, -127.01 (br, $\underline{CF_2}$-CF_3).

- **NP-C12/F10-e**

^{1}H-NMR (500 MHz, $CDCl_3$): δ = 0.90 (br, CH_3), 1.27 (br, (CH_2)); **^{19}F-NMR** (470 MHz, $CDCl_3$): δ = -81.51 (br, CF_3), -120.0 to -123.0 $(CF_2)_3$, -127.05 (br, $\underline{CF_2}$-CF_3).

- **NP-C12/F10-f**

^{1}H-NMR (500 MHz, $CDCl_3$): δ = 0.90 (br, CH_3), 1.27 (br, (CH_2)); **^{19}F-NMR** (470 MHz, $CDCl_3$): δ = -81.62 (br, CF_3), -120.0 to -122.8 $(CF_2)_3$, -127.12 (br, $\underline{CF_2}$-CF_3).

3.7.8.4. Synthetic details and NMR characterization data of NP-C8/F6

Table 3.11 Synthetic details for nanoparticles **NP-C8/F6**, obtained by direct synthesis.

Nanoparticles	$HAuCl_4$ (mmol)[a]	TOAB (mmol)[b]	Au/(total thiols)[c]	HS-C8/HS-F6 Initial ratio	$NaBH_4$ (mmol)[d]	Addition time
NP-C8/F6-a	0.140	0.360	3.0/1.0	7.0/1.0	1.43	all at once
NP-C8/F6-b	0.146	0.360	3.0/1.0	5.0/1.0	1.46	all at once
NP-C8/F6-c	0.183	0.450	3.0/1.0	3.0/1.0	1.80	3'30''
NP-C8/F6-d	0.128	0.315	3.0/1.0	1.5/1.0	1.28	3'30''
NP-C8/F6-e	0.154	0.382	3.0/1.0	2.0/1.0	1.54	3'30''
NP-C8/F6-f(C) **NP-C8/F6-f(H)** **NP-C8/F6-f(F)**	0.288	0.712	3.0/1.0	1.0/1.5	1.33	30'
NP-C8/F6-g(C) **NP-C8/F6-g(H)**	0.139	0.348	3.0/1.0	1.0/1.0	1.39	5''
NP-C8/F6-h	0.124	0.307	3.0/1.0	1.0/1.0	1.39	3'30''
NP-C8/F6-i(C) **NP-C8/F6-i(H)** **NP-C8/F6-i(F)**	0.133	0.330	3.0/1.0	1.0/2.0	1.33	3'45''
NP-C8/F6-j	0.178	0.444	3.0/1.0	1.0/5.0	1.78	30'
NP-C8/F6-k(C)[e] **NP-C8/F6-k(F)**[e]						

[a] Used as a 32 mM solution in deoxygenated milliQ water. [b] Added as a 35 mM solution in deoxygenated DCM. [c]The thiols were added as a solution in deoxygenated DCM, the solution was prepared with the specified **HS-C8/HS-F6** ratio, the total concentration of the thiols (**HS-C8+HS-F6**) was adjusted in order to add exactly 1.0 ml of the solution to the mixture containing $HAuCl_4$ and TOAB. [d] Added as a 0.42 M solution; [e] synthesized by place exchange reaction between **NP-C8** and **HS-F6**.

- **NP-C8/F6-a**

^{1}H-NMR (500 MHz, $CDCl_3$): δ = 0.90 (br, CH_3), 1.27 (br, (CH_2)); **^{19}F-NMR** (470 MHz, $CDCl_3$): δ = -80.83 (br, CF_3), -120.8 to -123.8 $(CF_2)_3$, -126.3 (br, $\underline{CF_2}$-CF_3).

- **NP-C8/F6-b**

^{1}H-NMR (500 MHz, $CDCl_3$): δ = 0.90 (br, CH_3), 1.27 (br, (CH_2)); **^{19}F-NMR** (470 MHz, $CDCl_3$): δ = -80.89 (br, CF_3), -120.8 to -124.0 $(CF_2)_3$, -126.22 (br, $\underline{CF_2}$-CF_3).

- **NP-C8/F6-c**

^{1}H-NMR (500 MHz, $CDCl_3$): δ = 0.90 (br, CH_3), 1.27 (br, (CH_2)); **^{19}F-NMR** (470 MHz, $CDCl_3$): δ = -81.01 (br, CF_3), -120.2 to -124.2 $(CF_2)_3$, -126.37 (br, $\underline{CF_2}$-CF_3).

- **NP-C8/F6-d: ^{1}H-NMR** (500 MHz, $CDCl_3$): δ = 0.90 (br, CH_3), 1.27 (br, (CH_2)); **^{19}F-NMR** (470 MHz, $CDCl_3$): δ = -81.19 (br, CF_3), -121.1 to -124.3 $(CF_2)_3$, -126.55 (br, $\underline{CF_2}$-CF_3).

- **NP-C8/F6-e**

^{1}H-NMR (500 MHz, $CDCl_3$): δ = 0.90 (br, CH_3), 1.27 (br, (CH_2)); **^{19}F-NMR** (470 MHz, $CDCl_3$): δ = -81.22 (br, CF_3), -120.8 to -124.4 $(CF_2)_3$, -126.5 (br, $\underline{CF_2}$-CF_3).

- **NP-C8/F6-f(C)**

^{1}H-NMR (500 MHz, $CDCl_3$): δ = 0.90 (br, CH_3), 1.27 (br, (CH_2)); **^{19}F-NMR** (470 MHz, $CDCl_3$): δ = -81.41 (br, CF_3), -121.2 to -124.6 $(CF_2)_3$, -126.73 (br, $\underline{CF_2}$-CF_3).

- **NP-C8/F6-f(H)**

^{1}H-NMR (500 MHz, $CDCl_3/C_6F_6$): δ = 0.90 (br, CH_3), 1.27 (br, (CH_2)); **^{19}F-NMR** (470 MHz, $CDCl_3/C_6F_6$): δ = -81.41 (br, CF_3), -120.7 to -123.7 $(CF_2)_3$, -126.73 (br, $\underline{CF_2}$-CF_3).

- **NP-C8/F6-f(F)**

^{1}H-NMR (500 MHz, $CDCl_3/C_6F_6$): δ = 0.90 (br, CH_3), 1.27 (br, (CH_2)); **^{19}F-NMR** (470 MHz, $CDCl_3/C_6F_6$): δ = -81.47 (br, CF_3), -120.6 to -123.6 $(CF_2)_3$, -126.85 (br, $\underline{CF_2}$-CF_3).

- **NP-C8/F6-g(C)**

^{1}H-NMR (500 MHz, $CDCl_3$): δ = 0.90 (br, CH_3), 1.27 (br, (CH_2)); **^{19}F-NMR** (470 MHz, $CDCl_3$): δ = -81.45 (br, CF_3), -121.8 to -124.2 $(CF_2)_3$, -126.76 (br, $\underline{CF_2}$-CF_3).

- **NP-C8/F6-g(H)**

^{1}H-NMR (500 MHz, $CDCl_3/C_6F_6$): δ = 0.90 (br, CH_3), 1.27 (br, (CH_2)); **^{19}F-NMR** (470 MHz, $CDCl_3/C_6F_6$): δ = -81.36 (br, CF_3), -120.6 to -124.3 $(CF_2)_3$, -126.8 (br, $\underline{CF_2}$-CF_3).

- **NP-C8/F6-h**

^{1}H-NMR (500 MHz, $CDCl_3$): δ = 0.90 (br, CH_3), 1.27 (br, (CH_2)); **^{19}F-NMR** (470 MHz, $CDCl_3$): δ = -81.45 (br, CF_3), -121.2 to -124.6 $(CF_2)_3$, -126.76 (br, $\underline{CF_2}$-CF_3).

- **NP-C8/F6-i(C)**

^{1}H-NMR (500 MHz, $CDCl_3$): δ = 0.90 (br, CH_3), 1.27 (br, (CH_2)); **^{19}F-NMR** (470 MHz, $CDCl_3$): δ = -81.45 (br, CF_3), -121.7 to -124.3 $(CF_2)_3$, -126.80 (br, $\underline{CF_2}$-CF_3).

- **NP-C8/F6-i(H)**

^{1}H-NMR (500 MHz, $CDCl_3/C_6F_6$): δ = 0.90 (br, CH_3), 1.27 (br, (CH_2)); **^{19}F-NMR** (470 MHz, $CDCl_3/C_6F_6$): δ = -81.51 (br, CF_3), -121.0 to -123.7 $(CF_2)_3$, -126.88 (br, $\underline{CF_2}$-CF_3).

- **NP-C8/F6-i(F)**

^{1}H-NMR (500 MHz, $CDCl_3/C_6F_6$): δ = 0.90 (br, CH_3), 1.27 (br, (CH_2)); **^{19}F-NMR** (470 MHz, $CDCl_3/C_6F_6$): δ = -81.58 (br, CF_3), -121.0 to -123.7 $(CF_2)_3$, -126.96 (br, $\underline{CF_2}$-CF_3).

- **NP-C8/F6-j**

^{1}H-NMR (500 MHz, $CDCl_3$): δ = 0.90 (br, CH_3), 1.27 (br, (CH_2)); **^{19}F-NMR** (470 MHz, $CDCl_3$): δ = -81.55 (br, CF_3), -121.2 to -123.7 $(CF_2)_3$, -126.96 (br, $\underline{CF_2}$-CF_3).

- **NP-C8/F6-k(C)**

^{1}H-NMR (500 MHz, $CDCl_3$): δ = 0.90 (br, CH_3), 1.27 (br, (CH_2)); **^{19}F-NMR** (470 MHz): δ = -81.64 (br, CF_3), -120.6 to -124.3 $(CF_2)_3$, -126.78 (br, $\underline{CF_2}$-CF_3).

- **NP-C8/F6-k(F)**

^{1}H-NMR (500 MHz, $CDCl_3/C_6F_6$): δ = 0.90 (br, CH_3), 1.27 (br, (CH_2)); **^{19}F-NMR** (470 MHz): δ = -81.53 (br, CF_3), -121.2 to -124.3 $(CF_2)_3$, -126.96 (br, $\underline{CF_2}$-CF_3).

3.7.8.5. Synthetic details and NMR characterization data of NP-brC12/F6

Table 3.12 Synthetic details for the preparation of nanoparticles **NP-brC12/F6**, obtained by direct synthesis.

Nanoparticles	$HAuCl_4$ (mmol)[a]	TOAB (mmol)[b]	Au/(total thiols)[c]	Initial ratio HS-brC12/HS-F6	$NaBH_4$ (mmol)[d,e]
NP-brC12/F6-a	0.150	0.373	4.0/1.0	10.0/1.0	1.50
NP-brC12/F6-b	0.162	0.405	4.0/1.0	3.0/1.0	1.62
NP-brC12/F6-c	0.122	0.304	4.0/1.0	1.0/1.0	1.22
NP-brC12/F6-d	0.066	0.1645	4.0/1.0	1.0/1.0	0.66
NP-brC12/F6-e	0.082	0.205	5.0/1.0	1.0/1.0	0.82
NP-brC12/F6-f	0.137	0.338	3.0/1.0	1.0/1.0	1.37
NP-brC12/F6-g	0.115	0.287	3.0/1.0	1.0/3.0	1.15
NP-brC12/F6-h	0.127	0.318	4.0/1.0	1.0/7.0	1.27
NP-brC12/F6-i	0.123	0.308	4.0/1.0	1.0/5.0	1.23

[a] Used as a 32 mM solution in deoxygenated milliQ water. [b] Added as a 34 mM solution in deoxygenated DCM. [c] The thiols were added as a solution in deoxygenated DCM, the solution was prepared with the specified **HS-brC12/HS-F6** ratio, the total concentration of the thiols (**HS-brC12+HS-F6**) was adjusted in order to add exactly 2.0 ml of the solution to the mixture containing $HAuCl_4$ and TOAB. [d] Added as a 0.4 M solution. [e] Added all at once.

- **NP-brC12/F6-a**

^{1}H-NMR (500 MHz, $CDCl_3$): δ = 0.90 (br, CH_3), 1.27 (br, (CH_2)); **^{19}F-NMR** (470 MHz, $CDCl_3$): δ = -80.84 (br, CF_3), -120.2 to -123.6 $(CF_2)_3$, -126.10 (br, $\underline{CF_2}$-CF_3).

- **NP-brC12/F6-b**

^{1}H-NMR (500 MHz, $CDCl_3$): δ = 0.90 (br, CH_3), 1.27 (br, (CH_2)); **^{19}F-NMR** (470 MHz, $CDCl_3$): δ = -80.98 (br, CF_3), -120.4 to -124.5 $(CF_2)_3$, -126.30 (br, $\underline{CF_2}$-CF_3).

- **NP-brC12/F6-c**

^{1}H-NMR (500 MHz, $CDCl_3$): δ = 0.90 (br, CH_3), 1.27 (br, (CH_2)); **^{19}F-NMR** (470 MHz,

$CDCl_3$): δ = -81.16 (br, CF_3), -120.7 to -124.5 $(CF_2)_3$, -126.50 (br, $\underline{CF_2}$-CF_3).

- **NP-brC12/F6-d**

^{1}H-NMR (500 MHz, $CDCl_3$): δ = 0.90 (br, CH_3), 1.27 (br, (CH_2)); **^{19}F-NMR** (470 MHz, $CDCl_3$): δ = -81.23 (br, CF_3), -121.0 to -124.5 $(CF_2)_3$, -126.50 (br, $\underline{CF_2}$-CF_3).

- **NP-brC12/F6-e**

^{1}H-NMR (500 MHz, $CDCl_3$): δ = 0.90 (br, CH_3), 1.27 (br, (CH_2)); **^{19}F-NMR** (470 MHz, $CDCl_3$): δ = -81.12 (br, CF_3), -120.6 to -124.5 $(CF_2)_3$, -126.40 (br, $\underline{CF_2}$-CF_3).

- **NP-brC12/F6-f**

^{1}H-NMR (500 MHz, $CDCl_3$): δ = 0.90 (br, CH_3), 1.27 (br, (CH_2)); **^{19}F-NMR** (470 MHz, $CDCl_3$): δ = -81.22 (br, CF_3), -121.0 to -124.6 $(CF_2)_3$, -126.50 (br, $\underline{CF_2}$-CF_3).

- **NP-brC12/F6-g**

^{1}H-NMR (500 MHz, $CDCl_3$): δ = 0.90 (br, CH_3), 1.27 (br, (CH_2)); **^{19}F-NMR** (470 MHz, $CDCl_3$): δ = -81.60 (br, CF_3), -120.2 to -123.9 $(CF_2)_3$, -126.90 (br, $\underline{CF_2}$-CF_3).

- **NP-brC12/F6-h**

^{1}H-NMR (500 MHz, $CDCl_3$): δ = 0.90 (br, CH_3), 1.27 (br, (CH_2)); **^{19}F-NMR** (470 MHz, $CDCl_3$): δ = -81.60 (br, CF_3), -120.6 to -124.3 $(CF_2)_3$, -126.95 (br, $\underline{CF_2}$-CF_3).

- **NP-brC12/F6-i**

^{1}H-NMR (500 MHz, $CDCl_3$): δ = 0.90 (br, CH_3), 1.27 (br, (CH_2)); **^{19}F-NMR** (470 MHz, $CDCl_3$): δ = -81.63 (br, CF_3), -120.6 to -124.3 $(CF_2)_3$, -127.0 (br, $\underline{CF_2}$-CF_3).

3.7.9. Synthesis of mixed monolayer NP-C12/F6-OH

Synthesis of NP – C12 of 4.4 nm

A $HAuCl_4$•$3H_2O$ (0.082 g, 0.21 mmoli) aqueous solution (20.7 mL) was added to tetraoctylammonium bromide (TOAB, 0.228 g, 0.42 mmol) in toluene (55.4 mL) and the mixture was vigorously stirred. The yellow aqueous solution became colorless, and the toluene phase turned orange. A solution of dodecanthiol (DT, 0.085 g, 0.42 mmol) in toluene (6.2 mL) was added and let to stir at room temperature for 10 minutes. A freshly prepared aqueous solution (20.7 mL) of $NaBH_4$ (0.079 g, 2.1 mmol) was added under vigorous stirring and the resulting solution was stirred for 18 h. After the separation of the two layers, the organic phase was evaporated at reduced pressure. The crude solid was heat-treated at 154 ^oC at the heating rate of 2 ^oC/min and held for 30 minutes at this temperature. The heat-treated product was dissolved in 30 mL toluene, mixed with 0.4 mmol DT and let to stir overnight. After the removal of the solvent, the solid was washed with MeOH (4x15 mL), dissolved in $CHCl_3$ and dried under argon, then washed again with MeOH (3x15 mL) and acetone (2x15 mL). The gold nanoparticles were obtained like a red-wine solid.

Synthesis of NP-C12/F6-OH

18.6 mg **NP-C12** were dissolved in 15 mL deoxygenated DCM and then a solution of **HS-F6-OH** (0.010 g, 0.405 mmol) in 0.480 mL deoxygenated DCM was added. The reaction was let to stir at 40 °C for 3 days. After one day was observed the precipitation of the nanoparticles and for this reason the reaction was stopped. The precipitate was separated and the nanoparticles were dissolved in MeOH and transferred in a centrifuge tube. Then the solvent was evaporated under argon and the solid was washed with DCM (3 x 10 mL) and $CHCl_3$ (2 x 10 mL). Then the nanoparticles were solubilize again in MeOH and the solvent was evaporated and after that the solid was washed again with DCM (2 X 10 mL) and $CHCl_3$ (2 x 10 mL). Ratio C12/F6-OH =1.2/1.

3.7.10. Synthesis of mixed monolayer NP-C16/F6-OH

Synthesis of NP – C16 of 4.1 nm

A $HAuCl_4 \cdot 3H_2O$ (0.076g, 0.192 mmoli) aqueous solution (19 mL) was added to tetraoctylammonium bromide (TOAB, 0.210 g, 0.385 mmol) in toluene (51 mL) and the mixture was vigorously stirred. The yellow aqueous solution became colorless and the toluene phase turned orange. Then was added hexadecanethiol (**HS-C16**, 0.1 g, 0.385 mmol) in toluene (5.7 mL) and let to stir for 10 minutes at room temperature. To the vigorously stirred solution, a freshly prepared aqueous solution (19 mL) of $NaBH_4$ (0.073 g, 1.93 mmol) was added and the resulting solution is stirred for 18 h. After the separation of the two layers, the organic phase was evaporated at reduced pressure. The crude solid was heat-treated at 154 ^oC at the heating rate of 2 ^oC/min and held at this temperature for 30 minutes. The heat-treated product was dissolved in 30 mL toluene, mixed with 0.09 g **HS-C16** and let to stir overnight. After the solvent removal, the solid was washed with MeOH (4x15 mL), dissolved in $CHCl_3$ and evaporated the solvent, then washed again with MeOH (3x15 mL) and acetone (2x15 mL). The gold nanoparticles were obtained like a red-wine solid.

Synthesis of mixed monolayer NP-C16/F6-OH

12.7 mg **NP-C16** were dissolved in 15 mL deoxygenated DCM (previously put under K_2CO_3) and a solution of **HS-F6-OH** (8.8 mg, 0.0218 mmol) in 0.44 mL deoxygenated DCM was added. The reaction was let to stir at 40 °C for 3 days. After one day, the precipitation of the nanoparticles was observed. The precipitate was separated and the nanoparticles were dissolved in MeOH and transferred in a centrifuge tube. The solvent was evaporated under argon and washed with DCM (3 x 10 mL) and $CHCl_3$ (2 x 10 mL). The nanoparticles were dissolved in MeOH, the solvent was evaporated and the solid was washed again with

DCM (2 x 10 mL) and $CHCl_3$ (2 x 10 mL). Ratio C16/F6-OH =1.2/1.

4. Synthesis of AuNPs for MRI applications

Magnetic Resonance Imaging (MRI) is a powerful technique and is actually a commonly used procedure in the practice of clinical diagnostics. Proton MRI is sensitive, but to provide sufficient contrast for practical applications it needs the use of compounds which are able to change the water protons relaxation times; these compounds are known as MRI contrast agents. Most of the contrast agents currently approved for clinical use are small molecules containing Gd(III) chelates. In seeking for improvements of the current contrast agents, the development of new species with enhanced relaxivity values, long lifetime in living body, no cyto- and systemic toxicity and ease of functionalization is currently being pursued. These features can be achieved by using water soluble gold nanoparticles decorated with Gd(III) chelates. Apart from reduced tumbling rates, nanoparticle-based contrast agents offer other advantages. Arguably the most important feature of these materials is multifunctionality which makes possible the attachment of several functional moieties to the same nanostructure, for multimodal detection or targeted delivery and/or recognition.[1]

Previously, in our group, water soluble gold nanoparticles[2] (Figure 4.1) coated with fluorinated ligands with suitable features for ^{19}F MRI applications have been designed and synthesized. It has been recently[3] demonstrated that these nanoparticles can be very good hosting scaffolds for small hydrophobic molecules. These are important results in order to obtain multimodal systems for a potential combination of imaging, targeting and drug delivery.

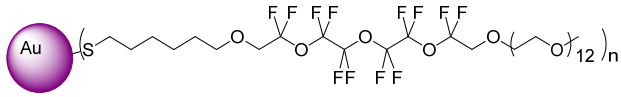

Figure 4.1 Water soluble AuNPs for ^{19}F MRI.

Based on these evidences, we have decided to investigate in closed details these systems and to improve their properties for application in MRI. In particular, we aim at decreasing the T1 and T2 relaxation times of proton and fluorine. For this purpose we have designed and synthesized the two classes of mixed monolayers AuNPs, represented in Figure 4.2.

[1] Warsi, M. F.; Adams, R.; Duckett, S.; Chechik, V., *Chem. Comm.,* **2010**, 46, 451.
[2] Boccalon, M.; Franchi, P.; Lucarini, M.; Delgrado, J. J.; Souza, F.; Stellacci, F., Zucca, I., Scotti, A.; Spreafico, R.; Pengo, P.; Pasquato, L., *Chem. Commun.,* **2013**, 49, 8794.
[3] Boccalon, M.; Bidoggia, S.; Romano, F.; Gualandi, L.; Franchi, P.; Lucarini, M.; Pengo, P.; Pasquato, L. *J. Mater. Chem. B*. **2015**, 3, 432 – 439.

The first type of nanoparticles is protected by the a mixture of thiolate **C8TEG** and a new ligand able to complex Gd(III) that was synthesized during this thesis: the gadolinium chelate, **C8-DO3AGd**. For the synthesis of the second class of nanoparticles we used a previously reported[2] fluorinated thiol and a derivative of this ligand which can bind the gadolinium ion.

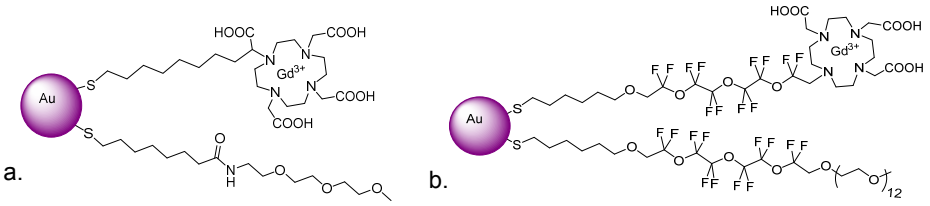

Figure 4.2 Design of AuNPs for MRI applications: a) **NP-C8TEG/C8-DO3AGd** and b) **NP-C6OF-PEG/C6OF-DO3AGd.**

The second activity developed during my PhD research work will be divided in two parts: the synthesis of the nanoparticles presented in Figure 4.2 and the description of some preliminary experimental results.

4.1. Synthesis of AuNPs for ^{1}H MRI

Previous studies[4] have shown that water soluble gold nanoparticles, **NP-C8TEG**, are very stable likely because the formation of stabilizing hydrogen bond between the ligands of the protective monolayer. To obtain these nanoparticles, very efficient synthetic routes and purification protocols have been developed. This type of nanoparticles results to be also compatible with the biological environment due to the presence of the triethylene glycol chain at the external surface of the monolayer.

These are the premises that prompted us to choose this system as scaffold for the synthesis of new and innovative AuNPs for ^{1}H MRI applications, Figure 4.2 and the monolayer of these nanoparticles will be functionalized by using a thiol able to complex the Gd(III).

The synthesis of **NP-C8TEG/C8-DO3AGd** have been realized in three steps: a) synthesis of small **NP-C8TEG** following the protocol reported previously by Pasquato[4]; b) synthesis of the new ligand able to complex the gadolinium ion, **HS-C8-DO3AGd** (Figure 4.3); c) place exchange reaction between **NP-C8TEG** and **HS-C8-DO3AGd**.

[4] Pengo, P.; Polizzi, S.; Battagliarin, M.; Pasquato, L.; Scrimin, P. *J. Mater. Chem.* **2003**, 13, 2471 – 2478.

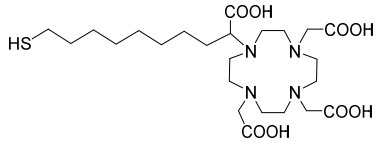

Figure 4.3 New hydrogenated ligand for complexing Gd(III).

4.1.1. Synthesis of NPs-C8TEG

4.1.1.1. Synthesis of thiol HS-C8TEG

The procedure for the synthesis of **HS-C8TEG** has been reported by Pasquato and Scrimin[4] in 2003. This thiol has been designed in order to give stable and water soluble gold nanoparticles. The stability is ensured by the alkyl chain present near the thiolated moiety, instead the solubility in water and polar solvents was obtained by attaching the triethylene glycol chain. The convergent synthesis of **HS-C8TEG** is presented in Scheme 4.1.

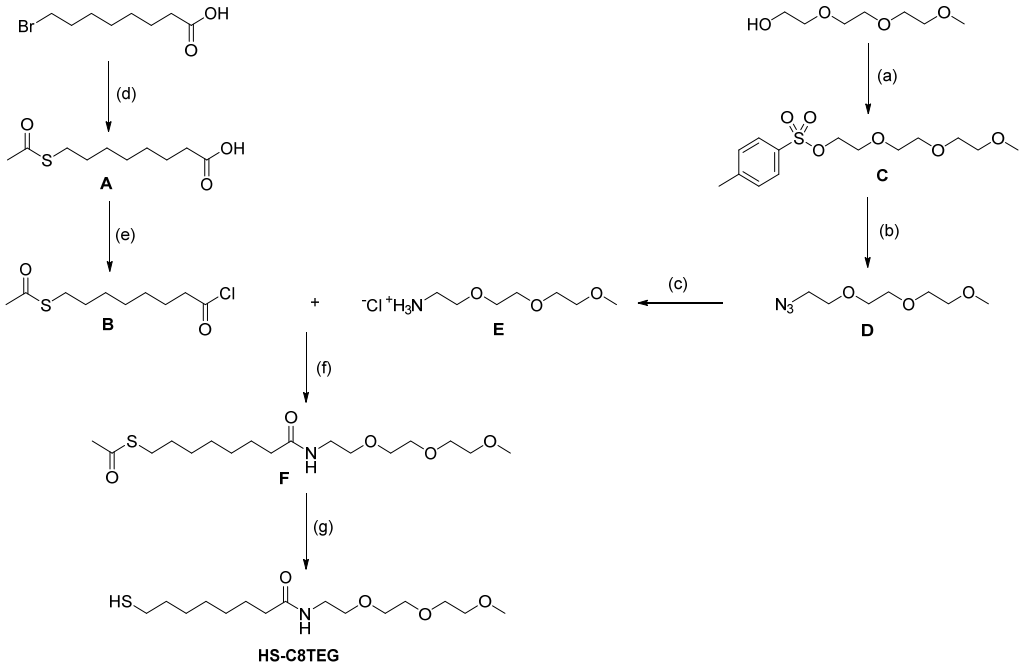

Scheme 4.1 Synthesis of thiol HS-C8TEG: a) TsCl, Et_3N, DCM, 0 °C to r.t., 18 h, 82%; b) NaN_3, MeOH/H_2O 1/2, 75 °C, 18 h, 95%; c) Triphenylphosphine, THF, 18 h, r.t., quant.; d) KSAc, DMF, 0 °C to r.t., 5 h, 92%.; e) $SOCl_2$, DCM, r.t., 3 h, quant.; f) DEA, DCM, r.t., 18 h, 75%.; g) $NaBH_4$.

In the first step, the commercially available 8-bromooctanoic acid has been converted to the corresponding thioacetate **A** by nucleophilic substitution with potassium thioacetate in dry DMF under argon atmosphere. Then, the carboxylic group was activated to the corresponding chloride **B** by reaction with thionyl chloride. On the other side, the alcohol group of the commercially available triethylene glycol monomethyl ether was transformed in a good living group by reaction with TsCl in the presence of Et_3N. The tosylate **C** has been converted into azide **D** through nucleophilic substitution with sodium azide. The reduction of the azido derivate with triphenylphosphine in THF gives the corresponding ammonium chloride **E.** The coupling of **E** with *S*-acetyl-8-thiooctanoyl chloride in the presence of triethylammine in DCM has been performed obtaining the protected thiol **F**. Subsequent removal of the acetyl group with $NaBH_4$ gave the thiol **HS-C8TEG** with 55% overall yield.

4.1.1.2. Synthesis of NPs-C8TEG

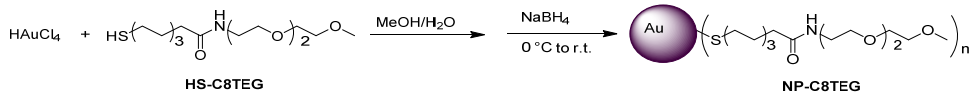

Scheme 4.2 Synthesis of **NPs-C8TEG.**

Nanoparticles **NPs-C8TEG** has been prepared using a homogenous phase synthesis in a mixture of methanol/water 1:1. In order to obtain nanoparticles with a core diameter at around 1.6 nm we have used an Au/thiol = 1/2 ratio. Briefly, a methanol solution of **HS-C8TEG** (3.2 mg/mL) has been added to an aqueous solution of tetrachloroauric acid (2 mg/mL). A freshly prepared solution of the $NaBH_4$ in water (15.6 mg/mL) was added in 10 s at 0 °C, the color of the solution turned brown indicating the formation of nanoparticles. The as obtained nanoparticles has been purified from unbound ligands with repeated washes with ethyl ether, and finally with gel permeation chromatography on *Sephadex*™ LH-20, eluting with methanol (Figure 4.4).

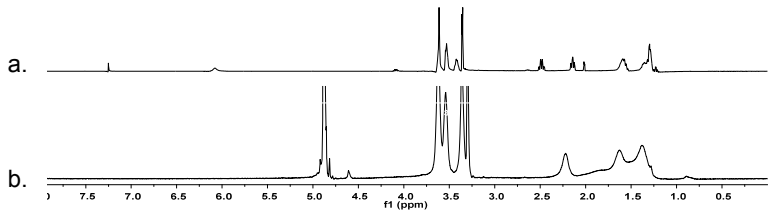

Figure 4.4 a) ^{1}H NMR (400 MHz, $CDCl_3$) of **HS-C8TEG** and b) ^{1}H NMR (400 MHz, CD_3OD) of **NP-C8TEG**.

In the UV-VIS absorption spectrum (Figure 4.5) of the NPs the surface plasmon

band at around 520 nm cannot be observed, qualitatively confirming that the nanoparticles are smaller than 2 nm. The size of the gold core of these nanoparticles was determined by TEM analysis, the diameter results to be 1.8 nm.

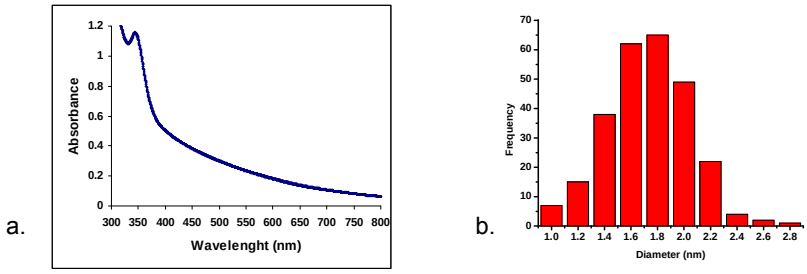

Figure 4.5 a) UV-VIS (0.1 mg/mL) spectrum of **NP-C8TEG** and b) Size histogram of **NP-C8TEG.**

The nanoparticles **NPs-C8TEG** were than used in the place exchange reaction with thiol **HS-C8-DO3AGd**, this species was synthesized as discussed below.

4.1.2. Synthesis of HS-C8-DO3AGd

The structure of **HS-C8-DO3AGd** is depicted in Figure 4.6 the hydrocarbon chain close to the thiol moiety was introduced to ensure stability to the obtained nanoparticles, the chelation of Gd(III) was ensured by using tri-*tert*-butyl 1,4,7,10-tetraazacyclododecane-1,4,7-triacetate, a derivate of DO3A. It has been demonstrated that the presence of a carboxyl group in the close proximity of this Gd(III) chelate[5] increases the relaxivity of the water protons coordinated to the Gd(III). For this reason the third important part of this ligand is the carboxylic group in the alpha position with respect to the DO3A chelating unit. The introduction of this carboxylic group was found to be the most difficult part in the synthesis of this thiol.

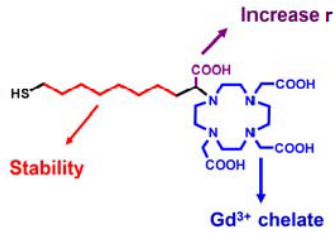

Figure 4.6 Structure of **HS-C8-DO3A**.

[5] Bernhard, C.; Moreau, M.; Lhenry, D.; Goze, C.; Boschetti, F.; Rousselin, Y.; Brunotte, F.; Denat, F. *Chem. Eur. J*. **2012**, 18, 7834 – 7841.

A first strategy for the synthesis of **HS-C8-DO3A** is presented in Scheme 4.3.

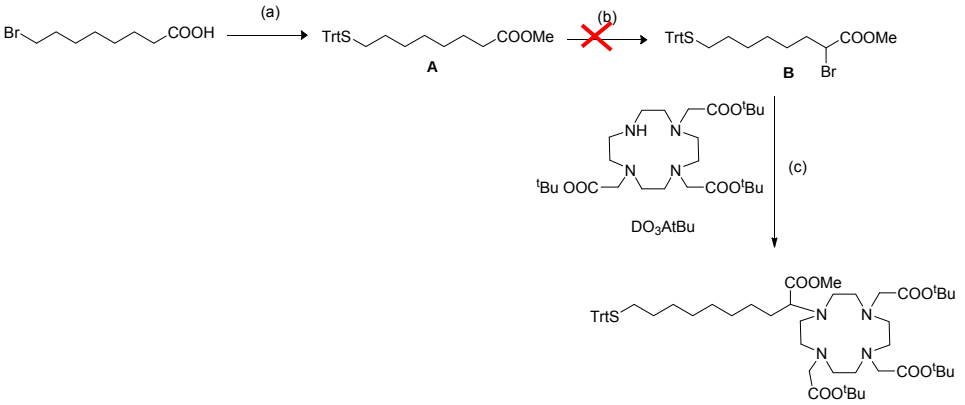

Scheme 4.3 First attempt for the synthesis of **HS-C8-DO3A** a) TrtSH, K_2CO_3, EtOH/H_2O; b) Br_2,PCl_3, CCl_4.

In a first attempt, we started from the commercially available 8-bromooctanoic acid and we have performed a nucleophilic substitution with TrtSH in the presence of K_2CO_3 to introduce the protected thiol group. The desired compound **A** was used as substrate for the next reaction, the bromination in the alpha position respect to the carboxylic moiety. The reaction was performed in the presence of Br_2 and PCl_3, but the resulting mixture did not shown the presence of the desired product. By changing the sequence of the first two steps, Scheme 4.4, to avoid the presence of the TrtSH group when adding Br_2, the nucleophilic substitution did not occur.

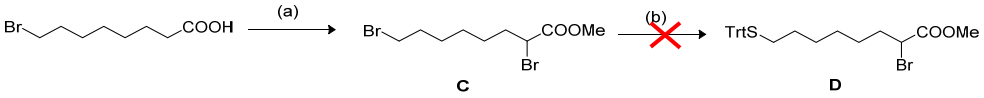

Scheme 4.4 Second procedure for the synthesis of **HS-C8-DO3A.**

To overcome these problems, we redesigned completely the strategy of synthesis, as reported in Scheme 4.5.

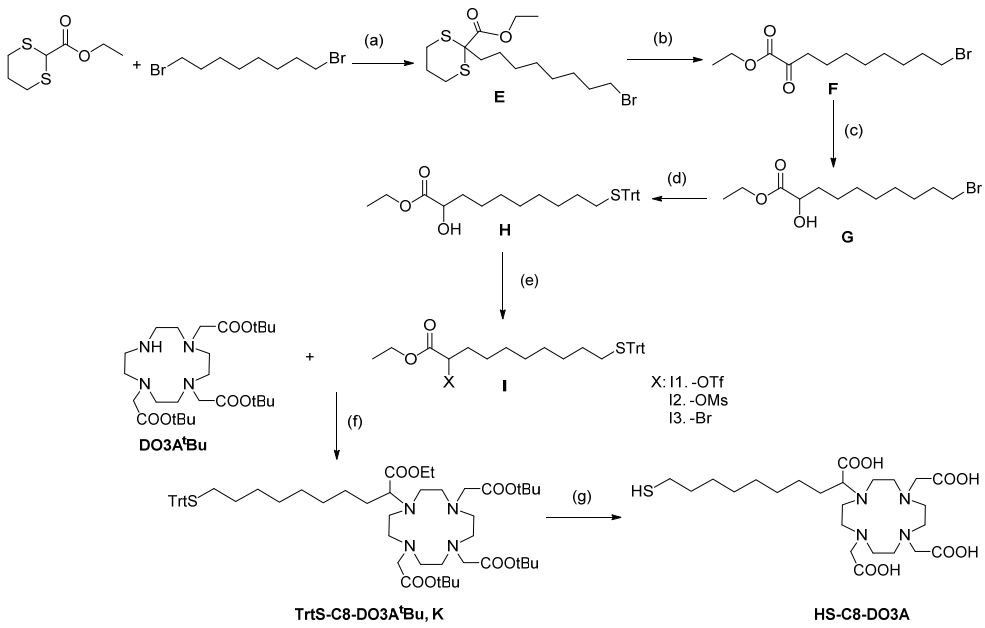

Scheme 4.5 Third strategy for the synthesis of **HS-C8-DO3A**: (a) NaH, DMF; (b) NBS, DMF/H_2O (c) $NaBH_4$, MeOH (d) NaH, TrtSH, DMF (e) I1: Tf_2O, Py; I2: MsCl, Et_3N; I3: MsCl, Et_3N; LiBr, THF; (f) K_2CO_3, DCM (g)1. NaOH; 2. TFA, TIPS, DCM.

Briefly, the commercially available 1,3-dithiane derivative reacts with 1,8-dibromooctane in the presence of a strong base, NaH, giving the product **E** which after purification by column chromatography was obtained with an overall yield of 52%. Then the carbonyl group was deprotected using NBS and the pure alpha ketoester **F** was obtained in 70% yield. The reduction of the keto group with sodium borohydride produced the pure secondary alcohol **G**. At this stage, the protected thiol group was introduced by reaction of the bromo-derivative with tritylthiol under basic conditions. After the purification of the product by column chromatography, compound **H** was obtained in 50% yield.

Different strategies have been followed in order to obtain the product **K**.

a) In the first strategy[6] the alcohol group was activated using trifluoromethane sulfonic anhydride in pyridine at 0 °C for 2 h obtaining brown oil. The as-obtained oil was reacted without further purifications or after a fast purification on a short column of silica gel with the **DO3A^{t}Bu** at room temperature overnight. In the ^{1}H NMR and mass spectra of the reaction no traces of the desired compound could be detected. To avoid the use of the very unstable triflate derivative, we have decided to pursue other strategies: the conversion of alcohol **H** to the corresponding bromide or mesyl derivative.

[6] Ansari, M.; Ahmad, M.; Dicke, K. Bioorg. *Med. Chem. Lett.* **1993**, 3, 1071 – 1072.

b) The second strategy required the activation of the alcohol group to its corresponding mesylate **I2** and the subsequent reaction with LiBr in anhydrous THF. The bromide **I3** was reacted for 1 day with **DO3A^{t}Bu** at 60 ºC using DCM as solvent. The ^{1}H NMR and the presence in the mass spectrum of a peak with m/z corresponding to the Na^+ adduct of compound **K** demonstrated the successful formation of **TrtS-C8-DO3A^{t}Bu** in 50% yield.

c) In order to increase the yield of this reaction, the mesyl derivative **I2** was reacted with DO3A^{t}Bu in the presence of K_2CO_3. In this case, the product **K** was obtained with a 58% yield. NMR experiments and mass spectroscopy have confirmed the presence of the desired compound **K**.

For the deprotection of compound **K** different procedures were tried. First, acidic and basic hydrolysis using HCl or KOH for one day were proved. The ESI-mass spectrum of the crude material demonstrated that the desired product could not be obtained and moreover, the *tert*-butyl groups were removed. To avoid this reaction we used 2 Equiv. of NaOH in a mixture of dioxane and water for five days at room temperature. After work up of the reaction, the presence of compound **K** was confirmed by ^{1}H-, ^{13}C-NMR spectra and mass analyses.

The solid was dissolved in TFA and let to stir overnight. The solvent was removed and the precipitate was dissolved in TFA/DCM and TIPS was added. The reaction mixture was left stirring for 2 hours and afterwards, the solvent was removed. The TIPS was washed with hexane and the white solid was thoroughly dried and used to place exchange with the previously synthesized **NPs-C8TEG**.

4.1.3. Synthesis of NP-C8TEG/C8-DO3AGd

4.1.3.1. Complexation of HS-C8-DO3A with Gd(III)

Thiol **HS-C8-DO3AGd** was used to complex the gadolinium ion, following the procedure reported by Penadez.[7] Briefly, the thiol **HS-C8DO3AGd** was dissolved in freshly prepared HEPES buffer (0.1 M, pH=7.4) previously deoxygenated by bubbling with argon. To the solution, 0.9 Equiv of a $GdCl_3$ solution were added and the reaction mixture was left stirring for 4 h at 25 ºC. The presence of free metal ion was assessed by using the complexometric indicator xylenol orange (Figure 4.7), a dye which displays a different color in the presence of free metal ions.

[7] Irure, A.; Marradi, M.; Arnaiz, B.; Genicio, N.; Padro, D.; Penadez, S. *Biomater. Sci.* **2013**, 658 – 668.

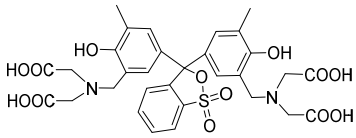

Figure 4.7 Structure of Xylenol Orange.

The color of an aqueous solution of xylenol orange depends on the pH. In fact, at acidic or neutral pH the solution is orange, when the pH is increased to basic values its color turns to violet. This change in color is determined by the deprotonation of the phenolic hydroxyl group which leads to an extended electronic delocalization. The coordination with the gadolinium ion takes place through the iminodiacetic moiety and the involvement of the phenolic oxygen which losses its proton with the consequent change of color from orange to violet. Owing a low thermodynamic stability (logK = 5.8) respect to the highly stable DO3A-Gd complexes, the xylenol orange-Gd(III) complex forms only in the presence of free Gd(III) ions. In acetate buffer (pH=5.6) solution, the xylenol orange dye shows two absorbtion maxima, at 433 and 573 nm. When the Gd(III) ion is added to the solution of the dye, the relative intensity of the two absorbtion bands changes. The free Gd(III) concentration is directly proportional to the ratio of the absorbances at 573 and 433 nm.

In order to determine the concentration of gadolinium after the complexation with **HS-C8-DO3A**, a calibration curve was realized, by calculating the ratio between of the absorbance at 573 nm and at 433 nm at increasing concentrations of Gd(III), as presented in the graphs below (Figure 4.8).

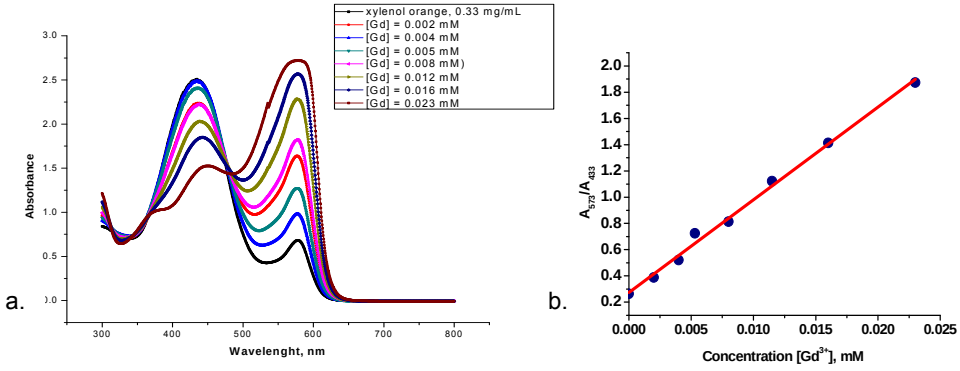

Figure 4.8 a) Spectrophotometric determination of Gd^{3+} complexed by xylenol orange; b) Calibration curve obtained by spectrophotometric changes of xylenol orange absrobtions in the presence of different amounts of Gd^{3+}.

After 4 hours the xylenol orange test suggests that the concentration of non complexed Gd(III) was below the limit of detection confirming quantitative complexation to the DO3A

moiety.

4.1.3.2. Synthesis of NP-C8TEG/C8-DO3AGd

The **HS-C8-DO3AGd** obtained according to the method outlined at point 4.1.3.1 was used to place exchange with the previously synthesized **NP-C8TEG**, as reported in Scheme 4.6.

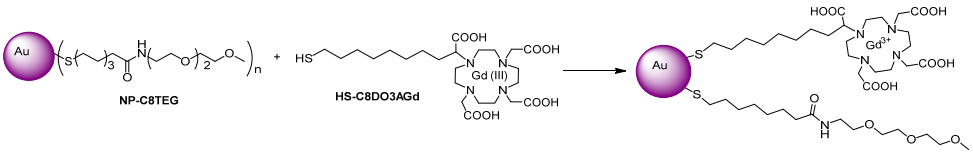

Scheme 4.6 Scheme for the synthesis of **NP-C8TEG/C8-DO3AGd.**

At the solution of **HS-C8-DO3AGd** in PBS were added 27.4 mg **NPs-C8TEG** dissolved in deoxygenated water (in a 1:1 ratio between **HS-C8TEG** present into the monolayer and **HS-DO3AGd**) and the reaction mixture was left stirring at 25 ºC for 3 days. After this time the nanoparticles were purified washing with water (7 x 30 mL). The ^{1}H NMR spectra (Figure 4.9) of these nanoparticles shown very broadened peaks determined by both the presence of the gold core and the presence of the Gd chelate.

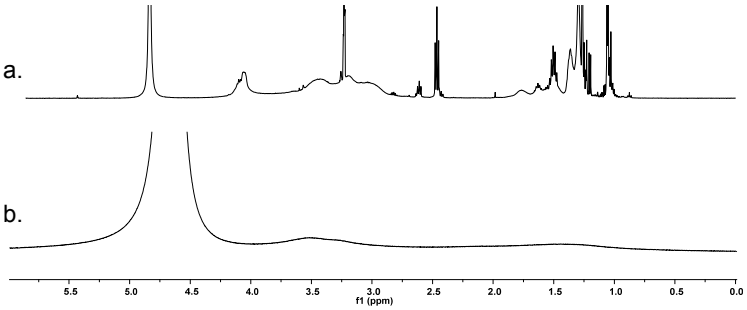

Figure 4.9 ^{1}H NMR (500MHz, CD_3OD) spectra of a) **HS-C8-DO3AGd** and b) **NP-C8TEG/C8-DO3AGd-a.**

In order to determine the number of Gd ions present into the monolayer of the nanoparticles we have considered that all the ligands **HS-C8-DO3A** are complexed with the Gd(III) ion and that free thiolates **C8-DO3A** are not present into the monolayer. The ratio between Au and Gd has been determined from ICP-AES analysis. Briefly, 1.3 mg of these nanoparticles were digested with *aqua regia* and the acqueous solution was analyzed. From the obtained emission spectra an [Au]/[Gd] = 17.4 ratio was determined. Combining these information with the size of the gold core, the average composition of the nanoparticles was assigned as follows: $Au_{201}C8TEG_{66}C8\text{-}DO3AGd_{12}$ Since the longitudinal relaxation time decreases with increasing the number of Gd ions, we aimed at further

increasing the number of **HS-C8-DO3AGd** present into the monolayer by increasing: a) the temperature at which the place exchange reaction was performed and b) the initial ratio between the incoming **HS-DO3AGd** and **HS-C8TEG** present into the monolayer.

For this purpose, 17.5 mg of **NP-C8TEG** (1 Equiv. of **HS-C8TEG**) were dissolved in deoxygenated milliQ water and this solution was added to the HEPES buffer solution of **HS-C8-DO3AGd** (1.8 Equiv.); the reaction mixture was allowed to stir at 40 ºC for 3 days. Then the nanoparticles were purified following the same procedure described for **NP-C8TEG/C8-DO3AGd-a** obtaining clean nanoparticles. The average composition of **NP-C8TEG/C8-DO3AGd-b** was determined to be $Au_{201}C8TEG_{54}C8DO3AGd_{24}$ with the loading of gadolinium chelates into the monolayer doubling when the temperature for the place exchange reaction increased from 25 ºC to 40 ºC. Further investigations will be performed in collaboration with BRACCO Imaging in order to determine the T1 and T2 of water protons relaxivity in the presence of the nanoparticles.

4.2. Synthesis of AuNPs for ^{19}F MRI

4.2.1. Synthesis of thiol HS-C6OF-PEG

In our group[3], a new fluorinated thiol (**HS-C6OF-PEG**) with suitable features for MRI applications has been designed and synthesized following the protocol reported in Scheme 4.7.

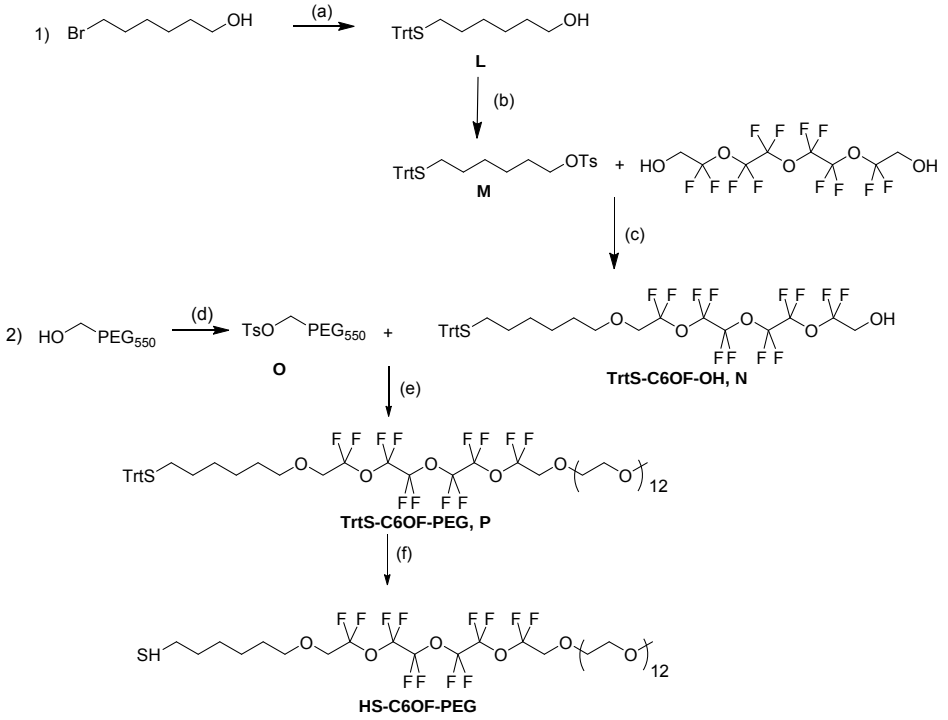

Scheme 4.7 Synthesis of thiol (a) TrtSH, K_2CO_3, EtOH/H_2O = 1/1, 90 ºC, overnight; (b) TsCl, Et_3N, DCM, r.t., overnight; (c) KOH, dioxane, reflux, overnight; (d) TsCl, DCM, r.t., overnight; (e) NaH dioxane, 50 ºC, overnight; (f) TFA, TIPS, DCM, r.t. 4 h.

The oxy-perfluorinated thiol **HS-C6OF-PEG** was synthesized in six steps. In the first step, 6-bromo-1-hexanol was reacted with TrtSH in a mixture EtOH/H_2O at reflux temperature for one day. The product **L** was obtained in quantitative yield. Then, **L** was reacted with TsCl in dry dichloromethane and after purification by flash chromatographic, pure **M** was obtained in 92% yield.

The following step includes the reaction between **M** and the oxy-perfluorinated tetraethylene glycol. The reaction of **M** with perfluorinated triethylene glycol in the presence of KOH at 80 ^{o}C gives the product **N** in 56% yield. The compound **N** reacted with PEG-OTs, **O**, in dry dioxane. The completion of the reaction was monitored by ^{1}H-NMR analysis because the purification of **P** proved to be non-practicable when traces of **O** are present.

Then, the thiol group was deprotected using TFA and TIPS and the desired product **HS-C6OF-PEG** was obtained as white solid with 30% yield.

4.2.2. Synthesis of PEG-ylated gold nanoparticles NP-C6OF-PEG

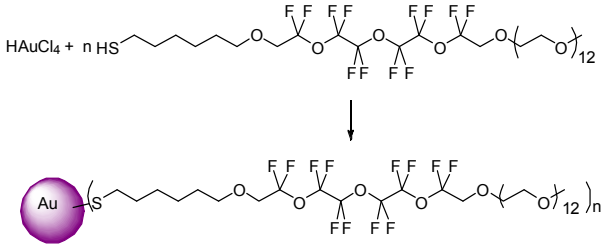

Scheme 4.8 Synthesis of **NP-C6OF-PEG.**

Water soluble gold nanoparticles protected by **HS-C6OF-PEG** have been synthesized by using a homogenous phase methanol/water procedure. Briefly, **HS-C6OF-PEG** (2 Equiv.) was added to a solution of tetrachloroauric acid (1 Equiv.) observing a color change from orange to yellow. After 1h, a freshly prepared solution of $NaBH_4$ was added all at once and the solution color change from pale yellow to brown. Then, the solution was concentrated and the nanoparticles were dialyzed against water for two days, changing the dialysis water seven times. The solution was concentrated again and purified by size exclusion chromatography using methanol as eluent. The ^{1}H NMR spectra demonstrated that the nanoparticles were clean because no sharp peaks were observed nor in the ^{1}H NMR or ^{19}F NMR spectra.

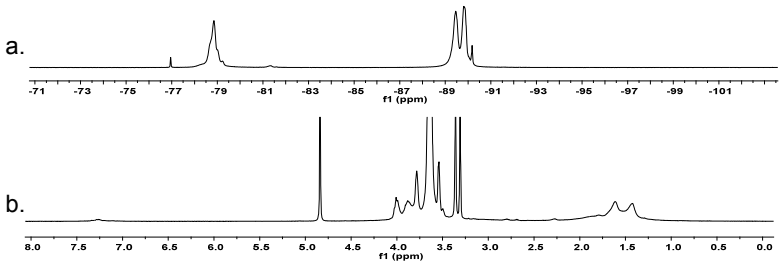

Figure 4.10 ^{19}F NMR spectrum of **NP-C6OF-PEG** and b) ^{1}H NMR of **NP-C6OF-PEG.**

By analyzing the ^{19}F NMR spectra, two signals, at -83 ppm and -94.4 ppm were observed. The T1 and T2 of these nanoparticles have been measured using the peak at -94.4 ppm, obtaining relaxation times of 588 ms and 67 ms for T1 and T2 respectively.

The UV-VIS spectrum is presented in Figure 4.11 and a very weak absorption band at around 540 nm can be seen, suggesting the presence of a population of nanoparticles with a diameter of the gold core larger than 3 nm.

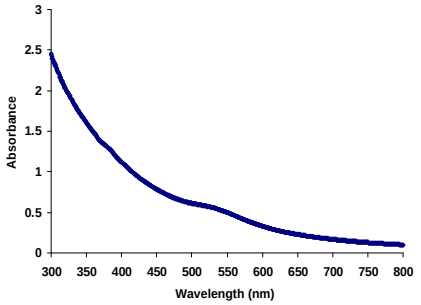

Figure 4.11 The UV-VIS absorbance spectra of **NP-C6OF-PEG.**

In order to investigate the interaction with HeLa cells, the uptake and cytotoxicity of these systems, the nanoparticles were place exchanged with a thiol presenting a BODIPY 650/665 dye unit. Cellular internalization of Bodipy labeled nanoparticles was studied by using confocal laser scanning microscopy and the presence of the nanoparticles is indicated by a red fluorescence. As can be seen in the images below (Figure 4.12), the nanoparticles are present only in the cytoplasm, being absent in the nucleus which shows a blu color.

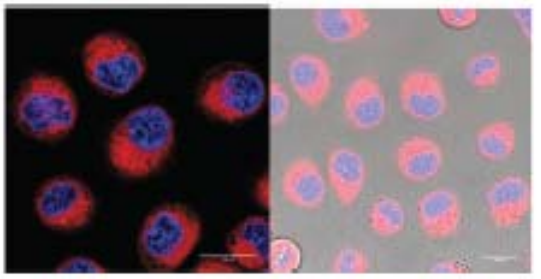

Figure 4.12 Confocal laser microscopy images, dark-field on the left and bright-field on the right, of HeLa cells (nucleus stained in blue, Hoechst dye) loaded with **NP-C6OF-PEG** (red fluorescent signal) for 4 h at 37 °C.

Preliminary results have shown that these nanoparticles have no significant toxicity in the conditions tested (4h, 37 ºC, with concentration ranging from 0.6 μM to 10 μM). For all concentrations, more than 95% of the cells were viable after the uptake of **NP-C6OF-PEG**. These promising results have determined us to design more complex systems in order to increase both the T1 and T2 and to obtain dual mode NPs for ^{1}H and ^{19}F MRI.

4.3. Synthesis of AuNPs for ^{1}H and ^{19}F MRI

4.3.1. Synthesis of HS-C6OF-DO3A

Previous studies suggested that the neighboring of fluorinated compounds and gadolinium chelates determine a huge improvement in the MRI signal. More specifically, the paramagnetic Gd(III) produces the decrease of the longitudinal and transversal relaxation times of fluorine and thus influences the performances of the nanoparticles. Starting from these previous data, we have designed and synthesized a new thiol, **HS-C6OF-DO3AGd**, presented in Scheme 0.7. This thiol has three components: a short alkyl chain in the proximity of the thiol group which gives stability to the gold nanoparticles; a fluorinated chain for the ^{19}F MRI signal and a DO3A derivative able to complex the gadolinium ion.

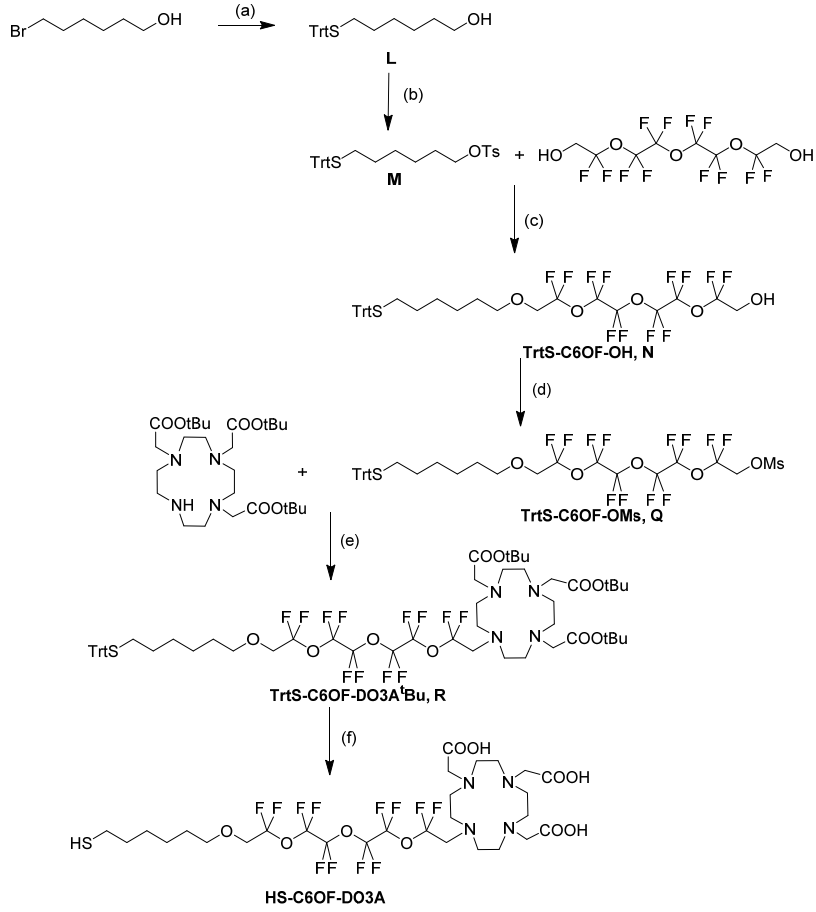

Scheme 4.13 (a) TrtSH, K_2CO_3, EtOH/H_2O; (b) TsCl, Et_3N, DCM; (c) NaH, dioxane;(d) MsCl, Et_3N, acetonitrile; (e) K_2CO_3, acetonitrile; (f) TFA, TIPS.

The compound **N** has been obtained as described previously. Then the hydroxyl group was activated using MsCl in acetonitrile giving the compound **Q**. Compound **Q** (0.8 Equiv) was added to a solution of 2 Equiv. of DO3A^{t}Bu in acetonitrile containing 8 Equiv. of K_2CO_3 and the reaction mixture was left stirring overnight at 55 ºC. After the purification of the product by flash chromatography eluting with dichloromethane, pure compound **R** was obtained with a 59 % yield. Finally, thiol **R** was deprotected using TFA and TIPS obtaining the product.

4.3.2. Synthesis of NP-C6OF-PEG/C6OF-DO3AGd

The synthesis of these nanoparticles has been performed using the same procedure reported for **NP-C8TEG/C8-DO3AGd** in Section 4.2.

Briefly, 0.04 mmol of thiol were dissolved in 2.5 mL HEPES buffer (0.1 M, pH = 7.4); under argon atmosphere, 0.41 mL of a 0.1 M aqueous solution of $GdCl_3$ were added to the thiol solution under vigorous stirring. The reaction was left stirring for 4h and afterwards an aqueous solution of **NP-C6OF-PEG** was added (in a 1:1.8 ratio respect to the **HS-C6OF-DO3AGd**). The reaction mixture was stirred for 3 days at 40 ºC. After this time the nanoparticles were transferred in two, Millipore 10000 cut off centrifugal filtration devices and washed several times with milliQ water since no free Gd (III) was observed in the permeate (using xylenol orange test). ^{1}H NMR and ^{19}F NMR analyses of these nanoparticles were performed, the spectra are reported in Figure 4.14.

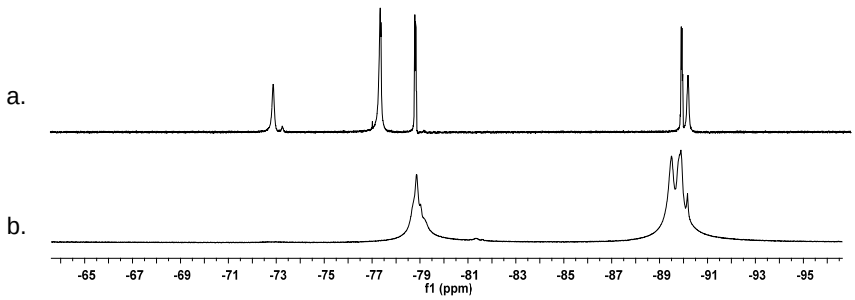

Figure 4.14 ^{19}F NMR (500 MHz, CD_3OD) of a) **HS-C6OF-DO3A** and b) ^{19}F NMR of **NP-C6OF-PEG/C6OF-DO3AGd.**

As it can be seen, the peaks of the nanoparticles are very broad with respect to the peaks of the free thiol. In fact, these spectra demonstrated that no free ligand is present. The ^{19}F NMR spectra of **NP-C6OF-PEG/C6OF-DO3AGd** present two signals, at -78.8 ppm and at -89.9 ppm. The peak at -72.8 ppm seen in the ^{19}F NMR spectra of the free thiol (Figure 4.14) disappears in the spectrum of the nanoparticles suggesting that this peak corresponds to the CF_2 group closer to the gadolinium complex. We have measured the longitudinal and

transversal relaxation times, T1 and T2 on the peak at -90 ppm by the inversion recovery procedure. The T1 for the peak at around -90 ppm was found to be 258 ms and the T2 for the same signal was found 33 ms. This demonstrates that the neighboring of a gadolinium complex with fluorine compound determines a strong decrease of the relaxation time respect with to the nanoparticles **NP-C6OF-PEG**. These preliminary results suggest that this kind of systems may function as bimodal contrast agents for MRI applications, both for ^{1}H and ^{19}F MRI. TEM analysis has shown that the nanoparticles have a gold core diameter of 1.6 nm. ICP-AES data have shown the presence of 9 moles of ligand which complex the gadolinium ion per nanoparticles. The characterization of these nanoparticles has to be completed with TGA analysis.

4.4. Experimental part

4.4.1. Synthesis of thiol HS-C8TEG

2-[2-(2-Methoxyethoxy)ethoxy]-1-ethyl-para-toluenesulfonate[8]

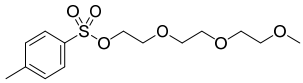

In a 100 mL round bottom flask charged with a solution of 4-toluenesulfonyl chloride (3.12 g, 16.3 x 10^{-3} mol) in dry dichloromethane (3.1 mL), a solution of triethylene glycol monomethyl ether (2.68 g, 15.8 x 10^{-3} mol) and 3.1 mL of triethylamine was added dropwise at 0 °C working under argon atmosphere. The mixture was allowed to stir at room temperature for 18 h observing the formation of a white precipitate, after completion of the reaction, the mixture was poured into water. The solution was extracted with dichloromethane (3 x 15 mL). The organic layer was washed with HCl 6 M (15 mL), $NaHCO_3$ 5% (15 mL), water (20 mL) and then dried over anhydrous Na_2SO_4. The solvent was removed under reduced pressure to yield 4.14 g as a colorless viscous oil. Yield: 82%.
^{1}H-NMR (270 MHz, $CDCl_3$): 7.80 (d, J = 8.20 Hz, 2H, Ar); 7.33 (d, J = 7.97 Hz, 2H, Ar); 4.16 (t, 2H, J = 4.82 Hz, C$\underline{H}_2$O); 3.68 (t, 2H, J = 4.83, C$\underline{H}_2$O); 3.52 -3.61 (m, 8H, (C$\underline{H}_2$O)$_4$); 3.37 (s, 3H, C$\underline{H}_3$O); 2.44 (s, 3H, C$\underline{H}_3$Ph). **^{13}C-NMR** (67.8 MHz, $CDCl_3$): 144.98 (C-Ar); 133.09 (C-Ar); 130.66 (C-Ar); 128.24 (C-Ar); 72.02 (CH_2O); 70.87 (CH_2O); 70.70 ($\underline{C}H_2$O); 69.36 ($\underline{C}H_2$O); 68.79 ($\underline{C}H_2$O); 59.16 ($\underline{C}H_3$O); 21.69 ($\underline{C}H_3$Ph). **MS-ESI** (CH_3OH) m/z: 341.2 [M + Na]$^+$.

2-[2-(2-Methoxyethoxy)ethoxy]ethyl azide

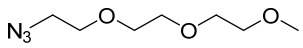

A 100 mL round-bottom flask was charged with a solution of 2-[2-(2-methoxyethoxy)ethoxy]-1-ethyl-para-toluenesulfonate (4.14 g, 13 x 10^{-3} mol) dissolved in 25 mL anhydrous DMF. To this solution, solid sodium azide (10.14 g, 156 x 10^{-3} mol) was added and the reaction mixture was heated at reflux for 18 h under stirring. Then the mixture was cooled down at room temperature and diluted with water (15 mL). The aqueous phase was extracted with dichloromethane (4 x 15 mL) and dried over anhydrous Na_2SO_4. The solvent was removed under reduced pressure giving 1.61 g of product as a colorless oil. Yield: 95%.

[8] Pengo, P.; Polizzi, S.; Battaglia, M.; Pasquato, L.; Scrimin, P. *J. Mater. Chem.* **2003**, 13, 2471-2478.

^{1}H-NMR (400 MHz, $CDCl_3$): 3.65 -3.72 (m, 8H, $(C\underline{H}_2O)_4$); 3.56 (m, 2H, $C\underline{H}_2O$); 3.38 (m, 5H, $C\underline{H}_3O+C\underline{H}_2N$). **MS-ESI** ($CH_3OH$) m/z: 341.2 $[M + Na]^+$.

2-[2-(2-Methoxyethoxy)ethoxy]ethyl ammonium chloride

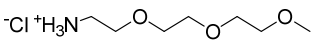

A 100 mL round-bottom flask was charged with a solution of 2-[2-(2-methoxyethoxy)ethoxy]ethyl azide (2.33 g, 12.3 x 10^{-3} mol), triphenylphosphine (6.46 g, 24.6 x 10^{-3} mol) and water (0.67 mL) in tetrahydrofuran (14 mL) The formation of bubbles of N_2 was observed. The reaction mixture was left to stir at room temperature for 18 h, then 150 mL of HCl 5% were added; a white precipitate was observed (phosphinoxide). The aqueous phase was treated with diethyl ether (6 x 15 mL) to remove any trace of phosphinoxide; the aqueous layer was dried at reduced pressure. Residual traces of water were removed by taking-up the residue with toluene and evaporating the solvent. The process was repeated several times obtaining 2.45 g of product as a pale yellow oil in quantitative yield.

^{1}H-NMR (400 MHz, $CDCl_3$): 8.22 (br, 3H, $N\underline{H}3$); 3.60- 3.90 (m, 10H, $(OC\underline{H}_2)_4$); 3.42 (s, 3H, $OC\underline{H}_3$); 3.23 (br, 2H, $C\underline{H}_2N$). **MS-ESI** (CH_3OH) m/z: 164.1 $[M + Na]^+$.

***S*-Acetyl-8-thiooctanoic acid**

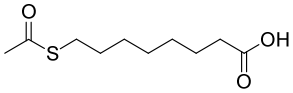

To a solution of 8-bromoctanoic acid (2.00 g, 8.96 x 10^{-3} mol) in dry DMF (5 mL) potassium thioacetate (2.00 g, 1.79 x 10^{-4} mol) was added at 0°C, under argon atmosphere. The mixture was left stirring 5 h at room temperature in the dark, and then it was diluted with water (5 mL) and diethyl ether (5 mL) The two phases were separated and the aqueous phase was extracted with diethyl ether (3 x 20 mL). The recombined organic layers were washed with water (6 x 20 mL) and brine (20 mL), the solution was dried over anhydrous Na_2SO_4 and the solvent was removed under reduced pressure affording 1.79 g of product as yellow solid. Yield: 92 %.

^{1}H-NMR (400 MHz, $CDCl_3$): 2.81 (t, 2H, J =7.3 Hz, $C\underline{H}_2S$); 2.30 (t, 2H, J = 7.3 Hz, $C\underline{H}_2CO$); 2.29 (s, 3H, $C\underline{H}_3$); 1.54 (m, 4H, $C\underline{H}_2CH_2S$ and $C\underline{H}_2CH_2CO$); 1.30 (m, 6H, $C\underline{H}_2$). **^{13}C-NMR** (68 MHz, CDCl3) : 196.13, 180.19, 33.98, 30.61, 29.36, 29.00, 28.79, 28.63, 28.46, 24.48.

_S_-Acetyl-8-thiooctanoyl chloride

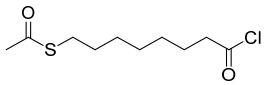

To a solution of *S*-Acetyl-8-thiooctanoic acid (1.50 g, 6.87 x 10^{-3} mol) in 30 mL of dry dichloromentane, thionyl chloride (0.56 mL, 7.69 x 10^{-3} mol) was added. The reaction mixture was stirred at room temperature under argon for 3 h. The solvent was removed under reduced pressure and the residue was co-evaporated with dry toluene (5 mL). The acetyl chloride was obtained in quantitative yield.

^{1}H-NMR (400 MHz, $CDCl_3$): 2.76 –2.94 (m, 4H, C$\underline{H}_2$CO and C$\underline{H}_2$S); 2.32 (s, 3H, C$\underline{H}_3$); 1.46 -1.85 (m, 4H, C$\underline{H}_2$CH$_2$S and C$\underline{H}_2$CH$_2$CO); 1.20 –1.45 (m, 6H, C$\underline{H}_2$).

7- ({2-[2-(2-Methoxyethoxy) ethoxy]ethyl}carbamoyl)heptyl ethanethioate

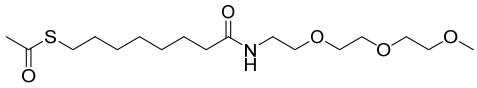

To a solution of 2-[2-(2-Methoxyethoxy)ethoxy]ethyl ammonium chloride (500 mg, 3.1 x 10^{-3} mol) in 12 mL of dry dichloromethane, a solution of *S*-Acetyl-8-thiooctanoyl chloride (1.09 g, 4.6 x 10^{-3} mol) in 10 mL of dry dichloromethane and 1.62 mL (9.3 x 10^{-3} mol) of dry diisopropylethylamine were added. The mixture was stirred at room temperature under argon atmosphere for 18 h. The mixture was extracted with 1 M HCl (2 x 10 mL), the organic layers were collected and dried over anhydrous Na_2SO_4. After solvent removal the crude product was purified by flash chromatography; eluent: ethyl acetate / petroleum ether 2 : 1. 0.845 g of product were obtained as a clear oil. Yield: 75%.

^{1}H-NMR (400 MHz, $CDCl_3$): 6.00 (br, 1H, N$\underline{H}$); 3.53 –3.67 (m, 10H, C$\underline{H}_2$O); 3.44 (m, 2H, C$\underline{H}_2$N); 3.39 (s, 3H, OC$\underline{H}_3$); 2.89 (t, 2H, J = 7.2 Hz, C$\underline{H}_2$S); 2.32 (s, 3H, C$\underline{H}_3$); 2.18 (t, 2H, J = 8.0 Hz, C$\underline{H}_2$CO), 1.45 –1.70 (m, 4H, C$\underline{H}_2$CH$_2$S and C$\underline{H}_2$CH$_2$CO);1.20 –1.45 (m, 6H, C$\underline{H}_2$). **^{13}C-NMR** (68 MHz, CDCl3): 195.94, 173.07, 71.85, 70.40, 70.36, 70.03, 69.85, 58.93, 39.01, 36.50, 30.55, 29.35, 29.02, 28.98, 28.73, 28.53, 25.54. **MS-ESI** (CH_3OH) m/z: 385 [M + Na^+].

***N*-1-{2-[2-(2-Methoxyethoxy)ethoxy]ethyl}-8-sulfanyloctanamide**

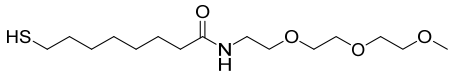

In a three neck round bottomed flask were dissolved 0.345 (0.169 mmol) of 7- ({2-[2-(2-Methoxyethoxy) ethoxy]ethyl}carbamoyl)heptyl ethanethioate in 15 mL of deoxygenated EtOH. At this solution was added $NaBH_4$ (0.53 g, 0.014 mol) and the mixture was allowed to stir for 1 h at r.t. The solution was acidified by adding HCl 1M to pH = 5. The mixture was

diluted with 10 mL of AcOEt and 20 mL of water. The aqueous phase was extracted with AcOEt (3x15 mL) and the organic phases were washed with water (1x20 mL), dried and the solvent was evaporated under reduced pressure, the product was recovered under argon.

^{1}H-NMR (500 MHz, $CDCl_3$) : 6.09 (br, 1H, NH); 3.57 -3.68 (m, 10H, $(OCH_2)_4$); 3.47 (m, 2H, CH_2N); 3.40 (s, 3H, OCH_3); 2.52 (m, 2H, CH_2S); 2.19 (t, 2H, J =7.23, CH_2CO); 1.55 -1.75 (m, 4H, CH_2); 1.28 -1.40 (m, 6H, CH_2).

4.4.2. Synthesis of NP-C8-TEG

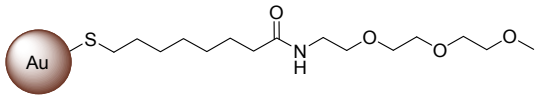

To a solution of $HAuCl_4$ (0.0807 mg, 0.205 mmol) in 40.35 mL of milliQ water a solution of HS-C8-TEG (0.132 g, 0.410 mmol) in 42.1 mL MeOH was added. The mixture was allowed to stir for 30 min and after this time, the solution was cooled at 0 °C for 30 min. To the mixture a solution of $NaBH_4$ (0.081 g, 21 mmol) in 5.65 mL of milliQ water was added in 10s and the reaction mixture was allowed to stir for 30 min at 0 °C and for 3h at r.t. The solvent was removed and the solid residue washed with diethyl ether (5 x 30 mL) then the nanoparticles were transferred in two centrifuge tubes and washed with diethyl ether (5 x 30 mL). Then purification was completed when the nanoparticles were passed through a Sephadex-LH20 column using methanol as eluent. Solubility properties: Good solubility in water, methanol and DCM. UV-VIS (CH_3OH): weak surface plasmon band at 502 nm. ^{1}H-NMR (CD_3OD, 400 MHz): δ: 1.33 (br, CH_2), 1.65 (br CH_2), 2.18 (br, CH_2CO), 3.40 (br, OCH_3), 3.55 (br, CH_2N), 3.64 (br, OCH_2), 6.09 (br, 1H, NH). TEM: X_m = 1.91 nm; σ = 0.35 nm; n = 217.

4.4.3. Synthesis of HS-C8-DO3AGd

2-(8-bromo-octyl)-[1,3]dithiane-2-carboxylic acid ethyl ester

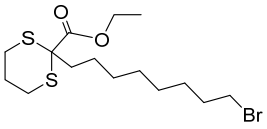

Working at 0 °C, a solution of 1,8-dibromooctane (3.5 mL, 19.03 mmol) and ethyl 1,3-dithiane-2-carboxylate (1.5 mL, 9.51 mmol) in dry DMF (3.5 mL) was added over 1 hour to a well stirred suspension of NaH (60% dispersion in mineral oil, 0.486 g, 10.46 mmol) in anhydrous toluene (10 mL). The suspension was stirred at room temperature overnight, then transferred into a separating funnel adding 40 mL of diethyl ether; the phase was washed with water (2 x 40 mL), dried and evaporated *in vacuo* to give a yellow oil. The

product was purified by flash chromatography on a silica gel column (EP to EP/AcOEt = 96/4), Yield: 55%.

10-bromo-2-oxo-decanoic acid ethyl ester

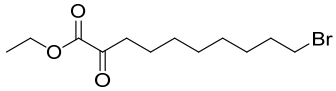

The **2-(8-bromo-octyl)-[1,3]dithiane-2-carboxylic acid ethyl ester** (1.9 g, 4.95 mmol) was dissolved in ACN (1 mL) and added over 1,5 hours to a well stirred suspension of NBS (7.06 g, 39.6 mmol) in 1.3 mL ACN and 2.4 mL maintained at 0 °C. After stirring for 2.5h, the red solution was poured into ice-cold DCM-hexane 1/1.4 (48 mL) and extracted with cold saturated $NaHSO_3$ (2 x 60 mL) and water (50 mL). The nearly colorless solution was cautiously washed with cold 20% Na_2CO_3 (1 x 30 mL), water (1 x 30 mL) and dried. Yield: 90%

^{1}H-NMR (500 MHz, $CDCl_3$): δ = 4.28 (q, 2H, $\underline{CH_2}$-COO), 3.40 (t, $\underline{CH_2}$-Br), 2.80 (t, 2H, $\underline{CH_2}$-CO), 1.8 ($\underline{CH_2}$-CH_2-Br), 1.6 ($\underline{CH_2}$-CH_2-CO), 1.2-1.4 (m, 21 H, CH_2). **^{13}C-NMR** (500 MHz, $CDCl_3$): δ = 195.00 (CO), 162,00 (COO), 62.30 ($\underline{CH_2}$-COO), 39.20 ($\underline{CH_2}$-CO), 33.90 ($\underline{CH_2}$-Br), 32.7 ($\underline{CH_2}$-CH_2-Br), 28.03-29.05 (CH_2), 22.80 ($\underline{CH_3}$-CH_2-COO).

10-bromo-2-hydroxy-decanoic acid ethyl ester

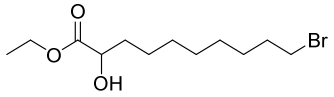

At a solution of 10-bromo-2-oxo-decanoic acid ethyl ester (1.2 g, 4 mmol) in 15 mL MeOH was added under stirring at 0 ºC $NaBH_4$ After 30 minutes, the solvent was removed then the residue was taken-up with DCM (10 mL) and the resulting solution was washed with water. The organic phase was dried and the solvent was evaporated affording the product as a yellowish oil with a 85 % yield.

^{1}H-NMR (500 MHz, $CDCl_3$): δ = 4.23 (q, 2H, $\underline{CH_2}$-COO), 4.14 (dd, 1H, CH-OH), 3.40 (t, $\underline{CH_2}$-Br), 1.80 (m, 2H, $\underline{CH_2}$-CH_2-Br), 1.75, 1.62 ($\underline{CH_2}$-CH-OH), 1.2-1.4 (m, 21 H, CH_2). **^{13}C-NMR**(500 MHz, $CDCl_3$): δ = 175.37 (CO), 70.34 (CH), 61.64 ppm($\underline{CH_2}$-COO), 34.30 ($\underline{CH_2}$-CH), 33.98($\underline{CH_2}$-Br), 28.07-29.14 (CH_2), 24.65 ($\underline{CH_3}$-CH_2-COO).

2-Hydroxy-10-tritylsulfanyl-decanoic acid ethyl ester

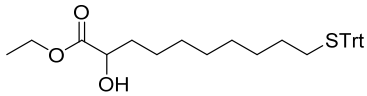

To a suspension of NaH (60% dispersion oil, 0.15 g, 3.73 mmol) in dry DMF (3,2 mL) maintained at 0 °C, was added TrtSH (0.939 g, 3.4 mmol). The mixture was allowed to stir

for 30 minutes and afterwards the compound **3** (1 g, 3.4 mmol) dissolved in 3.2 mL dry DMF was added. The mixture was left stirring overnight at room temperature and after that a mixture of EP/EE = 4/1 was added to precipitate the NaBr and the solid was filtered off. The product was purified by flash chromatography using silica gel, solvent EP/AcOEt =98/2 giving a yellow oil with a 70 % yield.

^{1}H-NMR (500 MHz, $CDCl_3$): δ = 7.2-7.4 (STrt), 4.23 (q, 2H, $\underline{CH_2}$-COO), 4.14 (dd, 1H, CH-OH), 2.14 (t, $\underline{CH_2}$-STrt), 1.60, 1.75 (m, 2H, CH_2-CH), 1.15-1.38 (m, 21 H, CH_2). **^{13}C-NMR** (500 MHz, $CDCl_3$): δ = 175.38 (CO), 145.044 (STrt), 126.46, 127.75, 129.57 (STrt) 70.40 (CH), 61.58 (CH_2-COO), 34.36 (CH_2-CH), 31.99 ($\underline{CH_2}$-STrt), 28.553-28.926 (CH_2), 24.66 (CH_3-CH_2-COO).

2-methanesulfonyl-10-tritylsulfanyl-decanoic acid ethyl ester

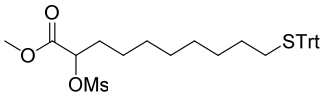

To a solution of 2-Hydroxy-10-tritylsulfanyl-decanoic acid ethyl ester (0.135 g, 0.275 mmol) in 1 mL ACN, triethylamine (80 µL, 0.55 mmol) and MsCl (70 µL, 0.826 mmol) were added dropwise at 0°. After 3.5 hours other 0.5 mL ACN, 40 µL Et_3N and 70 µL MsCl were added. After 7 hours the reaction was complete and the mixture was washed with saturated NH4Cl (1 x 20 mL) and the organic phases were washed with water brine (1 x 20 mL). The solvent was removed *in vacuo* and the product was purified by flash chromatography using silica gel, and eluting with EP/AcOEt = 98/2.

^{1}H-NMR (500 MHz, $CDCl_3$): δ = 7.2-7.4 (STrt), 4.98 (dd, 1H, CH-OH), 4.23 (q, 2H, $\underline{CH_2}$-COO), 3.13 (CH_3), 2.15 (t, $\underline{CH_2}$-STrt), 1.86 (m, 2H, CH_2-CH), 1.15-1.38 (m, 21 H, CH_2).

Coupling of the DO3A^{t}Bu with 2-methanesulfonyl-10-tritylsulfanyl-decanoic acid ethyl ester

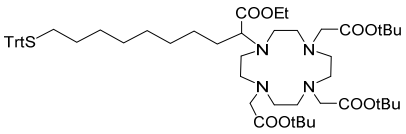

DO3A^{t}Bu (0.695 g) was added to a suspension of K_2CO_3 (0.466g, 3 Equiv.) in 8 mL acetonitrile and let to stir at 52 °C. At this mixture a solution of **2-methanesulfonyl-10-tritylsulfanyl-decanoic acid ethyl ester** (0.62g, 1 Equiv.) in 3 mL of ACN was added in 1 hour. The reaction mixture was left stirring overnight at 52 °C. The solvent was removed and the mixture was purified using a flash chromatography using DCM to DCM/MeOH = 98/2 as eluent. It was obtained the compound **6** with a 52% yield.

^{1}H-NMR (500 MHz, $CDCl_3$): δ = 7.2-7.4 ppm (STrt), 2.3-3.2 (br, 16 H, CH_2N), 3.13 (CH_3), 2.15 (t, $\underline{CH_2}$-STrt), 1.10-1.6 ppm (m, 21 H, CH_2, CH_3). ESI (MeOH) m/z: 1009 [M + Na^+], 987 [M + H^+].

Synthesis of thiol HS-C8-DO3A

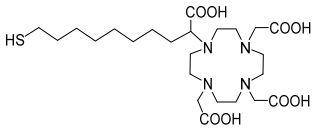

TFA (0.8 mL) was added to compound **TrtS-C8-DO3A^{t}Bu** (0.05 g, 0.052 mmol) and the solution became intense yellow, the mixture was diluted with 0.5 mL deoxygenated DCM and the reaction was let to stir overnight. Then the solvent was evaporated and to the yellowish solid was added TFA (0.2 mL) (the solution became yellow), TIPS (0.2 mL) (the solution became almost colorless) and deoxygenated DCM (1.5 mL). The reaction was allowed to stir for 2 hours and the solvent was removed *in vacuo*. Then the solid was washed five times with hexane, after removal of trace of hexane, a white solid was obtained. In the ^{1}H –NMR spectra, some small peaks at about 7.1 ppm could be seen and were assigned to the residual presence of triphenylmethane.

^{1}H-NMR (500 MHz, $CDCl_3$): δ = 2.6-3.7 (br, 16 H, CH_2N), 2.51 (t, $\underline{CH_2}$-SH), 1.10-1.6 ppm (m, CH_2). ESI **^{13}C-NMR** (500 MHz, $CDCl_3$): δ = 162.72 (CO), 61.49 (CH-COO), 49.00 – 54.95 ppm (CH_2-COO), 29.62 – 30.03 ppm (CH_2), 29.02 ($\underline{CH_2}$-SH).

Synthesis of HS-C8-DO3AGd

20 mg of **HS-C8-DO3A** (0.036 mmol) were dissolved in 1.5 mL of deoxygenated HEPES (pH = 7.4, 0.1 M in H_2O mQ). At this solution were added 0.330 mL of a 0.1 M $GdCl_3$ solution in water (0.033 mmol, 0.9 Equiv.) and the reaction was allowed to stir at 25 °C for 2 h. The Xylenol orange test suggests the complete complexation of the Gd(III). This solution will be used for the synthesis of mixed monolayers without further treatments.

4.4.4. Synthesis of NP-C8TEG/C8-DO3AGd

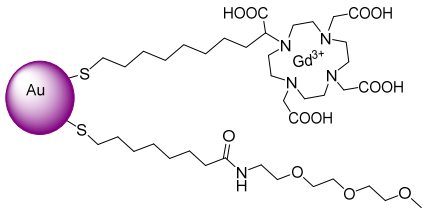

a) **NP-C8TEG/C8-DO3AGd-a:** 27.4 mg of **NP-C8TEG** were dissolved in 12 mL of deoxygenated mQ water and the solution was added at the **HS-C8DO3AGd** in HEPES buffer. The reaction mixture was allowed to stir at 25 °C for 3 days. After this time, the

nanoparticles were transferred in one Millipore centrifuge tube (10 000 MWCO)dried. Then the nanoparticles were washed with milliQ water (7 x 20 mL) and after that they were dried giving a brown solid. ICP-AES: [Au]/[Gd] = 17.4; 11.6 moli Gd/NPs. $Au_{201}C8TEG_{66}$/C8-$DO3AGd_{12}$

b) **NP-C8TEG/C8-DO3AGd-b:** 17.5 mg NP-C8TEG (1 Equiv. of **HS-C8TEG**) dissolved in 10 mL of deoxygenated milliQ water were added to 1 mL HEPES buffer solution containing **HS-C8DO3AGd** (1.8 Equiv) and the reaction was allowed to stir at 40 ºC for 3 days. Then the nanoparticles were purified following the same protocol as described for **NP-C8TEG/C8DO3AGd-a** obtaining clean nanoparticles. An aliquot of 1 mg of these nanoparticles was digested with *acqua regia* for the ICP-AES analysis, obtaining an Au/Gd ratio of 8.3. The average composition of **NP-C8TEG/C8-DO3AGd-b** was determined as $Au_{201}C8TEG_{54}C8DO3AGd_{24}$.

4.4.5. Synthesis of HS-C6OF-PEG

6-tritylthio-1-hexanol

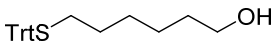

1-bromo-hexanol (2.5 mL, 19.1 mmol), tritylthiol (5.28 g, 19.1 mmol) and potassium carbonate (5.28 g, 38.2 mmol) were dissolved in 200 mL of H_2O/EtOH 1:1 mixture forming a suspension. The reaction mixture was refluxed at 90 ^oC for 18 hours. After the reaction was complete, the residue was neutralized with 1M HCl (150 mL) and extracted with DCM (5 x 100 mL). The organic layers were collected and washed with water (3 x 150 mL) and dried over Na_2SO_4. A yellow solid was obtained in quantitative yield.

^{1}H-NMR (400 MHz, $CDCl_3$): δ = 7.4-7.40 (m, 6H, Trt),7.30-7.25 (m, 6H, Trt), 7.22-7.18 (m, 3H, Trt), 3.57 (t, 2H, J = 6.6 Hz, C$\underline{H}_2$OH); 2.14 (t, 2H, J=7.3 Hz, CH_2STrt), 1.55-1.40 (m, 4H, CH_2), 1.27-1.22 (m, 4H, CH_2). **^{13}C-NMR** (67.8 MHz, $CDCl_3$): δ = 145.15 (C1 Trt), 129.68 (C3 Trt), 127.88 (C2 Trt), 126.59 (C4 Trt), 66.36 (C_q), 62.80 (CH_2OH), 32.39 (CH_2), 31.78 (CH_2), 28.60 (CH_2), 28.41 (CH_2), 25.15 (CH_2).

6-tritylthio-1-paratoluenesulfonylhexane

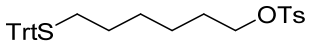

The *p*-toluenesulfonyl chloride (TsCl) (789 mg, 4.14 mmol) was dissolved under argon atmosphere in 3 mL dry DCM. The mixture was cooled at 0°C and added drop wise to a mixture of 6-tritylthio-1-hexanol (1.5 g, 3.98 mmol), triethylammine (1.11 mL, 7.96 mmol) in 1 mL of dry DCM. After two hours the reaction mixture was diluted with DCM (30 mL) and water (30 mL). The aqueous layer was extracted with DCM (4 x 30 mL). The organic layers were collected and washed with HCl 6 N (1 x 30 mL) ($NaHCO_3$ 5 % (2 x 40 mL) and H_2O (2

x 40 mL), dried over Na_2SO_4, filtered and the solvent removed under reduced pressure. The product was purified by flash chromatography, using $CHCl_3$/Petroleum ether 6/4 as eluent obtaining a white solid. Yield: 92%.

^{1}H-NMR (270 MHz, $CDCl_3$): δ = 7.79 (m, 2H, Ts), 7.42-7.21 (m, 17H, Trt+Ts), 3.98 (m, 2H, CH_2OTs); 2.44 (s, 3H, CH_3), 2.11 (t, 2H, J=7.3 Hz, CH_2STrt), 1.53 (m, 2H, CH_2), 1.28 (m, 2H, CH_2), 1.18 (m, 2H, CH_2) ppm. **^{13}C-NMR** (67.8 MHz, $CDCl_3$): δ = 145.15, 144.77, 133.30, 129.9, 127.9, 126.64, 70.41, 66.42, 31.63, 28.47, 24.78, 22.54, 21.51, 13.99 ppm. **MS-ESI** (m/z): 553.2 [M+Na^+], 569.2 [M+K^+].

Coupling of 6-tritylthio-1-paratoluenesulfonylhexane with oxy-fluorinated tetraethylene glycol, HS-C6OF-OH

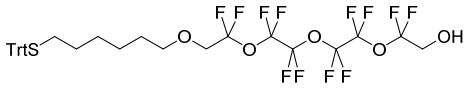

To a solution of perfluorinated tetraethylene glycol (1.383g, 3.382 mmol) in 2 mL of dry dioxane was added a solution of 6-tritylthio-1-paratoluenesulfonylhexane (0.816g, 1.537 mmol) in 2 mL of dry dioxane, the addition was completed in 10 minutes. To the solution, KOH pellets (0.283 g, 5.07 mmol) was added and the reaction mixture was stirred overnight at 100 ^oC. After the reaction was complete, the residue was dissolved in 30 mL of water and the mixture was extracted with ethyl acetate (5 x 20 mL). The organic phase was then washed with water (2 x 25 mL) and brine (2 x 25 mL) and dried over Na_2SO_4., filtered and evaporated under reduced pressure. The product was purified by flash chromatography using hexane/AcOEt 9/1 as eluent. Yield 56%.

^{1}H-NMR (400 MHz, $CDCl_3$): δ = 7.43 (m, 6H, Trt), 7.28 (m, 6H, Trt), 7.26 (m, 3H, Trt), 3.89 (t, J=9.6 Hz, 2H, $HOC\underline{H}_2CF_2$); 3.78 (t, J=9.7 Hz, 2H, $OC\underline{H}_2CF_2$); 3.55 (t, J=6.5 Hz, 2H, $OC\underline{H}_2CH_2$); 2.15 (t, 2H, J=7.3 Hz, CH_2STrt), 1.50 (m, 2H, CH_2), 1.28 (m, 2H, CH_2), 1.18 (m, 4H, CH_2). **MS-ESI** (m/z): 791.3 [M+Na^+].

TsOPEGOMe

A solution of TsCl (789 mg, 4.14 mmol) in 3 mL dry DCM was added drop wise to a mixture of HO-PEG-OMe (2.01 mL, 3.98 mmol), triethylammine (1.11 mL, 7.96 mmol) diluted with 1 mL dry DCM and kept at 0 °C. The mixture was allowed to stir at room temperature for 18 hours. The mixture was then diluted with in DCM (50 mL) and water (50 mL). The aqueous layer was extracted with DCM (3 x 50 mL); the organic layers were collected and were washed with HCl, $NaHCO_3$ 5 % (3 x 30 mL) and H_2O (3 x 30 mL), dried over Na_2SO_4. After removal of the solvent under reduced pressure, the crude product was purified by flash chromatography using $CHCl_3$ as eluent. A white solid was obtained in 92% yield.

Coupling of HS-C6OF-OH with TsOPEGOMe

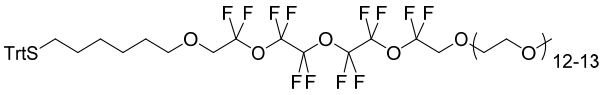

The alcohol **HS-C6OF-OH** (0.29 g, 0.377 mmol) was dissolved in 3 mL dry dioxane under Ar atmosphere. At the solution was added NaH (36.2 mg, 1.508 mmol, previously washed 5 times with petroleum ether) and the mixture was stirred for 20 minutes. To the solution was added TsOPEGOMe (0.266 g, 0.377 mmol) dissolved in 2 mL dry dioxane over a time period of 10 minutes, the solution became yellow. The reaction mixture was heated under stirring for 18 h at 50 °C. then it was cooled at room temperature, diluted with $CHCl_3$. The organic layer was washed with brine (2 x 30 mL) and dried over Na_2SO_4. After filtration and removal of the solvent, the product was purified by flash chromatography using $CHCl_3$/AcOEt 9/1 as eluent.

^{1}H-NMR (400 MHz, $CDCl_3$): δ = 7.44 (m, 6H, Trt), 7.25 (m, 6H, Trt), 7.23 (m, 3H, Trt), 3.96 (t, J=9.9 Hz, 2H, $OC\underline{H}_2CF_2$); 3.6-3.5 (m, 4 H, CH_2O + OCH_2CF_2); 3.36 (s, 3H, OCH_3); 2.13 (t, 2H, J=7.3 Hz, CH_2STrt), 1.49 (m, 2H, CH_2), 1.38 (m, 2H, CH_2), 1.21 (m, 4H, CH_2).

Synthesis of thiol HS-C6OF-PEG

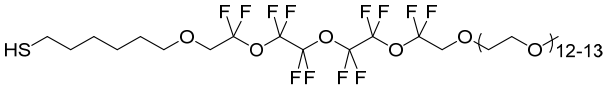

Compound **TrtS-C6OF-PEG** (518 mg, 0.399 mmol) was dissolved in deoxygenated dichloromethane (5 mL) under argon atmosphere. At the mixture, trifluoroacetic acid (0.59 mL, 7.98 mmol) and then triisopropyl silane (0.16 mL, 0.798 mmol) were added. The reaction mixture was stirred at room temperature for 4 hours and then the solvent was removed *in vacuo,* the residue was co-evaporated with methanol. The crude product was purified by column chromatography over silica gel using chloroform-ethyl acetate (9:1 v/v) as eluent, compound **HS-C6OF-PEG** was obtained as a colorless oil (Yield 409 mg, 97%).

^{1}H-NMR (400 MHz, $CDCl_3$): δ = 3.92 (t, J=9.9 Hz, 2H, $OC\underline{H}_2CF_2$); 3.76 (m, 4 H, CH_2O + OCH_2CF_2), 3.67 (s, 3H, CH_2O); 3.39 (s, 3H, OCH_3), 2.15 (t, 2H, J=7.3 Hz, CH_2SH), 1.49 (m, 2H, CH_2), 1.38 (m, 2H, CH_2), 1.21 (m, 4H, CH_2). ^{19}F NMR (470 MHz, CD_3OD) = -83.6 to -84.0 (m, CF_2), -94.6 to -95.12 (m, CF_2-O)

4.4.6. Synthesis of PEG-ylated gold nanoparticles NP-C6OF-PEG

The tetrachloroauric acid (0.058 g, 0.1465 mmol) was dissolved in 50 mL of deoxygenated water and the thiol **HS-C6OF-PEG** (0.310 g, 0.293 mmol) was added dissolved in 50 mL deoxygenated methanol. The mixture was stirred for 30 minutes at room temperature and for 30 minutes at 0°C. At 0°C a freshly prepared solution of $NaBH_4$ (0.061 g, 1.6115 mmol)

was added rapidly. Then the reaction mixture was stirred for 1 hour at 0 °C and 2 hours at room temperature. After this time the reaction was stopped and the precipitation of the nanoparticles was attempted without prior concentrating the solution using solvent such as methanol, hexane, pentane, diethyl ether, acetone but no precipitation could be obtained. The ethanol was then removed without exceedingly concentrating the solution and adding mQ water at small portions. The resulting solution was dialyzed for 3 days against water. Then the solvent was removed and the brown solid was purified by size exclusion chromatography on Sephadex LH 20, using methanol as mobile phase. Then the crude product was dialyzed again for 4 days against water. We obtained 0.080 g of **AuNPs-C6OF-PEG**. ^{1}H-NMR (CD_3OD, 400 MHz): δ= 3.38 (br, CH_3O), 3.48-3.77 (br, CH_2O), 4.10 (br, CF_2CH_2O). UV-VIS absorbance: 540 nm (weak). TEM: X_m = 1.5 nm ± 0.3 nm.

4.4.7. Synthesis of HS-C6OF-DO3AGd

TrtS-C6OF-OMs

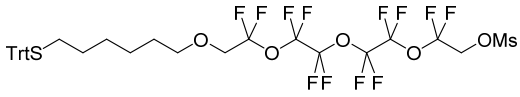

To a solution of 0.195 g (0.254 mmol) of **TrtS-C6OF** in 3.5 mL acetonitrile Et_3N (0.113 mL, 0.812 mmol) and MsCl (0.127 mL, 1.653 mmol) were added dropwise at 0ºC. The reaction was let to stir for 3 hours under argon atmosphere. Then the solvent was removed and the crude mixture was purified by flash chromatography eluting with DCM. The pure product was used rapidly for the next reaction.

TrtS-C6OF-DO3A^{t}Bu

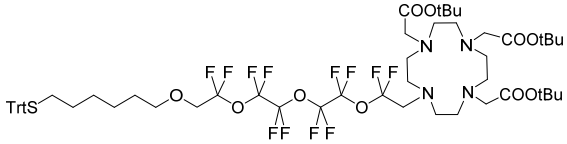

The TrtS-C6OF-OMs (0.170 g, 0.2 mmol) dissolved in 2 mL of acetonitrile was added over a time span of 2 hours to a solution prepared by dissolving DO3A^{t}Bu (0.205 g, 0.4 mmol) in 2 mL of acetonitrile, containing K_2CO_3 (0.220 g, 1.6 mmol), and kept at 60ºC. The reaction mixture was left stirring overnight. The next day 0.111 g K_2CO_3 and 0.0985 g of DO3A^{t}Bu were added and the mixture was stirred at 60ºC for further 18 h. A further amount of 0.094 g of K_2CO_3 and 0.076 g of DO3AtBu was added and the reaction mixture was maintained at 60 °C for other 6 hours. After the last addition of reagents, the ^{1}H NMR spectrum demonstrated the disappearance the signals corresponding to **TrtS-C6OF-OMs**.

^{1}H-NMR (400 MHz, CD_3OD): δ = 7.43 (m, 6H, Trt), 7.28 (m, 6H, Trt), 7.26 (m, 3H, Trt), 3.82;3.88 (br, 2 H, CH_2N), 3.78 (t, J=10.3 Hz, 2H, $OC\underline{H_2}CF_2$), 3.53 (t, J=6.5 Hz, 2H, $OC\underline{H_2}CH_2$); 3.32 (N-$\underline{CH_2}$-CF_2); 3.26 (br, $\underline{CH_2}$-COO); 2.95; 2.76 (br, CH_2N), 2.13 (t, 2H, J=7.3 Hz, CH_2STrt), 1.6-1.15 (m, CH_2, tBu).

Synthesis of HS-C6OF-DO3A

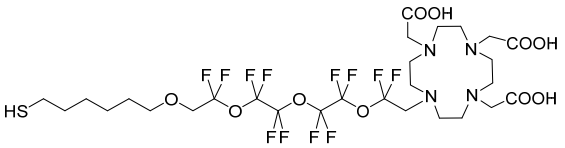

Trifluoroacetic acid (0.9 mL, 11.8 mmol) was added to a solution of TrtS-C6OF-DO3AtBu (0.075 g, 0.059 mmol) in 1 mL anhydrous DCM; the reaction mixture was allowed to stir overnight. Then the solvent was removed and to the solid residue were added 2 mL anhydrous deoxygenated DCM, 0.28 mL TFA and 0.28 mL of TIPS. The reaction was left stirring for 2h, the solvent was removed and the solid was washed 5 times with deoxygenated hexane. The solid was dried under argon and the product was obtained as a white solid.

^{1}H-NMR (400 MHz, CD_3OD): δ = 3.8-3.92 (br, 2 H, CH_2N), 3.79 (t, J=10.3 Hz, 2H, $OC\underline{H_2}CF_2$), 3.55 (t, J=6.5 Hz, 2H, $OC\underline{H_2}CH_2$); 3.04-2.66 (CH_2N, 2.53 (t, 2H, J = 7.3 Hz, CH_2-SH,)1.50 (m, 2H, CH_2); 1.28 (m, 2H, CH_2), 1.18 (m, 4H, CH_2). ^{19}F NMR (470 MHz, CD_3OD) = -76.9 (m, CF_2-CH_2N), -81.6 to -80.9 (m, CF_2), -82.79 (m, CF_2), -94.11 to -93.6 (m, CF_2-O).

Synthesis of HS-C6OF-DO3AGd

0.045 g of **HS-C6OF-DO3A** (0.045 mmol) were dissolved in 2.5 mL of deoxygenated HEPES (pH = 7.4, 0.1 M in H_2O mQ). To this solution were added 0.413 mL of a 0.1 M $GdCl_3$ solution (0.041 mmoli, 0.9 Eq.) and the reaction mixture was stirred for 2 h at 25 °C. This solution was used for the place exchange reaction without further purifications.

4.4.8. Synthesis of NP-C6OF-PEG/C6OF-DO3AGd

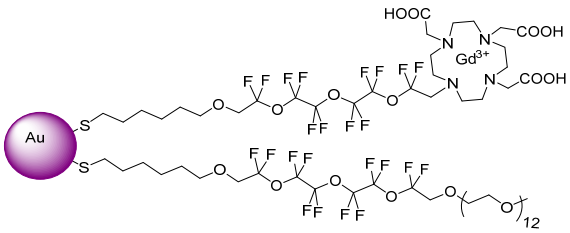

25 mg of NP-C6OF-PEG were dissolved in 2 mL of deoxygenated mQ water and the solution was added at **HS-C6OF-DO3AGd** in HEPES reaction was let under stiring at 40 °C for 3 days After this time, the nanoparticles were transferred in one Millipore (10 000

MWCO) centrifugal filtration device and the solution was centrifuged at 4500 rpm for 30 minutes and washed with milliQ water (7 x 20 mL). After that the nanoparticles were dried giving a brown solid. ICP-AES: [Au]/[Gd] = 11.4; 9 moli Gd/NPs. TEM: X_m = 1.5 nm ± 0.3 nm.

5. Conclusions

This PhD thesis is focused on two projects and the main objective are: a) the study of the morphology of mixed monolayers on the surface of gold nanoparticles composed of hydrogenated and fluorinated ligands using NMR techniques and b) the design of gold nanoparticles coated with gadolinium chelates for MRI applications.

In the first part of this project, we have investigated how a mixture of hydrogenated and fluorinated thiolates organize on the surface of the gold core. In order to gain information about the influence of the structure of the ligands and of the length mismatch between them on the shape of the resulting domains, we have synthesized three classes of nanoparticles. Varying the initial ratio between the *H*- and the *F*- thiolates, we have obtained gold nanoparticles with different percentages of the fluorinated ligand into the monolayer. For all these nanoparticles we have performed ^{19}F NMR experiments in order to investigate the dependence of the chemical shift of the CF_3 group of the fluorinated thiolates with the composition of the monolayer.

The first type of nanoparticles is protected by ligands having different length, *i.e.* **NP-C16/F6** and **NP-C12/F6**. Plotting the chemical shift of the CF_3 group as a function of the ligand composition for **NP-C16/F6**, a sigmoidal trend has been found, with a plateau region between 40 % and 80 % of the *F*-ligand. At percentages of the fluorinated ligand lower than 40% a linear decay was obtained suggesting that increasing the amount of fluorinated ligand into the monolayer the CF_3 group experiences very different chemical surroundings. In the region between 40% and 80% the chemical shift of the CF_3 group is less sensitive to the composition of the monolayer, indicating that the thiolate **F6** experiences very similar surroundings even though the percentage of the fluorinated ligand into the monolayer increases. When more than 80% of the **F6** thiolate is introduced in the monolayer, the chemical shift of the terminal CF_3 group becomes again sensitive to the influence of the neighboring thiols. Multiscale molecular simulations for this type of nanoparticles suggested that the two ligands organize in stripes on the surface of the gold core. In **NP-C12/F6** are present ligands with different length but the graph obtained plotting the chemical shift of the CF_3 group as a function of the ligand composition is different with respect to that of **NP-C16/F6**. In this case the plateau region was found in the first 25% of fluorinated thiolate in the monolayer; this trend is followed by a sudden decrease of the chemical shift with a small increase of **F6** introduced into the monolayer. At higher percentages, a plateau region is observed up to the 100% of **F6**. For these

nanoparticles, multiscale simulations suggest the formation of irregular domains, in some cases stripes in other cases patches. This is an indication that the length mismatch of four carbon atoms is not sufficient to create a highly ordered system, but it can be surely stated that the obtained organization is not random. This means that the ligands are able to phase segregate forming domains, but the small difference in length is not sufficient to gain the entropy necessary to organize in stripes or regular patches.

The second type of nanoparticles that we have investigated is represented by nanoparticles protected by ligands of equal length, **NP-C12/F10** and **NP-C8/F6**. The behavior curves obtained for **NP-C12/F10** shows an exponential decay of the chemical shift of the CF_3 and close CF_2 peaks as a function of the percentage of the fluorinated ligand into the monolayer. A steep decay was observed when the loading of the fluorinated ligand was less than 40 %, followed by a smooth decrease of the chemical shift up to the 100% of **F6**. This indicates a strong evolution of the surface area at the interface in the first region of the curve which determines a significant downfield shift of the NMR signals of the fluorinated ligands. When the loading increases over 60%, no important changes at the interface are observed and the chemical shift remains nearly constant. Multiscale simulations on selected nanoparticles **NP-C12/F10** suggest that the two ligands phase separate in two big domains forming Janus nanoparticles. The behavior of the chemical shift *vs.* the percentage of **F6** in the monolayer of **NP-C8/F6** is different with respect to the previous types of nanoparticles and seems to be an intermediate situation between an exponential and a linear decay. This trend is somewhat unexpected since we thought that **NP-C8/F6** and the previously discussed **NP-C12/F10** should have had a very similar Janus organization of the monolayer. Multiscale simulations are consistent with the NMR chemical shift behaviour and show that the two ligands self-sort in small domains.

For nanoparticles protected by ligands with similar bulkiness and different length, **NP-brC12/F6**, the broad peak of the nanoparticles shifts gradually downfield when the composition of the **F6** into the monolayer increases from 6% to 100%. In the case of these nanoparticles, the linear decay suggests that the average composition of the first nearest neighbor shell for one ligand coincides with the overall composition of the monolayer. This was in agreement with the multiscale simulations. It has been demonstrated that bidimensional heteronuclear experiments and in particular, ^{1}H-^{19}F HOESY, are very sensitive but are not suited to distinguish between different organization of the monolayer because cross peaks between the CF_2 central groups of the fluorinated ligand and the methylene groups of the either hydrogenated or fluorinated thiolates can be observed even when a small number of interactions are present.

The preparation of such a large number of samples of nanoparticles protected by blend of hydrogenated and fluorinated thiolates enable us to analyze the composition of the monolayers in comparison with the ratio of thiols used for the synthesis. Moreover, we observed that the solubility properties of the nanoparticles depends on the morphology, as expected, and are consistent with the NMR and multiscale molecular simulations data. These results have been reported in a recent paper: "Routes to the preparation of mixed monolayers of fluorinated and hydrogenated alkanetiolates grafted on the surface of gold nanoparticles" M. Şologan, C. Cantarutti, S. Bidoggia, S. Polizzi, P. Pengo, L. Pasquato, *Faraday Discussion* 2016, DOI: 10.1039/C6FD00016A. A second manuscript is in preparation.

In the second part of this PhD thesis preliminary results about the synthesis of new ligands able to complex the Gd(III) for the synthesis of AuNPs for MRI applications are presented. Three classes of nanoparticles have been designed:

a) **NPs-C6OF-PEG** protected by a oxyfluorinated ligand for ^{19}F MRI applications.
b) **NPs-C8TEG/C8-DO3AGd** protected by a mixture of thiolates, **C8TEG** and a new ligand able to complex the Gd(III), **HS-C8-DO3A**, for ^{1}H MRI applications.
c) **NPs-C6OF-PEG/C6OF-DO3AGd** which may be a first example for dual imaging, both for ^{1}H and ^{19}F MRI applications.

The preliminary results described in the thesis suggest that this kind of systems could be promising candidates as contrast agents for MRI applications. Moreover, it has been found that the neighbouring of fluorine atoms with Gd(III) determine a decrease of the T1 and T2 relaxations times from 588 ms and 67 ms respectively for **NP-C6OF-PEG** to 258 ms and 33 ms for **NP-C6OF-PEG/C6OF-DO3AGd**.